5-1990

Laramide Deformation in Precambrian Granitic Rocks, Northeastern Wind River Range, Wyoming

Mark A. DuBois
Utah State University

LARAMIDE DEFORMATION IN PRECAMBRIAN GRANITIC ROCKS, NORTHEASTERN WIND RIVER RANGE, WYOMING

by

Mark A. DuBois

A thesis submitted in partial fulfillment
of the requirements for the degree

of

MASTER OF SCIENCE

in

Geology

Approved:

UTAH STATE UNIVERSITY
Logan, Utah

1990

ACKNOWLEDGMENTS

I am grateful to many people for thesis-related help over the last few years. First, I'd like to thank and praise the Lord - for the direction to come to Utah State and for allowing me to maintain my sanity through the experience. My parents taught me to love learning and supported me in my educational endeavors - for which I am grateful. To Diana, my loving and uncomplaining wife, thank you. Your patience (and at times, impatience) expedited this process.

My advisor, Dr. Evans introduced me to the beautiful Dubois (sic) area and suggested the research. His numerous reviews of the manuscript and insightful comments and questions facilitated unification of the anastomosing threads of this research. Partial funding for this research was made through Dr. Evans and a U.S.U. Faculty Research Grant as well as from the donors of Petroleum Research Fund, administered by the American Chemical Society, Grant #GB-19752. Thank you Dr. Evans. Dr.'s Fiesinger and Kolesar made numerous suggestions which improved the structure and reading of the manuscript. Dr. Chris Schmidt accompanied me to the field and was helpful with his suggestions and explanations. Dr. Forster made useful comments in the early stages of this research. All of the Geology Department faculty have been quite accessible, whether for class- or thesis-related questions. Friday afternoon meetings with them and fellow grad students at the White Owl were also helpful. Thank you all.

In Wyoming, Mr. Pete Peterson and Mr. Clarence Allison graciously allowed access to the study area. Merle and Dorothy at the Forest Service took messages. To all of them I'd like to express my sincere gratitude.

Mark A. DuBois

TABLE OF CONTENTS

Page

ACKNOWLEDGMENTS ii

LIST OF TABLES vi

LIST OF FIGURES vii

ABSTRACT ix

INTRODUCTION AND OBJECTIVES 1

LOCATION 3
GEOLOGIC SETTING 3
PREVIOUS WORK 6

Laramide Deformation and the Wind River Mountains 6
Fracture Mapping in Crystalline Rock and Analysis in General 12
Microfracture Analysis and Mapping 12
Interrelated Fluid Flow, Mineralization, Microstructure and Deformation Mechanism(s) 14

METHODS 16

FRACTURE ANALYSIS 16

Airphoto 16
Outcrop 19

Grid Area 20
Traverse Area 21

Thin Section 25

SAMPLING 25
THIN SECTION PREPARATION AND ANALYSIS 25
X-RAY ANALYSIS 26

Procedures 26

Powdering 26
Random Mounts 27
Oriented Mounts 27
Montmorillonite, Kaolinite, and Chlorite Determinations 27
Machine Parameters 28

SEM ANALYSIS 28

RESULTS OF INVESTIGATION 29

FRACTURE ANALYSIS 31

Airphoto 34
Outcrop 34

Grid Area 36
Traverse Area 38

Thin Section 38

Traverse Area 40
Grid Area 46

COMPOSITIONAL ANALYSIS 48

Thin Section and X-ray Analyses.....48

Traverse Area 48
Grid Area 48

SEM Analysis 54

DISCUSSION AND INTERPRETATION 55

SAMPLING AND NUMBER OF DATA 55
SCALES OF OBSERVATION AND TREATMENT OF DATA 56
DEFORMATIONAL FEATURES AND MECHANISMS 57

Traverse Area 58
Area Along Jakey's Fork Fault (Gridpoints 4,5,6) 64
Central Part of Study Area (Gridpoints 7,8,16,17) 67
Ross Lakes Fault - Jakey's Fork Fault Intersection Area ..69

RELATIVE TIMING OF FAULTING 69
PRECAMBRIAN - PALEOZOIC CONTACT 73
FLUID-FLOW AND GEOCHEMISTRY 75

CONCLUSIONS 81

RECOMMENDATIONS FOR FUTURE WORK 84

REFERENCES 87

APPENDICES 93

APPENDIX A. EXPLANATION FOR AND DISCUSSION OF APPENDIX INFORMATION 94
APPENDIX B. TRAVERSE AREA: SAMPLE AND ANALYSIS DESCRIPTIONS 95
APPENDIX C. GRID AREA: SAMPLE AND ANALYSIS DESCRIPTIONS 97
APPENDIX D. TRAVERSE AREA SAMPLES: COMPOSITION AND THIN SECTION DEFORMATION DATA 101
APPENDIX E. GRID AREA SAMPLES: COMPOSITION AND THIN SECTION DEFORMATION DATA 109
APPENDIX F. TRAVERSE AREA: RESULTS OF FRACTURE ORIENTATION AND DENSITY ANALYSES 119
APPENDIX G. GRID AREA: RESULTS OF FRACTURE ORIENTATION AND DENSITY ANALYSES 131
APPENDIX H. TRAVERSE AREA: THIN SECTION PHOTONEGATIVES AND FRACTURE TRACINGS 156
APPENDIX I. GRID AREA: THIN SECTION PHOTONEGATIVES AND FRACTURE TRACINGS 166

LIST OF TABLES

Table Page

1. TRAVERSE FRACTURES: DENSITY AND ORIENTATION 43

2. GRID FRACTURES: DENSITY AND ORIENTATION 49

LIST OF FIGURES

Figure — Page

1. Wyoming location map for study area 4
2. Topographic map showing location of Jakey's Fork study area 5
3. Topographic map showing locations of Jakey's Fork study area and Whiskey Mountain and Torrey Creek areas 8
4. Generalized geologic map for study area 10
5. Northern Wind River Range - downplunge projection 11
6. Map view of study area 17
7. Orientations of airphoto fractures/lineaments and groupings in the study area 18
8. Photograph of Traverse Area viewing due south 22
9. Photograph of Traverse Area viewing perpendicular to fold axis .22
10. Photographs of Precambrian granite - Cambrian Flathead Sandstone contact 23
11. Cross-sectional diagram of Traverse Area showing displacement and tilting of Cambrian Flathead Sandstone 30
12. Equal-area plot with Kamb contours of poles to bedding for measurements taken in traverse across Ross Lakes Fault 32
13. Rose diagrams of outcrop fracture orientations at Gridpoint 3 ..33
14. Equal-area stereonets of major fracture orientations (planes) or deformation zone orientations in the northeastern Wind River Range 35
15. Map of Gridpoint Area with rose diagrams showing outcrop fracture orientations 37
16. Map of Traverse Area with rose diagrams showing outcrop fracture orientations 39
17. Photonegative of thin section with mapped intergranular fractures and quartz fractures 41

18. Traverse Area - combined fracture orientation data: outcrop, intergranular, and quartz (primarily intragranular) 42

19. Flathead Sandstone - vertical thin section photonegative showing subhorizontal fractures and zones of granulation in steeply east-dipping beds 44

20. Thin section microphotograph of Flathead Sandstone quartz grains in contact with microcline grain from granite 45

21. Grid Area - combined fracture orientation data: airphoto, outcrop, intergranular, quartz (primarily intragranular) 47

22. Thin section microphotographs showing progressive deformation of rocks along Jakey's Fork Fault 50

23. Thin section microphotographs showing fractured quartz aggregates from Traverse Point E 59

24. Horizontal thin section photonegative of granitic sample from small zone near Traverse Point F showing folded, fractured, discontinuous nature of elongated quartz-grain aggregates 60

25. Thin section microphotograph of a folded quartz-grain aggregate from Figure 24 61

26. Photograph of outcrop at Gridpoint 5 66

27. Photograph of typical outcrop in central Grid Area 68

28. Horizontal thin section photonegative of sample from Gridpoint 3 - near the intersection of Jakey's Fork Fault and Ross Lakes Fault showing mylonitic, breccia, and veined angular clasts 70

29. Photograph of Ross Lakes Shear Zone 71

30. Photograph of quartz and breccia vein crossing the Precambrian-Paleozoic contact near Traverse Point E 74

31. Thin section microphotograph of quartz vein through a highly altered feldspar grain from the Traverse Area 77

ABSTRACT

Laramide Deformation in Precambrian Granitic Rocks,

Northeastern Wind River Range, Wyoming

by

Mark A. DuBois, Master of Science

Utah State University, 1990

Major Professor: James P. Evans
Department: Geology

Fractures and faults in the Jakey's Fork area, northeastern Wind River Range, Wyoming, caused by brittle Laramide deformation in the Precambrian granitic basement have been studied in detail at airphoto, outcrop, and thin-section scales. The study area is bounded on the south by the approximately east-west and vertical Jakey's Fork Fault and on the east by the approximately northwest-southeast and vertical Ross Lakes Fault. Both were active during Laramide deformation. Four distinct structural domains, defined by fracture patterns and proximity to the two major faults have emerged in this study. The areas are: 1) Along Ross Lakes Fault granite cores a fold defined by shallowly and steeply east-dipping Cambrian Flathead Sandstone. Laramide movement on Ross Lakes Fault appears to have post-dated Jakey's Fork Fault movement and was discordant with Precambrian zones. Fractures at all scales studied strike approximately northeast-southwest, consistent with the inferred maximum Laramide principal stress. 2) Along east-west striking Jakey's Fork Fault, Laramide movement appears to have reactivated Precambrian mylonite zones as evidenced by the chlorite-rich, foliated cataclasite along its

trace. Fractures at all scales have an approximate east-west orientation. 3) Near the intersection of the two faults, deformation was intense, as shown by mylonitic, breccia, and veined clasts. Discrete airphoto fractures were not recognized due to intense deformation in this interaction zone. 4) In the central area, away from the two faults, airphoto and outcrop fracture orientations have a north to northeast strike. Fracture orientations at the thin-section scale are more variable and do not agree with macroscopic orientations; they strike west to northwest. The central area is a 'block', possibly divided into 'sub-blocks', bounded by zones along which much of the deformation occurred. Thus, these zones had an insulating effect at thin-section scale. The Paleozoic rocks were at least partially decoupled from the basement during deformation, suggested by gouge along the contact and different fracture orientations on opposite sides of the contact. At least two fluid systems are represented in the study area. Relatively wide-spread, pre-Laramide chlorite development occurred at temperatures and pressures higher than those present during Laramide deformation. A Laramide (or post-Laramide) pervasive fluid system (especially near Ross Lakes Fault) is reflected by abundant fracture porosity, advanced feldspar alteration, and kaolinite development.

(204 pages)

INTRODUCTION AND OBJECTIVES

Recent work which has related observable deformation features on the macroscale (i.e., regional or airphoto) and microscale (thin section) to tectonic events and stress fields has not systematically examined the relationship between the distributions of microfractures, macroscopic fractures, and faults in granitic rocks and fluid flow properties in these areas. Fluids have a fundamental role in nearly all natural fracture processes in rocks (Knipe,1989). Evidence for fluids is found in microscopic and macroscopic fractures in fault zones (Simpson,1987; Segall and Pollard,1983a) but it is not known how the fluids penetrated to these areas. Fluids may penetrate granitic rocks during fault development (to significant depths, $\geq$ 5 km) (McCaig,1988; Reynolds and Lister,1987; Gough,1986; Kerrich et al.,1984) and such fluids have been implicated as being responsible for the weakening of the rocks through mechanical and/or chemical effects (Kronenberg and Segall,1987; Segall,1987; Mase and Smith,1987; Kirby,1984; Janecke and Evans,1988). However, the mechanisms of fluid flow through, and possible weakening of, these (originally) low permeability rocks are unknown (Brace,1984; Neuzil,1986; Nesbitt and Muehlenbachs,1989). Fluid flow may range from channeled flow in large fractures (little rock-fluid interaction, Sibson,1981) to mineralization (and/or alteration) along microfractures (pervasive interaction, e.g. in breccia zones, Wood and Walther,1986).

The Jakey's Fork area, northeastern Wind River Mountains, Wyoming, is an ideal setting to investigate structural patterns and the (possible) related fluid flow in deformed granitic rocks from the macro- to the

microscale. Laramide deformation, responsible for formation of the Wind River Range, has been discussed by Brown (1988) and refers to basement-involved features that developed in Late Cretaceous through Eocene time. Air photo interpretation of the Jakey's Fork area revealed several faults and large fracture patterns in granitic rocks that previously had not been mapped in detail. Optical microscopy of Jakey's Fork samples further revealed that fractures and faults exist on the microscale. In addition, fieldwork showed that outcrops exhibited three-dimensional exposures which were desirable for sampling, data gathering, and fluid-flow interpretation.

In this study, systematic mapping of fractures and faults was performed at several scales to identify fault-fracture and (possible) associated fluid-flow patterns. This research systematically examined the distributions of microfractures, macroscopic fractures, and faults in the granitic rocks of the Jakey's Fork area at airphoto, outcrop, and thin-section scales. Mineralogical, textural, and deformational evidence for the types of fluid interaction and the mechanical response of Precambrian rocks to Laramide deformation were also evaluated. These analyses allowed a continuum of data to be evaluated with respect to the scale of fractures, the role of fluids, types of fluid flow, and possible failure mechanisms in the granitic rocks.

The overall goals of this study were to investigate and characterize Laramide deformation and the paleohydrologic flow system of Precambrian rocks in the Jakey's Fork area as well as to examine the role of basement rock deformation in the geologic evolution of the Wind River Range. These

were accomplished by examining: (1) the distribution (orientation and density) of fractures and faults from the macro- to microscale in deformed granitic rocks; and (2) mineralogical, textural, and deformational evidence for fluid interaction along these fractures and faults. The fracture distribution data also allowed evaluation of scale with respect to orientations and densities of (possible) hydraulic conduits.

The scope of the original objectives was necessarily broad. As field and lab work progressed however, the work became more focused - as some aspects of the proposed work proved impractical and/or as interpretation of accumulated data dictated the subsequent course of the research.

LOCATION

The Jakey's Fork area is approximately 16 km southwest of Dubois, WY in the northeastern part of the Wind River Range (Figure 1). The specific study area is located in the Simpson Lake, WY (1:24,000) quadrangle: T.41N,R.107W, Sections 33,34,35; and T.40N,R.107W, Sections 2,3,4 (enclosed in heavy dashed lines, Figure 2).

GEOLOGIC SETTING

The Wind River Range is the largest Laramide thrust sheet in Wyoming (Figure 1). The structural and topographic relief expressed in the Wind River Range is thought to have resulted from regional deformation occurring between late Cretaceous and middle Eocene time (Love,1960) and from Oligocene-age crestal uplift of the range (Steidtman et al.,1989)

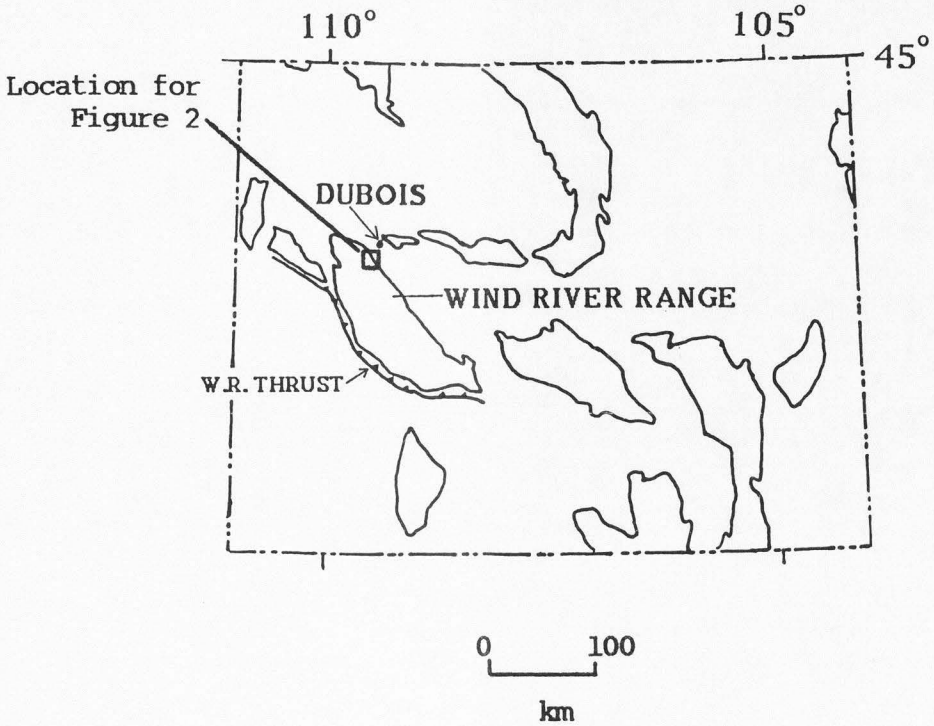

Figure 1. Wyoming location map for study area. W.R. THRUST = Wind River Thrust.

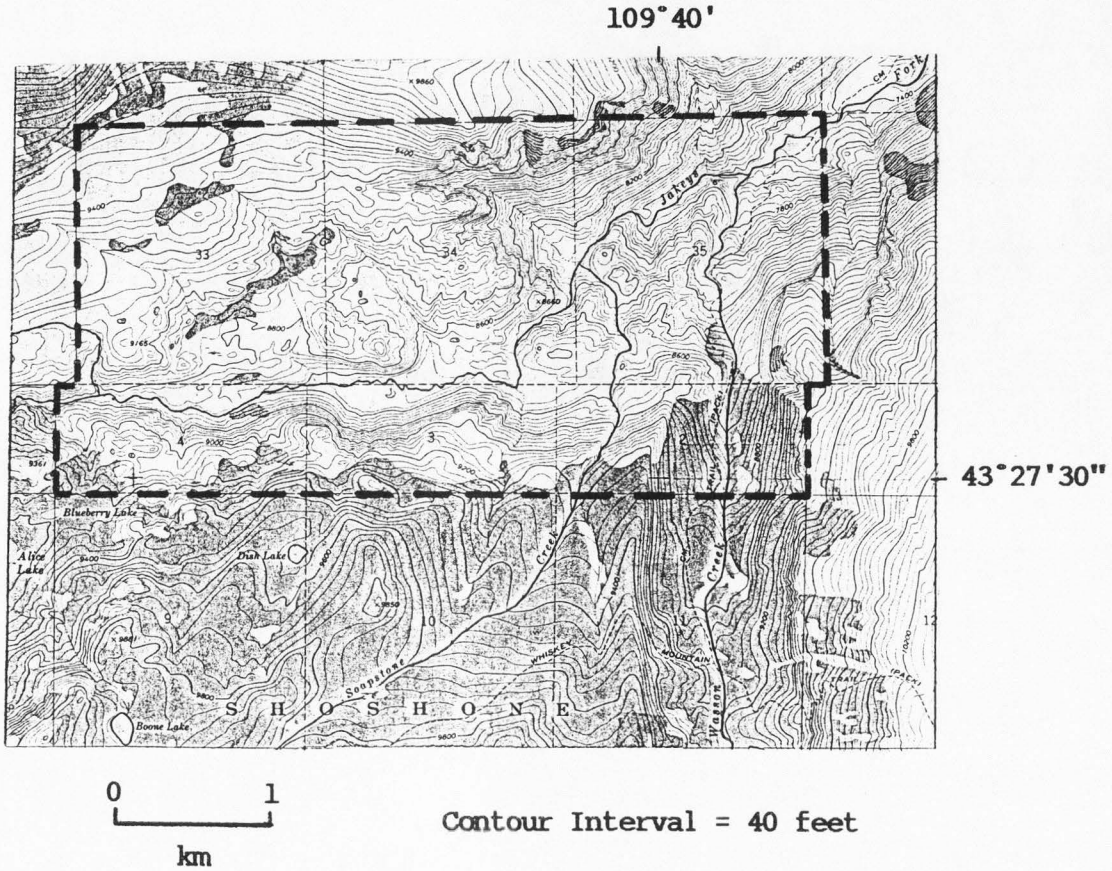

Figure 2. Topographic map showing location of Jakey's Fork study area (as described in text).

followed by regional uplift and erosion. Laramide deformation from N40E-S40W oriented horizontal compressive stresses (Brown,1988) resulted in this northwest-trending, thrusted asymmetric anticline with an extensive exposed core of Precambrian crystalline rocks. The range trends northwest-southeast with a length of ≈ 220 km, a width of ≈ 70 km, and was formed from a west- to southwest-directed thrust sheet. Originally horizontal sedimentary rocks in the Green River Basin to the west of the uplift are overthrust by the Precambrian rocks of the Wind River Mountains along a moderately dipping (30-35^0 NE, Smithson, et al.,1978) thrust surface.

The Jakey's Fork area is located near the northeastern flank of the Wind River Range where the Precambrian crystalline rocks are overlain by Paleozoic and younger rocks which dip ≈ 15^0 into the Wind River Basin forming an east-facing homocline. Low-to-moderate east dips in the Paleozoic rocks increase to near vertical in the hinge area and are accompanied by abundant fractures and faults in the exposed Precambrian rocks. Two approximately vertical large faults cut through the study area - Jakey's Fork Fault (JFF) trending ≈ east-west and Ross Lakes Fault or Shear Zone (RLF or RLSZ) trending ≈ north-south.

PREVIOUS WORK

Laramide Deformation and the Wind River Mountains

Brown (1988) described Laramide deformation as being concentrated along primary northwest trends, with brittle crustal yielding due to

horizontal compressive stresses (N40E-S40W). Deformation also occurred along secondary structural trends striking east and northeast, possibly a result of reactivation of Precambrian zones of weakness. In the Wyoming Province, Prucha et al. (1965) reported dominant structural trends of N40W and that deformation of sedimentary rocks was a consequence primarily of differential movement of discrete fault blocks in the underlying basement. Hoppin and Palmquist (1965) reported that the positions and attitudes of Laramide structures in the Bighorn Mountains may reflect Precambrian lines of weakness or may be in response to Laramide stress systems uninfluenced by basement and that any combination is possible. They suggested evaluation in the mountain flanks where both basement and cover rocks could be mapped (and the relative effects of Precambrian zones and Laramide deformation on Paleozoic and Precambrian rocks could be estimated). Wise (1964) mapped microjoints ($\geq$ 4 macroscopic subparallel fractures spaced closer than 3 mm) in Precambrian basement outcrops in Montana and Wyoming. He reported common local patterns of two nearly vertical, perpendicular sets and suggested that there was a regional system of eight recurring fracture directions (between N70W and N85E). Measurements near the range front in the southern Wind River Mountains showed two nearly vertical NE-SW and NW-SE fracture sets (Wise,1964, Plate 4).

Gilliland (1959) measured 100 joint strikes in the Precambrian rocks from air photos in the Whiskey Mountain area (just south to southeast of the Jakey's Fork area, Figure 3) and found two dominant sets with 70°-80° and 310°-320° azimuths. Other workers, e.g., Keefer (1970), have described

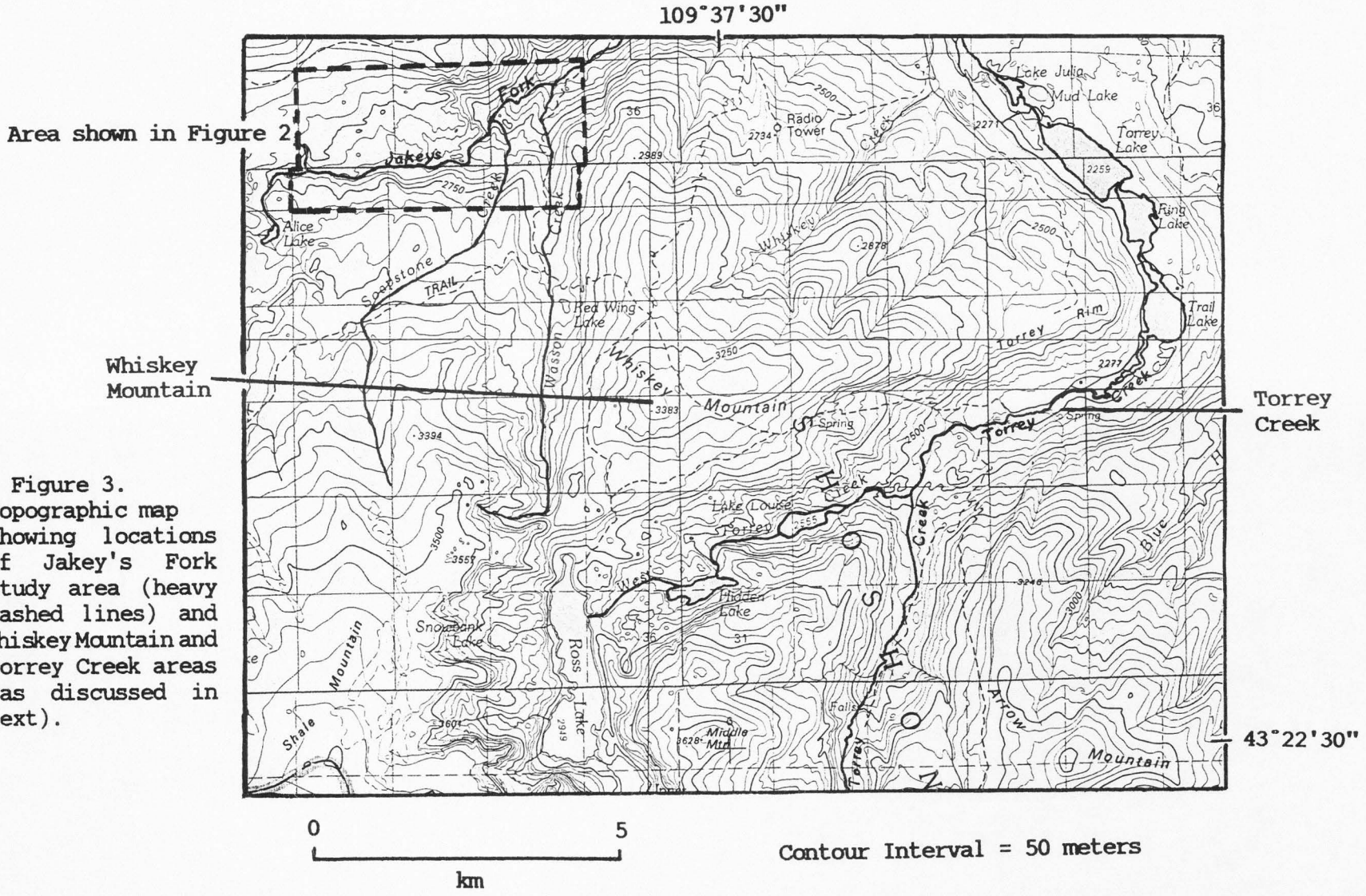

Figure 3. Topographic map showing locations of Jakey's Fork study area (heavy dashed lines) and Whiskey Mountain and Torrey Creek areas (as discussed in text).

dominant NW structural trends within the Wind River Range. Steidtman et al. (1989) contrasted the modern Wind River Range crest trend of N45W (≈ parallel to the Wind River Fault) with mapping in the core of the range which showed a dominant N25W fault trend and suggested that the N25W trend resulted from reactivation(s) of Precambrian shear zones. Mitra and Frost (1981) recognized early Precambrian, late Precambrian, and Laramide deformation zones in the Wind River Mountains along Torrey Creek southeast of the Jakey's Fork and east of the Whiskey Mountain areas (Figure 3) but stated that extensive recrystallization in the Precambrian rocks caused them to behave as a massive and homogeneous basement during Laramide deformation. In their study area, they recognized seven distinct sets of Laramide deformation zones (characterized by intense fracturing).

A generalized geologic map with the Jakey's Fork study area outlined (Figure 4, redrawn from a 1971 study by Granger et al.) shows the northern end of the Wind River Range. The goal of Granger et al.'s (1971) mapping was to produce, using airphotos with field-checking, a geological reconnaissance map (at a 1:62,500 scale and covering ≈ 886 km^2) for a U.S.G.S. mineral survey. Two major faults (or shear zones) have been mapped in the Jakey's Fork area by Granger et al. (1971, Figure 4). The shear zones trend north-south (Ross Lakes Fault, RLF or RLSZ) and east-west (Jakey's Fork Fault, JFF). A southwest-northeast cross section through the northern Wind River Range (Figure 5, based on Mitra,1984 and Evans,unpublished) shows the major Wind River Thrust, a probable imbricate - the White Rock Thrust (Yonkee et al.,1984), and the subparallel (in a horizontal plane) Ross Lakes Fault which cuts through the study area. The

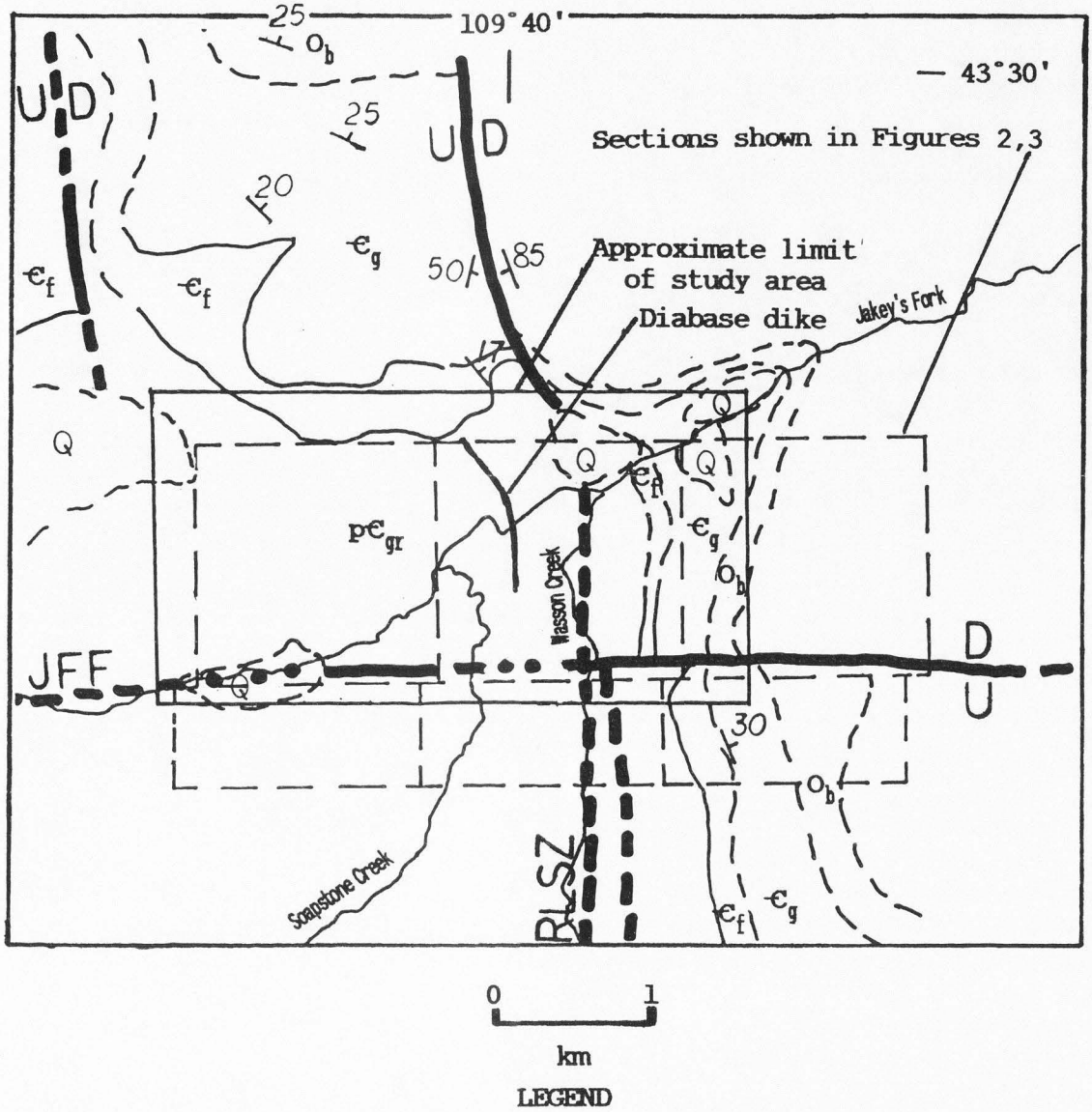

Figure 4. Generalized geologic map for study area (adapted from Granger et al., 1971). JFF = Jakey's Fork Fault. RLSZ = Ross Lakes Shear Zone. Geologic units are: $p\epsilon_{gr}$, Precambrian granite; ϵ_f, Cambrian Flathead Sandstone; ϵ_g, Cambrian Gallatin and Gros Ventre Formations; O_b, Ordovician Bighorn Dolomite; Q, Quaternary deposits.

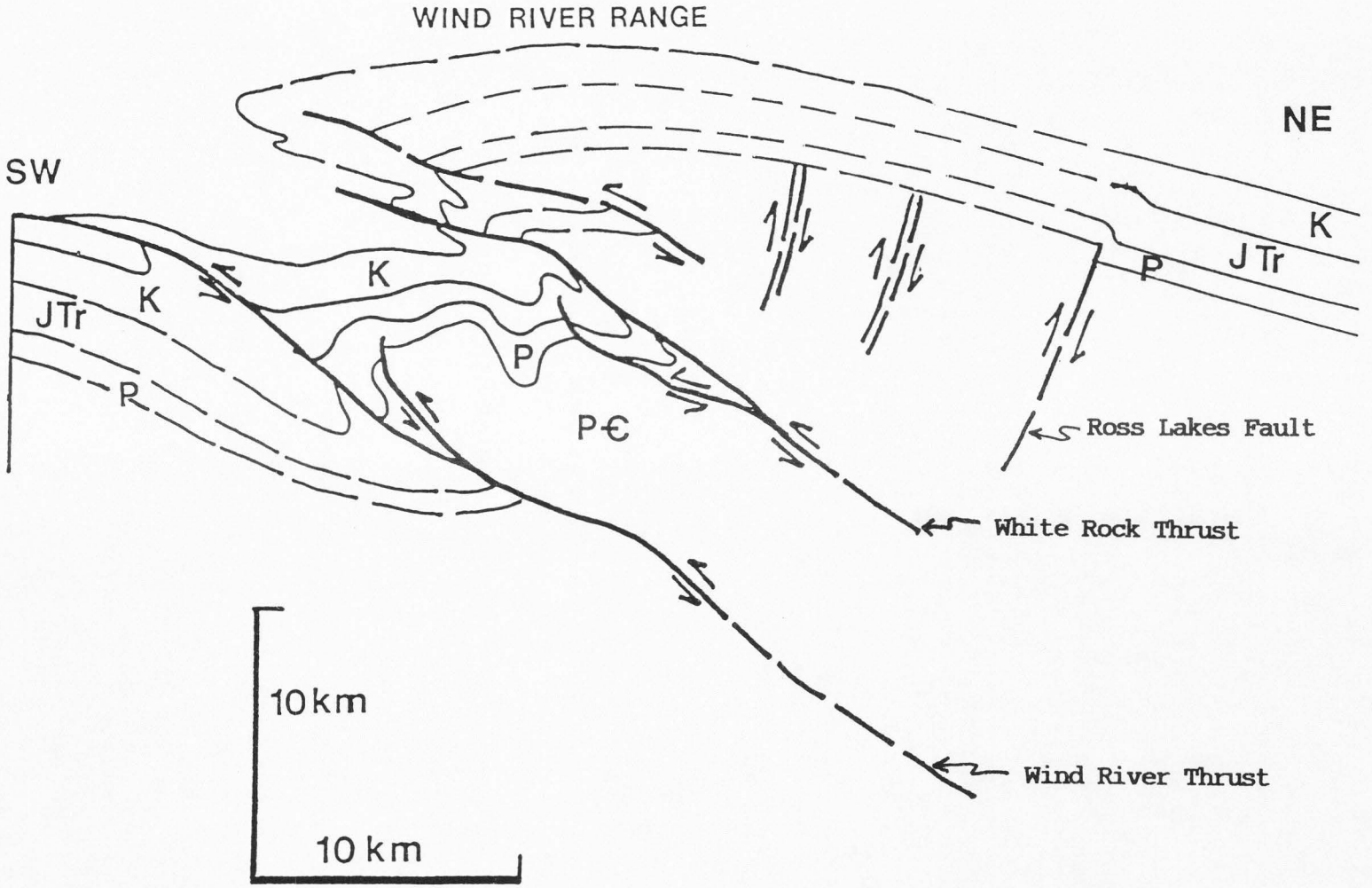

Figure 5. Northern Wind River Range - downplunge projection (based on Mitra, 1984; and Evans, unpublished). Rock units are: PC, Precambrian granite and gneiss; P, Paleozoic rocks; JTr, Jurassic-Triassic rocks; K, Cretaceous rocks.

cross section suggests that RLF (or RLSZ) is a possible 'back thrust' which accommodated internal deformation of the Wind River thrust sheet.

Portions of this work have been described in DuBois and Evans (1989), DuBois and Evans (1990), and Evans et al. (1990). Others who have worked on and reported various aspects of geology in the Wind River Mountains include: Baker, 1946; Berg, 1962; Erslev, 1986; Mitra et al.,1988.

Fracture Mapping in Crystalline Rock and Analysis in General

Segall and Pollard (1983a,b) mapped and studied fractures and strike-slip fault nucleation in granitic rocks in the Sierra Nevada. Their work indicated that the faults nucleated on earlier formed joints oriented approximately parallel to the local maximum-inferred compressive stress and grew through a linking of adjacent faults by secondary dilatational fractures. They also presented a method of field mapping in fractured granites.

Microfracture Analysis and Mapping

Groshong (1988) described the relationship between principal stresses and orientations of extension fractures (fractures that exhibited opening perpendicular to their planes and no shear displacement of the planes). Extension fractures form parallel to sigma-1 (maximum principal stress) and open perpendicular to sigma-1 (or parallel to sigma-3 - least principal stress).

Dula (1981) correlated deformation lamellae and microfractures in quartz (from lower Paleozoic quartzites) with macrofractures and in situ

stress measurements in Colorado. He found that microfracture and joint orientations were very similar which suggested that they were both related to the same stress field (Laramide stresses which have continued to the present). Dula (1981) also stated that these types of analyses are best suited for slightly to moderately deformed rocks which have a relatively simple stress history where recrystallization has not obliterated useful fabric elements or produced preferred crystallographic orientations.

Lespinasse and Pêcher (1986) correlated sets of fluid-inclusion planes (healed microfractures in quartz) in granites with several well-documented regional deformational events in France. They reported orientations similar to those of micro- and mesoscale fractures with the dominant fluid-inclusion trail direction parallel to the main direction of regional shortening. They also suggested that the trails appear to be fossilized pathways of hydrothermal solution migration.

Kowallis et al. (1987) studied healed microcracks (primarily intragranular fractures) in quartz grains from borehole granite in Illinois and concluded that their relatively uniform orientation suggested a paleostress field with a maximum horizontal compressive stress oriented parallel to them (and about 90° from its present orientation) existed at the time the microcrack set formed. They also noted that the healed microcracks had a more uniform orientation than open microcracks which formed by stress relief when the core was removed from the borehole.

Ren et al. (1989) investigated healed microfractures (those which showed no evidence of shearing, i.e., tensile fractures) in quartz grains in plutons of known ages and related their orientations to changes in regional tectonic stresses in the Basin and Range province.

Brace (1971) reviewed experimental rock deformation and discussed crack formation parallel to maximum horizontal stress direction and fault formation.

Engelder (1974) described characteristics of gouge and cataclastic deformation. He found microfractures in cataclastic sandstone associated with gouge to be strongly oriented parallel to the maximum principal compressive stress.

Interrelated Fluid Flow, Mineralization, Microstructure and Deformation Mechanism(s)

Mitra and Frost (1981) characterized Laramide deformation in the Wind River Range as primarily brittle (expressed by intense fracturing and granulation) and pre-Laramide deformation (i.e., Precambrian) as ductile (dominated by crystal-plastic mechanisms). They also explained that fluid flux along the Laramide shear zones was small since kaolinite was lacking in the samples they studied (with the following assumed conditions: 150°C, SiO_2-saturated water, 1 kb pressure, K-spar alteration to kaolinite).

Mitra (1984) studied fractures in thin sections of rocks from the White Rock Thrust and recognized two main types which could be used to distinguish between mainly brittle and mainly ductile deformation. He characterized brittle deformation by fractures that propagated spontaneously across grains and grain boundaries and that are observed as continuous fractures which cut across grains of different compositions and orientations. Ductile deformation (close to the brittle-ductile transition regime) was characterized by fractures that die out within individual grains or are terminated at grain boundaries.

Bruhn et al. (1987) discussed the role of chemically reactive fluids

and fracture permeability with respect to deformation zone growth and brittle vs ductile deformation mechanisms.

METHODS

Fieldwork was conducted from June to September, 1988. In order to realize the objectives, 17 gridpoints were established in the study area (at 610 m, equal to 2000', centers on the 1:12,000 base map, Figure 6) to systematically gather structural data and collect representative samples. The grid area was chosen so as to include the Ross Lakes Shear Zone (and breached Paleozoic rocks) on its eastern edge and Jakey's Fork Fault on its southern boundary. The intended study area was extended west in order to include the prominently fractured area visible on the airphoto (Figure 7).

FRACTURE ANALYSIS

Fracture orientation data for this study are graphically depicted on equal-area rose diagrams or stereonets which were constructed using "STEREONET" version 3.6, an academic shareware computer plotting program for the Macintosh computer. The program was written by Richard W. Allmendinger of the Department of Geological Sciences at Cornell University. The significance of stereonet data is shown by Kamb contours. Kamb (1959) suggested this method for constructing data point density contours to show concentrations which depart significantly from a uniform distribution of data.

Airphoto

Subsequent to completion of fieldwork and to establish large-scale

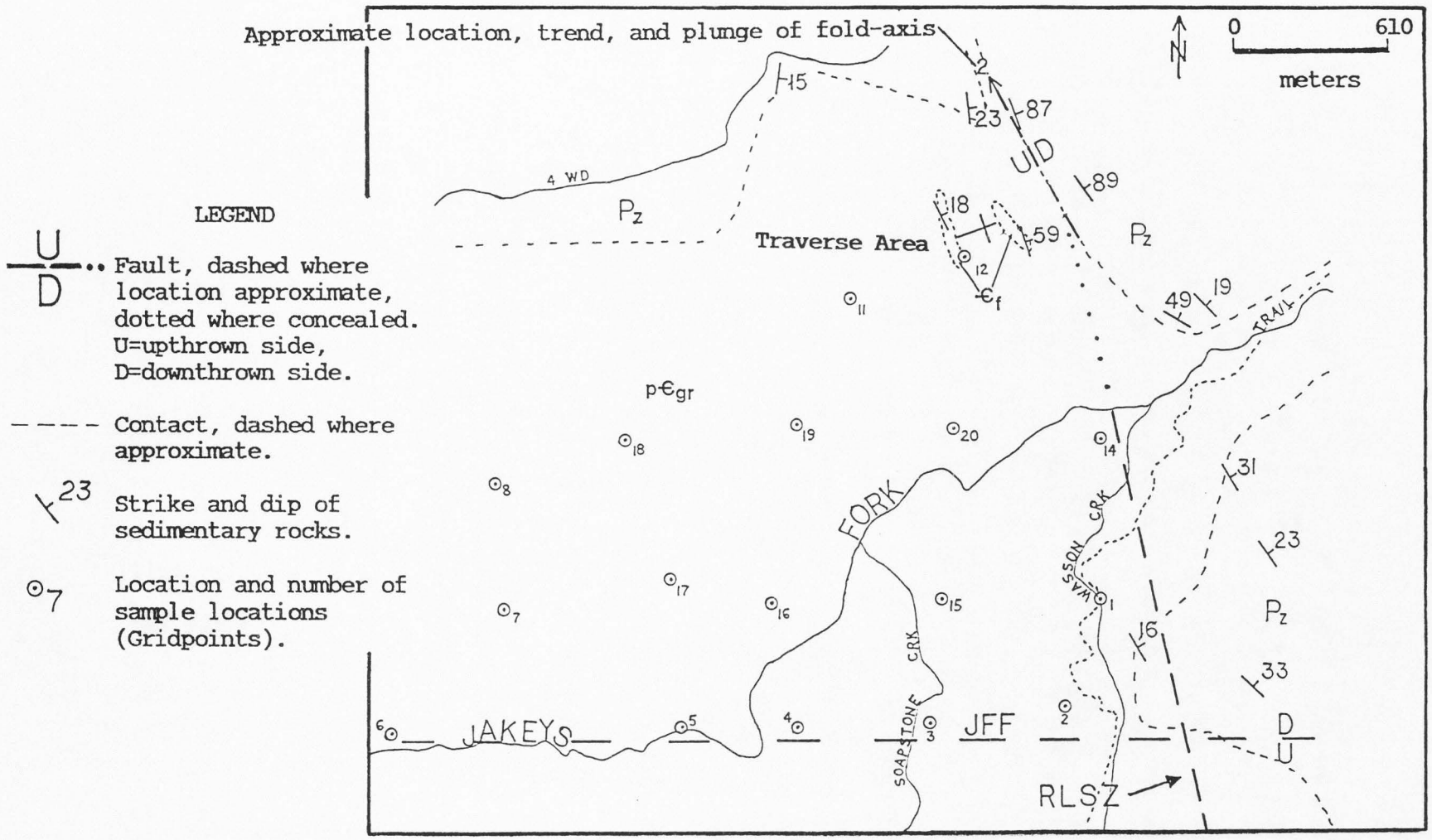

Figure 6. Map view of study area. Rock units are: p€gr, Precambrian granite; €f, Cambrian Flathead Sandstone; Pz, Paleozoic rocks (undifferentiated). 4WD = Four-wheel drive road. JFF = Jakey's Fork Fault. RLSZ = Ross Lakes Shear Zone.

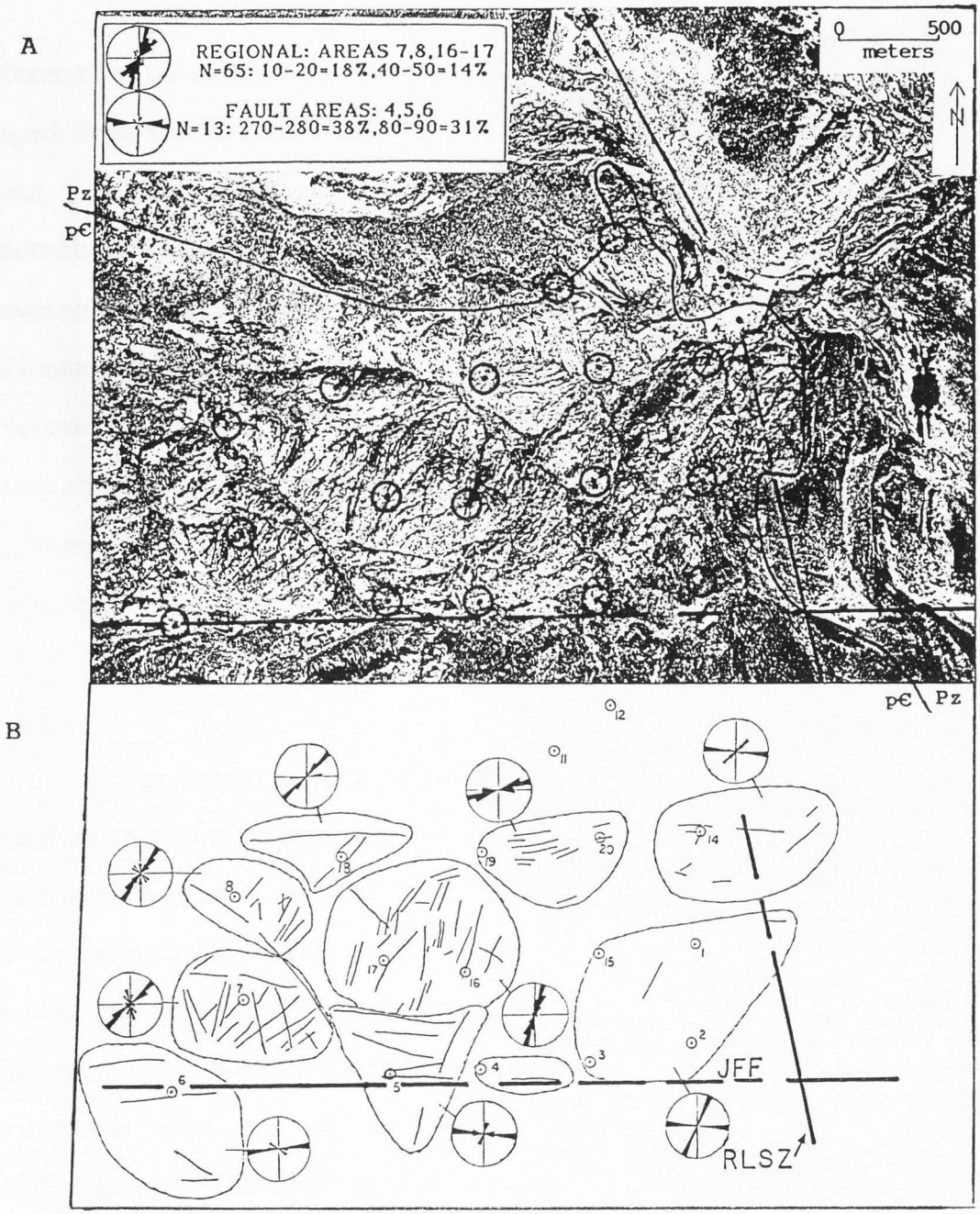

Figure 7. Orientations of airphoto fractures/lineaments and groupings in the study area. JFF = Jakey's Fork Fault, RLSZ = Ross Lakes Shear Zone, dashed where approximate and dotted where concealed. pC = Precambrian rocks, Pz = Paleozoic rocks (on opposite sides of contact). Numbered circles indicate gridpoints. Unnumbered circles in airphoto (A) correspond to numbered circles in fracture tracing from overlay (B).

deformation characteristics, distinct lineaments in the study area were mapped from the airphoto (scale ≈ 1:12,000) and grouped with respect to their gridpoint proximity (using Ray (1960) as a general reference). Fracture orientations and lengths were recorded. Analyses included grouping the data into ten degree intervals and plotting rose diagrams (orientation frequency) as well as fracture density histograms (cumulative fracture lengths per 10 degree interval per unit area). Fracture orientations and lengths were checked on the USGS 1:24,000 Simpson Lake, WY Orthophotoquad in order to estimate measurement errors. No field-checking of the lineament data was performed.

Outcrop

Outcrop mapping of fractures and veins was performed in order to investigate patterns possibly associated with those visible on airphotos. Mapping methods were adapted from LaPointe and Hudson (1985). In general, all individual fractures were not measured but were grouped with respect to recognizable sets from outcrops which could show them in three dimensions and set characteristics were recorded. The primary data recorded at each outcrop included: representative fracture orientations (strike and dip) of each set, the number and length of fractures in each set, and approximate outcrop dimensions (for surface area or volume and density calculations). From these data, comparisons were made with data obtained at other scales of observation and with data reported by other workers in the area (e.g., Mitra and Frost,1981). Additional types of fracture data (important for fluid-flow considerations as discussed by

Barton et al.,in press) considered for gathering included:

(1) age relations - Fracture intersections, abutments, and cross-cutting or off-setting relations could help determine characteristics of (or possibly define) various fracture sets which, if of different ages, should differ with respect to deformation characteristics, fluid flow, etc.

(2) roughness - A similar roughness (for an unweathered surface) would suggest a similar age, origin, and/or history. Roughness is important in controlling aperture variation and, therefore, flow characteristics. This parameter could be estimated qualitatively by the density and angularity of fracture-surface asperities (on unweathered surfaces).

(3) aperture - Fracture widths are important in controlling fluid flow. Representative measurements should be obtained on minimally weathered/mineralized surfaces.

(4) mineralization and/or alteration - This aspect was investigated because mineralization or alteration in fractures may reveal their relative ages and network paleohydrology.

(5) connectivity - Fluid-flow properties are affected by the degree of fracture connections, therefore it was desirable to determine the ratios of fractures (or sets) which terminate (blind fractures), abut, or cross others.

Grid Area. The above types of fracture data were gathered at outcrops located near the plotted gridpoints (Figure 6). Outcrops were chosen for their accessibility, quality, and proximity to plotted

gridpoints. Outcrop quality was a somewhat subjective criterion but was based on three-dimensionality, resistance to erosion, and rock type. Granitic (as opposed to gneissic) outcrops and samples were preferred because they should exhibit less (Precambrian) structural interference, especially at the microscale. Gridpoints 9, 10, and 13 were not sampled due to lack of proximal suitable outcrops and are not plotted on Figure 6.

Traverse Area. In addition to the Grid Area, fracture data were collected in the Traverse Area (shown in the upper right of Figure 6) where the tightly folded Cambrian Flathead Sandstone is breached by underlying, highly cataclastically deformed Precambrian granitic rocks. Photographs of the Traverse Area are shown in Figures 8 and 9. This structural arrangement provided the rare opportunity and bonus (in addition to examining the deformation of the granite in the context of Wind River Range development) of examining Precambrian rocks in the core of a fold in the Foreland Province. Equal-area stereonet analysis was used to define the fold axis from the attitudes of the surrounding Paleozoic rocks. Traverses with a Brunton compass and tape measure were conducted through the granitic rocks perpendicular and parallel to the fold axis to obtain data and samples at suitable outcrops. The area of the perpendicular traverse is shown in Figure 9. Some data and samples were also gathered from the Flathead Sandstone at opposite ends of the perpendicular traverse. Photographs of the Flathead Sandstone - Precambrian granite contacts are presented in Figure 10.

Figure 8. Photograph of Traverse Area viewing due south. Steeply east-dipping Cambrian Flathead Sandstone (C_f) is on east side (left) and shallowly east-dipping Flathead Sandstone is on west side (middle right) of Precambrian granite (gr) exposed in the core of the fold.

Figure 9. Photograph of Traverse Area viewing perpendicular to fold axis. View direction is $\approx 250^{\circ}$, parallel to traverse direction. Traverse Point E is in center of photograph (arrow).

A

B

Figure 10. Photographs of Precambrian granite - Cambrian Flathead Sandstone contact. A,B - views of upper contact. Shallowly east-dipping Flathead Sandstone is above hammer. C - view of lower contact, approximately at Traverse Point E. Bottom of approximately vertical stick rests on contact. Steeply east-dipping Flathead Sandstone is above contact.

Figure 10. (Continued).

C

Thin Section

Photonegatives were prepared from oriented horizontal thin sections, and fractures and veins were traced on acetate overlays. Optical microscopy was used to differentiate intergranular (i.e., brittle, Mitra,1984), intragranular (in quartz), open, closed, and healed fractures and also to determine the nature of fracture coatings or vein fillings. Orientations and lengths of individual fractures were recorded and analyzed similarly to those at airphoto and outcrop scales.

SAMPLING

Oriented hand-samples were collected at all Grid and Traverse outcrops for compositional and microstructural analyses. At outcrops with visible, highly deformed zones, both high- and low-deformation samples were collected. Qualitatively, dense fracture or shear zones (usually with gouge) were judged to be high-deformation zones. Relatively unfractured zones such as the areas between high-deformation zones were classified as low-deformation zones.

THIN SECTION PREPARATION AND ANALYSIS

Oriented horizontal and vertical 1"x3" thin sections were prepared from most collected hand-samples using standard methods. The majority of samples had to be impregnated with epoxy resin in order to withstand cutting and grinding. Horizontal slabs were cut in order to intersect the major fracture orientations (as close to perpendicular as possible) recorded at outcrop scale or the major discontinuities visible in hand-

sample. Vertical slabs were cut perpendicular to the horizontal slabs in order to examine the fractures in two dimensions. 2"x3" thin sections were also prepared to examine larger areas of the more deformed samples.

In addition to fracture analysis (described above), point counts were made on relatively undeformed samples to determine background mineral compositions and on some samples from highly deformed areas to detect any resultant differences. Individual mineral grains were also examined with respect to their relative sizes and appearances (shape, alteration, deformation characteristics). Fractures and veins were investigated with respect to offset, fillings, and interaction with wall rock including deformation/failure mechanisms. References used for these analyses included Simpson (1985,1986), Tullis and Yund (1977,1987), Knipe (1989), and Schmid (1983) who described deformation mechanisms in quartz and feldspar grains and their recognition at the microscale.

X-RAY ANALYSIS

X-ray diffraction (XRD) was employed primarily for mineral identification of opaque or very fine-grained minerals. Identifications were made based on standard tables for mineral d-spacings.

Procedures

Powdering. Approximately 20 g of pea-sized fragments of the handsamples were ground in the Spex Mill until virtually all of the powder passed through a 115 M. sieve. Spot sampling was performed on a few samples using a dental grinder or engraver to deposit powder from the

desired area onto a glass slide.

Random Mounts. The powdered sample was shaken through a 115 M. sieve to produce a uniform layer on a glass slide (≈ 2" x 2") which had been coated with a thin layer of petroleum jelly. Excess material was removed from the slide with gentle tapping.

Oriented Mounts. Slurries were prepared by mixing the various powders with distilled water and about 2 ml were deposited onto glass slides with an eyedropper. The samples were air-dried in a fume hood prior to analysis.

Montmorillonite, Kaolinite, and Chlorite Determinations. After initial x-ray diffraction spectra had been obtained, samples suspected of containing montmorillonite were glycolated. The slides were placed in a closed desiccator which contained ethylene glycol and heated in a 55-65°C. oven for ≥ 1 hour. The samples were allowed to return to ambient temperature in the desiccator and were reanalyzed to determine if a peak at ≈ 14 Å shifted to ≈ 17 Å.

In samples which exhibited 7 Å but no 14 Å peaks, the presence of kaolinite was determined by heating the sample in a furnace at ≈ 550-600°C. for ≈ 1 hour. After cooling, the samples were re-run to check for the disappearance of the 7 Å peak, indicative of kaolinite. In the presence of chlorite (with 14 and 7 Å peaks) the detection of kaolinite by a decrease in the 7 Å peak height after heating is ambiguous. For this study, ≈ 3 g (accurately weighed) of < 115 M. sample suspected of containing both minerals was boiled for 30 minutes in 50 ml 2N HCl to decompose the chlorite. These samples were dried, washed with distilled

water, redried and weighed to note possible weight differences due to loss of chlorite. Oriented mounts were then prepared as described above to determine if kaolinite was present. This procedure was adapted from Starkey et al. (1984).

Machine Parameters. Diffraction peaks were obtained using Ni-filtered Cu Kα radiation. The peak positions and relative intensities were recorded by a strip-chart recorder, set at 2 cm/min. Random mounts were scanned from 2^0 to 41^0 2θ and oriented mounts were scanned from 2^0 to 28^0 2θ at a speed of 2^0 2θ per minute.

SEM ANALYSIS

Preliminary SEM analysis was performed on 5-micron-polished chips to determine whether additional and/or complementary information could be obtained from this technique.

RESULTS OF INVESTIGATION

As mapped in Figures 4 and 6 the Jakey's Fork area was found to be primarily coarse-crystalline granite flanked by a linear outcrop belt of Paleozoic rocks striking north-northwest with a fairly uniform dip of ≈ 20-30° east, except where modified by faulting. The east-west trending, approximately vertical Jakey's Fork Fault (JFF) parallels the southern boundary of the study area (Figure 6). North-side down movement (of ≈ 202 m or 662' - from the base of Flathead Sandstone with approximately a 30° dip, Figure 4) is shown by the offset of moderately east-dipping Paleozoic rocks in the southeastern part of the study area and the fault continues west along the pronounced lineament visible in the airphoto (Figure 7). The approximately vertical Ross Lakes Fault or Shear Zone (RLF or RLSZ, Figures 4,6) trends north-northwest with down on the east displacement. The amount of displacement on RLF may be indeterminable from exposures in the study area since the bedded rocks have been deformed (tilted) by the faulting and are not adjacent on opposite sides of the fault (Figure 11). From the upper and lower Precambrian-Paleozoic contacts in the Traverse Area (Figure 6), throw and heave could be estimated to be 107 m (350') and 153 m (500') respectively, if it was assumed that the Flathead Sandstone outcrops were once continuous. Then the estimation could be made by projecting the shallowly and steeply dipping Flathead Sandstone to their point of intersection and calculating relative to a shallowly dipping continuous bed (Figure 11). Tilting or rotation of the Flathead Sandstone also occurred resulting in the steeper dip at the lower contact - in addition to the calculated displacement.

Field mapping improved on Granger et al.'s (1971; Figure 4) contact

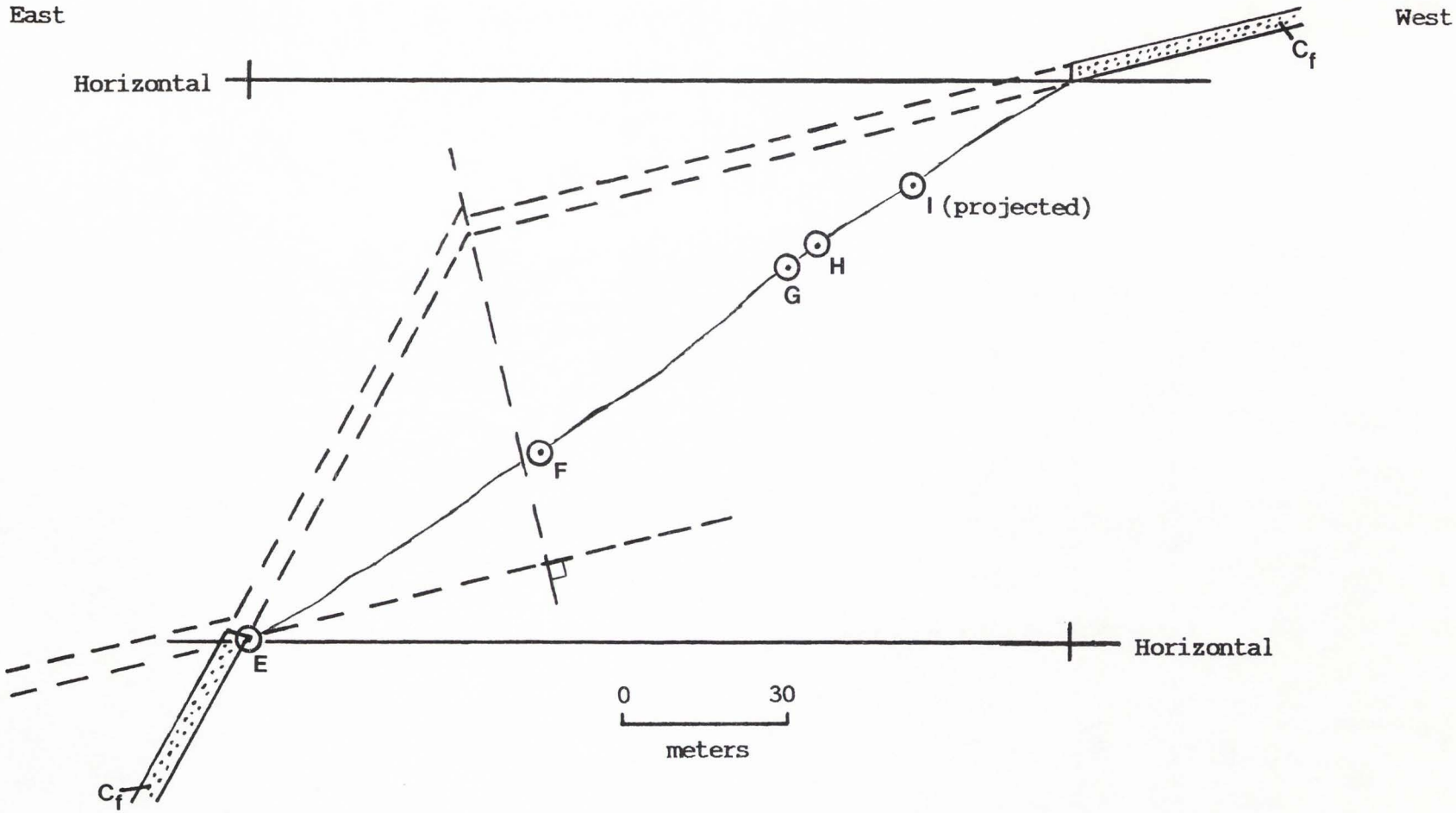

Figure 11. Cross-sectional diagram of Traverse Area showing displacement and tilting of Cambrian Flathead Sandstone (C_f). View is approximately parallel to fold axis, Traverse Points are indicated, and ground surface is sketched in. Thickness of Flathead Sandstone is not to scale.

and fault trace locations. The Ross Lakes Fault has one trace in the study area; south of Jakey's Fork (River) it cuts Precambrian and moderately east-dipping Paleozoic rocks and north of Jakey's Fork it separates steeply east-dipping to vertical Paleozoic rocks and Precambrian rocks that define a northwest-trending, sharply folded structure. The fold-axis trend of 331° and plunge of 2° were determined by equal-area stereonet analysis (Figure 12) of bedding attitudes in the surrounding rocks. The Traverse Area (where data and samples were collected parallel and perpendicular to the fold axis), located between outcrops of tightly folded and breached Flathead Sandstone, is also shown in Figure 6.

FRACTURE ANALYSIS

Data for individual and combined Traverse Points and Gridpoints are given in Appendices A-I and are referred to below for comparison purposes. Overall, fracture densities were greatest for the dominant orientations (shown by rose diagrams), but the results suggested that interpretive problems could result from data gathered near localized deformation zones or from an insufficient number of data points. These problems are demonstrated by an example from Gridpoint 3, where two slightly dissimilar areas (A and B) were found at the outcrop and subsequently were analyzed both separately and together (Figure 13). Figure 13 demonstrates that an insufficient number of data or too small a sampling area could yield results that might lead to interpretive problems (i.e., 0-10° would be classified the major interval if only area A was considered.).

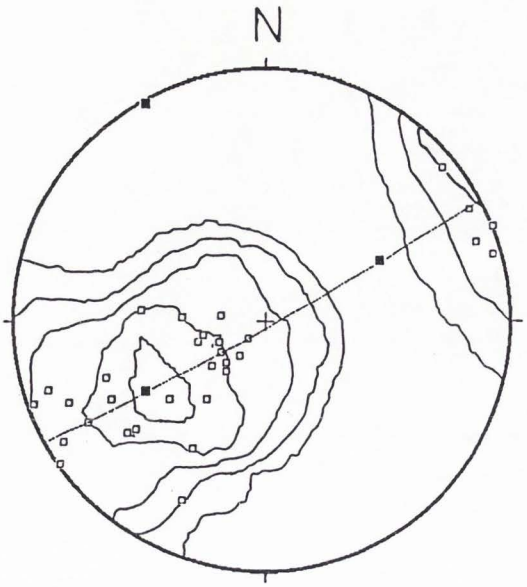

N = 35 C.I. = 2 sigma

Trend and plunge of fold axis: 331°/2°

Figure 12. Equal-area plot with Kamb contours of poles to bedding for measurements taken in traverse across Ross Lakes Fault.

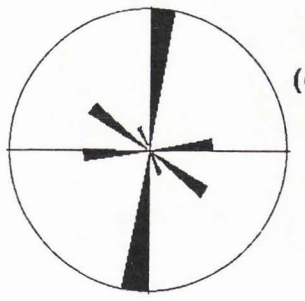

GRIDPT 3 (A)
(Outcrop Fractures)
N=59:0-10=46%

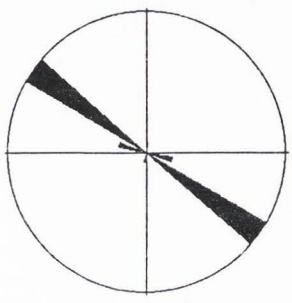

GRIDPT 3 (B)
(Outcrop Fractures)
N=95:120-130=79%

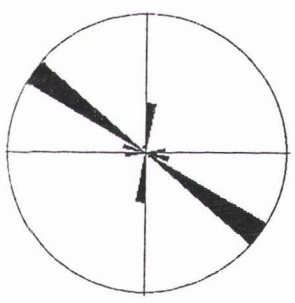

GRIDPT 3 (A+B)
(Outcrop Fractures)
N=154:120-130=58%

Figure 13. Rose diagrams of outcrop fracture orientations at Gridpoint 3. Fracture orientations are listed for the major ten-degree intervals. Diagrams show results for two slightly dissimilar areas - individually: 3(A), 3(B); and combined: 3(A+B). The diagram for 3(A+B) demonstrates that an insufficient number of data or unrepresentative data may indicate an erroneous or unrepresentative major fracture orientation - such as, if area 3(A) only was considered.

Airphoto

Figure 7 shows the airphoto locations of gridpoints as well as lineament trends for each area. The two dominant trends for the combined data are approximately east-west along Jakey's Fork Fault and a possible regional or background north-northeast trend (in the central area away from the major faults). Lineament densities were generally greatest for the dominant orientations and these data have been included in Appendix G. It should be noted that the lack of dominant lineaments in the Gridpoint 1-2-3-15 area (Figure 7) corresponds to the intersection of the two faults. This area will be discussed further below. Qualitatively, approximately east-west lineaments appear to be longer than lineaments of orientations oblique to them and these oblique lineaments appear to terminate against (or abut) the east-west lineaments (supported quantitatively by airphoto fracture density graphs, Appendix G, and discussed further below). From comparisons with the orthophotoquad, fracture measurements made from the airphoto were determined to be within 4° of actual orientation and fracture/lineament lengths were ≈ 20-30% lower.

Outcrop

Most fractures measured at outcrops in the study area were steeply dipping (Figure 14 A,B,C) and equal-area rose diagrams were used for subsequent orientation comparisons with airphoto and thin section data (for which dip data were limited). Figure 14D shows the orientations of

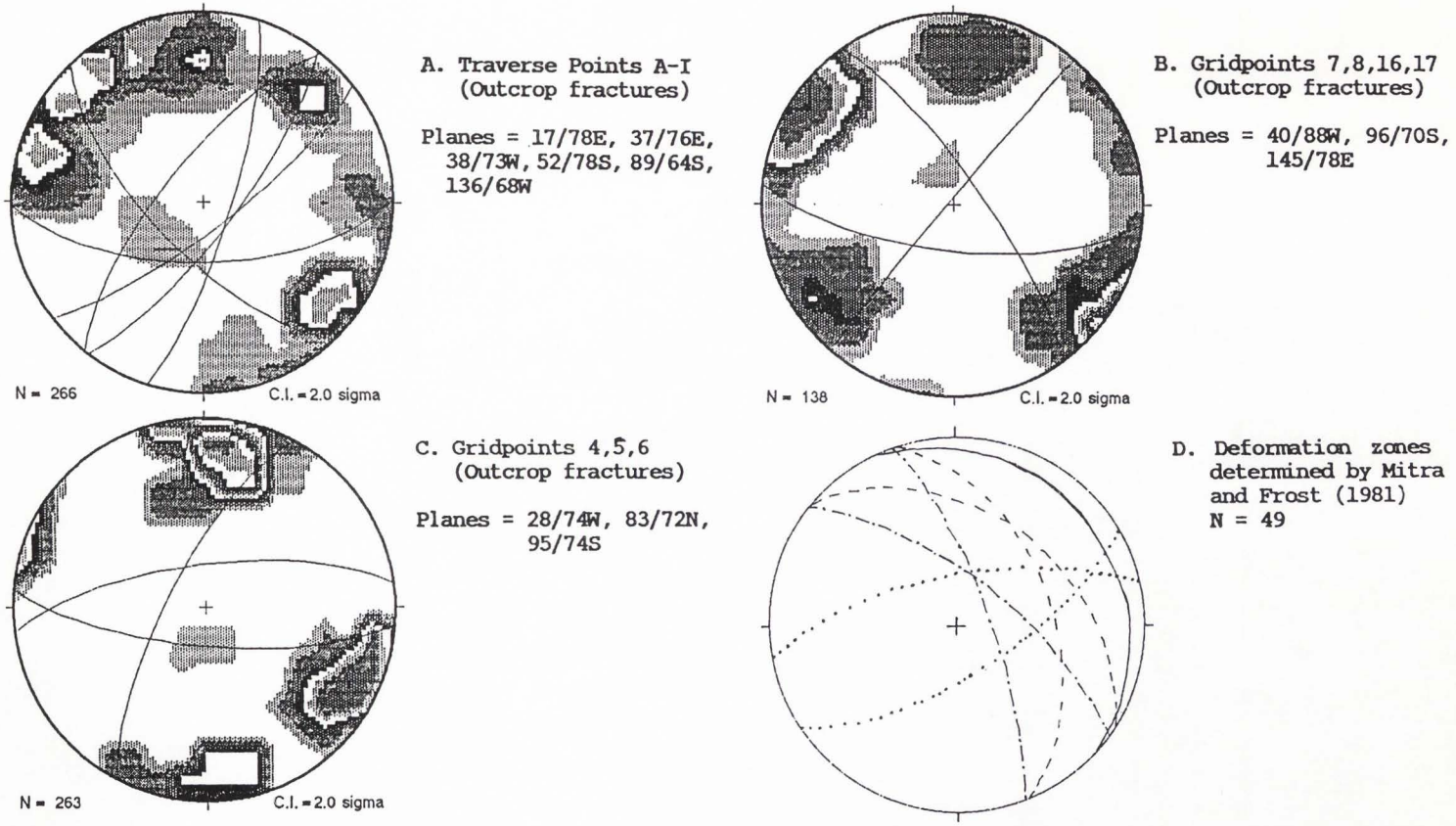

Figure 14. Equal-area stereonets of major fracture orientations (planes) or deformation zone orientations in the northeastern Wind River Range. A, B, C are Kamb-contoured plots of poles to outcrop fracture orientations in the Jakey's Fork area. Dominant fracture orientations are shown by great circles which correspond to major pole concentrations and great circle (plane) orientations are listed. D is a plot of the orientations of 7 major sets of Laramide deformation zones (great circles) determined by Mitra and Frost (1981) in the Torrey Creek area.

7 sets (N=49) of Laramide deformation zones reported by Mitra and Frost (1981). Compared to Figures 14 A-C, Figure 14D (with much fewer data) shows a greater tendency for northwest-southeast orientations and shallower dips. Fracture characteristics such as age relations, roughness, aperture, mineralization, and connectivity were deprioritized due to the overall nature of the outcrops which were studied; the fractures observed at the outcrops generally showed weathered surfaces and separations across these surfaces appeared to be due to minor block rotations or adjustments (which would affect roughness and aperture to a much greater extent than orientation and length). Also, the fractures investigated were generally cross-cutting (with little/no visible offsets) and of outcrop size. Typical outcrop maximum dimensions ranged from a few meters to a few tens of meters. Age relations were difficult to establish and connectivity (if desired) could be estimated from measured orientations and lengths (LaPointe,1988). These simplifications were also made in order to maximize the number of data and samples obtainable and to facilitate their collection. Slickensides were observed on a small percentage of the fracture surfaces measured, primarily in the Traverse Area, and indicated predominantly dip-slip movement with a minor oblique component (of inconsistent orientation).

Grid Area. Outcrop fracture orientations are shown in Figure 15. Visually, there is good agreement in general between Figures 15 (outcrop) and 7 (airphoto) for data obtained along Jakey's Fork Fault (Gridpoints 4,5,6 and ≈ E-W orientations) and in the central area of the Grid (Gridpoints 7,8,16,17 and ≈ NE-SW orientations) although differences can

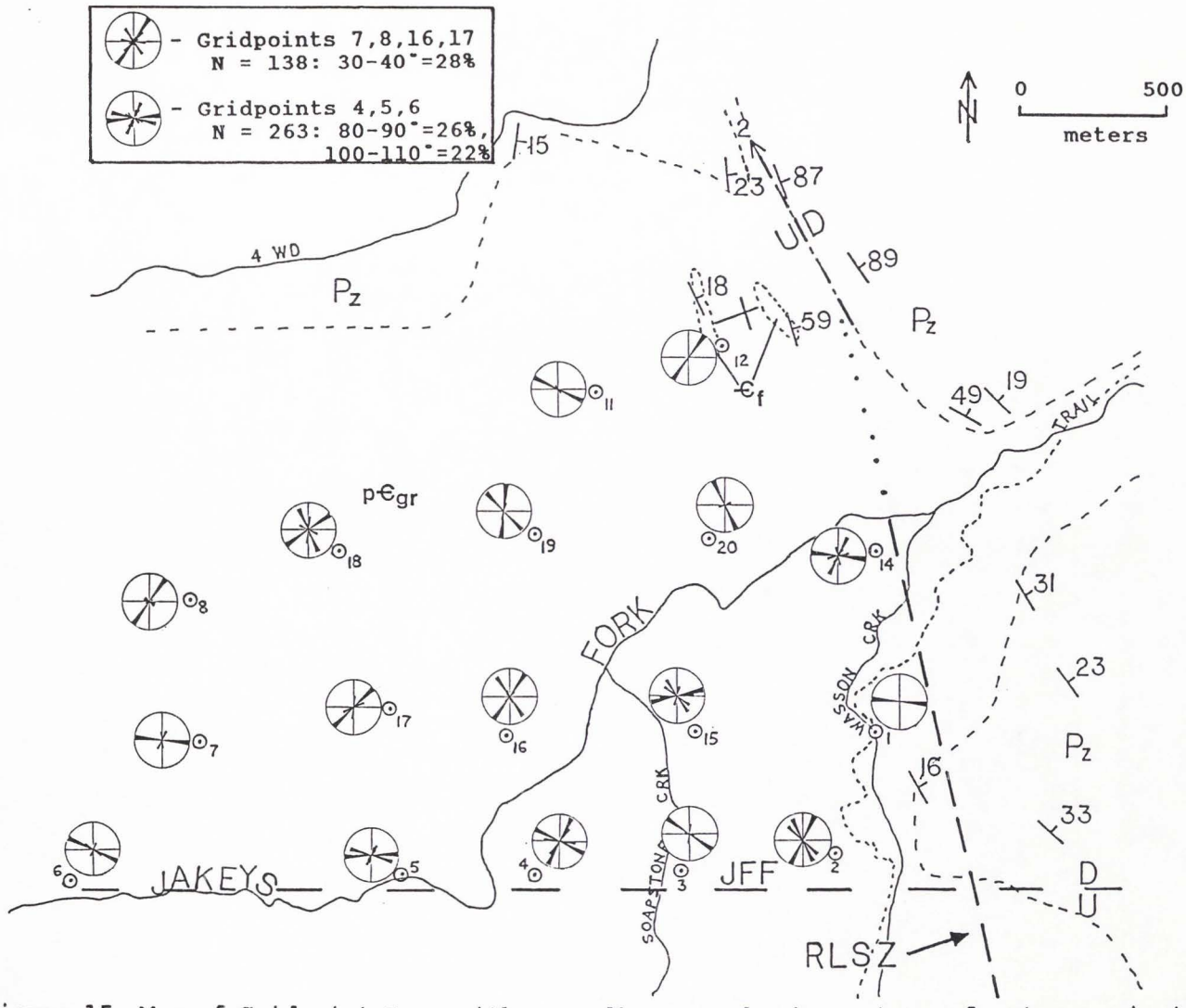

Figure 15. Map of Gridpoint Area with rose diagrams showing outcrop fracture orientations. Legend and explanations are same as in Figure 6.

be seen at individual gridpoints.

Traverse Area. Fracture orientations for Traverse outcrops are shown in Figure 16. The combined data show a dominant northeast-southwest orientation similar to the airphoto and grid data for the central grid area but only a minor east-west component is indicated. Limited fracture data obtained in the overlying Flathead Sandstone show a dominant trend approximately parallel to the fold axis which is quite different from that in the granite. No outcrop fracture measurements were made at Point E due to its extremely shattered and 'gougey' nature (visible in Figure 10C).

Thin Section

Fracture orientation data at thin-section scale were obtained for every (possible) Gridpoint (1-20) and for the Traverse Points perpendicular to the fold axis (E-I). Data from both high- and low-deformation areas were obtained when possible. Copies of the photonegatives and fracture tracings as well as all data for individual and combined sampling points are included in the Appendices. Initially it was thought that open fracture data would or could be related to the most recent deformation event. This is possible and these data are included in the Appendices, but Kowallis et al. (1987) suggested that the open fractures could also be related to relatively recent events such as stress relief during unroofing. It is also possible that open fractures could result from sample collection and/or thin section preparation procedures (Richter and Simmons,1977) but open fracture orientations (40-50°) are nearly identical to closed fracture (50-60°) and outcrop fracture (40-50°) combined data orientations for the Traverse Area (Appendix F).

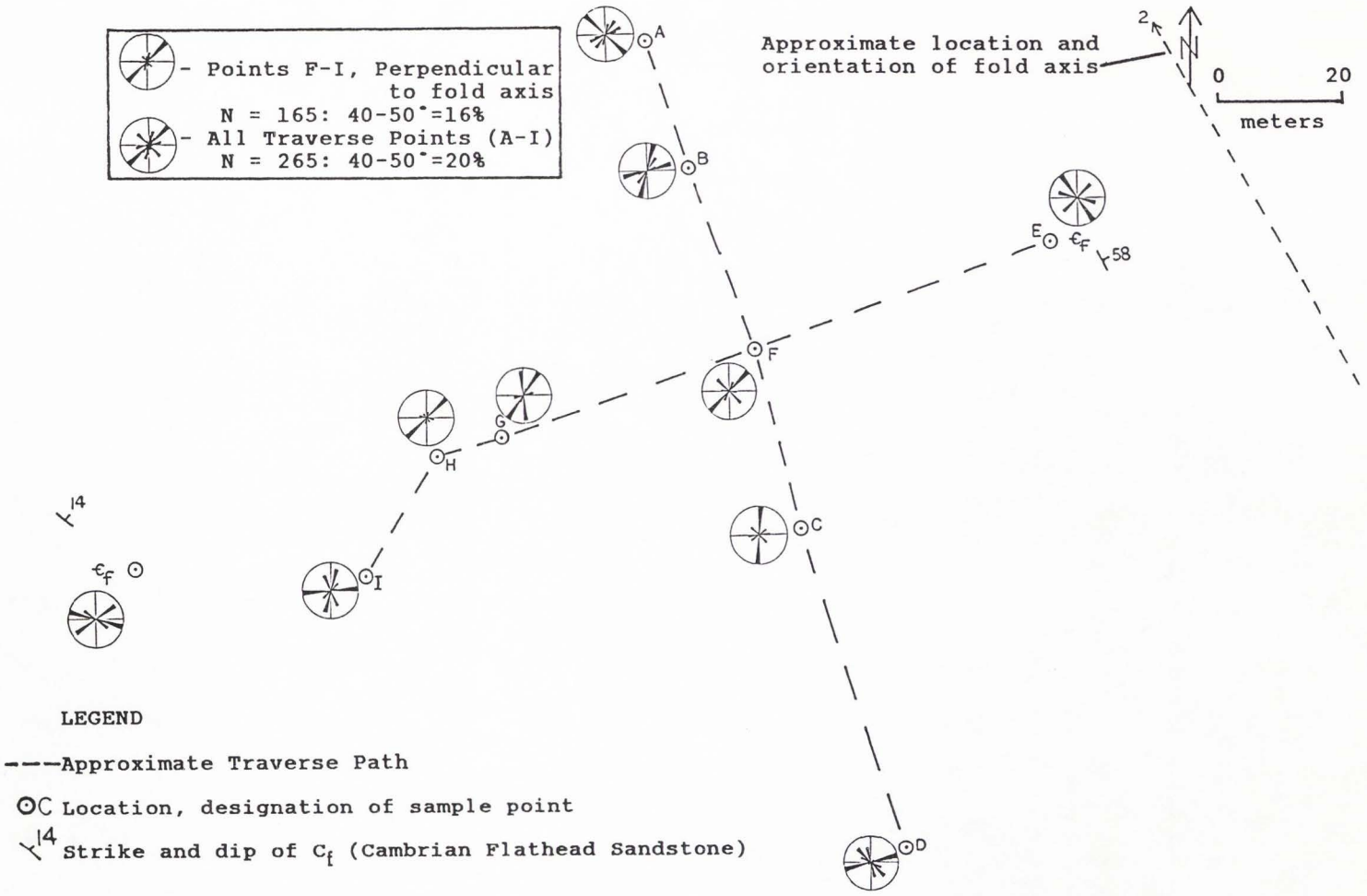

Figure 16. Map of Traverse Area with rose diagrams showing outcrop fracture orientations.

Overall (including Grid Area data), no consistent relation(s) was (were) observed between open fractures, closed fractures, and outcrop or airphoto fracture data. Quartz (fracture) data generally indicated the same major orientations as (intergranular) fracture data.

Traverse Area. Intergranular (brittle) fracture and intra- and intergranular quartz fracture orientation data from the Traverse Area show a dominant northeast-southwest trend and are quite similar to those obtained at outcrop scale. Figure 17 shows one of the thin section photonegatives along with its fracture tracing. A summary diagram (Figure 18) and Table 1 show the similarities of dominant trends for intergranular, quartz, and outcrop fractures. Thin sections from areas qualitatively judged to be high-deformation zones (at outcrop scale) yielded results in better agreement with outcrop determinations than did samples from relatively low-deformation areas. Similar to fractures observed at outcrop scale (Figure 14A), fractures at thin-section scale (in granite) were primarily vertical to steeply dipping. These observations were made from matched fractures in perpendicular thin sections or from the hand-samples. Also similar to outcrop scale results (Figure 16), fractures (or fracture patterns) in the overlying Flathead Sandstone appeared to be quite different. Figure 19 shows a vertical thin section of steeply dipping Flathead Sandstone from near Traverse Point E where fractures and zones of granulation are subhorizontal - in contrast to those in adjacent Precambrian rocks. Figure 20 shows differences in the type and amount of deformation across the shallowly east-dipping contact where relatively undeformed Flathead Sandstone grains are juxtaposed with a fractured microcline grain from the granite.

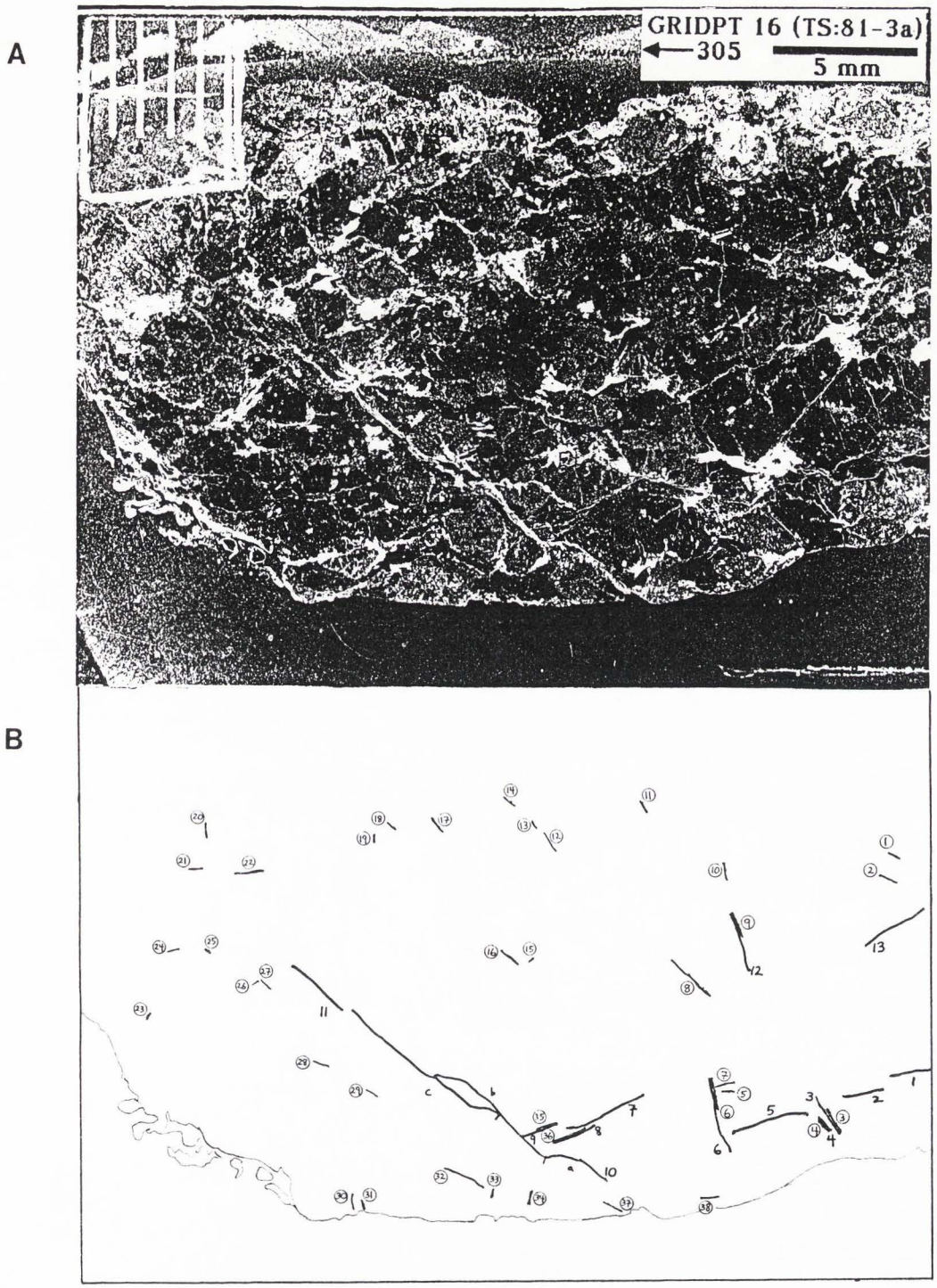

Figure 17. Photonegative of thin section with mapped intergranular fractures and quartz fractures. A. Photonegative, B. Fracture tracings from overlay. Circled numbers represent quartz fractures.

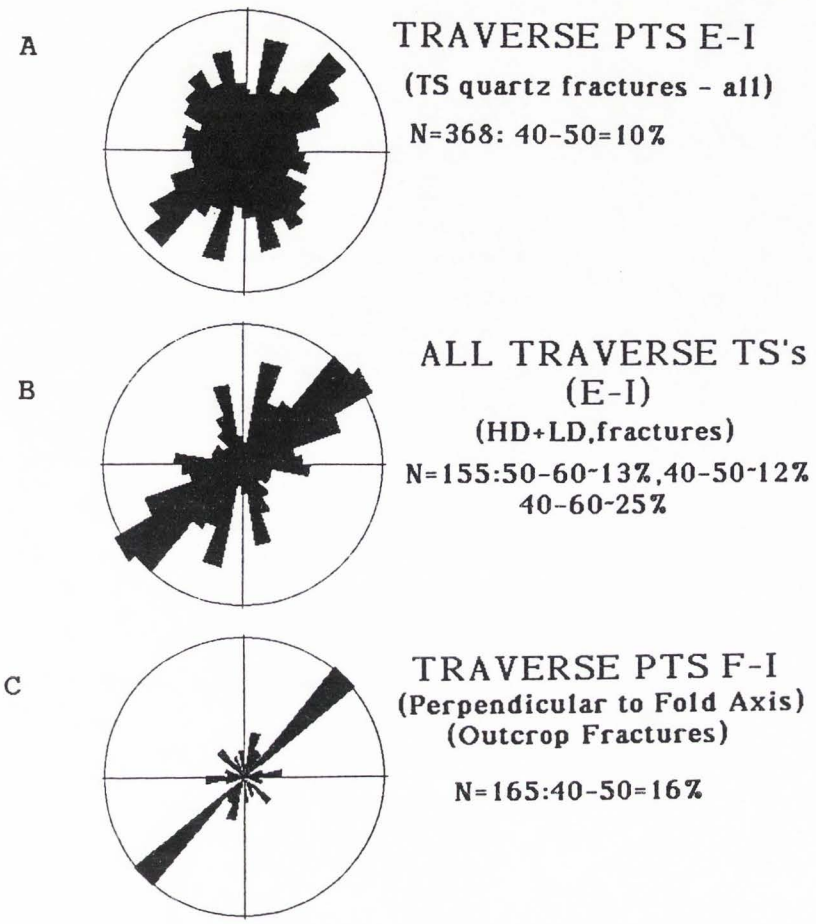

Figure 18. Traverse Area - combined fracture orientation data: outcrop, intergranular, and quartz (primarily intragranular). A. Quartz fractures. B. Intergranular fractures. C. Outcrop fractures. TS = thin section, HD = high deformation sample, LD = low deformation sample.

TABLE 1. TRAVERSE FRACTURES: DENSITY AND ORIENTATION

Traverse Point	Quartz		Intergranular		Outcrop	
	≈ D	AZ	≈ D	AZ	≈ D	AZ
E (density)	1.2	80-90	9.7	60-70	-	-
(rose)	16%	80-90	23%	50-60, 90-100		
F (density)	0.6	50-60	7.1	40-50	170	40-50
(rose)	18%	50-60	22%	40-50	45%	40-50
G (density)	1.7	160-170	4.6	160-170	280	30-40
					252	160-170
(rose)	18%	160-170	16%	20-30, 160-170	39%	30-40
					36%	170-180
H (density)	1.2	40-50	4.6	50-60	149	40-50
(rose)	20%	30-50	34%	50-60	60%	40-50
I (density)	2.0	10-20	7.5	10-20	251	10-20
(rose)	20%	10-20	22%	10-20	33%	80-90
					26%	10-20
E-I (density)	0.7	40-50	3.7	40-50	137	40-50
(rose)	10%	40-50	13%	50-60	16%	40-50

D = density (from density graphs, Appendix F) and density units are mm/sq mm x 100 for thin section measurements and m/sq m for outcrop measurements. D for rose diagrams indicates the % of total measurements in the listed (major) ten-degree interval (also from Appendix F). AZ = azimuthal orientation of dominant ten-degree interval of fractures.

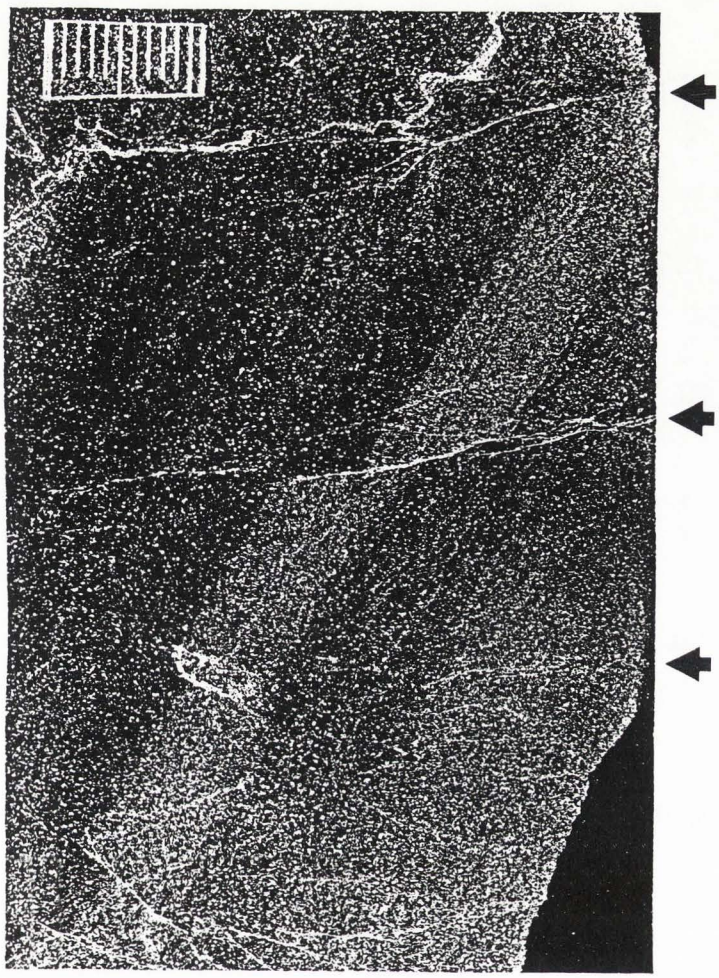

Figure 19. Flathead Sandstone - vertical thin section photonegative showing subhorizontal fractures and zones of granulation (arrows) in steeply east-dipping beds. Fractures and granulation zones can be seen to be subhorizontal in hand-sample 623-3a from which thin section was made. Sample was collected just east of Traverse Area (Figure 15) near Point E. Offsets of beds are probably due to brittle extension caused by approximately vertical movement along Ross Lakes Fault. Small tic marks in scale are 1 mm apart.

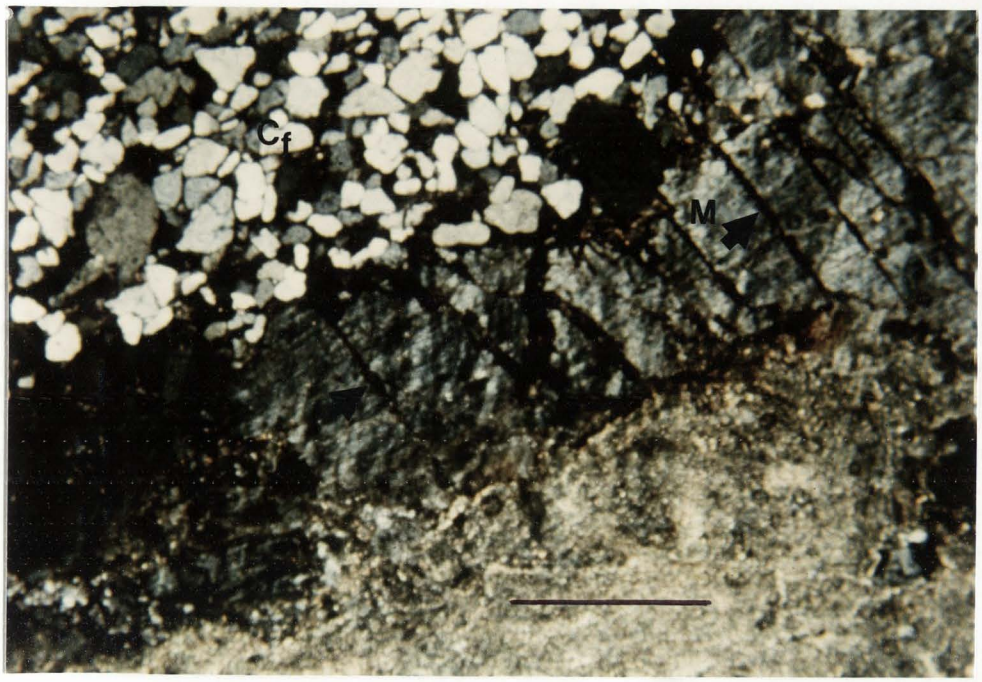

Figure 20. Thin section microphotograph of Flathead Sandstone quartz grains in contact with microcline grain from granite. Sample was collected near upper (shallowly east-dipping) granite - Flathead Sandstone contact. Deformation in the Flathead Sandstone (C_f) shows little relation to that in the granite (represented by dense fractures, arrows, in the microcline grain, M). Cross-polarized light. Scale bar is 1 mm long.

Deformation visible at the microscale is also detailed in Appendix D. Generally, brittle deformation characterized by grain-scale fracture, granulation, and cataclasis was evident but with no observable textural development, such as foliation.

Grid Area. The good agreement between outcrop and thin section fracture data in the Traverse Area was not as evident from grid samples except for those from Gridpoints 4,5,6 along Jakey's Fork Fault. These data also agreed quite well with the airphoto data (Figure 21). The lack of general agreement between thin section intergranular fractures and outcrop and airphoto fracture data led to the investigation of quartz fractures and fracture densities. Lespinasse and Pêcher (1986) and Ren et al. (1989) successfully used quartz fractures in paleostress determinations and reported that although orientations of quartz fractures were similar to those of intergranular fractures, quartz fractures were preferable in the determinations. The reported advantages (Lespinasse and Pêcher,1986; Ren et al.,1989) of using quartz fractures were: (1) they were less sensitive to grain-scale heterogeneities; (2) quartz has poor cleavage so cracks may form in any direction without crystallographic bias; and (3) since quartz grains are generally more transparent and less altered than feldspars, the fractures are more easily identified. For this study in general, quartz fractures were intragranular, more abundant (but shorter and less dense) than intergranular fractures, and gave better-defined data groupings than intergranular fractures, but quartz fractures indicated the same dominant orientations (i.e., they are in poor agreement with major outcrop and airphoto orientations). Figure 21 and

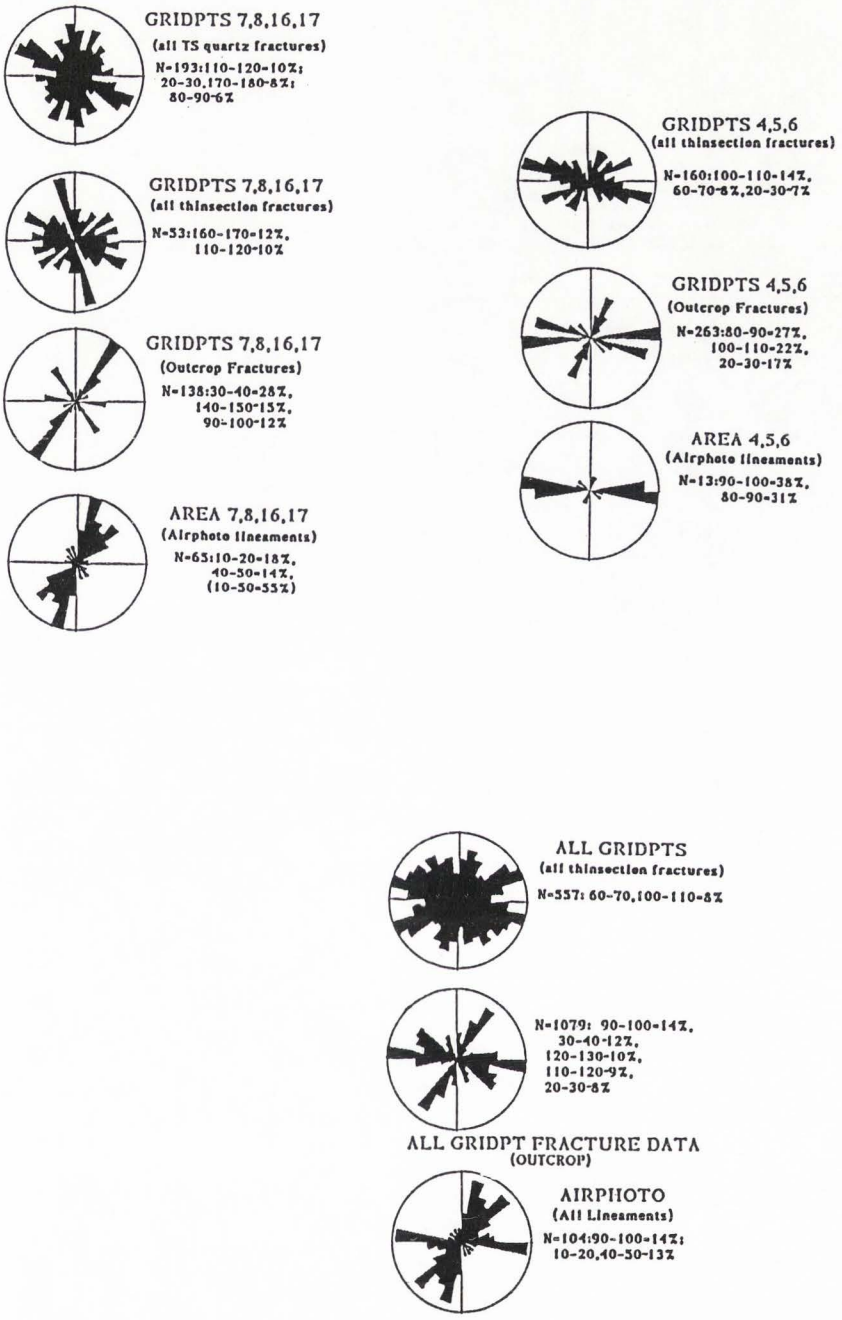

Figure 21. Grid Area - combined fracture orientation data: airphoto, outcrop, intergranular, quartz (primarily intragranular). TS = thin section. Thin section fractures = intergranular fractures.

Table 2 summarize these data and comparisons. Also, fracture orientations from high-deformation samples (from thin section data) were not as well related to outcrop results as were the data from Traverse samples.

Deformation on the microscale (Appendix E) appears to have been much less intense (in the brittle sense) for most Grid Area samples compared to Traverse Area samples, and is characterized by more plastic deformation in quartz and feldspar with a brittle overprint. Intense (brittle) deformation is shown however, by samples collected along Jakey's Fork Fault (Gridpoints 4,5,6). A general progression in the amount of deformation (grain-size reduction) from protolith to mylonite is shown by 4 samples from Gridpoints 4 and 5 (Figure 22). Open fractures are rare in these samples - in contrast to those from the Traverse Area.

COMPOSITIONAL ANALYSIS

Thin Section and X-ray Analyses

Traverse Area. Point-count data were collected for 4 thin sections representative of high- and low-deformation samples and are presented in Appendix D. The 'protolith' (low-deformation sample) is granite (IUGS classification) while the samples from dense fracture and gouge zones (using additional information from XRD) contain much altered (sericitized?) and unidentifiable feldspar, noticeable kaolinite, chlorite (up to ≈ 12%), and fracture porosity (up to ≈ 26%).

Grid Area. Point-count data (Appendix E) were collected for 2 thin

TABLE 2. GRID FRACTURES: DENSITY AND ORIENTATION

Gridpt	Quartz		Intergranular		Outcrop		Airphoto	
	≈D	AZ	≈D	AZ	≈D	AZ	≈D	AZ
7 (density)	0.8	50-60	1.0	30-40	177	20-30	286	50-60
					172	90-100		
(rose)	32%	40-60	40%	30-40	61%	90-100	28%	40-50
8 (density)	3.3	110-120	4.1	170-180	161	30-40	213	30-40
(rose)	20%	110-120	28%	110-130	56%	30-40	28%	30-40
16(density)	0.7	170-180	1.4	50-60	222	140-150	-	-
					218	30-40		
(rose)	12%	0-10	12%	90-100	40%	30-40	-	-
17(density)	1.1	40-50	4.7	50-60	130	40-50	-	-
(rose)	12%	70-80, 150-160	25%	50-60, 70-80,160-170	55%	40-50	-	-
16-17(density)	0.7	170-180	2.4	50-60	107	140-150	294	10-20
					105	30-40		
(rose)	40%	330-10	14%	160-170	30%	30-40	32%	10-20
7-8-16-17								
(density)	0.8	110-120	1.4	50-60	103	30-40	187	10-20
(rose)	10%	110-120	12%	160-170	28%	30-40	18%	10-20
4-5-6(density)	-	-	2.0	110-120	612	100-110	259	90-100
(rose)	-	-	14%	110-120	27%	80-90	38%	90-100

D = density (from density graphs, Appendix G) and density units are mm/sq mm x 100 for thin section measurements, m/sq m for outcrop measurements, and km/sq km x 100 for airphoto measurements. D for rose diagrams indicates the % of total measurements in the listed (major) ten-degree interval (also from Appendix G). AZ = azimuthal orientation of dominant ten-degree interval of fractures.

A

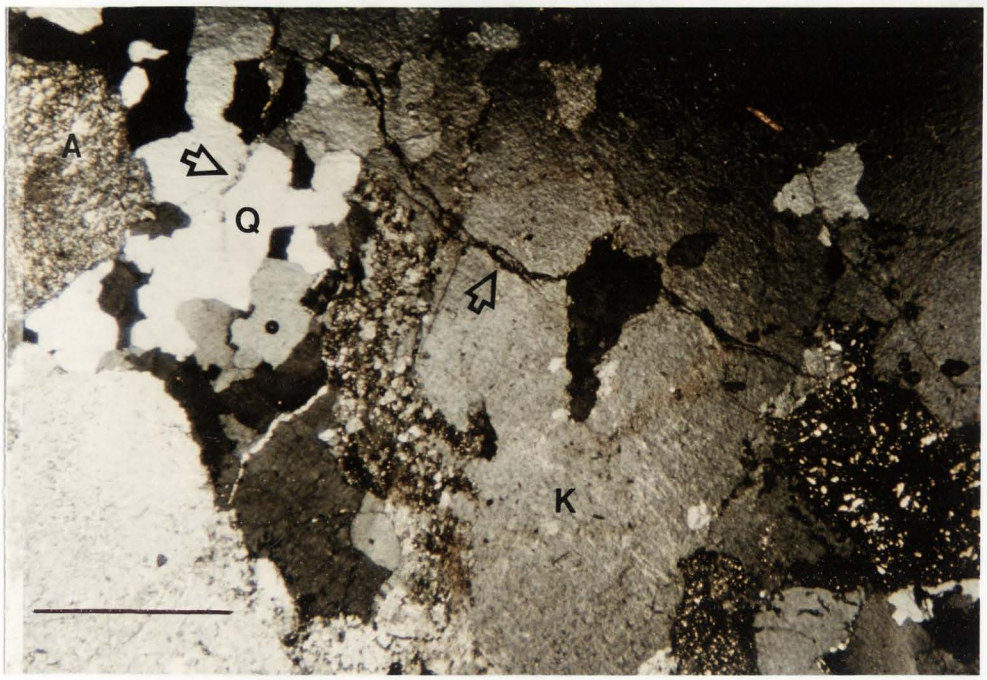

Figure 22. Thin section microphotographs showing progressive deformation of rocks along Jakey's Fork Fault. For all photographs: cross-polarized light, scale bar = 1 mm.
A. Sample 727-3c1 from Gridpoint 5. This sample represents relatively undeformed protolith. Large K-feldspar grains (K), moderate fracturing (arrows), alteration of plagioclase grains (A), and grain-sized aggregates of quartz grains (Q) are visible.
B1,B2. Sample 81-2a from Gridpoint 4. This sample shows increased deformation from sample 727-3c1 (Figure 22A) evidenced by reduced feldspar (F) grain size and deformed quartz-grain aggregates (Q).
C1,C2. Sample 713-1 from Gridpoint 4. Grain-size reduction is more advanced than in B resulting in a mylonitic texture.
D. Sample 81-2b from Gridpoint 4. This sample shows extreme grain-size reduction resulting in an ultramylonite.

Figure 22. (Continued).

B1

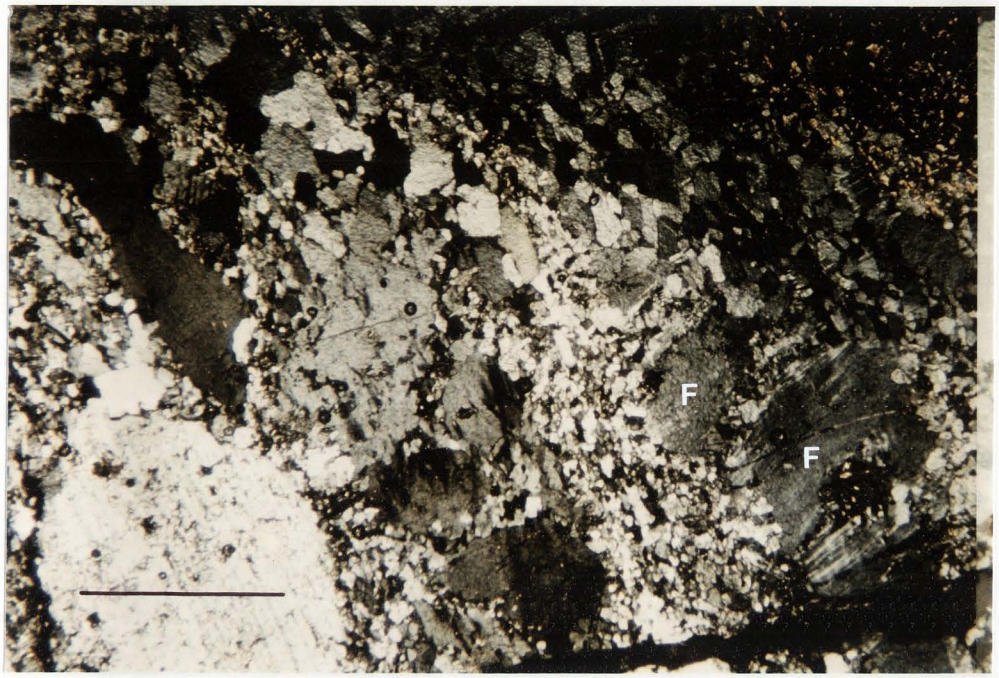

B2

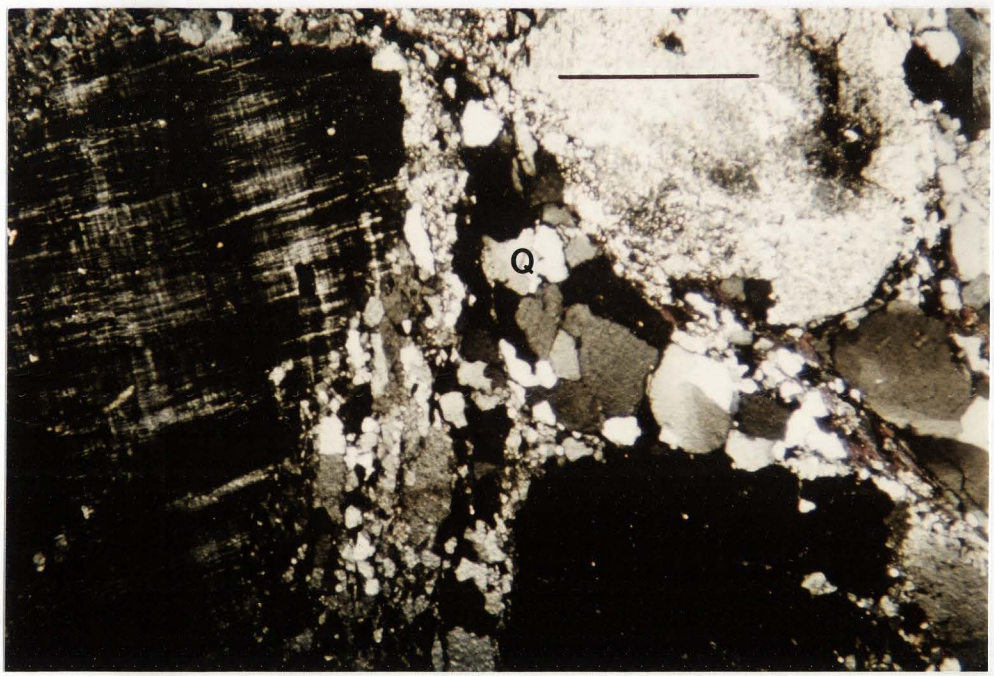

Figure 22. (Continued).

C1

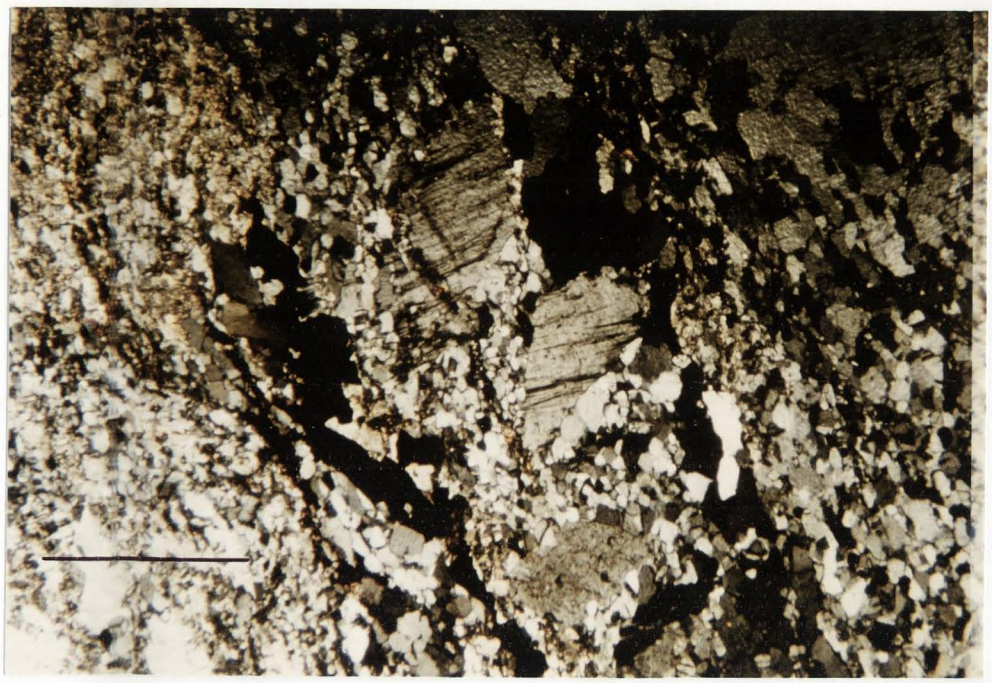

C2

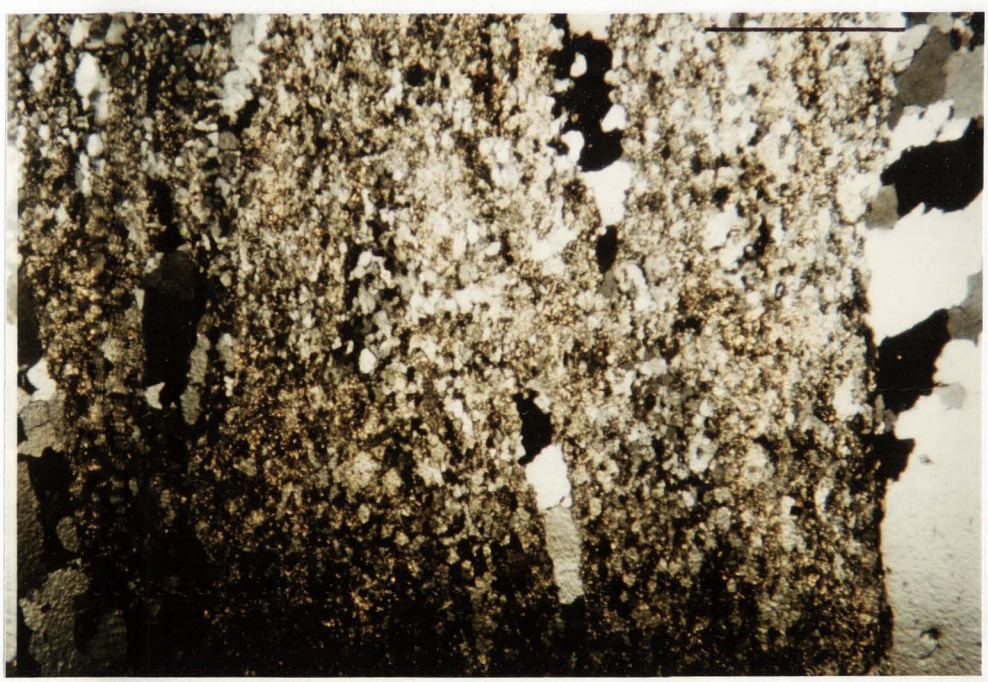

Figure 22. (Continued).

D

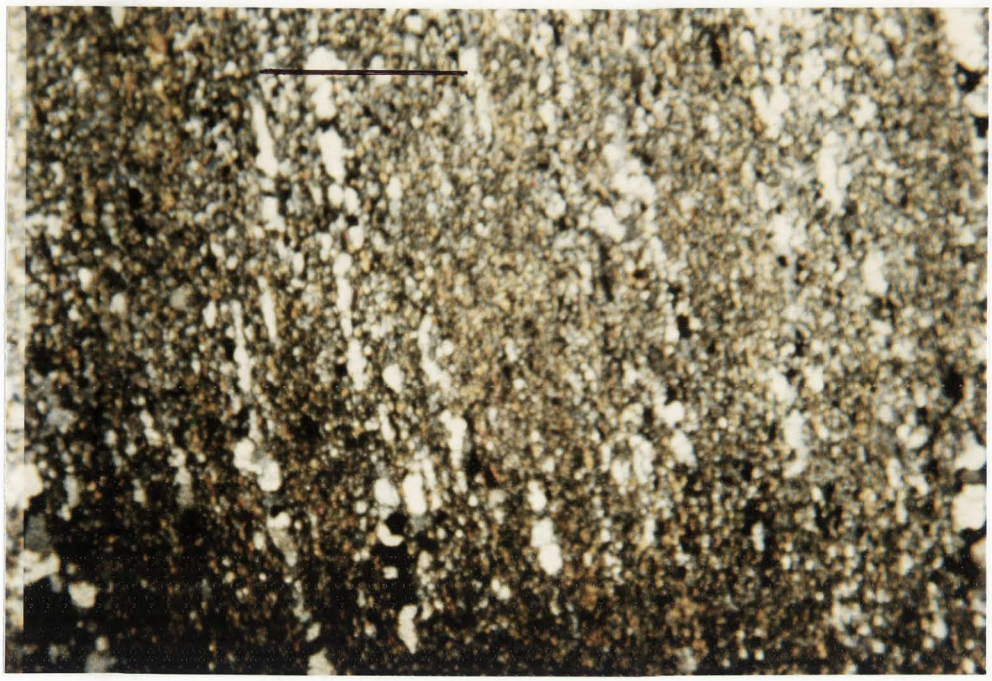

sections prepared from relatively undeformed and unaltered samples to determine background (protolith) mineral compositions. These data indicate the protolith is granite (IUGS classification).

X-ray analyses (Appendix E) were performed on 15 grid samples. The dominant phyllosilicate, especially in the mylonitic samples from along JFF, was chlorite (up to ≈ 13%). Kaolinite was definitely identified in only one sample - from Gridpoint 12, near RLF and the Traverse Area.

SEM Analysis

SEM analysis suggested that the major opaque mineral in the breccia zones near Ross Lakes Fault is hematite (which was later confirmed by x-ray diffraction).

DISCUSSION AND INTERPRETATION

SAMPLING AND NUMBER OF DATA

Fracture orientation observations, results of analyses, and thus interpretations of the results may have been biased or influenced due to sampling criteria, especially accessibility and exposure quality of outcrops, and it is recognized that more data would be required to ensure an accurate and representative interpretation. The grid with sampling points was set up in an attempt to systematically obtain representative samples and data from as much of the study area as possible. Problems are suggested by the agreement of thin section and outcrop data for the Traverse Area and lack of agreement among thin section, outcrop, and airphoto data for most of the Grid Area. Within the Grid Area, airphoto and outcrop data are similar, but they do not agree with thin section data. Along Jakey's Fork Fault, thin section, outcrop, and airphoto data agree. The possible problems relate to the initial assumption that deformation visible on the macroscale resulted from deformation on the microscale and should be visible on the microscale (as discussed and reported by, among others, Segall and Pollard, 1983a,b; Dula,1981; Lespinasse and Pêcher,1986). The lack of scale agreement suggests the unequal influence of deformation on the various scales (i.e., brittle fracture and related deformation is a scale-dependent process) and/or that insufficient data were collected.

Although there may have been some problems with the data, interpretations have been based on the available information because: (1) it was assumed that data possibly lost or unobtainable due to intense

deformation, lack of exposure, or an insufficient number of samples was represented to some degree by the data collected or generated for this research; and (2) other forms of bias (discussed by LaPointe and Hudson, 1985) were reduced or eliminated by the methods employed, since sampling and data generation methods were consistent and both outcrop and thin section data accounted for three dimensions.

SCALES OF OBSERVATION AND TREATMENT OF DATA

Initially, thin section fracture observations were grouped for both high- and low-deformation samples as open intergranular or closed intergranular (Appendices F,G). Since no consistent differences were recognized, intergranular fracture data were combined for individual sampling points and used for comparisons with airphoto and/or outcrop data. Combinations of sampling point data were generally made for thin section and outcrop comparisons with airphoto data such as for Areas 16-17 or Areas 19-20 (Figure 7) where no definite area of lineaments could be assigned to a single Gridpoint. Data combinations were also used for making scale comparisons (with more data) for areas with similar lineament patterns (Areas 7,8,16-17 and 4,5,6 from Figures 7,15,21).

Thin section quartz fractures were primarily intragranular although some fractures crossed grain and subgrain boundaries. Since quartz fractures generally indicated the same major orientations as intergranular fractures (from rose diagrams or density graphs - Appendices F,G), quartz fractures were not analyzed for all thin sections. Quartz fractures were

initially analyzed because of reported successes in stress orientation determinations (Lespinasse and Pêcher,1986; Ren et al.,1989; Dula,1981), but since quartz fracture data were very similar to intergranular fracture data, these analyses were not pursued.

DEFORMATIONAL FEATURES AND MECHANISMS

Four main areas characterized by deformational features and mechanisms have emerged in the Jakey's Fork study area from observations at the microscale to macroscale and will be discussed below. At the thin-section scale, differences in the type and amount of quartz deformation helped to define these areas. In thin sections from hand-samples that exhibit relatively little deformation, grain-sized aggregates of recrystallized quartz grains are commonly about the same size as feldspar grains (Figure 22A). Individual quartz grains about the same size as coexisting feldspar grains are rare (Appendices D,E) and since Laramide deformation conditions were more conducive to brittle mechanisms (fracturing and granulation), the grain-sized aggregates of quartz grains were considered to represent the 'background' or pre-Laramide appearance for this mineral. Subsequent (i.e., Laramide) deformation was then inferred from how the quartz-grain aggregates were deformed. Deformation characteristics could also be inferred from the types and/or amounts of alteration and deformation shown by microcline and plagioclase grains. Microcline deformation was characterized primarily by fracturing and grain-size reduction with minor recrystallization. Plagioclase grains

exhibited fracturing and much alteration (sericitization? and/or kaolinization, primarily near the Traverse Area). At the macroscale, fracture orientations and characteristics were used to distinguish areas of different types of deformation. The macroscopic deformation features are probably related to the relative orientations of Laramide stresses and the existence and orientation of preexisting Precambrian zones of weakness (i.e., deformation zones).

Traverse Area

Quartz deformation in the Traverse Area is characterized primarily by fragmented aggregates (Figure 23) and minor discontinuous boudins (Figure 24). The pre-Laramide deformation was dominated by fracturing, veining, and folding and was followed by Laramide brittle deformation, discordant with preexisting fabric. The quartz 'ribbons' appear to be subparallel to Ross Lakes Fault and the fold axis (Figure 24), but they are somewhat discontinuous in horizontal section and more discontinuous in vertical section which indicates their orientation was unfavorable for Laramide deformation. The 'ribbons' also demonstrate pre-Laramide folding (compression subparallel to the orientation of the Laramide fold axis and therefore inconsistent with the inferred Laramide sigma-1, Figures 24,25). The friable hand-sample from which the thin section was prepared was collected from a dense fracture/shear zone with an orientation of 255°/90° which is subparallel to the inferred sigma-1 but ≈ perpendicular to the 'ribbons'. This is probably an isolated zone or a zone of limited extent since this was the only foliated sample found in the Traverse Area.

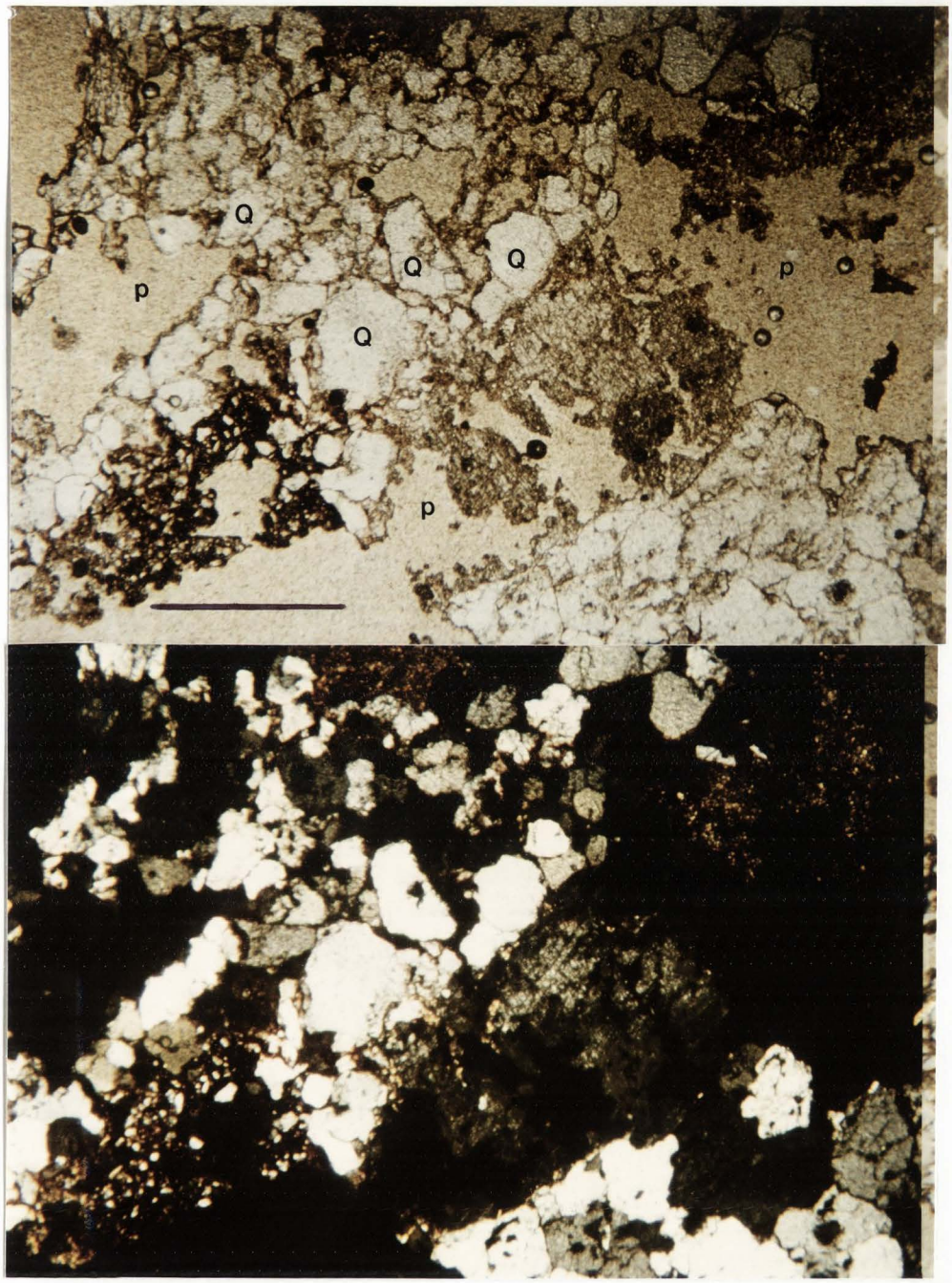

Figure 23. Thin section microphotographs showing fractured quartz aggregates from Traverse Point E. Scale bar is 1 mm long. Q denotes individual quartz grains.
A. Plane-polarized light. Note the abundant porosity (P).
B. Cross-polarized light. High-colored, very fine-grained material is probably kaolinite.

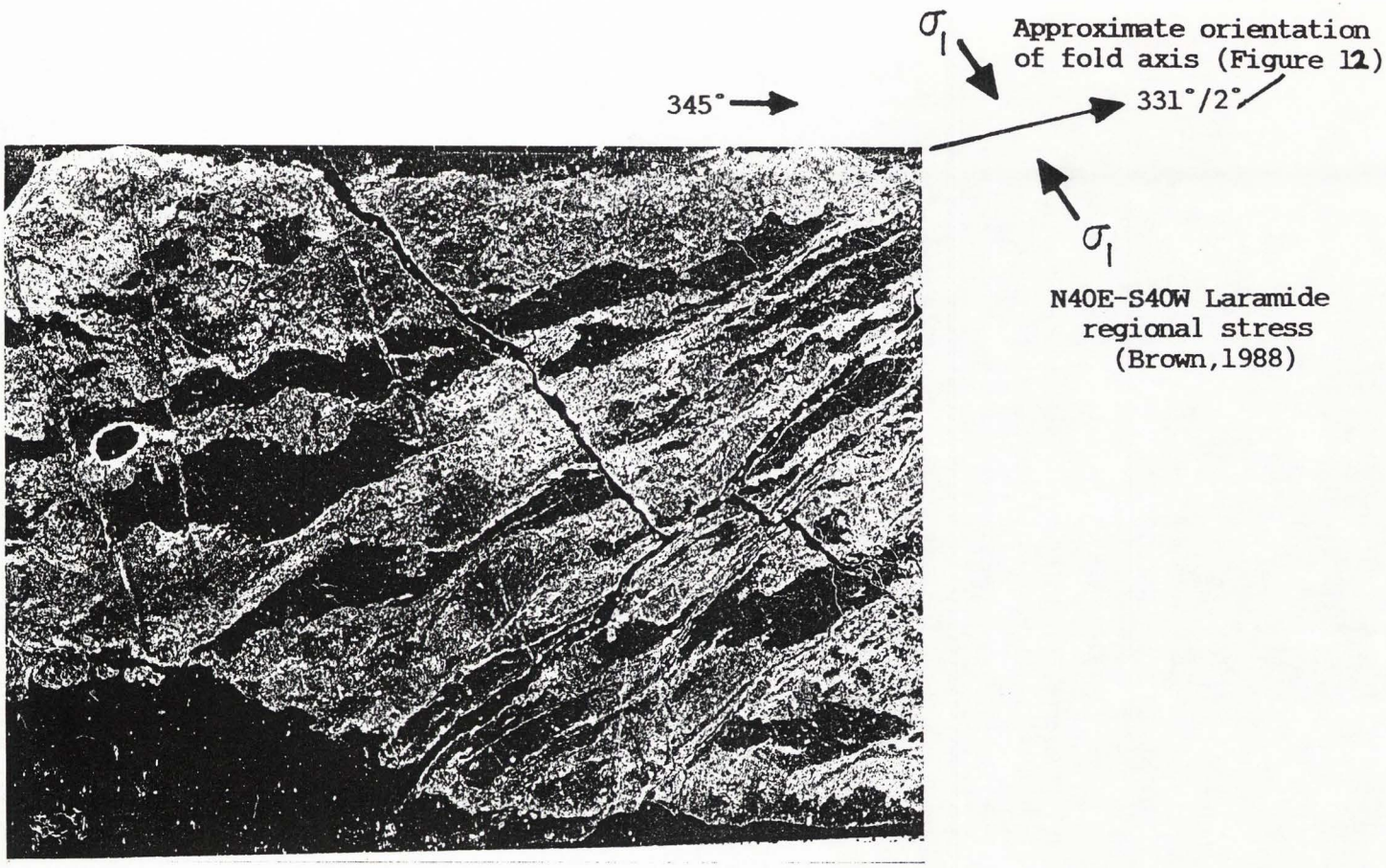

Figure 24. Horizontal thin section photonegative of granitic sample from small zone near Traverse Point F showing folded, fractured, and discontinuous nature of elongated quartz-grain aggregates (in black). The quartz-grain aggregates appear to be pre-Laramide quartz veins which have been disrupted in three dimensions. The 345° arrow denotes the orientation of the thin section. Long dimension of photonegative is equivalent to 3.1 cm. See text for discussion.

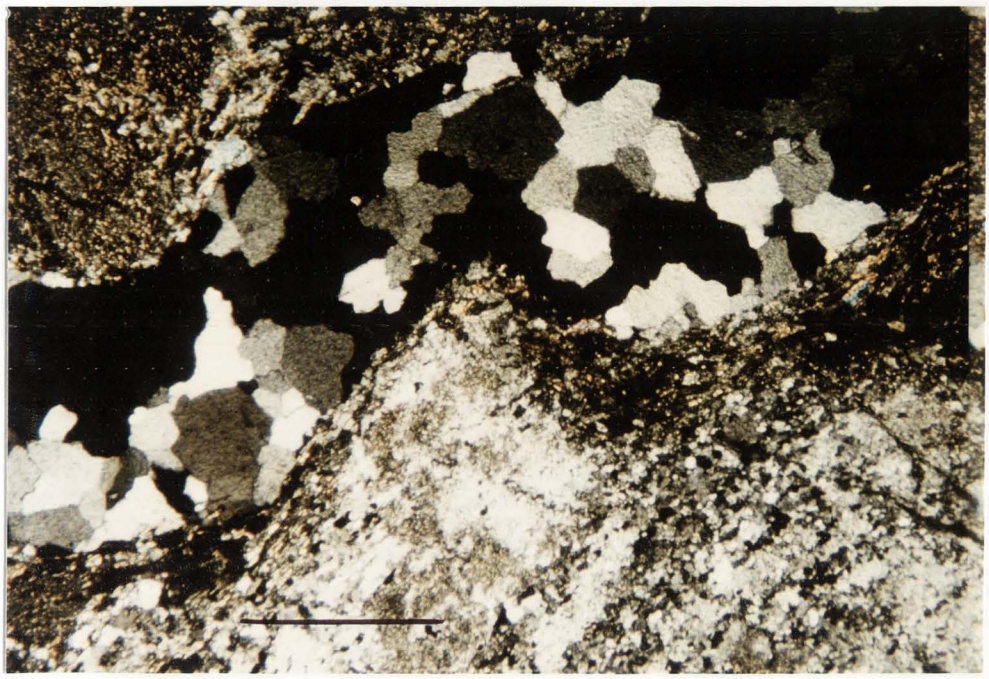

Figure 25. Thin section microphotograph of a folded quartz-grain aggregate from Figure 24. Cross-polarized light. Scale bar is 1 mm long. See text for discussion.

Generally, quartz veins were abundant in the Traverse Area. The veins usually were irregular in form and contained evidence of cataclastic deformation such as granitic fragments.

Macroscopic brittle deformation is demonstrated by numerous shear zones and dense fracture zones. Outcrop and thin section fracture data show strong correlation with a dominant orientation of primarily NE-SW; the dominant orientation of $\approx$ 40-60° is approximately parallel to the maximum Laramide regional (compressive) stress of N40E-S40W reported by Brown (1988). The lack of airphoto-scale lineaments in the Traverse Area (Figure 7) is probably due to intensity of deformation, lowered erosional resistance, and the lack of preexisting zones or favorable orientations of these zones.

The locations of the upper (shallowly east-dipping) and lower (steeply east-dipping) Precambrian-Paleozoic contacts in the Traverse Area (Figures 11,15,16) were used to constrain the amount of displacement or deformation undergone by the granite in the core of the fold. As previously mentioned, it is difficult or impossible to determine the absolute amount of displacement on Ross Lakes Fault, but the amount of displacement appears to be comparable to that on Jakey's Fork Fault. Gilliland (1959) reported 470 feet of displacement on Ross Lakes Fault near the study area, but he did not state where it was measured or how it was calculated. The manner in which the granite deformed was by brittle cataclasis and fracture orientations remained fairly consistent (NE-SW, Figures 16,18). However, the intensity of deformation at Traverse Points E-I perpendicular to the fold axis (Table 2) showed little change,

contrary to what might be expected. This could be due to the manner in which fracture data were obtained and although orientations were accurately represented at the Traverse Points, zones of densest fractures representing the areas of most intense deformation probably were not represented in outcrops that could be sampled.

The nature of the fractures in the Precambrian granite and their orientations is somewhat problematic. Although the strikes of fracture orientations in the granite are approximately parallel to sigma-1, they exhibit nearly vertical dips (Figure 14A) whereas subhorizontal fractures would be expected with a vertical sigma-3, inferred from reverse faulting along RLF, as discussed by Groshong (1988). The observation of different fracture orientations between Precambrian and Paleozoic rocks was made at both thin section and outcrop scale (Figures 16,19,20) and is probably due, at least in part, to a 'decoupling' of the Flathead Sandstone from the granite (discussed further below) and possibly to the influence of unrecognized pre-Laramide zones in the granite. It is also possible that stress was not transferred (or was inefficiently transferred) across the Paleozoic-Precambrian contact due to differences in the mechanical properties of the Precambrian and Paleozoic rocks: (1) differences across the contact - bedded Paleozoics vs more isotropic granite; or (2) the granite is not isotropic due to preexisting zones; or (3) the granite is not homogeneous due to alteration or textural differences ranging from porphyritic to equigranular to foliated. Experimental deformation of granite by Wawersik and Brace (1971) demonstrated that fracture mechanisms were complex and depended on confining pressure, mineral composition, and

grain size. For example, at high confining pressures, fractures were inclined to sigma-1 or propagated in initial planes which could explain the orientations observed in this study. Wise (1964) discussed similar phenomena in his study of microjoint orientations in Precambrian rocks from Montana and Wyoming. In thin section, he observed fluid inclusions parallel to and locally reopening older planes of fluid inclusions and interpreted them as a system of Precambrian weakness directions that partially controlled orientations of all subsequent fracture systems. Microjoints were then interpreted as a system of late Laramide fractures influenced by the pervasive Precambrian weakness directions. Wise (1964) also offered an explanation for the vertical nature of the microjoints; they were expansion features and developed subsequent to the bulk of Laramide deformation as blocks were lifted free of adjacent basin floors. Similar arguments could be proposed for observed fracture orientations in the Jakey's Fork study area, although the specific types of joints ($\geq$ 4 subparallel fractures spaced closer than 3 mm) studied by Wise (1964) were uncommon in the study area. Typical subparallel fracture spacings in the study area ranged from approximately 1 cm in high-deformation areas to $\geq$ 30 cm in low-deformation areas.

Area Along Jakey's Fork Fault
(Gridpoints 4,5,6)

Laramide deformation along Jakey's Fork Fault was concentrated in narrow zones and a wide range of brittle-deformation intensity was observed (Figure 22). Pre-Laramide zones were characterized by

subparallel quartz folia which are either elongated aggregates of recrystallized and elongate quartz grains, or possibly quartz veins in which recrystallization occurred. The quartz folia were subparallel to Jakey's Fork Fault and dominant fracture orientations at all scales (Figure 21). Brittle Laramide deformation was concordant with these zones because the folia remained continuous while granulation occurred parallel to the folia (Figure 22). It appears that the 'background' quartz aggregates were plastically deformed to form the 'ribbon' or foliated quartz with individual grains elongated parallel to the folia along a Precambrian deformation zone. The quartz folia, the abundant fine-grained subparallel chlorite (up to 13%), and penetrative deformation are indicative of temperatures and pressures in excess of those present during Laramide deformation (Mitra and Frost,1981). Brittle Laramide deformation along JFF was concordant with these preexisting zones and produced extreme grain-size reduction (Figure 22D).

Fair-to-good agreement for fracture orientations is shown at all scales studied (thin section, outcrop, airphoto; Figure 21). The planar foliation observed in thin section was also evident at outcrop scale - both with orientations similar to those of fractures (Figure 26).

The amount of displacement on Jakey's Fork Fault (202 m) appears to be comparable to that on Ross Lakes Fault. However, the Jakey's Fork Fault displacement is confined to a more narrow zone in the Paleozoic rocks and is much better constrained due to reactivation of a Precambrian zone of weakness.

Figure 26. Photograph of outcrop at Gridpoint 5. View is approximately due east parallel to Jakey's Fork Fault. Walking stick lies on top of the densely fractured and veined outcrop. Most fractures and veins are nearly vertical, strike ≈ east-west, and project through the offset Paleozoic rocks shown in Figure 29.

Central Part of Study Area
(Gridpoints 7,8,16,17)

Brittle Laramide deformation (as well as Precambrian deformation) appears to have been much less intense in this part of the study area (compared with the Traverse Area or Gridpoints 4,5,6, discussed above). Quartz grains were observed to be in relatively undeformed and intact aggregates. The quartz grains showed only minor plastic deformation (such as undulose extinction and deformation banding) and the aggregates exhibited only minor fracturing or 'molding' around the more resistant feldspar grains similar to that shown in Figure 22B2.

Good agreement was obtained between airphoto and outcrop fracture data for this part of the study area (Figures 7,15,21) with a major orientation approximately NE-SW (azimuth $\approx$ 10-50°). Thin section data did not agree with data from larger scales of observation (Figure 21) however, and indicate a dominant orientation of approximately NW-SE. Since this area is approximately centrally located and at some distance from the two major faults in the study area (Figure 15), I speculate that the regional Laramide deformation exhibited at outcrop and airphoto scales may not have been sufficiently intense in this area to overcome/replace background patterns or grain-scale heterogeneities, that is, to become penetrative. Typical outcrops in the central area have less dense and more sheet-like fractures (Figure 27) whereas representative outcrops along Jakey's Fork Fault exhibit dense, subparallel, and approximately vertical fractures (Figure 26). This phenomenon is similar to that described by Mitra (1978) for crystalline basement rocks in northern Virginia; during deformation

Figure 27. Photograph of typical outcrop in central Grid Area. Vertical fracture densities are relatively low and exfoliation-type slab jointing is common.

much of the strain was taken up by narrow ductile deformation zones and the blocks between these zones remained relatively undeformed.

Ross Lakes Fault - Jakey's Fork Fault Intersection Area

The general area of the fault intersection is Gridpoint Area 1-2-3-15 (Figure 7). Recognizable lineaments in the airphoto are rare, probably due to the intensity of deformation in this area, lowered erosional resistance of densely fractured areas, and unfavorable orientations of (possible) preexisting zones. Figure 28 shows veined, mylonitic, and breccia clasts in a sample collected at Gridpoint 3. The nature of the clasts indicates that the deformation: (1) was brittle, from the angular clasts; (2) was discordant with preexisting zones, from the mylonitic clast (compare with concordant deformation discussed above); and (3) formed in more than one distinct episode, from the veined and breccia clasts.

RELATIVE TIMING OF FAULTING

Several observations need to be mentioned here:

(1) Jakey's Fork Fault offsets moderately east-dipping Paleozoic rocks east of Ross Lakes Fault and Gridpoint 2 (Figure 6).

(2) South of Jakey's Fork Fault, the continuation of Ross Lakes Fault (or Shear Zone) is expressed as sheared granitic rocks (Figure 29) whereas just north of Jakey's Fork Fault, Ross Lakes Fault offsets Paleozoic rocks or is covered by talus primarily from the Cambrian

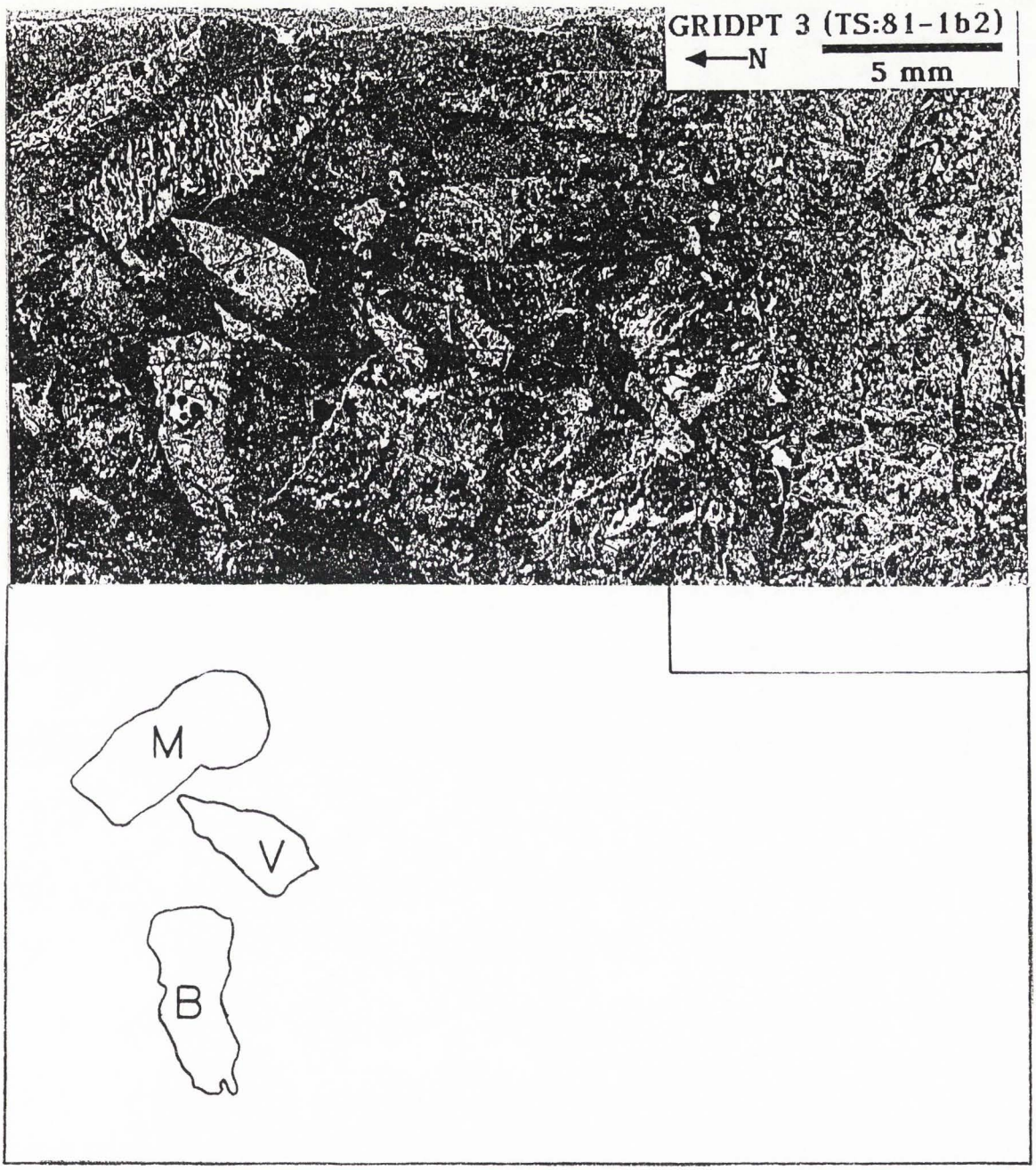

Figure 28. Horizontal thin section photonegative of sample from Gridpoint 3 - near the intersection of Jakey's Fork Fault and Ross Lakes Fault showing mylonitic (M), breccia (B), and veined (V) angular clasts.

Figure 29. Photograph of Ross Lakes Shear Zone. View is approximately 119°. Shear zone is mainly visible in granite at extreme right (arrow). North of the arrow (left), the fault is probably covered by Cambrian Flathead Sandstone talus. Jakey's Fork Fault offsets the moderately east-dipping Paleozoic rocks (south side up, dashed line) just north of where the shear zone is visible in granite.

Flathead Sandstone. (1) and (2) suggest that movement on Ross Lakes Fault occurred after movement on Jakey's Fork Fault (south side up, followed by some erosion).

(3) Qualitatively, east-west airphoto lineaments (Figure 7) appear to be longer than those of different orientations and the oblique lineaments appear to terminate on the east-west lineaments. This is quantitatively supported by thin section, outcrop, and airphoto data in Table 2 (combined data for Gridpoints 7-8-16-17 vs Gridpoints 4-5-6) where approximately east-west fracture orientations generally exhibit both a higher percentage of total fractures and a higher density (i.e., they are longer) than those of other orientations. Similar observations in granitic rocks of other areas have been interpreted to mean that the longer fractures formed earlier, although it may be difficult to determine whether the shorter fractures resulted from the same or a later deformational event (Segall and Pollard,1983a; Pollard and Aydin,1988). East-west striking fractures parallel to Jakey's Fork Fault would result from the same stresses which actuated movement on Jakey's Fork Fault and movement on Jakey's Fork Fault prior to that on Ross Lakes Fault is indicated.

(4) There is a lack of distinct lineaments in Grid Area 1-2-3-15 (Figure 7). This fact by itself as discussed above, suggests intense deformation such as would have occurred near the intersection of two faults. The breccia, mylonitic, and veined clasts (Figure 28) indicate that more than one deformational event occurred. The texture and composition of the mylonitic clast are very similar to those of samples

from Gridpoints 4 and 5 (Appendix E) which suggests concordant (to the Precambrian zone) deformation along Jakey's Fork Fault was followed by discordant deformation along Ross Lakes Fault.

Without knowing the number and timing of (Laramide) faulting events on each fault, it is difficult to say more from the above observations than some Ross Lakes Fault movement occurred after some movement on Jakey's Fork Fault.

PRECAMBRIAN - PALEOZOIC CONTACT

Decoupling of the Cambrian Flathead Sandstone from the Precambrian granite during Laramide deformation was already discussed with respect to different fracture orientations across the contact in the Traverse Area. North of Jakey's Fork (River) and near the Traverse Area, the inferred orientation of Ross Lakes Fault changes slightly (Figure 6). South of Jakey's Fork, Ross Lakes Fault is marked primarily by the shear zone in granite (Figure 29) whereas north of Jakey's Fork, it is defined by the fold axis. The change in fault orientation also suggests at least partial decoupling - since above the contact, the attitudes of Paleozoic rocks more strongly reflect Laramide stress orientations. The intensely deformed granite below the contact (and more intact Flathead Sandstone) shown in Figure 10 supports the decoupling idea.

Precambrian-Cambrian decoupling is not thought to be complete however, due to the presence of a quartz vein laminated with quartz and granite fragments crossing the contact (Figure 30). The vein is syntectonic and indicates at least partial welding or coupling across the

Figure 30. Photograph of quartz and breccia vein crossing the Precambrian-Paleozoic contact near Traverse Point E. View is ≈ 345° and steeply east-dipping Cambrian Flathead Sandstone is on the right. The contact orientation is approximately 321°/60°E. The several-generation vein extends through granite and gouge and ≈ 150 cm into the basal Flathead Sandstone. Walking stick is approximately parallel to and lies below vein. Small divisions on stick are 2.54 cm apart.

contact because the vein crosses the contact, records several episodes of deformation, and incorporates granitic fragments. Where visible, the vein measured approximately 20 cm wide in the granite and tapered to approximately 5 cm wide in the basal Flathead Sandstone. More extensive decoupling could occur in the less competent overlying Cambrian Gros Ventre Shale (suggested by Hoppin and Palmquist, 1965, for differing Precambrian and Paleozoic fracture patterns in the Bighorn Mountains).

FLUID-FLOW AND GEOCHEMISTRY

Plagioclase grains are generally altered (sericitized?) in the study area and the degree of alteration appears to be related to location. The grains are very altered and the presence of kaolinite is noticeable in the Traverse Area and at nearby Gridpoint 12. Plagioclase is altered to a lesser degree and the presence of kaolinite is questionable in the rest of the study area. Microcline alteration/deformation appears to be limited to fracturing, cataclasis, and minor recrystallization (no alteration to muscovite as reported by Mitra and Frost (1981) was observed). Plagioclase alteration is generally favored over microcline alteration at near-surface conditions (Guilbert and Sloane,1968) and may be related to Ca content (higher Ca, less stable) or a higher dislocation density which facilitates dissolution (Berner and Holdren,1977), but it is unclear how the relative abundance of the numerous dislocations associated with extensive polysynthetic twinning in both microcline and plagioclase (Berner and Holdren,1979) could be determined. Alteration of plagioclase to kaolinite would be favored at near-surface conditions where

Fe could be tied up with oxygen (Hurst and Kunkle,1985) - possibly related to abundant black, brown, and specular hematite associated with veins in the Traverse Area.

Chlorite is the major phyllosilicate in the Grid Area (up to ≈ 13%) especially along Jakey's Fork Fault and is present in the Traverse Area up to approximately 12% (Appendices D,E). In the central part of the Grid Area, biotite is present up to approximately 5%. The degradation of chlorite and gravimetric analysis for loss of chlorite from samples was not tested with a blank or standard, but point counting yielded comparable chlorite contents for the one sample where both methods were employed. Since chlorite appears to be present in approximately equal amounts in the Traverse Area and the Grid Area and microcline does not appear to be weathered, alteration of plagioclase to kaolinite is indicated near Ross Lakes Fault in the northern part of the study area. This alteration is probably related to the abundance of open fractures and the availability of water from the overlying Flathead Sandstone. At least some of the kaolinite development appears to be post-deformational in the Traverse Area since the very altered feldspars in some samples have undergone little grain-size reduction or fracturing. Figure 31 shows a fractured/veined feldspar grain from the Traverse Area which has been almost completely altered. The clearly defined grain boundaries suggest alteration occurred after brittle fracturing and veining (which probably would have deformed an altered grain). It is unlikely that the development of phyllosilicates in the Traverse Area facilitated continued deformation (Evans,1988) since foliated (cataclasite) zones were not

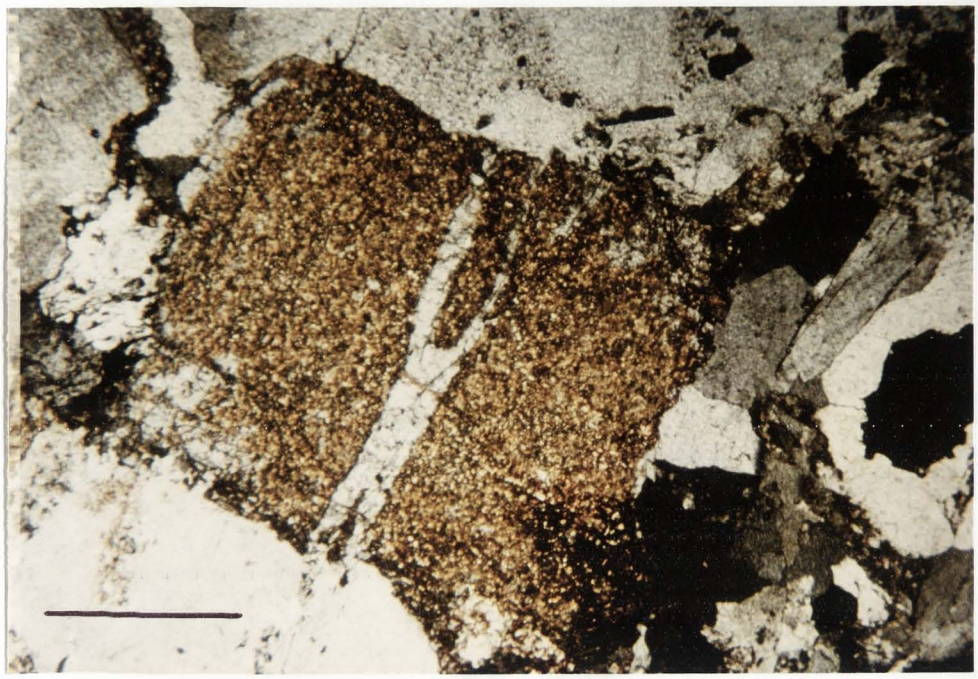

Figure 31. Thin section microphotograph of quartz vein through a highly altered feldspar grain from the Traverse Area. Alteration to very fine-grained phyllosilicates probably occurred after brittle deformation. Cross-polarized light. Scale bar is 1 mm long.

observed (as they were along Jakey's Fork Fault) and this may also indicate post-deformational kaolinite development.

Chlorite development along Jakey's Fork Fault may have contributed to localization of deformation there. That kaolinite did not develop along Jakey's Fork Fault is probably due to few open fractures and also because this area was deeper in the intrusion (temperatures were higher) and it was a greater distance from the Flathead Sandstone, the probable source of water. Depending on assumptions made (overburden; activities, natures, and availabilities of reactants; water pressure; etc.) kaolinite might be stable at temperatures associated with this part of the intrusion (stable up to $\approx$ 300°C; Hurst and Kunkle,1985). Temperatures probably would have been less than 300°C, since according to Mitra and Frost (1981), sedimentary overburden was approximately 3 km and the additional depth to this part of the intrusion must have been $\leq$ 3 km which is the approximate distance to the moderately east-dipping Paleozoic rocks (Figure 6). With the rather high geothermal gradient of 40°/km used by Mitra and Frost (1981), temperatures then would have been $\leq$ about 240°C, and kaolinite would be stable and expected if other conditions necessary for its formation were similar to those in the Traverse Area. It appears though, that water necessary for feldspar reaction (Janecke and Evans,1988) would have been unavailable or limited due to the very fine-grained nature of the rocks. In addition, the fine-grained nature of the rocks would favor recrystallization or diffusive mass transfer over fracturing (Knipe,1989) in the deformation zones along Jakey's Fork Fault.

The development of chlorite along Jakey's Fork Fault would have

required the influx of Fe- and Mg-rich fluids (probably) associated with alteration of diabase inclusions or original mafic components (possibly minor biotite in the study area) of the granite (Knipe and Wintsch,1985). Chlorite development was probably pre-Laramide since it would occur at a higher temperature-pressure regime than was present during Laramide deformation (Mitra and Frost,1981) and fault movement would have resulted in increased fracture permeability before extensive granulation occurred along the deformation zones. No diabase or diabase dikes were found in the study area (as reported and mapped by Granger et al., 1971, Figure 4), but altered (chloritized) diabase 'pods' were common.

Fluid flow appears to have been pervasive in the Traverse Area (partially syntectonic due to numerous breccia veins and the vein across the contact), based on relatively abundant kaolinite (possibly along unrecognized zones), dense fracture zones and open fractures - usually with weathered and/or altered surfaces, and abundant veining. Brittle deformation discordant with (possible) preexisting zones would have enhanced fracturing and would be consistent with the irregular orientations of many veins. The same fluid regime could not lead to development of approximately equal abundances of chlorite along Jakey's Fork Fault and in the Traverse Area and also to kaolinite development in the Traverse Area, so a minimum of 2 separate (in time and space) fluid systems are indicated. More than one fluid system is indicated in the Traverse Area by laminated quartz veins which often contain black, brown, and minor specular hematite. In the Grid Area relatively less pronounced fluid effects are indicated by less pronounced plagioclase alteration,

minor epidote emplacement (veining), rare calcite veining, and quartz (plastic) deformation and dissolution (healing of microcracks).

CONCLUSIONS

Laramide deformation in the Jakey's Fork study area was dominated by brittle fracture, grain-size reduction, and cataclasis. Pre-Laramide deformation of the Precambrian granitic rocks partially controlled the orientations of subsequent fracture systems at all scales studied (thin section, outcrop, airphoto). This finding contradicts Mitra and Frost (1981) who stated that during Laramide deformation, the Precambrian rocks behaved as massive, homogeneous basement but agrees with Wise (1964) who reported that microscopic fluid inclusion planes reflected Precambrian weakness directions and partially controlled the orientations of all subsequent fracture systems, including Laramide joints. Wise (1964) also observed that the persistent vertical orientation of microjoints developed subsequent to the bulk of Laramide deformation and that they were expansion features that formed as blocks lifted free of confines of adjacent basin floors. Data gathered in this study are insufficient to determine whether the fractures in the Jakey's Fork area are late expansion features because the fractures investigated do not meet Wise's (1964) description of microjoints and no absolute or relative ages for the various fracture sets have been obtained.

The two main zones of Laramide deformation in the study area lie along Ross Lakes Fault and Jakey's Fork Fault. Deformation with similar orientations developed in areas proximal to the faults and shows that these areas were influenced by the same stresses that caused movement on the faults. Laramide displacement on both faults was comparable, although

Jakey's Fork Fault is interpreted to have developed from a Precambrian deformation zone. Laramide deformation along Jakey's Fork Fault produced extreme grain-size reduction to the foliated cataclasite (mylonite). The Ross Lakes Fault is primarily a Laramide feature along which displacement occurred subsequent to some movement on Jakey's Fork Fault. The fold axis coincides with the inferred Ross Lakes Fault location in the northeastern part of the study area and its orientation is consistent with reported Laramide stress orientations (Brown,1988). Abundant irregular fractures and veining, poor fracture preservation, and fracture porosity indicate that Ross Lakes Fault does not follow a preexisting zone, but its orientation was probably influenced by Precambrian zones.

Mitra (1978) studied ductile deformation zones and discussed how they could develop in massive homogeneous rocks when they were deformed; planar inhomogeneities developed along which much of the later deformation takes place. The relatively undeformed homogeneous basement rocks were essentially passive blocks of basement bounded by these zones. Deformation in the Jakey's Fork area can be explained in a similar way. Laramide deformation primarily occurred along the two faults in the area. The central Grid Area may be thought of as a 'block' with deformation zones (Ross Lakes Fault and Jakey's Fork Fault) along its eastern and southern boundaries. Since outcrop and airphoto fracture data agree, the central 'block' is possibly divided into 'sub-blocks' the size of individual outcrops. Lesser amounts of deformation (compared to along the faults) occurred in the central area 'block' and 'sub-blocks' which appear to have had an insulating or shielding effect at thin-section scale.

The Paleozoic cover rocks were at least partially decoupled from the Precambrian basement. The decoupling is suggested from the 'gougey' granite at the contact and by different fracture orientations in the granite. Laramide stresses are reflected to a larger extent in the Paleozoic rocks.

At least two fluid systems are represented in the study area. Pre-Laramide chlorite development occurred at a depth of perhaps $\geq$ 6 km (related to temperatures associated with this retrograde metamorphism). Later (Laramide or post-Laramide) fluids along Jakey's Fork were minimal and their effects were limited to minor recrystallization in the fine-grained ductile matrix and relatively late-stage undeformed calcite veins. The distribution of fluids was probably limited by low fracture permeability. A Laramide (or post-Laramide) pervasive fluid system (especially in the Traverse Area) is reflected by the abundant fracture porosity and permeability, advanced feldspar alteration, and kaolinite development. A number of veins indicate several episodes of deformation with similar orientations and with similar fluids (laminated white quartz and hematite veins with or without breccia are common) and the larger veins may indicate channeled flow.

RECOMMENDATIONS FOR FUTURE WORK

As always, more work could be done and more data could be collected or generated in order to provide more specific and detailed interpretations and conclusions.

A more detailed analysis of the Paleozoic rocks near RLF would probably give a better idea of the amount and nature of the decoupling. Only limited fracture data were obtained in the Flathead Sandstone and none were obtained in younger units. An investigation of the Gros Ventre Shale and/or the Gallatin Limestone revealed complete decoupling above the less competent Gros Ventre Shale (Evans et al.,1990). More detailed/extensive investigations of individual outcrops might allow relative ages of the fracture sets to be determined and possibly assigned to individual deformation events.

Additional techniques which might be employed to supplement results and enhance interpretations are described below.

Thin section preparation and analysis (as described by Richter and Simmons,1977; Dula,1981; Kowallis et al.,1987) would facilitate three-dimensional analysis of intergranular fractures and quartz fractures. Inferred stress orientations on the microscale could then be better evaluated. Fracture (open, closed, healed) interrelations could also be better evaluated and possibly allow relative age determinations to be made. Extrapolation of the results to the macroscale might then be improved.

Cathodoluminescence may reveal microveins not visible in plane- or

cross-polarized light (Groshong,1988).

Microthermometry of fluid inclusions could enable a chronology to be devised from the physico-chemical characteristics of the fluids (Lespinasse and Pêcher,1986; Pêcher et al.,1985) since experimental work by Smith and Evans (1984) and Brantley et al. (1990) has suggested that microcracks in quartz have geologically short lifetimes at temperatures $\geq$ 200°C. Data on salinities (from melting temperatures) and densities (from homogenization temperatures) of fluid inclusions could be combined with orientation data to develop a chronology since both temperature and salinity tend to decrease with time in the evolution of hydrothermal systems. The nature of the fluids may also allow discrimination of primary (from initial crystallization) or secondary (from healing of microcracks) fluid inclusions to be made. This work could be combined with isotopic analyses of fluid inclusions ($\delta^{18}O$, for example) to indicate the nature(s) of the water circulating during and/or after deformation, and it could possibly give an indication of the amount of circulating water (Nesbitt and Muehlenbachs,1989; Kerrich et al.,1984).

Electron microprobe analyses (e.g., An contents of plagioclase grains and identification of alteration products) could enhance knowledge of operative alteration processes and conditions (as described by Guilbert and Sloane,1968; Berner and Holdren,1977).

Universal-stage microscopic analyses of quartz grain c-axes and deformation lamellae could supplement and/or improve interpretations based on regional or in situ stress orientations (discussed by Schmid,1983; Dula,1981).

Scanning or transmission electron microscopy to determine the morphology of kaolinite found in samples from near the Traverse Area could indicate whether kaolinite developed as a result of weathering after uplift and exposure or from hydrothermal alteration (Keller,1979).

Drilling could provide oriented core samples for compositional and deformational analysis. Results of core-sample analyses could improve interpretations through recognition of surface or near-surface effects (Kowallis et al.,1987). Possible results would indicate whether kaolinization occurred post-uplift and exposure and whether vertical fracture orientations are post-Laramide expansion features as suggested by Wise (1964). The results could also improve interpretations about the overall mechanical response of the basement rocks to Laramide deformation by providing compositional, fracture, and fault data at depth.

The possibility of fractal relations could be investigated for the fracture data acquired during this study. Using methods such as those suggested by LaPointe (1988), calculated fracture densities (for the different scales of observation) could be examined.

Finally, a method which would provide absolute ages for the various deformational events in the Jakey's Fork area is desirable. Absolute ages would add the most significant improvements to interpretations with respect to the manner and controls of basement deformation in the northern Wind River Range in response to Laramide stresses.

REFERENCES

Baker, C.L., 1946, Geology of the northwestern Wind River Mountains, Wyoming: Geological Society of America Bulletin, v. 57, p. 565-596.

Barton, C.C., Larsen, E., Page, W.R., and Howard, T.M., in press, Characterizing fractured rock for fluid-flow, geomechanical, and paleostress modeling: methods and preliminary results from Yucca Mountain, Nevada: U.S. Geological Survey Open-File Report.

Berg, R.R., 1962, Mountain flank thrusting in Rocky Mountain foreland, Wyoming and Colorado: American Association of Petroleum Geologists Bulletin, v. 46, p. 2019-2032.

Berner, R.A., and Holdren, G.R., Jr., 1977, Mechanism of feldspar weathering: some observational evidence: Geology, v. 5, p. 369-372.

Berner, R.A., and Holdren, G.R., Jr., 1979, Mechanism of feldspar weathering - II. observations of feldspars from soils: Geochimica et Cosmochimica Acta, v. 43, p. 1173-1186.

Brace, W.F., 1971, Micromechanics in rock systems, *in* Te'eni, M., ed., Structure, solid mechanics and engineering design: New York, Wiley-Interscience, p. 187-204.

Brace, W.F., 1984, Permeability of crystalline rocks: new in situ measurements: Journal of Geophysical Research, v. 89, p. 4327-4330.

Brantley, S.L., Evans, B., Hickman, S.H., and Crerar, D.A., 1990, Healing of microcracks in quartz: implications for fluid flow: Geology, v. 18, p. 136-139.

Brown, W.G., 1988, Deformational style of Laramide uplifts in the Wyoming foreland, *in* Perry, W.J., Jr., and Schmidt, C.J., eds., Interaction of the Rocky Mountain foreland and the Cordilleran thrust belt: Geological Society of America Memoir 171, p. 1-25.

Bruhn, R.L., Yonkee, W.A., and Parry, W.T., 1987, Faulting processes in the brittle-ductile transition regime: Eos, v. 68, p. 1472.

DuBois, M.A., and Evans, J.P., 1989, Laramide deformation in Precambrian granitic rocks, northeastern Wind River Range, Wyoming: Geological Society of America Abstracts with Programs, v. 21, p. 74.

DuBois, M.A., and Evans, J.P., 1990, Internal deformation of the Wind River thrust sheet along Laramide and Precambrian zones: detailed structural analyses and scales of brittle deformation, NE Wind River Range, Wyoming: Geological Society of America Abstracts with Programs, (in press).

Dula, W.F., Jr., 1981, Correlation between deformation lamellae, microfractures, and in situ stress measurements, White River uplift, Colorado: Geological Society of America Bulletin, v. 92, p. 37-46.

Engelder, J.T., 1974, Cataclasis and the generation of fault gouge: Geological Society of America Bulletin, v. 85, p. 1515-1522.

Erslev, E.A., 1986, Basement balancing of Rocky Mountain foreland uplifts: Geology, v. 14, p. 259-262.

Evans, J.P., 1988, Deformation mechanisms in granitic rocks at shallow crustal levels: Journal of Structural Geology, v. 10, p. 437-443.

Evans, J.P., Batatian, D., Derr, D., DuBois, M., Harlan, S., Malizzi, L., McDowell, R., Nelson, G., Parke, M., Schmidt, C., and Weberg, E., 1990, Mechanisms and kinematics of a Precambrian-cored fold and fault structure: Jakey's Fork, Wyoming: Geological Society of America Abstracts with Programs, (in press).

Gilliland, J.D., 1959, Geology of the Whisky Mountain area, Fremont County, Wyoming: Laramie, Wyoming, University of Wyoming, Unpublished M.S. Thesis.

Gough, D.I., 1986, Seismic reflectors, conductivity, water and stress in the continental crust: Nature, v. 323, p. 143-144.

Granger, H.C., McKay, E.J., Mattick, R.E., Patten, L.L., and McIlroy, P., 1971, Mineral resources of the Glacier Primitive Area, Wyoming: U.S. Geological Survey Bulletin 1319-F, 113 p.

Groshong, R.H., Jr., 1988, Low-temperature deformation mechanisms and their interpretation: Geological Society of America Bulletin, v. 100, p. 1329-1360.

Guilbert, J.M., and Sloane, R.L., 1968, Electron-optical study of hydrothermal fringe alteration of plagioclase in quartz monzonite, Butte district, Montana: Clays and Clay Minerals, v. 16, p. 215-221.

Hoppin, R.A., and Palmquist, J.C., 1965, Basement influence on later deformation: the problem, techniques of investigation, and examples from Bighorn Mountains, Wyoming: American Association of Petroleum Geologists Bulletin, v. 49, p. 993-1003.

Hurst, V.J., and Kunkle, A.C., 1985, Dehydroxylation, rehydroxylation, and stability of kaolinite: Clays and Clay Minerals, v. 33, p. 1-14.

Janecke, S.U., and Evans, J.P., 1988, Feldspar-influenced rock rheologies: Geology, v. 16, p. 1064-1067.

Kamb, W.B., 1959, Ice petrofabric observations from the Blue glacier, Washington, in relation to theory and experiment: Journal of Geophysical Research, v. 64, p. 1891-1909.

Keefer, W.R., 1970, Structural geology of the Wind River Basin, Wyoming: U.S. Geological Survey Professional Paper 495-D, 35 p.

Keller, W.D., 1979, Kaolinization of feldspar as displayed in scanning electron micrographs: Geology, v. 6, p. 184-188.

Kerrich, R., La Tour, T.E., and Willmore, L., 1984, Fluid participation in deep fault zones: evidence from geological, geochemical, and $^{18}O/^{16}O$ relations: Journal of Geophysical Research, v. 89, p. 4331-4343.

Kirby, S.H., 1984, Introduction and digest to the special issue on chemical effects of water on the deformation and strengths of rocks: Journal of Geophysical Research, v. 89, p. 3991-3995.

Knipe, R.J., 1989, Deformation mechanisms - recognition from natural tectonites: Journal of Structural Geology, v. 11, p. 127-146.

Knipe, R.J., and Wintsch, R.P., 1985, Heterogeneous deformation, foliation development, and metamorphic processes in a polyphase mylonite, in Thompson, A.B., and Rubie, D.C., eds., Metamorphic reactions kinetics, textures, and deformation: Advances in Physical Geochemistry, v. 4, New York, Springer-Verlag, p. 180-210.

Kowallis, B.J., Wang, H.F., and Jang, B.-A., 1987, Healed microcrack orientations in granite from Illinois borehole UPH-3 and their relationship to the rock's stress history: Tectonophysics, v. 135, p. 297-306.

Kronenberg, A.K., and Segall, P., 1987, Fluid inclusions along healed microcracks and dislocations within a ductile shear zone: implications for fluid access and hydrolytic weakening: Eos, v. 68, p. 1471.

LaPointe, P.R., 1988, A method to characterize fracture density and connectivity through fractal geometry: International Journal of Rock Mechanics and Mining Sciences and Geomechanics Abstracts, v. 25, p. 421-429.

LaPointe, P.R., and Hudson, J.A., 1985, Characterization and interpretation of rock mass joint patterns: Geological Society of America Special Paper 199, 37p.

Lespinasse, M., and Pêcher, A., 1986, Microfracturing and regional stress field: a study of the preferred orientations of fluid-inclusion planes in a granite from the Massif Central, France: Journal of Structural Geology, v. 8, p. 169-180.

Love, J.D., 1960, Cenozoic sedimentation and crustal movement in Wyoming: American Journal of Science, v. 258-A, p. 204-214.

Mase, C.W., and Smith, L., 1987, The role of pore fluids in tectonic processes: Reviews of Geophysics, v. 25, p. 1348-1358.

McCaig, A.M., 1988, Deep fluid circulation in fault zones: Geology, v. 16, p.867-870.

Mitra, G., 1978, Ductile deformation zones and mylonites: the mechanical processes involved in the deformation of crystalline basement rocks: American Journal of Science, v. 278, p. 1057-1084.

Mitra, G., 1984, Brittle to ductile transition due to large strains along the White Rock thrust, Wind River Mountains, Wyoming: Journal of Structural Geology, v. 6, p. 51-61.

Mitra, G., and Frost, B.R., 1981, Mechanisms of deformation within Laramide and Precambrian deformation zones in basement rocks of the Wind River Mountains: Contributions to Geology, University of Wyoming, v. 19, p. 161-173.

Mitra, G., Hull, J.M., Yonkee, W.A., and Protzman, G.M., 1988, Comparison of mesoscopic and microscopic deformational styles in the Idaho-Wyoming thrust belt and the Rocky Mountain foreland, *in* Perry, W.J., Jr., and Schmidt, C.J., eds., Interaction of the Rocky Mountain foreland and the Cordilleran thrust belt: Geological Society of America Memoir 171, p. 119-141.

Nesbitt, B.E., and Muehlenbachs, K., 1989, Origins and movement of fluids during deformation and metamorphism in the Canadian Cordillera: Science, v. 245, p. 733-736.

Neuzil, C.E., 1986, Groundwater flow in low-permeability environments: Water Resources Research, v. 22, p. 1163-1195.

Pêcher, A., Lespinasse, M., and Leroy, J., 1985, Relations between fluid inclusion trails and regional stress field: a tool for fluid chronology - an example of an intragranitic uranium ore deposit (northwest Massif Central, France): Lithos, v. 18, p. 229-237.

Pollard, D.D., and Aydin, A., 1988, Progress in understanding jointing over the past century: Geological Society of America Bulletin, v. 100, p. 1181-1204.

Prucha, J.J., Graham, J.A., and Nickelsen, R.P., 1965, Basement-controlled deformation in Wyoming province of Rocky Mountains foreland: American Association of Petroleum Geologists Bulletin, v. 49, p. 966-992.

Ray, R.G., 1960, Aerial photographs in geologic interpretation and mapping: U.S. Geological Survey Professional Paper 373, 230 p.

Ren, X., Kowallis, B.J., and Best, M.G., 1989, Paleostress history of the Basin and Range province in western Utah and eastern Nevada from healed microfracture orientations in granites: Geology, v. 17, p. 487-490.

Reynolds, S.J., and Lister, G.S., 1987, Structural aspects of fluid-rock interactions in detachment zones: Geology, v. 15, p. 362-366.

Richter, D., and Simmons, G., 1977, Microcracks in crustal igneous rocks: microscopy, *in* Heacock, J.G., ed., The earth's crust (its nature and physical properties): American Geophysical Union, Monograph 20, p. 149-180.

Schmid, S.M., 1983, Microfabric studies as indicators of deformation mechanisms and flow laws operative in mountain building, *in* Hsü, K.J., ed., Mountain building processes: San Diego, Academic Press, p. 95-110.

Segall, P., 1987, Observations of interrelated brittle and ductile deformation accompanying faulting in granitic rocks: Eos, v. 68, p. 1471.

Segall, P., and Pollard, D.D., 1983a, Joint formation in granitic rock of the Sierra Nevada: Geological Society of America Bulletin, v. 94, p. 563-575.

Segall, P., and Pollard, D.D., 1983b, Nucleation and growth of strike slip faults in granite: Journal of Geophysical Research, v. 88, p. 555-568.

Sibson, R.H., 1981, Fluid flow accompanying faulting: Field evidence and models, *in* Simpson, D.W., and Richards, P.G., eds., Earthquake prediction: An international review: American Geophysical Union, Maurice Ewing Series 4, p. 593-603.

Simpson, C., 1985, Deformation of granitic rocks across the brittle-ductile transition: Journal of Structural Geology, v. 7, p. 503-511.

Simpson, C., 1986, Fabric development in brittle-to-ductile shear zones: Pure and Applied Geophysics, v. 124, p. 269-288.

Simpson, C., 1987, Exhumed fault zones: the role of fractures in ductile deformation: Eos, v. 68, p. 1472.

Smith, D.L., and Evans, B., 1984, Diffusional crack healing in quartz: Journal of Geophysical Research, v. 89, p. 4125-4135.

Smithson, S.B., Brewer, J., Kaufman, S., Oliver, J., and Hurich, C., 1978, Nature of the Wind River thrust, Wyoming, from COCORP deep-reflection data and from gravity data: Geology, v. 6, p. 648-652.

Starkey, H.C., Blackmon, P.D., and Hauff, P.L., 1984, The routine mineralogical analysis of clay-bearing samples: U.S. Geological Survey Bulletin 1563, 32 p.

Steidtman, J.R., Middleton, L.T., and Shuster, M.W., 1989, Post-Laramide (Oligocene) uplift in the Wind River Range, Wyoming: Geology, v. 17, p. 38-41.

Tullis, J., and Yund, R.A., 1977, Experimental deformation of dry Westerly Granite: Journal of Geophysical Research, v. 82, p. 5705-5718.

Tullis, J., and Yund, R.A., 1987, Transition from cataclastic flow to dislocation creep of feldspar: mechanisms and microstructures: Geology, v. 15, p. 606-609.

Wawersik, W.R., and Brace, W.F., 1971, Post-failure behavior of a granite and diabase: Rock Mechanics, v. 3, p. 61-85.

Wise, D.U., 1964, Microjointing in basement, Middle Rocky Mountains of Montana and Wyoming: Geological Society of America Bulletin, v. 75, p. 287-306.

Wood, B.J., and Walther, J.V., 1986, Fluid-flow during metamorphism and its implications for fluid-rock ratios, in Wood, B.J., and Walther, J.V., eds., Fluid-rock interactions during metamorphism: Advances in Physical Geochemistry, v. 5, New York, Springer-Verlag, p.89-108.

Yonkee, A., Mitra, G., and Hull, J., 1984, Basement-cover relationships in Laramide foreland thrust sheets of the Wyoming province: Geological Society of America Abstracts with Programs, v. 16, p. 702.

APPENDICES

APPENDIX A. EXPLANATION FOR AND DISCUSSION OF APPENDIX INFORMATION

The following appendices present more detailed deformational and compositional data for the study area than could be reasonably be included in the body of the thesis. These data are presented in this form not only to keep the text readable, but also to provide a fairly complete and accessible record of observations 'distilled' from field notes for future reference. Data are given from airphoto, outcrop, hand-sample, and thin section observations for both the Traverse and Grid Areas. Individual appendices present certain types of data and/or descriptions for Traverse or Grid Area observations and more complete explanations for individual appendices are given at the beginning of each appendix.

APPENDIX B. TRAVERSE AREA: SAMPLE AND ANALYSIS DESCRIPTIONS

Appendix B briefly describes samples, analyses performed, and data collected from the Traverse Area.

Data Pt	Sample I.D.	Description	Types of Analyses Performed
A	720-3a	granite, high deformation	Outcrop: fracture orientations; combined with B,C,D,F and with all Traverse Pts - fracture orientations Thin sections: deformation characteristics
	720-3b	granite, low deformation	
B	720-2a	granite, high deformation	Outcrop: fracture orientations Thin sections: deformation characteristics
	720-2b	granite, low deformation	
C	720-4a	granite - very fractured, high deformation	Outcrop: fracture orientations Thin sections: deformation characteristics, Point-counts (-4a,-4c) X-ray diffraction: (-4a,-4c)
	720-4b	granite-gouge, high deformation	
	720-4c	granite, low deformation	
D	720-5a	granite, high deformation	Outcrop: fracture orientations Thin sections: deformation characteristics
	720-5b	granite-gouge with quartz vein, high deformation	
	720-5c	granite, low deformation	
E	719-1a	granite-gouge with quartz veins, high deformation	Thin sections: deformation characteristics; (-1e): fractures, quartz fractures - orientations and densities X-ray diffraction: (-1c)
	719-1b	granite-gouge, high deformation	
	719-1c	"	
	719-1d	"	
	719-1e	"	
≈E	623-3a	Flathead Sandstone, high deformation, vertical thin section only	Thin sections: deformation characteristics, Point-counts (-3c) X-ray diffraction: (-3c,-3e)

	623-3b	gouge zone between sandstone and granite, high deformation	
	623-3c	"	
	623-3d	"	
	623-3e	'granite', high deformation	
F	720-1a	granite, low deformation	Outcrop: fracture orientations and densities; combined with G, H,I - fracture orientations and densities Thin sections: deformation characteristics; (-1a,-1d) fractures, quartz fractures - orientations and densities
	720-1b	anastomosing quartz veins and shear zone in granite, high deformation	
	720-1c	quartz vein in granite, high deformation	
	720-1d	granite with > 1 generation of quartz veins, high deformation	
	720-1e	'foliated' granite from dense fracture - shear zone, high deformation	
G	721-1a	granite, high deformation	Outcrop: fracture orientations and densities Thin sections: deformation characteristics; fractures, quartz fractures - orientations and densities
	721-1b	granite, low deformation	
H	721-2a	granite, high deformation	Outcrop: fracture orientations and densities Thin sections: deformation characteristics; fractures, quartz fractures - orientations and densities; Point-counts (822-1) X-ray diffraction: (822-1)
	822-1	granite, low deformation	
I	721-3a	granite, high deformation	Outcrop: fracture orientations and densities Thin sections: deformation characteristics; fractures and quartz fractures - orientations and densities
	721-3b	granite, low deformation	

APPENDIX C. GRID AREA: SAMPLE AND ANALYSIS DESCRIPTIONS

Appendix C briefly describes samples, analyses performed, and data collected from the Grid Area.

Data Pt	Sample I.D.	Description	Types of Analyses Performed
1	82-3a	granite, low deformation	Outcrop: fracture orientations
	82-3b	(altered) diabase from 'pod'	Thin sections (-3a,-3c): deformation characteristics; fracture orientations and densities
	82-3c	granite - fractured and veined, high deformation	X-ray diffraction: (-3b)
			Airphoto: (with 2,3,15) lineament orientations
2	829-1	granite, low deformation	Outcrop: fracture orientations
			Thin section: deformation characteristics; fracture orientations and densities
3(A)	81-1a	granite, low deformation	Outcrop: fracture orientations
(B)	81-1b1	(altered) diabase	Thin sections (-1a,-1b2): deformation characteristics; fracture orientations and densities
	81-1b2	granite with irregular quartz veins, high deformation?	X-ray diffraction: (-1b1)
4	713-1	'foliated' granite, high deformation	Outcrop: fracture orientations
	81-2a	granite (least deformed sample)	Thin sections (all): deformation characteristics; (713-1,81-2a): fracture orientations and densities
	81-2b	granite, altered/high deformation?	X-ray diffraction: (all)
			Airphoto (with 5,6): lineament orientations, densities for comparison with thin section, outcrop
5(A)	727-3a	granite (with black veins)	Outcrop: fracture orientations
(B)	727-3b	granite	Thin sections (-3c1,-3d): deformation characteristics; fracture orientations and densities; Point-counts (-3c1)
(C)	727-3c1	granite, low deformation?	X-ray diffraction: (-3c1,-3c2)
	727-3c2	(altered) diabase	Airphoto: lineament orientations and densities
	727-3d	granite with conjugate fractures, veins, high deformation	

≈5 (south of JF)	824-2a	granite with 'cross veins', high deformation	Thin section (-2a): deformation characteristics X-ray diffraction: (-2a)
	824-2b	granite(?) with quartz veins, high deformation	
6	824-1a	granite(?) from dense fracture zone, high deformation	Outcrop: fracture orientations Thin sections (all): deformation characteristics; fracture orientations and densities Airphoto: lineament orientations and densities
	824-1b	granite(?) from dense fracture zone, high deformation	
	824-1c	granite(?), quartz veined, least deformed sample	
7	823-2a	granite(?)	Outcrop: fracture orientations and densities Thin section (-2b): deformation characteristics; fracture, quartz fracture orientations and densities; Point-counts X-ray diffraction: (-2b) Airphoto: lineament orientations, densities; combined with 8,16,17 for comparison with thin section and outcrop
	823-2b	granite, low deformation	
8	823-1	granite, low deformation	Outcrop: fracture orientations, densities Thin section: deformation characteristics; fracture, quartz fracture orientations and densities X-ray diffraction Airphoto: lineament orientations, densities
11	725-2	granite (+ gouge?) from dense fracture zone	Outcrop: fracture orientations Thin section (-2): deformation characteristics; fracture orientations and densities
	725-2a	"	
12	721-4a	granite from densely quartz-veined zone, high deformation (?)	Outcrop: fracture orientations Thin section (-4c): deformation characteristics; fracture orientations and densities

	721-4b	quartz-veined zone with granitic clasts, high deformation (?)	
	721-4c	granite, least deformed sample	
≈12	725-1a	Flathead Sandstone (+ gouge), high deformation, vertical thin section	Thin section (-1d): deformation characteristics; fracture orientations and densities X-ray diffraction: (-1a,-1d)
	725-1b	granite/gouge, high deformation	
	725-1c	"	
	725-1d	granite, high deformation (?)	
≈12	624-4a	Flathead Sandstone (orange-colored), high deformation(?)	Thin section (-4a,-4c): deformation characteristics
	624-4b	" - unoriented	
	624-4c	Flathead Sandstone (reddish-colored), high deformation(?)	
	624-5	granite, high deformation (?)	
14	82-2a	granite from dense quartz-vein zone, high deformation	Outcrop: fracture orientations Thin sections (-2b,-2c): deformation characteristics; fracture orientations and densities Airphoto: lineament orientations and densities
	82-2b	granite (breccia), high deformation	
	82-2c	granite, least deformed sample	
15	82-1a	coarse-grained pegmatite vein(?)	Outcrop: fracture orientations Thin section (-1b): deformation characteristics; fracture orientations and densities X-ray diffraction: (-1a)
	82-1b	granite, low deformation	
16	81-3a	granite from dense fracture zone, high deformation	Outcrop: fracture orientations and densities Thin sections (-3a,-3b): deformation characteristics; fracture, quartz fracture - orientations and densities X-ray diffraction: (-3b) Airphoto (combined with 17; 7,8): lineament orientations, densities for comparison with
	81-3b	granite, least deformed sample	

			thin section and outcrop
17	727-2a	granite, low deformation	Outcrop: fracture orientations and densities
	727-2b	"	Thin section (-2a): deformation characteristics; fracture, quartz fracture - orientations and densities
18	727-1a	granite(?) from coarse-grained pegmatite(?) vein	Outcrop: fracture orientations Thin section (-1c): deformation characteristics; fracture orientations and densities Airphoto: lineament orientations, densities
	727-1b	granite, low deformation(?)	
	727-1c	granite, low deformation	
19	726-3a	granite from dense fracture zone, high deformation	Outcrop: fracture orientations Thin sections (all): deformation characteristics; fracture orientations and densities Airphoto (combined with 20): lineament orientations, densities for comparison with thin section and outcrop
	726-3b	granite, least deformed sample	
	726-3c	granite, proximal to 'diabase' pod	
20	726-1a	granite, near dense fracture zone, high deformation(?)	Outcrop: fracture orientations Thin section (-1a): deformation characteristics; fracture orientations and densities
	726-1b	quartz vein with granitic fragments, high deformation(?)	
≈20	726-2	(altered) diabase sill/dike/pod	X-ray diffraction

APPENDIX D. TRAVERSE AREA SAMPLES: COMPOSITION AND THIN SECTION DEFORMATION DATA

Appendix D summarizes the results of optical (microscopic) and XRD analyses of Traverse Area samples. Individual minerals are described with respect to their deformation characteristics, appearances, and abundances. In general, most potassium feldspar is represented by microcline with tartan twinning. Plagioclase is primarily altered and exhibits albite twinning. C_f = Cambrian Flathead Sandstone.

Traverse Point A

Sample 720-3a

* Thin section deformation characteristics:

This sample contains numerous intergranular fractures, many with fine- to medium-grained quartz and minor opaques.

Feldspars: Almost all grains exhibit moderate-dense (transgranular) fractures, are an- to subhedral, and show relatively minor alteration and recrystallization. Microcline grains have many quartz-filled fractures and range in size from 4-16 mm. Plagioclase grains show minor grain-scale faults (offset albite twins) and average ≈ 3 mm in size.

Quartz grains are all mainly an- to subhedral, ≈ 0.5-1.5 mm in size, and show undulose extinction to subgrain formation as well as minor polygonization. Numerous fractures through subgrains were observed.

Sample 720-3b

* Thin section deformation characteristics:

This sample is similar to 720-3a, with slightly more recrystallization of microcline and quartz and many open fractures. A shear fracture with angular microcline and very fine-grained quartz is also present. Quartz grains are primarily anhedral.

Traverse Point B

Sample 720-2a

* Thin section deformation characteristics:

This sample has numerous intergranular fractures, some of which are open, and two relatively large shear fractures.

Feldspar grains have numerous fractures and shear fractures, are present as subhedral grains to angular fragments, and show minor recrystallization. Grain sizes range from 11 mm (microcline) to < 0.5 mm (plagioclase).

Quartz grains and deformation are very similar to that described for Point A. Also present are vein quartz grains up to ≈ 6 mm which show evidence of shearing.

Sample 720-2b

* Thin section deformation characteristics:

This sample contains numerous intergranular fractures. Many fractures are open but some contain fine-grained (minor very fine-grained) quartz and opaques. More than one opening event can be seen.

Feldspar grains are similar to those described for sample 720-2a, with minor recrystallization and moderate to dense fractures - many with

quartz fillings. Plagioclase is generally altered.

Quartz grains are generally elongate to subequant with undulose extinction and average ≈ 1 mm in size. Subgrain formation and sutured grain boundaries were also noted. A few angular grains were also present.

Traverse Point C

Sample 720-4a

* Thin section deformation characteristics:

Overall, much grain-size reduction is evident in this sample (compared to 720-4c). Phyllosilicates are present in irregularly shaped areas and are fairly uniformly dispersed. Most grains are angular to subrounded and < 0.5 mm in size.

Feldspars grains show minor recrystallization and much alteration. Rare recognizable microcline and plagioclase range up to 24 and 2.5 mm in size respectively.

Quartz grains range up to 2.5 mm and show primarily undulose extinction and subgrain formation with minor polygonization.

* X-ray analysis: quartz, microcline, plagioclase, chlorite (up to 11.5%), illite/micas, kaolinite

* Point-count (176 points): quartz (31.8%), microcline (5.7%), plagioclase (6.8%), unidentified feldspar (30.7%), very fine-grained with high birefringence (5.1%), biotite (5.1%), chlorite (11.9%), calcite (1.7%), unidentified (1.1%)

Sample 720-4b

* Thin section deformation characteristics:

Feldspar grains are all moderately to densely fractured and some fractures are quartz-filled. Microcline grains range from ≈ 15 to < 3 mm and show minor recrystallization. Plagioclase 'grains' are primarily altered and range up to 2 mm.

Quartz occurs primarily in fractured aggregates of small (recrystallized) grains (88 microns to ≈ 0.5 mm) which have attained somewhat polygonal shapes. The aggregates are irregular to feldspar-conforming in shape. Subhedral, fractured vein quartz grains of 1-4 mm in size are also present.

Numerous open relatively large fractures are evident.

Sample 720-4c

* Thin section deformation characteristics:

This sample contains relatively few fractures of thin section size and moderate intergranular fractures.

Feldspar grains show much evidence for brittle fracturing and grain-size reduction. Microcline grains range from about 3 to 15 mm and show minor recrystallization. The larger grains are subhedral while the smaller are primarily angular. Plagioclase grains are sub- to anhedral, show much alteration (sericitization?), and are 2-4 mm in maximum dimension.

Quartz grains are primarily anhedral, occur up to 3-4 mm in size, and show undulose extinction to deformation banding types. Most quartz occurs in moderately fractured, rounded aggregates of irregular to polygonal small grains (0.5 - 1 mm).

* X-ray analysis: quartz, plagioclase, microcline, chlorite, biotite?

* Point-count (265 points): quartz (37.7%), microcline (30.6%), plagioclase (10.9%), unidentified feldspar (10.9%), very fine-grained with high birefringence (2.3%), chlorite (4.9%), opaques (0.8%), open (1.9%)

Traverse Point D

Sample 720-5a

* Thin section deformation characteristics:

This sample shows moderate numbers of intergranular fractures which are generally open.

Feldspars: Microcline is present as moderately fractured, subhedral to anhedral grains with minor recrystallization, 7+ to ≈ 0.5 mm. Plagioclase is primarily anhedral and altered. Intact recognizable fragments range up to 4 mm.

Quartz: Deformation in quartz is expressed by undulose extinction, deformation lamellae, subgrain formation, and minor polygonization. Quartz generally occurs as aggregates (about 4 mm in maximum dimension) of anhedral and subequant to elongate (sub-?)grains (≤ 0.5 mm).

Sample 720-5b

* Thin section deformation characteristics:

Deformation is expressed by numerous intragranular fractures, many cross-cutting and open. Alteration is minor. Two shear fractures were observed containing coarse- to fine-grained material.

Feldspars: Microcline grains are primarily anhedral, ≈ 3 mm in size, show minor recrystallization and alteration, and are moderately fractured. Plagioclase grains are primarily anhedral, 2-3 mm in size, altered, and contain grain-scale faults.

Quartz grains are primarily anhedral, and show undulose extinction to subgrain formation. Grain sizes range from 1 to < 0.5 mm.

Sample 720-5c

* Thin section deformation characteristics:

This sample shows (relatively) very few intergranular fractures or veins.

Feldspars: Microcline grains are primarily subhedral and moderately fractured (with minor recrystallization) with maximum dimensions of ≈ 7 to 18 mm. Plagioclase grains are somewhat altered, anhedral, moderately fractured, and range from 1 to 2 mm in size.

Quartz grains are anhedral, range from < 0.5 to 2 mm in size, and exhibit undulose extinction and moderate subgrain formation. The grains occur in moderately fractured, generally subequant to elongate 'pods' ≈ 5 mm in maximum dimension.

Traverse Point E

These samples were collected at the steeply dipping granite - Flathead Sandstone contact and are similar in description to (623-3, below). This locality however, is where the vein crosses the contact as described above in the Interpretation.

Sample 719-1a

* Thin section deformation characteristics:

This sample consists primarily of a quartz vein with shear fractures. Densely fractured feldspars are present (primarily microcline) and range from 15 mm at the edge of the shear zone to 0.5 mm in size.

Vein quartz (larger grains up to 5 mm) grains are subhedral to angular and show minor undulose extinction. Fractured grains and fragments are $\leq$ 125 microns in size and in addition to undulose extinction, show subgrain formation and recrystallization.

Sample 719-1b

* Thin section deformation characteristics:

Feldspars: Microcline grains are moderately fractured (containing very fine-grained quartz and highly birefringent grains), sub- to anhedral (4.5 to 12 mm), and sub-angular (1.5 to 6.5 mm). Plagioclase grains are highly altered and almost unrecognizable. Minor (open) fracturing occurs in these sub-rounded grains about 5 mm in size.

Quartz grains are anhedral and subequant to slightly elongate (0.25-2 mm) with minor edge suturing, exhibit undulose extinction, and occur in 5-15 mm aggregates.

Sample 719-1c

* Thin section deformation characteristics:

Feldspars: Microcline grains are densely fractured, range in size from $\approx$ 3 to 11 mm in size, and show minor recrystallization. The rounded, highly altered feldspar (plagioclase?) grains range up to 7 mm.

Quartz grains are anhedral but overall are more equant and show less undulose extinction and more polygonization than those in sample 719-1b. Grains range in size up to 2 mm, but most grains are 177-500 microns and occur in 5-6 mm subequant aggregates.

* X-ray analysis: quartz, microcline, illite/micas, chlorite?, kaolinite?

Sample 719-1d

* Thin section deformation characteristics:

Observed deformation features are very similar to those described for samples 719-1b and 719-1c.

Sample 719-1e

* Thin section deformation characteristics:

Observed deformation features are very similar to those described for samples 719-1b and 719-1c.

$\approx$ Traverse Point E (just south of actual point)

Overall, samples 623-3 are densely fractured and show much alteration. Opaque minerals are concentrated along zones of deformation in some thin sections but are usually disseminated. The samples were collected across the steeply dipping Precambrian granite - Cambrian Flathead Sandstone (Cf) contact.

Sample 623-3a

* Thin section deformation characteristics:

This sample consists primarily of 125-250 micron, subangular to subrounded, fairly well-sorted (Cf) quartz grains. Some zones of comminution with concentrated opaques and minor undulose extinction are also present. These zones show minor offset and are approximately horizontal - cutting across bedding planes.

Sample 623-3b

* Thin section deformation characteristics:

Feldspar grains are intensely fractured (with many open fractures) with reddish opaque coatings and are subhedral to subangular. Microcline grain sizes range up to 6 mm and down to ≈ 1 mm for fragments. Plagioclase grains are moderately altered and up to 4 mm in size.

Quartz occurs primarily as anhedral grains with undulose extinction. Most grains are ≈ 125-250 microns but range up to 1 mm in size.

Sample 623-3c

* Thin section deformation characteristics:

This sample from a mid-gouge zone primarily shows intense fracturing and grain-size reduction with minor alteration and much fracture porosity. Some fractures contain abundant very fine-grained, highly birefringent material.

Feldspars: Microcline grains are subhedral (up to 7 mm) to angular (down to < 1 mm). Recognizable plagioclase is a very minor component.

Quartz grains are generally the smallest (<350 micron) fragments observable, are subangular to angular, show dense fracturing to undulose extinction, and range in size up to ≈ 2 mm.

* X-ray analysis: quartz, microcline, illite/micas, kaolinite

* Point-count (160 points): quartz (32.5%), microcline (16.9%), unidentified feldspar (1.3%), very fine-grained with high birefringence (18.8%), opaques (4.4%), open (26.3%)

Sample 623-3d

* Thin section deformation characteristics:

Characteristics are very similar to sample 623-3c. There appear to be fewer open fractures and microcline grains appear to be more intact. One shear fracture was observed which contains grains and fragments from < 62 microns up to 1 mm in size.

Sample 623-3e

* Thin section deformation characteristics:

This sample exhibits deformation similar to sample 623-3d. There are fewer open fractures, more (consolidated) areas of phyllosilicates (altered plagioclase?), and microcline grains appear to be less fractured. Quartz grains generally show undulose extinction and range from 4 mm in size down to very fine recrystallized grains at microcline grain boundaries.

* X-ray analysis: quartz, microcline, illite/micas, kaolinite

Traverse Point F

Sample 720-1a

* Thin section deformation characteristics:

This sample contains numerous intergranular fractures (some open) and some of which cross the quartz grain aggregates.

Feldspar grains exhibit both grain-scale and through-going faults. Microcline occurs primarily as ≈ 0.8-11 mm angular fragments with very fine-grained quartz and phyllosilicates in fractures and shows minor recrystallization. Plagioclase grains are densely fractured, show minor to moderate alteration, and are ≈ 1-4 mm in size with some bent albite twins present.

Quartz grains are primarily anhedral, subequant to elongate (≈0.5-1.5 mm) with undulose extinction. Subgrain formation with edge suturing and minor polygonization are also evident. The grains commonly occur in irregular to elliptical 'pods' or aggregates ≈ 5x2 mm in size.

Sample 720-1b

* Thin section deformation characteristics:

This sample consists primarily of quartz with minor, relatively clean (unaltered), rounded to angular (≈1 mm) feldspar fragments. Moderate thin section-size open fractures and minor phyllosilicate development were noted. Vein quartz occurs as anhedral to subhedral, up to 5 mm in size, subequant to elongate grains showing primarily undulose extinction. The vein is juxtaposed with a sub-parallel, much finer-grained shear(?) zone which contains primarily angular quartz grains $\leq$ 0.25 mm and minor 1-2 mm fragments. These grains show undulose extinction with minor subgrain formation and recrystallization.

Sample 720-1c

* Thin section deformation characteristics:

This sample consists primarily of quartz grains in a wide range of sizes. A poorly defined cataclastic foliation (≈N-S) is also evident sub-parallel to foliation defined by opaques, chlorite, and quartz 'stringers'. Minor elongate quartz 'pods' up to 6-7 mm long and oriented N-S are composed of subhedral, elongate (E-W) 0.5+ mm grains with undulose extinction. Relatively unaltered plagioclase grains are present $\leq$ 0.25 mm. Most grains are angular, subequant to elongate ≈ parallel to foliation, and range in size from 0.71 mm to $\leq$ 0.062 mm.

Sample 720-1d

* Thin section deformation characteristics:

This sample is primarily coarse-grained with a major (≈ 7 mm x 4.5 cm) shear zone sub-parallel to an earlier-formed quartz vein. Fractures are open, closed, mineral-filled (coarse- and very fine-grained quartz, phyllosilicates), and primarily trend ≈ NE-SW. Open fractures trend both parallel and perpendicular to the shear zone and show little alteration along their traces. Feldspar grains away from the shear zone are moderately fractured with little evidence of shear. Microcline grains are subhedral (up to 9 mm) to angular (1.5 mm fragments) with minor recrystallization. Plagioclase grains are moderately altered and fractured, generally anhedral, 1-4 mm in size, and show some bent and perpendicular albite twins. Quartz grains (outside of the vein) occur in fractured aggregates, are subequant to elongate (≈0.5-1 mm in size) and

show undulose extinction to subgrain formation.

Sample 720-1e

* Thin section deformation characteristics:

Foliation (lineation) in this sample is defined by folded and fractured quartz 'boudins' which trend ≈ NW-SE. Open and closed (with primarily very fine-grained quartz) fractures trend both sub-parallel and sub-perpendicular to foliation in this sample from a macroscopically dense fracture/shear zone oriented ≈ 075°/vertical. Quartz grains in the boudins are primarily an- to subhedral, subequant to minor elongate, 0.2-1 mm in size, and exhibit undulose extinction to subgrain formation with sutured boundaries. The matrix (between boudins) consists of very fine-grained quartz and phyllosilicates and angular quartz and highly altered feldspar grains up to 2.5 mm in maximum dimension. The vertical thin section shows the boudins to be very discontinuous or broken up.

Traverse Point G

Sample 721-1a

* Thin section deformation characteristics:

Feldspars: Microcline grains are moderately fractured, an- to subhedral, and range in size from 11 mm down to 1 mm fragments. Plagioclase grains are moderately altered, an- to subhedral, and range in size from 3 to << 1 mm. Bent and perpendicular albite twins were observed.

Quartz occurs primarily as irregular to elongate aggregates (≈8 mm in maximum dimension) of 0.5-1 mm grains and shows minor undulose extinction, subgrain formation, sutured boundaries, and polygonization. The aggregate areas appear to be molded around the more equant feldspars. Quartz grains outside of the aggregates are anhedral, up to 3 mm in size, and show undulose extinction.

Sample 721-1b

* Thin section deformation characteristics:

This sample contains numerous fractures and shear fractures (zones of granulation).

Feldspars: Microcline grains are very fractured and veined. Veins contain very fine-grained quartz and phyllosilicates. Sizes range from 15 mm (subhedral grains) to 1 mm (angular fragments). Plagioclase grains are moderately altered and generally fractured to form 0.8 to 4 mm angular fragments. Some perpendicular albite twins were observed.

Quartz grains are generally moderately fractured, anhedral, and show undulose extinction. Sizes range up to 4 mm but average ≈ 0.5-1 mm. Minor subgrain formation was also observed. The grains primarily occur in rounded to elongate to irregular aggregates 5-7 mm in maximum dimension.

Traverse Point H

Sample 721-2a

* Thin section deformation characteristics:

Feldspars: Microcline grains are primarily subhedral, 4-13 mm in size, moderately fractured, and show minor alteration and/or recrystallization at grain/fragment edges. Fragments range in size down

to 1 mm. Plagioclase grains are highly altered and 2-3 mm in maximum dimension.

Quartz occurs primarily as 2.5 mm aggregates of $\leq$ 1 mm grains with minor undulose extinction, subgrain formation with sutured boundaries, and polygonization. Some 'molding' of these aggregates around the more equant feldspars is apparent.

Sample 822-1

* Thin section deformation characteristics:

Feldspars: Microcline occurs as moderately fractured, sub- to anhedral grains, 3 - 7 mm in size. Angular fragments range down to $\approx$ 0.6 mm. Plagioclase grains generally are altered, subhedral, and range in size from 0.5-4 mm.

Quartz grains range in size from 4 mm down to < 1 mm and are generally anhedral, moderately fractured, and show undulose extinction. Minor healed intergranular fractures (in quartz, but expressed as linear concentrations of opaques in feldspars) and relatively strain-free polygonal grains are also present.

* X-ray analysis: quartz, plagioclase, microcline, phyllosilicates?

* Point-count (240 points): quartz (38.8%), microcline (30.4%), plagioclase (9.2%), unidentified feldspar (12.9%), very fine-grained with high birefringence (2.1%), biotite? (4.2%), opaques (1.7%)

Traverse Point I

Sample 721-3a

* Thin section deformation characteristics:

Feldspars: Microcline grains are subhedral, 2.5-6.5 mm, and moderately fractured with minor recrystallization on edges. Plagioclase grains are moderately fractured, generally anhedral and altered and range from 1-3 mm in size.

Quartz grains are very similar to those described in sample 721-2a (Traverse Point H) and occur in $\approx$ 4 mm rounded to elongate 'pods' as aggregates of 0.18-0.5 mm grains with undulose extinction.

Sample 721-3b

* Thin section deformation characteristics:

Feldspars: Microcline occurs as 2-13 mm, moderately fractured, subhedral grains. Fractures are open or contain quartz and have reddish opaque linings. Plagioclase grains are an- to subhedral, 0.3 to 2.5 mm, moderately fractured, and show minor alteration.

Quartz grains are primarily anhedral, 0.25-1 mm in size, and show undulose extinction to subgrain formation with sutured boundaries to minor polygonization. The grains are generally present in moderately fractured, rounded aggregates approximately 5 mm in maximum dimension.

APPENDIX E. GRID AREA SAMPLES: COMPOSITION AND THIN SECTION DEFORMATION DATA

Appendix E summarizes the results of optical (microscopic) and XRD analyses of Grid Area samples. Individual minerals are described with respect to their deformation characteristics, appearances, and abundances. In general, potassium feldspar is represented by microcline with tartan twinning. Plagioclase grains are primarily altered and exhibit albite twinning.

Gridpoint 1

Sample 82-3a

* Thin section deformation characteristics:

Overall, this thin section has a framework of feldspars in a quartz matrix with few through-going fractures.

Feldspar grains are generally subangular to subrounded and frequently show recrystallization, especially at contacts and often associated with chlorite(?) and opaques. Microcline grains are sub- to anhedral, 2-15 mm, and are moderately fractured. Some grains are relatively unaltered while some show recrystallization. Plagioclase grains are an- to subhedral, 2-3 mm, and show minor alteration (sericitization?), fractures, grain-scale faults, and minor recrystallization.

Quartz grains are primarily recrystallized. Largest grains are ≈ 0.2 mm but they are generally much smaller.

Sample 82-3b

* X-ray analysis: quartz, chlorite

Sample 82-3c

* Thin section deformation characteristics:

A prominent ≈ E-W vein/shear fracture in this sample records ≥ 2 events.

Feldspar: Microcline grains are sub- to anhedral, 2-8 mm, and relatively unaltered with some intragranular fracturing. Minor recrystallization is evident on some grain edges. Plagioclase is primarily altered (sericitized?), sub- to anhedral, and 1-4 mm. Perpendicular albite twins were observed.

Quartz grains are primarily anhedral and < 1 mm, although they range in size up to 2 mm, and show undulose extinction to deformation banding. Minor subgrain formation, polygonization, and suturing were also observed. The 0.35-0.71 mm quartz grains generally occur in subequant to elongate to irregular aggregates 5-6 mm in maximum dimension.

Gridpoint 2

Sample 829-1

* Thin section deformation characteristics:

This sample is very similar to 82-3c described above.

Feldspars: Microcline grains are sub- to anhedral, 3-11 mm, and are relatively unaltered. Minor recrystallization on grain boundaries and intragranular fractures were observed. Plagioclase grains are primarily

altered (sericitized?), an- to subhedral, and 2-6 mm in size.

Quartz grains are mainly anhedral and range in size from 0.1-2 mm (average ≈ 0.2 mm). Undulose extinction, deformation banding, and some subgrain formation and polygonization were observed. Larger grains generally showed less recovery (primarily undulose extinction). The grains generally occur in moderately fractured, irregularly shaped aggregates ≈ 2-5 mm in size.

Gridpoint 3

Sample 81-1a

* Thin section deformation characteristics:

Feldspar: Microcline grains are primarily anhedral (subangular to subrounded) and range in size from 1 to 9 mm. Minor recrystallization (and subgrain formation?) was observed at grain boundaries. Plagioclase grains are sub- to anhedral (sub-rounded to sub-angular), range in size from 2-10 mm (average ≈ 3-4 mm), and are primarily altered (sericitized?).

Quartz grains generally occur in aggregates, range in size from 0.1-4 mm (most ≈ 0.5-1 mm) and are mainly anhedral. Larger grains show undulose extinction and subgrain formation while the smaller grains exhibit undulose extinction and minor polygonization.

Sample 81-1b1

* X-ray analysis: quartz, hematite, plagioclase, kaolinite?, chlorite?

Sample 81-1b2

* Thin section deformation characteristics:

Overall, this sample is very fine-grained compared to sample 81-1a and consists primarily of angular fragments (cemented clasts?). One foliated clast and fragments of recrystallized quartz are visible in thin section. Grain sizes were generally between 1 mm and 62 microns. In the vertical section, both steep anastomosing and subhorizontal fracture/shear zones were visible.

Feldspar: No microcline was observed. Plagioclase grains are primarily unaltered and range from 0.1 to 1 mm in size. Perpendicular albite twins were observed.

Quartz grains are primarily angular to subangular and very fine-grained (average < 1 mm), although some grains up to 2 mm were observed (possibly from irregular or deformed veins). Much recrystallization was evident in the matrix. Larger grains show some polygonization with recrystallization at their edges.

Gridpoint 4

Sample 713-1

* Thin section deformation characteristics:

Overall, this sample appears to be a more deformed 'version' of sample 81-2a (below). Angular feldspar fragments, more narrow and regular banding, and very few to no regular, open fractures are present. The fabric is approximately parallel to measured outcrop orientations. The vertical section shows vertical to steeply S-SW dipping zones with approximately parallel elongated quartz grains (in aggregates) and feldspar fragments. Altered feldspars are less recognizable as grains (more flattened) than in 81-2a. Chlorite- and opaque-rich zones help to

define the foliation.

Feldspar: Microcline grains show much fracturing and recrystallization. Grains range in size up to 3 mm but most are $\leq$ 0.2 mm. Plagioclase grains show much alteration and grain-size reduction. Largest grains are 3 mm in maximum dimension but most are much smaller.

Quartz grains show undulose extinction, subgrain formation, and recrystallization. Largest grains are elongate, $\approx$ 1-2 mm (vein quartz?), with undulose extinction, subgrain formation, and suturing but most are smaller. Quartz aggregates are more strung out than in 81-2a with dimensions of $\approx$ 1-3 mm wide by 19 mm long.

* X-ray analysis: quartz, plagioclase, microcline, illite/micas, chlorite (up to 11%)

Sample 81-2a

* Thin section deformation characteristics:

Overall, this sample appears to be a foliated cataclasite from the angularity and range of grain sizes and the crude segregation of quartz grains into bands (former veins?). The horizontal section shows a lineation of $\approx$ 120° while the vertical section shows vertical to steeply S-SW dipping zones.

Feldspar grains are densely fractured (and rotated?) to form rounded to angular fragments. Microcline grains are primarily angular fragments and show grain-size reduction (largest fragments $\approx$ 4 mm), but some subgrain formation and recrystallization especially at grain boundaries and along fractures were also observed. Recrystallized quartz appears to be abundant in microcline fractures. Plagioclase grains are primarily fractured and sericitized (largest grains $\approx$ 3-3.5 mm) but some subgrain formation and recrystallization along fractures were also observed. Grains which appear to have been almost completely altered to very fine-grained (< 62 microns) material also appear to have been 'mashed-out' sub-parallel to the bands of quartz.

Quartz grains show a wide size-range. Largest grains appear to be (late-stage) vein quartz (1.5 mm). These grains are sub- to anhedral and exhibit undulose extinction and moderate fracturing. Quartz grains are primarily in elongate aggregates 0.5-3 mm wide by 19 mm long. These subequant grains mainly show undulose extinction with minor polygonization and range from 0.088-0.71 mm (average $\approx$ 0.25 mm) in size. Very fine-grained (< 62 micron) recrystallized quartz grains are also present in the finer-grained folia.

* X-ray analysis: quartz, plagioclase, microcline, chlorite?, illite/micas?

Sample 81-2b

* Thin section deformation characteristics:

This sample appears to be a more deformed version of sample 713-1 (above) with extreme grain-size reduction. The thin sections show foliation orientation to be $\approx$ 120° with a vertical to steep N-NE dip. Quartz aggregates are elongate but discontinuous, with the largest measuring 1x5 mm. Grains in the aggregates range in size from 0.18-0.35 mm and are more subequant, polygonal, and relatively strain-free than those in 713-1. The largest grains are possibly remnant vein quartz (0.3

mm) but these are rare. Grains in the matrix are << 62 microns in size. There are few/no regular or open fractures.

* X-ray analysis (random mount): quartz, plagioclase?, phyllosilicates?

Gridpoint 5

Sample 727-3c1

* Thin section deformation characteristics:

Feldspar: Microcline grains are moderately fractured, sub- to anhedral (angular), range in size from 2-20 mm (average ≈ 5 mm), and show minor undulose extinction and recrystallization at edges. Intragranular fractures are both open and quartz-filled. Plagioclase grains are fractured and rotated, subangular to subrounded, altered -mainly sericitized(?), and average ≈ 3 mm in size (range 2-5 mm). Perpendicular albite twins were observed.

Quartz grains are primarily anhedral and show a range of deformation from undulose extinction to deformation banding to subgrain formation and edge suturing. They occur mainly in moderately fractured, irregularly shaped aggregates up to 5 mm in maximum dimension. Individual grains range up to 4 mm in size but are usually 0.25-1 mm.

* X-ray analysis: (unoriented) quartz, microcline, others?

* Point-count (232 pts): quartz (22.0%), microcline (48.7%), plagioclase (20.7%), unidentified feldspar (4.3%), chlorite (3.0%), open (0.9%), biotite?

Sample 727-3c2

* X-ray analysis: quartz, plagioclase, chlorite, illite/micas?

Sample 727-3d

* Thin section deformation characteristics:

Dense fractures, shear fractures, and zones of granulation can be seen in the thin sections with orientations of ≈ 100°/vertical (to steep S dip). Opaque minerals and minor chlorite outline the edges of the shear zones.

Feldspar: Microcline grains show large (moderate to dense) fracturing with quartz filling and no offset. The primarily angular fragments range in size from 0.2 to 6 mm and average ≈ 2 mm. Plagioclase grains are also moderately to densely fractured with some offsets of albite twins (as well as perpendicular twins) visible. Highly birefringent very fine-grained material generally decorates the fractures and the grains themselves show only minor to negligible alteration. The angular fragments range in size from 1-3 mm with most ≈ 1 mm.

Vein quartz grains range up to 10 mm in size, show little deformation, and are sub- to euhedral. 'Original' quartz grains are primarily angular fragments ≈ 1 mm in size and mainly show undulose extinction. Very fine-grained quartz (≈ 62 microns) is abundant and possibly recrystallized.

≈5 (just south of 5)

Sample 824-2a

* Thin section deformation characteristics:

Cross-cutting zones of granulation were observed in this sample. The zones strike ≈ 015° and most dip moderately south, although a few dip moderately to the north. Grain sizes in these zones ranged from 1 mm to < 62 microns. Zones of elongate quartz grains (≈015°) were also observed. The (0.5-1 mm) grains showed strong undulose extinction to deformation banding, and most had sutured boundaries.

Feldspar grains are primarily angular and < 1 mm in size. Recognizable plagioclase fragments are sericitized.

Quartz grains primarily show undulose extinction to deformation banding. Some subgrain formation and edge suturing were also observed.

* X-ray analysis: quartz, plagioclase, chlorite (up to 13%)

Gridpoint 6

Sample 824-1a

* Thin section deformation characteristics:

This sample is a mylonite or a foliated cataclasite. Deformation descriptions are very similar to those given below for 824-1c. Foliation dips primarily steeply to the south.

Sample 824-1b

* Thin section deformation characteristics:

This sample consists primarily of fine-grained (minor coarse-grained) quartz with characteristics similar to those described below for 824-1c. Foliation is approximately vertical. Late-stage calcite veins are also present.

Sample 824-1c

* Thin section deformation characteristics:

Most deformation zones (and the more coarse-grained elongate quartz) in this sample are vertical to steeply dipping. Some conjugate zones are present but most zones and grains have an orientation of ≈ 120°.

Plagioclase is present as fine grains (≤ 1 mm) in minor amounts. Kinked albite twins and undulose extinction were observed.

The sample consists primarily of 'vein' (≈ 10% up to 2 mm) and matrix (≈ 62-125 micron) quartz. The larger grains are anhedral to angular and elongate. They show primarily undulose extinction and deformation banding with recrystallization at grain edges. The smaller recrystallized grains are generally subequant and show strain-free polygonization. Some subgrain formation and elongate grains with sutured boundaries and a 138° lineation were also observed.

Gridpoint 7

Sample 823-2b

* Thin section deformation characteristics:

This sample is a relatively undeformed, fine- to medium-grained, equigranular granite.

Feldspars: Microcline grains are generally subequant and an- to subhedral, range in size up to 5 mm (average 1-2 mm), and show minor recrystallization at edges. Plagioclase grains are generally subequant,

sericitized(?), and range in size from 1-2 mm.

Quartz grains primarily show undulose extinction and are subequant (0.5-1 mm) and anhedral. Deformation banding and subgrain formation with suturing were present to a lesser degree. The grains generally occur in irregularly shaped aggregates up to 3 mm in maximum dimension.

* X-ray analysis: quartz, plagioclase, microcline, chlorite (minor)

* Point-count (225 points): quartz (41.4%), microcline (35.1%), plagioclase (13.8%), unidentified feldspar (2.7%), chlorite? (3.1%), unidentified(4.0%)

Gridpoint 8

Sample 823-1

* Thin section deformation characteristics:

Feldspar: Microcline grains are primarily subhedral, unaltered, and have intragranular fractures with minor recrystallization. Grain (and fragment) sizes range from 1-12 mm and average ≈ 4 mm. Plagioclase grains are generally altered, anhedral, and average ≈ 2 mm in size. Perpendicular albite twins were observed.

Quartz grains are mainly anhedral, show primarily undulose extinction with some deformation banding and subgrain formation. They generally occur in moderately fractured, irregularly shaped aggregates up to 5 mm in maximum dimension. Grains average ≈ 1 mm (0.125-2 mm) in size within the aggregates.

* X-ray analysis: quartz, microcline, plagioclase, biotite?

Gridpoint 11

Sample 725-2

* Thin section deformation characteristics:

Most grains in this sample ranged in size from 1-3 mm, showed recrystallization at grain boundaries, and were angular to subrounded in shape. The vertical and horizontal thin sections showed numerous (moderate to dense) intergranular fractures (many open) of diverse orientations.

Feldspar: Microcline grains primarily showed recrystallization (at grain boundaries and in fractures) and undulose extinction. Plagioclase grains were generally altered and fractured but also showed undulose extinction and bent albite twins.

Quartz generally was present as moderately to densely fractured, irregularly to rounded-shaped aggregates 4-5 mm in maximum dimension. Individual grains showed undulose extinction to subgrain formation with sutured boundaries and minor polygonization. They ranged in size from 0.25-0.71 mm.

Gridpoint 12

Sample 721-4c

* Thin section deformation characteristics:

Moderate to dense fractures in this sample were open, quartz-filled, or filled with angular fragments, opaque minerals, and very fine-grained material.

Feldspar: Microcline grains (and fragments) range in size from $\leq$ 1 mm up to 10 mm and show some undulose extinction and subgrain formation.

Plagioclase grains (and fragments) are moderately altered and range in size from ≈ 1-2 mm down to 0.088 mm.

Quartz grains (outside the breccia zone) primarily show undulose extinction to subgrain formation with suturing. The anhedral and subequant to elongate (0.35-0.71 mm) grains generally occur in moderately fractured, irregular aggregates up to 4 mm in maximum dimension.

Sample 725-1a

* X-ray analysis: hematite, quartz, microcline?, plagioclase?

Sample 725-1d

* Thin section deformation characteristics:

Fractures in this sample are moderate to dense, primarily open, and show phyllosilicate development along their traces.

Feldspar: Microcline grains show undulose extinction and many intragranular fractures. They are angular to rounded in shape and range in size from 1-12 mm. Plagioclase was not recognized in this sample, possibly due to complete alteration.

Quartz grains are generally anhedral, 0.25-0.71 mm, and show undulose extinction and deformation banding to subgrain formation with sutured boundaries and minor polygonization. The grains generally occur in moderately fractured, irregularly shaped aggregates, ≈ 5 mm in maximum dimension.

* X-ray analysis: quartz, kaolinite, illite/micas

≈12(Flathead Sandstone southwest of 12 near shallow-dipping contact)

Samples 624-4a,-4c

* Thin section deformation characteristics:

These samples consist primarily of subangular to rounded, < 0.5 mm quartz grains. The clasts generally show low deformation exhibited by minor undulose extinction. Both vertical and horizontal fractures were visible in thin section.

Gridpoint 14

Sample 82-2b

* Thin section deformation characteristics:

This sample consists primarily of a vertical shear zone but both vertical and subhorizontal open fractures are also present.

Feldspar: Microcline fragments are generally angular to subangular, show undulose extinction and minor recrystallization, and range from ≤ 0.25 up to 2 mm in size. Plagioclase fragments are generally unaltered, show undulose extinction, minor recrystallization, bent and perpendicular albite twins, and range from ≤ 0.18 up to 2 mm in size.

Quartz grains exhibit undulose extinction to subgrain formation and apparent recrystallization in the smaller grains. Sizes range from ≈ 1 mm to < 62 microns.

Sample 82-2c

* Thin section deformation characteristics:

Overall, this sample shows brittle deformation with dense fractures, numerous grain-scale faults, and granulation (but to a lesser extent than

in 82-2b). The vertical section shows several subhorizontal fractures.

Feldspar: Average grain size is ≈ 1 mm but microcline fragments range up to 6 mm. Plagioclase grains are relatively unaltered, angular with undulose extinction, and show kinked albite twins. Grain-scale faults were also evident from offsets of albite twins.

Quartz grains ranged from 2 mm to very fine-grained and generally showed undulose extinction to subgrain formation with recrystallization at grain edges.

Gridpoint 15

Sample 82-1a

* X-ray analysis: quartz, plagioclase, microcline?, phyllosilicates?

Sample 82-1b

* Thin section deformation characteristics:

This sample shows some evidence of hydrothermal alteration with an epidote (high birefringence - XPL, high relief and almost colorless -PPL) + chlorite (rather dark - XPL, light green to dark green pleochroism) vein, minor disseminated epidote and chlorite, and minor sphene.

Feldspar: Microcline grains were generally anhedral, ranged in size from 1-7 mm, and showed some subgrain formation and recrystallization at grain edges. Plagioclase grains are generally altered, anhedral, and 1-2 mm in size. Kinked albite twins were observed.

Quartz grains generally were ≈ 0.18-1.0 mm in size, anhedral, and showed deformation which ranged from relatively strain-free polygonization to undulose extinction and subgrain formation with sutured grain boundaries. The grains occurred in irregularly shaped to rounded aggregate ≈ 4 mm in maximum dimension.

Gridpoint 16

Sample 81-3a

* Thin section deformation characteristics:

Moderate to dense intergranular fractures in this sample appear to be associated with chlorite and recrystallized very fine-grained material.

Feldspar grains are generally fractured (and rotated?) fragments which appear to have been more resistant compared to quartz grains which have 'flowed' around them and defined a crude foliation. Microcline grains range in size from 1-10 mm, are moderately to densely fractured, and show evidence of some subgrain formation and recrystallization (usually on grain boundaries or in fractures). Most plagioclase grains are altered and range from 1-2 mm in size.

Quartz grains generally occur in irregular to feldspar-conforming aggregates and range in size from 0.35-0.71 mm. Deformation is shown primarily by undulose extinction but subgrain formation and suturing are also present.

Sample 81-3b

* Thin section deformation characteristics:

This sample contains about the best examples of biotite from samples in the study area (with light to dark brown pleochroism). The grains are irregularly shaped and disseminated.

Feldspar: Microcline grains are anhedral, 1-10 mm in size, and show undulose extinction and minor recrystallization. Plagioclase grains are altered, 2-3 mm in size, and show some recrystallization and kinked albite

twins.

Quartz deformation has resulted in primarily undulose extinction and subgrain formation with some polygonization. Most grains are anhedral, range from 0.25-1 mm in size, and occur in irregularly shaped aggregates up to 6 mm in maximum dimension.

* X-ray analysis: quartz, plagioclase, microcline, illite/micas (biotite), kaolinite?

Gridpoint 17

Sample 727-2a

* Thin section deformation characteristics:

Feldspar: Microcline grains are moderately fractured and show some recrystallization on edges and in fractures. Sizes average ≈ 3 mm but range from 1-10 mm. Plagioclase grains are moderately fractured and altered and average 2 mm in size. Perpendicular as well as bent albite twins were observed.

Quartz grains range in size from 0.18 to 0.71 mm and show undulose extinction and deformation bands to subgrain formation with suturing and minor polygonization. The grains generally occur in irregularly shaped aggregates 3-7 mm in size.

Gridpoint 18

Sample 727-1c

* Thin section deformation characteristics:

All grains are moderately fractured. Feldspar grains appear to form a framework of 2-3 mm-sized grains. Microcline grains range in size from 1-7 mm (average ≈ 3 mm), are an- to subhedral, and show some recrystallization, primarily along fractures. Plagioclase grains are primarily altered and range in size from 1-2 mm.

Quartz grains range in size from 2 to 0.25 mm (average ≈ 0.5 mm) and show primarily undulose extinction to minor deformation banding, subgrain formation and polygonization. The grains generally occur in irregularly shaped and moderately fractured aggregates approximately 4 mm in maximum dimension.

Gridpoint 19

Sample 726-3a

* Thin section deformation characteristics:

Feldspar: Microcline grains are anhedral, moderately fractured and show undulose extinction and recrystallization. Average grain size is ≈ 2-3 mm with a 2-11 mm range. Plagioclase grains are generally sericitized(?) and 1-2 mm in size. Perpendicular albite twins and possible recrystallization were observed. Untwinned feldspar grains were generally altered and showed undulose extinction.

Quartz grains generally occurred in elongate to irregularly shaped aggregates ≈ 5 mm in size. Grains were generally anhedral, subequant, ranged from 0.25-0.71 mm in size, and showed undulose extinction to subgrain formation and minor polygonization.

Sample 726-3b

* Thin section deformation characteristics:

This sample is very similar to 726-3a (above).

Feldspar: Microcline grains are primarily ≈ 3 mm in size, fractured, and show undulose extinction. Plagioclase grains are mainly altered, 1-2 mm in size, and show undulose extinction with minor recrystallization at grain edges.

Quartz grains are generally fractured, ≤ 1 mm in size, and show undulose extinction and subgrain formation to recrystallization and polygonization.

Sample 726-3c

* Thin section deformation characteristics:

Generally, feldspars form a framework of 2-3 mm (ranging up to 5-6 mm) subhedral to anhedral, moderately fractured grains with a quartz and biotite matrix. Moderate recrystallization can be seen on grain edges. Untwinned feldspar grains are generally altered and show undulose extinction. Plagioclase grains are 1-2 mm in size, altered and some show undulose extinction as well as bent and perpendicular albite twins.

Aggregates of quartz grains are rounded to elongate and show a greater size range than 726-3a and 726-3b above (≈ 2-7 mm). Grains are primarily 0.18-1 mm and show undulose extinction and subgrain formation to polygonization.

Gridpoint 20

Sample 726-1a

* Thin section deformation characteristics:

Feldspar grains exhibit primarily intragranular fractures but also show intergranular fractures. Microcline grains are anhedral to rounded in appearance, moderately fractured, and range in size from < 0.5 to 5 mm (average ≈ 2 mm). Undulose extinction and recrystallization at grain edges were observed. Plagioclase grains are mainly altered and subrounded, range in size from 2-4 mm, and show minor subgrain formation and recrystallization at grain boundaries. Perpendicular albite twins were observed.

Quartz occurs mainly as irregularly shaped grain aggregates 2-5 mm in maximum dimension. The aggregates were seen to 'conform' to/around feldspar grains in places. The grains generally showed undulose extinction (with minor deformation banding) but subgrain formation and edge suturing were also prominent. Polygonization was observed but was minor. The grains were primarily anhedral and ranged in size from 0.18-0.71 mm in size.

≈20

Sample 726-2

* X-ray analysis: quartz, plagioclase, chlorite

APPENDIX F. TRAVERSE AREA: RESULTS OF FRACTURE ORIENTATION AND DENSITY ANALYSES

Appendix F graphically presents the results of fracture orientation and density analyses for the Traverse Area at the various scales of observation. Data from individual and combined sampling points are given.

Abbreviations used:

TS	= thin section
HD, Hi-defm	= high deformation
LD, Lo-defm	= low deformation

For some density graphs, the numbers in parentheses on top of the columns refer to the number of observations (or fractures) represented by that particular column. Apparent discrepancies between numbers (of observations) on graphs (rose diagrams and density) and those shown on the photonegatives (Appendix H) result from some fractures being used for orientation analyses that were prominent in thin section but were outside of the area photographed. Also, fractures observed on vertical outcrop faces were not included in outcrop density calculations.

TRAVERSE PT A
(Outcrop Fractures)
N=15:130-140=33%;
30-40,60-70=20%

TRAVERSE PT B
(Outcrop Fractures)
N=25:10-20=36%,
70-80=32%

TRAVERSE PT C
(Outcrop Fractures)
N=41:0-10=46%

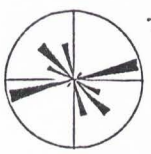

TRAVERSE PT D
(Outcrop Fractures)
N=19:70-80=37%,
130-140=25%

TRAVERSE PTS (A-D,F)
(Parallel to Fold Axis)
(Outcrop Fractures)
N=149:130-140=20%

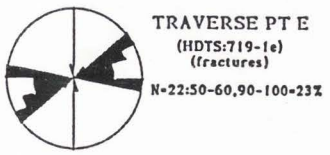
TRAVERSE PT E
(HDTS:719-1e)
(fractures)
N=22:50-60,90-100=23%


TRAVERSE PT E
(TS quartz fractures,HI-defm)
N=25: 80-90=16%

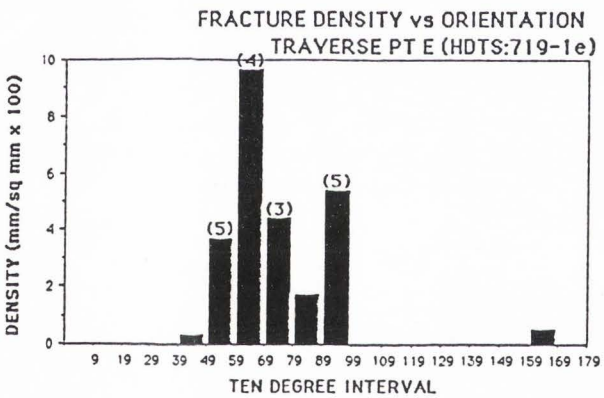
FRACTURE DENSITY vs ORIENTATION
TRAVERSE PT E (HDTS:719-1e)
DENSITY (mm/sq mm x 100)
TEN DEGREE INTERVAL
9 19 29 39 49 59 69 79 89 99 109 119 129 139 149 159 169 179
(4)
(5)
(3)
(5)

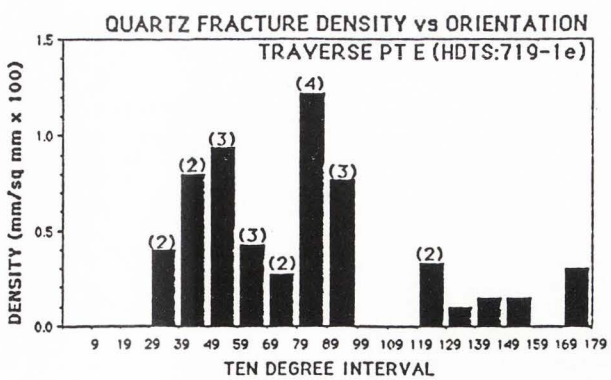
QUARTZ FRACTURE DENSITY vs ORIENTATION
TRAVERSE PT E (HDTS:719-1e)
DENSITY (mm/sq mm x 100)
TEN DEGREE INTERVAL
9 19 29 39 49 59 69 79 89 99 109 119 129 139 149 159 169 179
(2)
(2)
(3)
(3)
(2)
(4)
(3)
(2)

TRAVERSE PT F
(HD+LD TS fractures)
N=53:40-50=22%

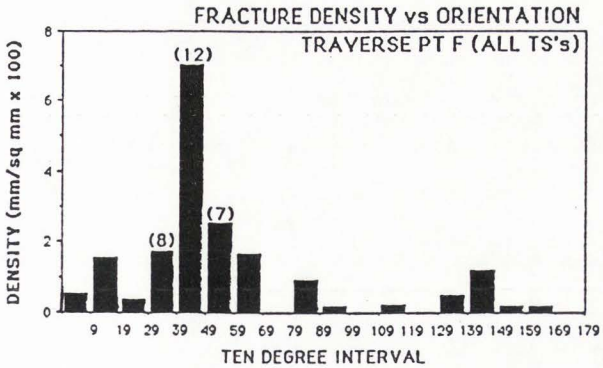

TRAVERSE PT F
(TS quartz fractures - all)
N=54: 50-60=18%

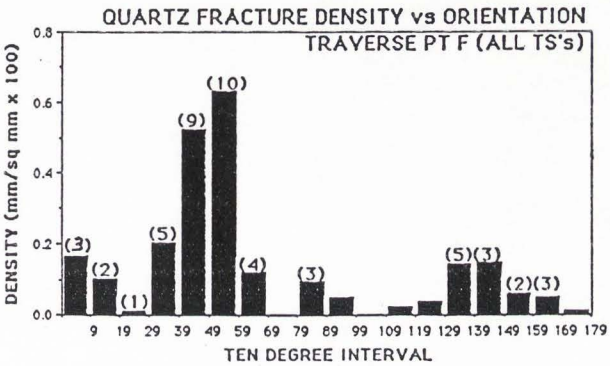

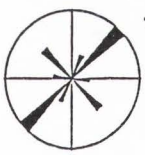

TRAVERSE PT F
(Outcrop Fractures)
N=49:40-50=45%,
130-140=27%

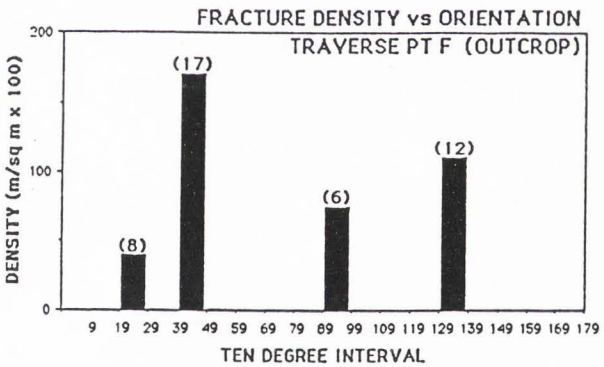

TRAVERSE PT F
(LDTS:720-1a)
(fractures)
N=24:20-30,30-40,
50-60,60-70,140-150=13%

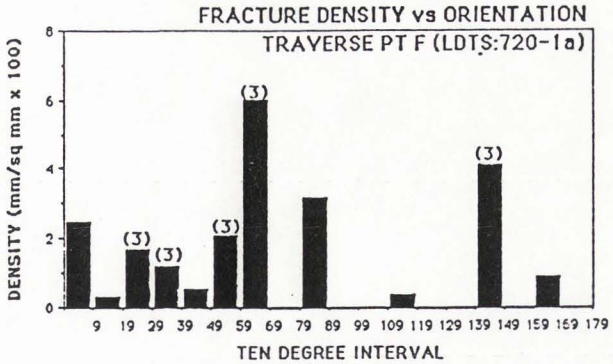

TRAVERSE PT F
(HDTS:720-1dh)
(fractures)
N=29:40-50=34%

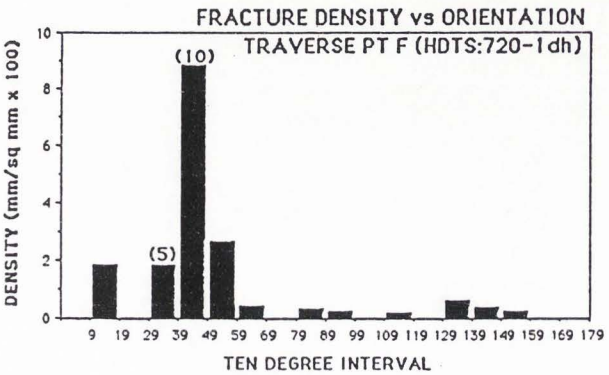

TRAVERSE PT F
(TS quartz fractures,Lo-defm)
N=31: 50-60,60-70,
130-140=12%

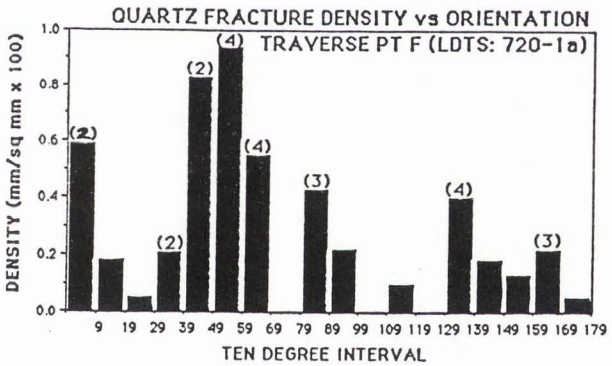

TRAVERSE PT F
(TS quartz fractures,Hi-defm)
N=23: 40-50=30%

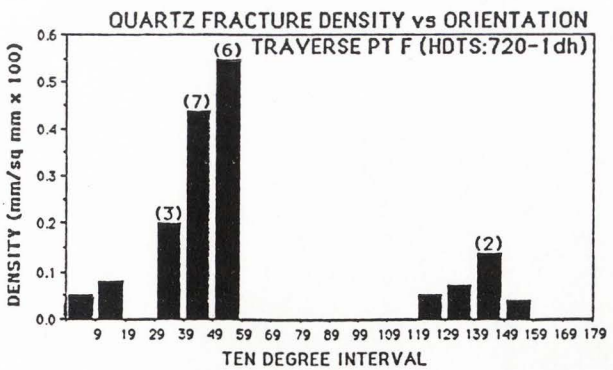

TRAVERSE PT G
(HD+LD TS fractures)
N=31:20-30,160-170=16%

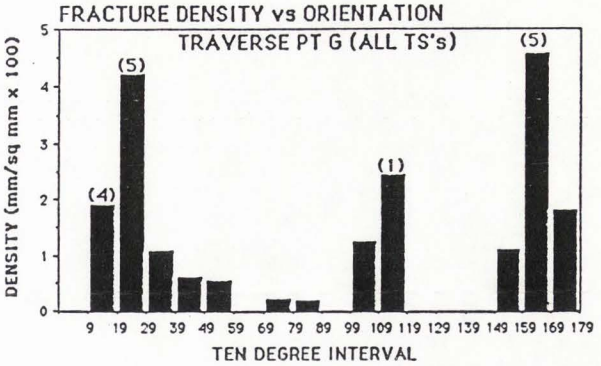

TRAVERSE PT G
(TS quartz fractures - all)
N=88: 160-170=18%

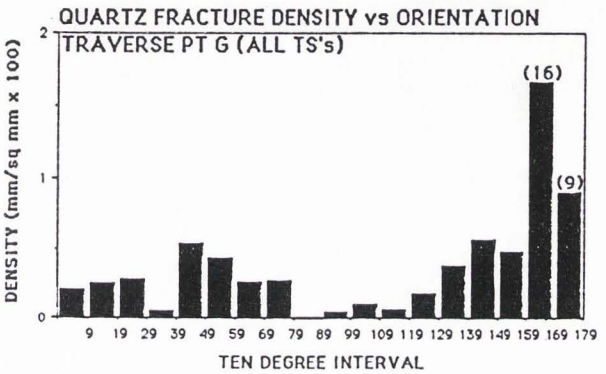

TRAVERSE PT G
(Outcrop Fractures)
N=28:30-40=39%,
170-180=36%

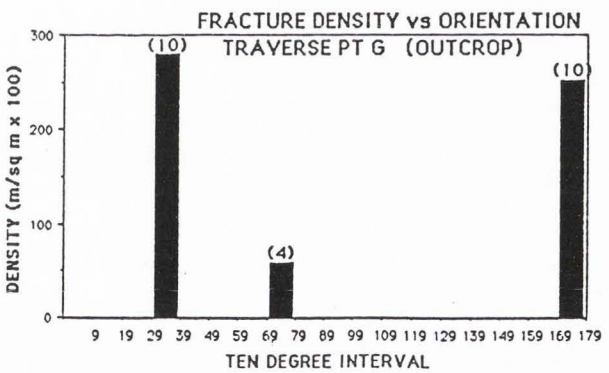

TRAVERSE PT G
(LDTS:721-1b)
(fractures)
N=14:160-170=36%

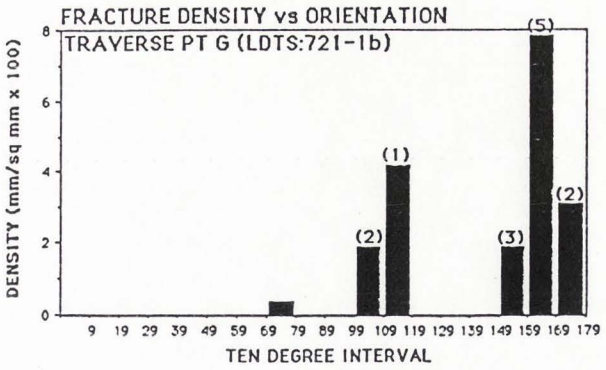

TRAVERSE PT G
(HDTS:721-1a)
(fractures)
N=17:20-30=29%

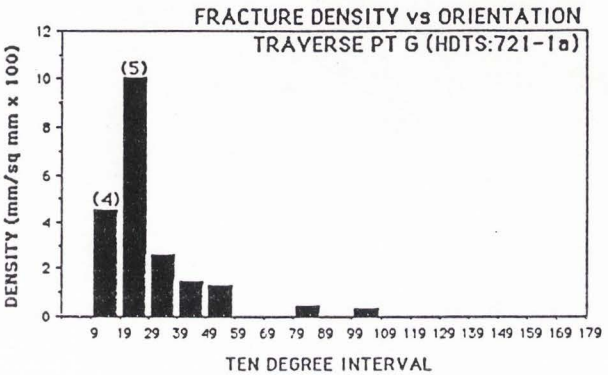

TRAVERSE PT G
(TS quartz fractures,Lo-defm)
N=42: 160-170=26%

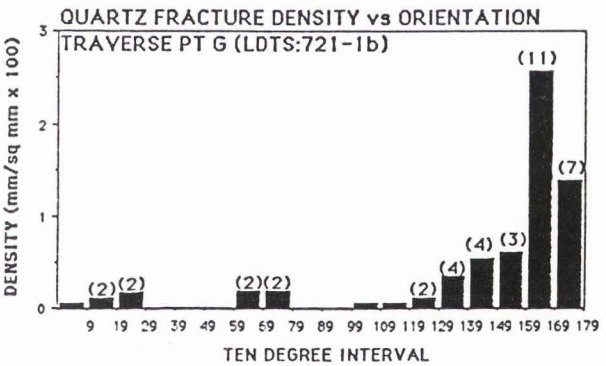

TRAVERSE PT G
(TS quartz fractures,HI-defm)
N=46: 50-60,140-150,
160-170=10%

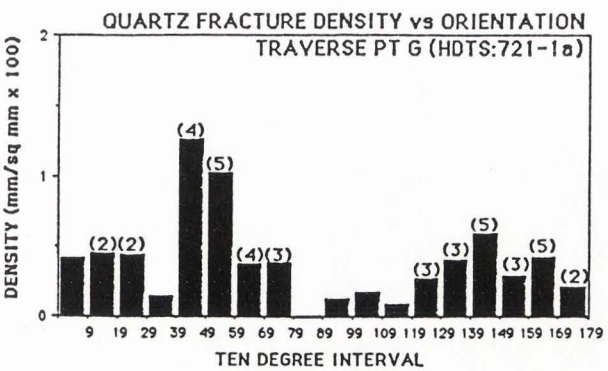

TRAVERSE PT H
(HD+LD TS fractures)
N=18:50-60=34%

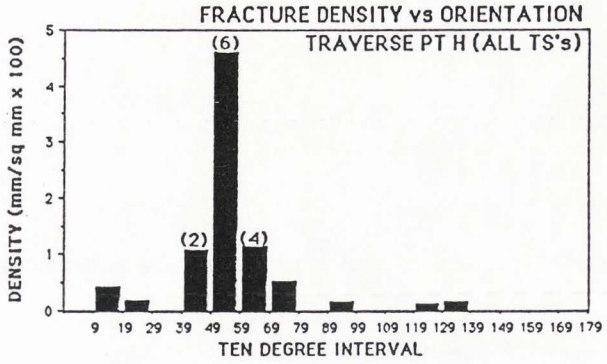

TRAVERSE PT H
(TS quartz fractures - all)
N=109: 30-40,40-50,
100-110=10%

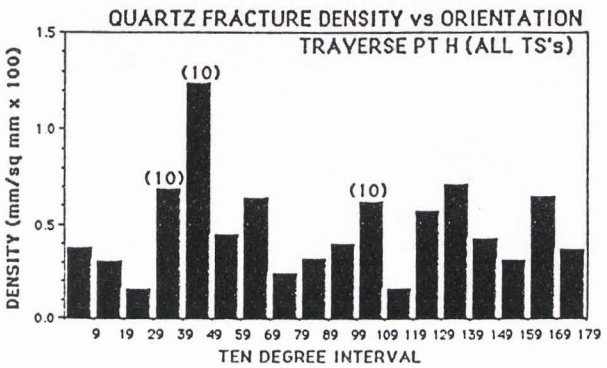

TRAVERSE PT H
(Outcrop Fractures)
N=45: [illegible]-60%

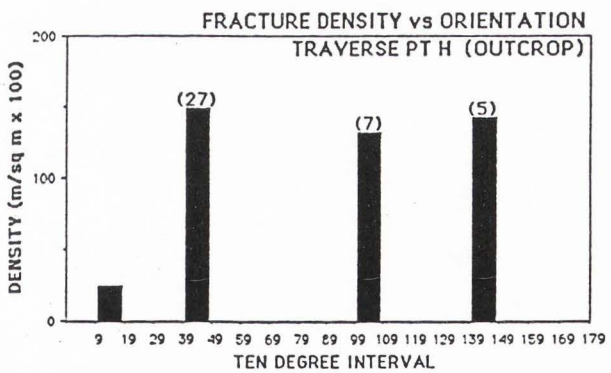

TRAVERSE PT H
(LDTS:822-1)
(fractures)
N=8:40-50,50-60,=25%

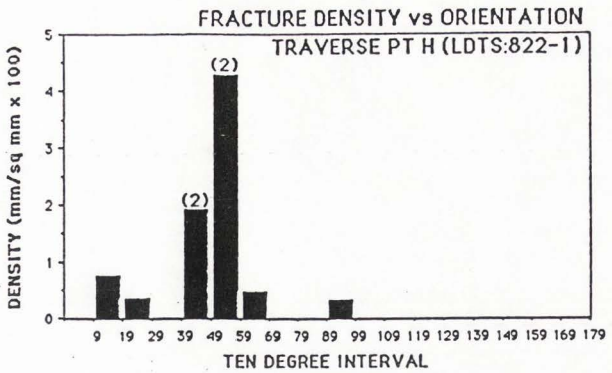

TRAVERSE PT H
(HDTS:721-2a)
(fractures)
N=10:50-60=40%

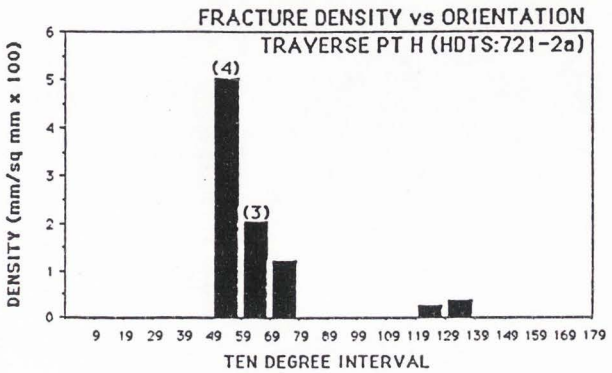

TRAVERSE PT H
(TS quartz fractures,Lo-defm)
N=50: 90-100,120-130,
160-170=10%

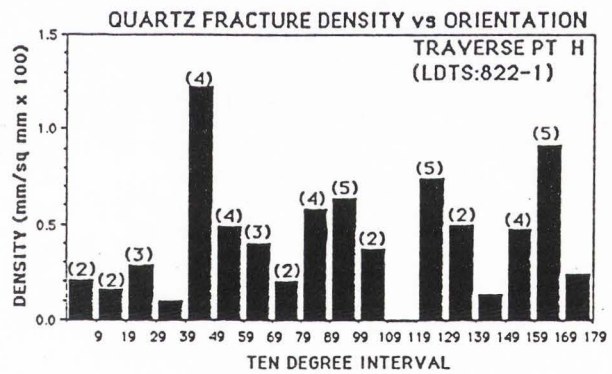

TRAVERSE PT H
(TS quartz fractures,Hi-defm)
N=59: 30-40=16%

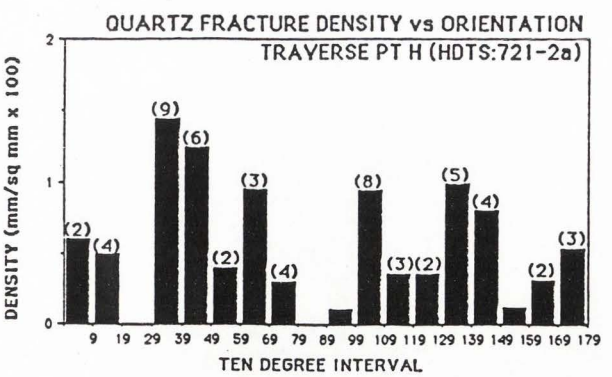

TRAVERSE PT I
(HD+LD TS fractures)
N=31:10-20-22%

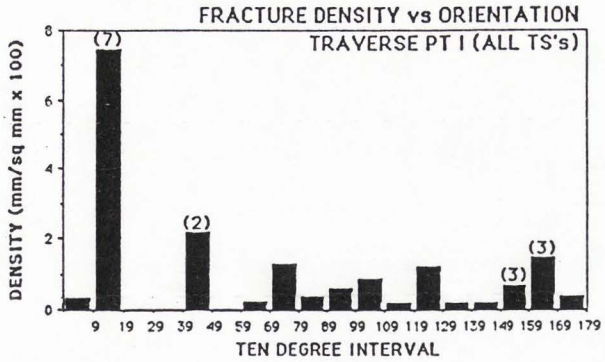

TRAVERSE PT I
(All TS quartz fractures)
N=92: 10-20-20%

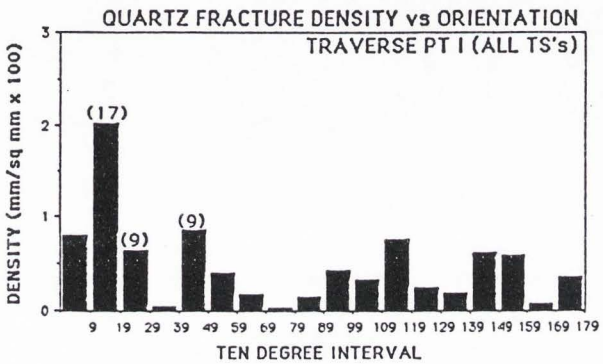

TRAVERSE PT I
(Outcrop Fractures)
N=43:80-90-33%,
10-20-26%

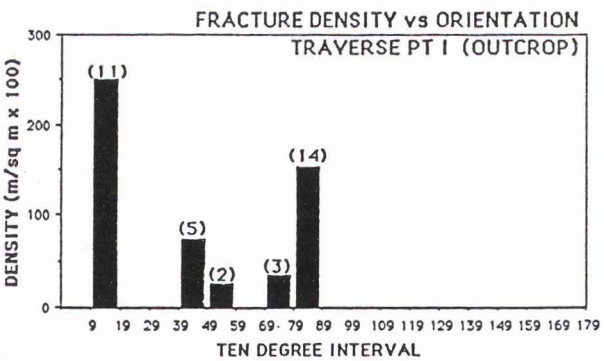

TRAVERSE PT I
(LDTS:721-3b)
(fractures)
N=18:130-160,
160-170=17%

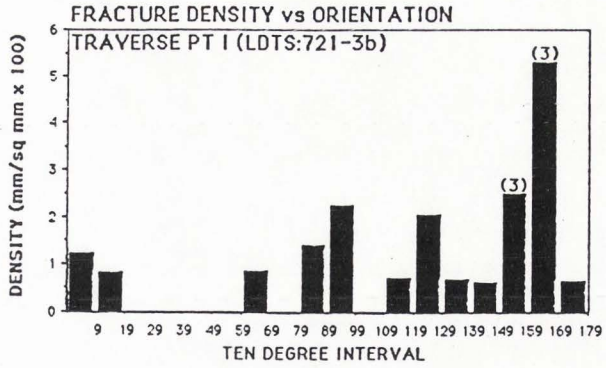

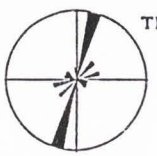

TRAVERSE PT I
(HDTS:721-3a)
(fractures)
N=13:10-20=46%

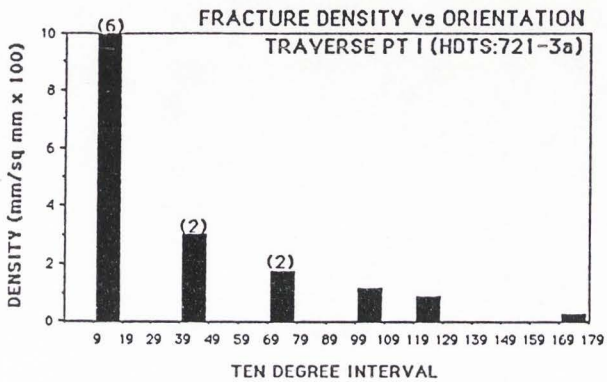

TRAVERSE PT I
(TS quartz fractures,Lo-defm)
N=33: 10-20=18%

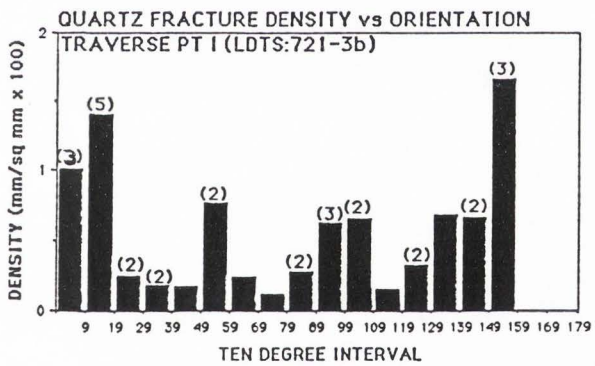

TRAVERSE PT I
(TS quartz fractures,Hi-defm)
N=59: 10-20=20%

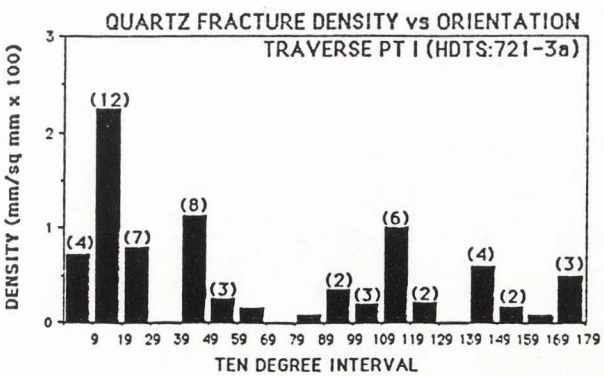

TRAVERSE PTS E-I
(HI-defm TS's,all fracture data)
N=91:40-50,50-60=16%

N=23: 40-50=30%

HI-DEFORMATION TS'S (E-I)
OPEN FRACTURE DATA

N=68: 50-60=16%

HI-DEFORMATION TS'S (E-I)
VEIN, CLOSED FRACTURE DATA

TRAVERSE PTS F-I
(All LDTS Fracture data)
N=64:160-170=16%

ALL TRAVERSE TS's
(E-I)
(HD+LD,fractures)
N=155:50-60=13%,40-50=12%
40-60=25%

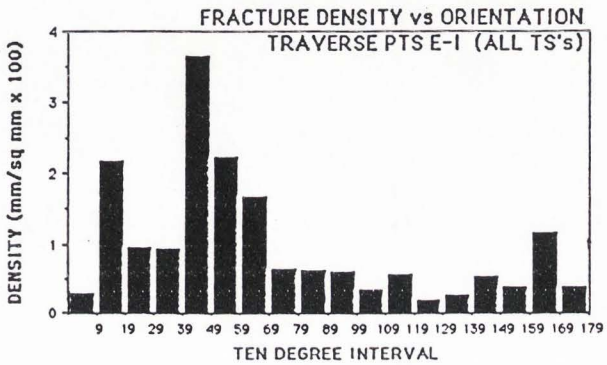

TRAVERSE PTS E-I
(TS quartz fractures - all)
N=368: 40-50=10%

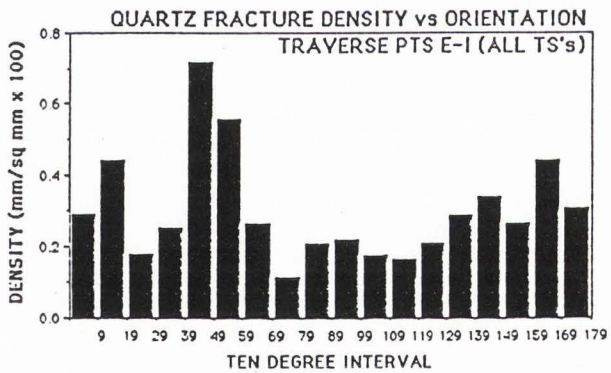

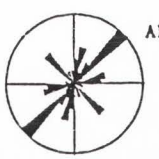

ALL TRAVERSE PTS
(A-I)
(OUTCROP DATA)
N=265: 40-50=20%

TRAVERSE PTS F-I
(Perpendicular to Fold Axis)
(Outcrop Fractures)
N=165:40-50=16%

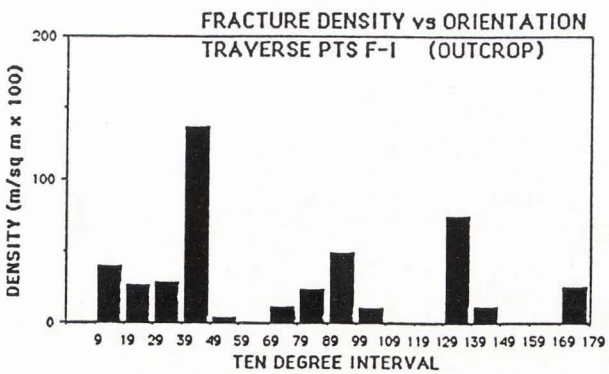

APPENDIX G. GRID AREA: RESULTS OF FRACTURE ORIENTATION AND DENSITY ANALYSES

Appendix G graphically presents the results of fracture orientation and density analyses for the Traverse Area at the various scales of observation. Data from individual and combined sampling points are given.

Abbreviations used:

TS	= thin section
HD, Hi-defm	= high deformation
LD, Lo-defm	= low deformation

For some density graphs, the numbers in parentheses on top of the columns refer to the number of observations (or fractures) represented by that particular column. Apparent discrepancies between numbers (of observations) on graphs (rose diagrams and density) and those shown on the photonegatives (Appendix I) result from some fractures being used for orientation analyses that were prominent in thin section but were outside of the area photographed. Also, fractures observed on vertical outcrop faces were not included in outcrop density calculations.

GRIDPT 1 (TS:82-3a)
(Lo-defm,closed fractures)
N=17: 150-160=36%

GRIDPT 1 (TS:82-3a)
(Lo-defm,open+closed fractures)
N=20: 150-160=35%

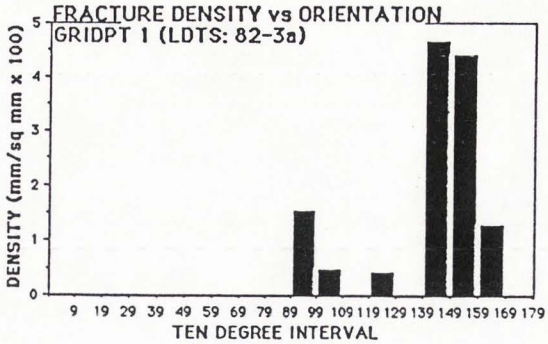

GRIDPT 1 (TS:82-3c)
Hi-defm,open fractures)
N=6: 10-20,20-30,40-50,
80-90,100-110,150-160=16%

GRIDPT 1 (TS:82-3c)
(closed+open fractures)
N=20: 100-110=25%

GRIDPT 1 (TS:82-3c)
(Hi-defm,closed fractures)
N=14: 100-110,110-120=28%

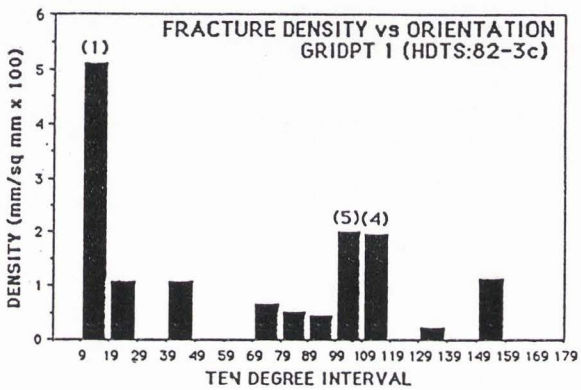

GRIDPT 1
Thinsection
(all fracture data)
N=40:150-160=22%,
100-110 = 15%

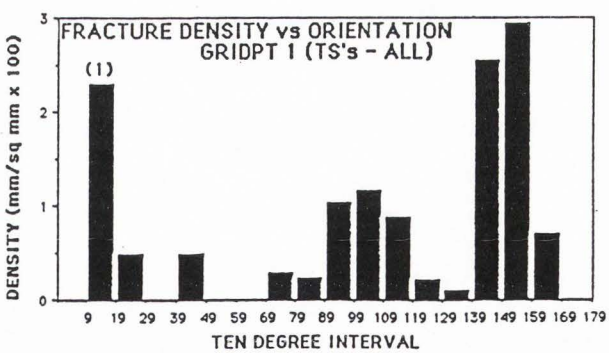

GRIDPT 1
(Outcrop Fractures)
N=89:90-100=98%

GRIDPT 2 (TS:829-1)
(Le-defm,open+closed fractures)
N=16: 10-20-19%

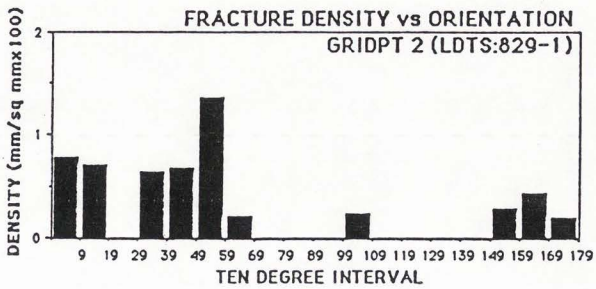

GRIDPT 2
(Outcrop Fractures)
N=18:20-30-39%,
150-160-33%,
130-140-28%

GRIDPT 3 (TS:81-1a)
(Lo-defm,closed fractures)
N=10: 70-80,130-140,
160-170=20%

GRIDPT 3 (TS:81-1a)
(Lo-defm,open+closed
fractures)
N=12: 70-80,90-100,130-140,
160-170=17%

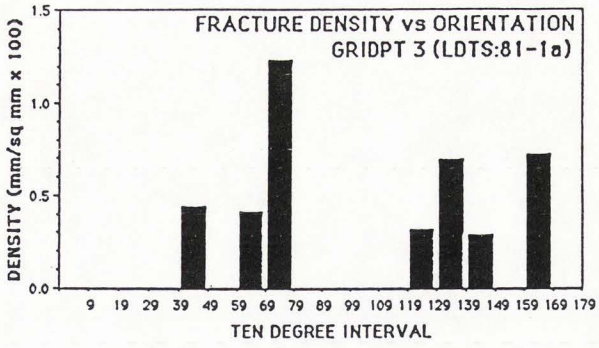

GRIDPT 3 (TS:81-1b2)
(Hi-defm?,all fractures closed)
N=22: 0-10,20-30,170-180=14%

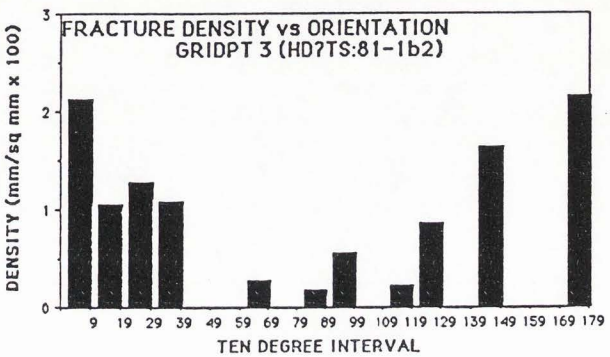

GRIDPT 3
Thinsection
(all fracture data)
N=34:90-100-12%

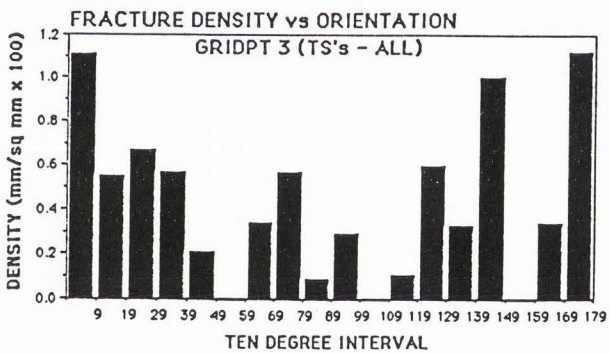

GRIDPT 3 (A)
(Outcrop Fractures)
N=59:0-10=46%

GRIDPT 3 (A+B)
(Outcrop Fractures)
N=154:120-130=58%

GRIDPT 3 (B)
(Outcrop Fractures)
N=95:120-130=79%

GRIDPT 4 (TS:81-2a)
(Lo-defm?,closed fractures)
N=4: 60-70=50%

GRIDPT 4(TS:81-2a)
(Lo-defm?,open+closed fractures)
N=5: 60-70=40%

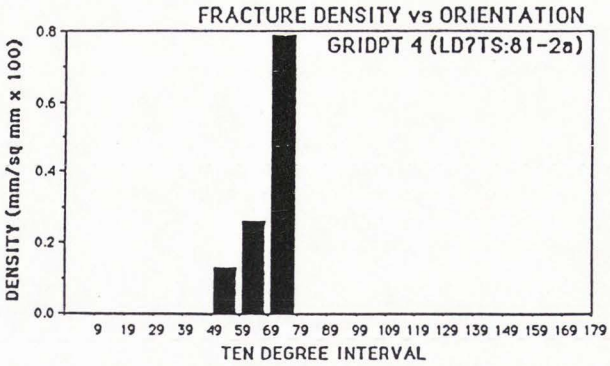

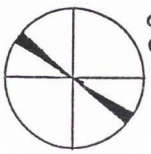

GRIDPT 4 (TS:713-1)
(HI-defm?,all fractures closed)
N=6: 120-130=83%

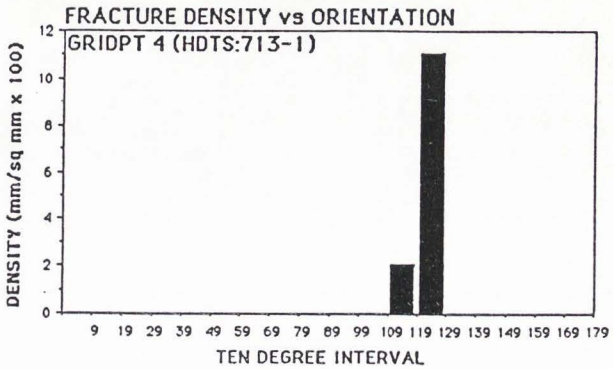

GRIDPT 4
(all thinsection fractures)
N=11:120-130=46%,
60-70=19%

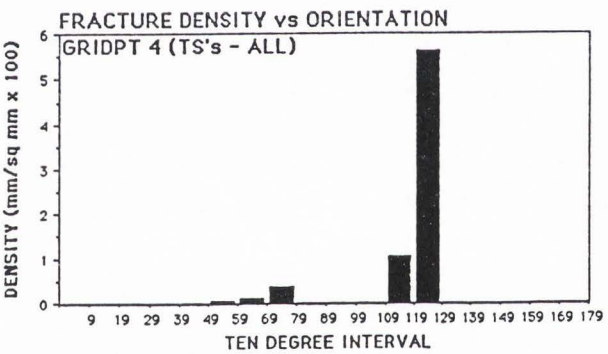

GRIDPT 4
(Outcrop Fractures)
N=44:110-120=33%,
20-30=30%,
90-100=21%

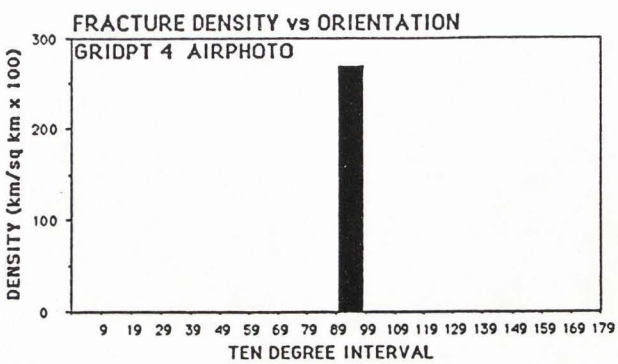

GRIDPT 5 (TS727-3c1)
(Lo-defm,open fractures)
N=5: 60-70-60%

GRIDPT 5 (TS:727-3c1)
(Lo-defm,open+closed fractures)
N=21:90-100-24%

GRIDPT 5 (TS:727-3c1)
(Lo-defm,closed fractures)
N=16: 90-100-25%

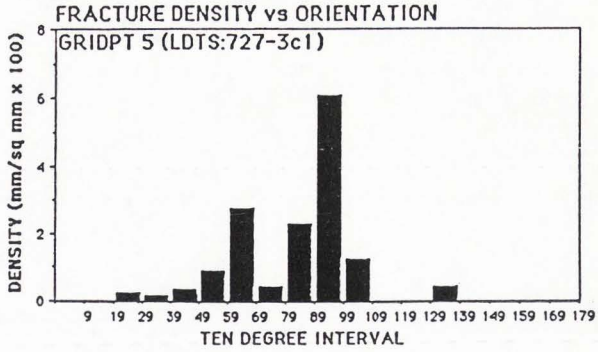

GRIDPT 5 (TS:727-3dh)
(Hi-defm,open fractures)
N=9: 60-70,80-90,100-110-22%

GRIDPT 5 (TS:727-3dh)
(Hi-defm,open+closed fractures)
N=22: 100-110-41%

GRIDPT 5 (TS:727-3dh)
(Hi-defm,closed fractures)
N=13: 100-110-54%

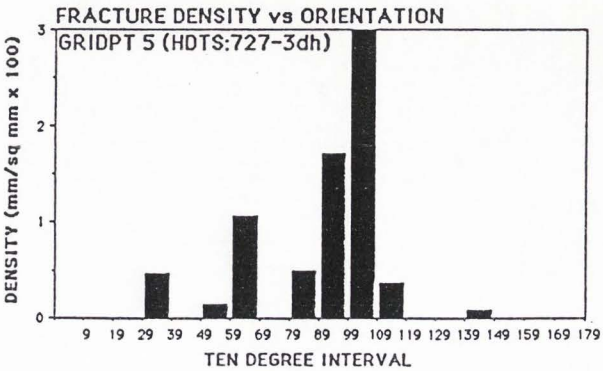

GRIDPT 5
(all thinsection fractures)
N=43:100-110-26%,
60-70-19%

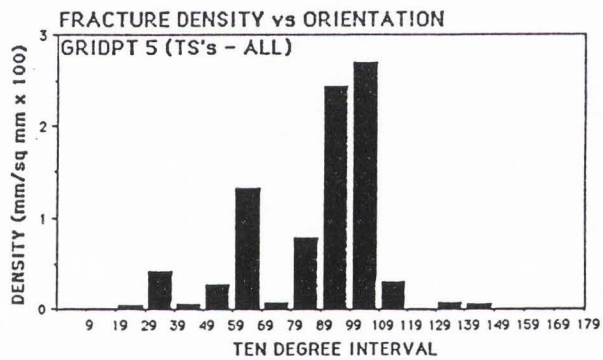

GRIDPT 5 (A)
(Outcrop Fractures)
N=25:40-50-24%

GRIDPT 5 (B)
(Outcrop Fractures)
N=63:10-20-34%,
80-90-33%,
30-40-27%

GRIDPT 5 (A+B+C)
(Outcrop Fractures)
N=206:80-90-34%,
100-110-28%

GRIDPT 5 (C)
(Outcrop Fractures)
N=118:100-110-42%,
80-90-38%

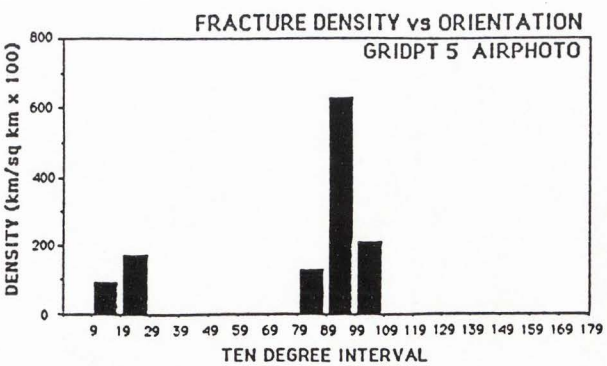

AREA 5
(Airphoto lineaments)
N=7:90-100-42%

GRIDPT 6 (TS:824-1c)
(Lo-defm,open fractures)
N=13: 110-120-30%

GRIDPT 6 (TS:824-1c)
(Lo-defm,open+closed fractures)
N=30: 110-120-20%

GRIDPT 6 (TS:824-1c)
(Lo-defm,closed fractures)
N=17: 20-30,130-140, 140-150-18%

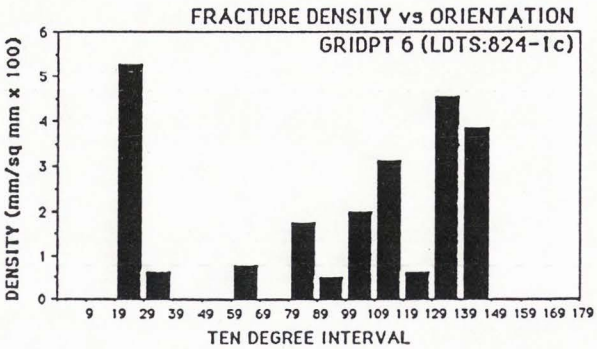

GRIDPT 6 (TS:824-1b)
(HI-defm,open fractures)
N=19: 10-20-16%

GRIDPT 6 (TS:824-1b)
(HI-defm,open+closed fractures)
N=57: 30-40-12%

GRIDPT 6 (TS:824-1b)
(HI-defm,closed fractures)
N=38: 110-120-16%

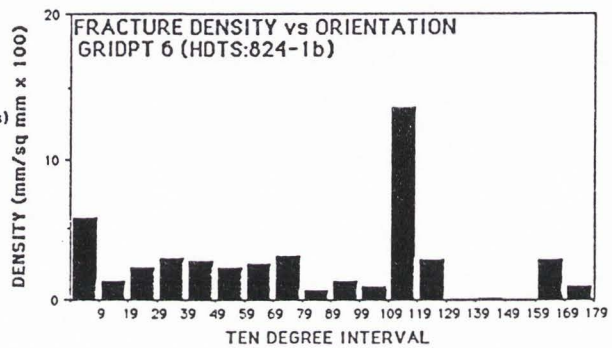

GRIDPT 6 (TS:824-1a)
(HI-defm,open fractures)
N=14: 150-160-22%

GRIDPT 6 (TS:824-1a)
(HI-defm,open+closed fractures)
N=19: 100-110-21%

GRIDPT 6 (TS:824-1a)
(HI-defm,closed fractures)
N=5: 100-110-40%

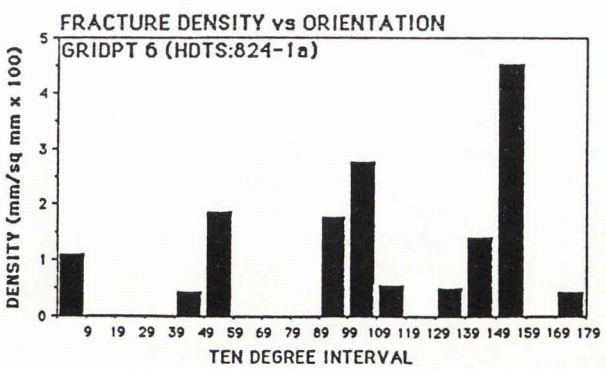

GRIDPT 6
(all thinsection fractures)
N=106:110-120-12%,
20-30-9%

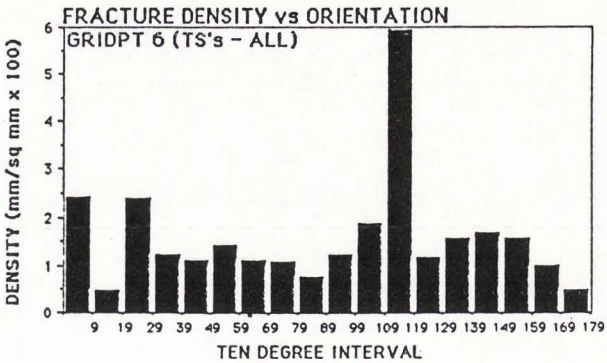

GRIDPT 6
(Outcrop Fractures)
N=13:110-120-62%

AREA 6
(Airphoto lineaments)
N=5:80-90-60%

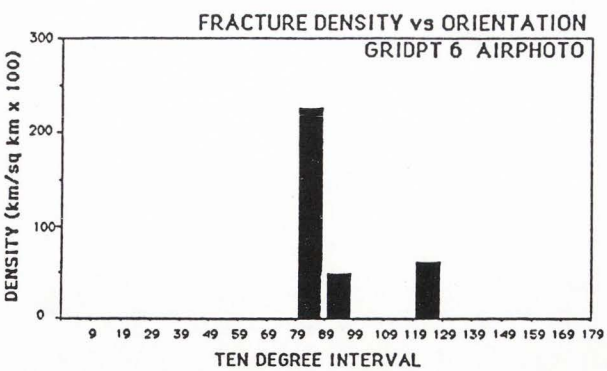

GRIDPT 7 (TS:823-2b)
(Lo-defm,all fractures closed)
N=5: 30-40-40%

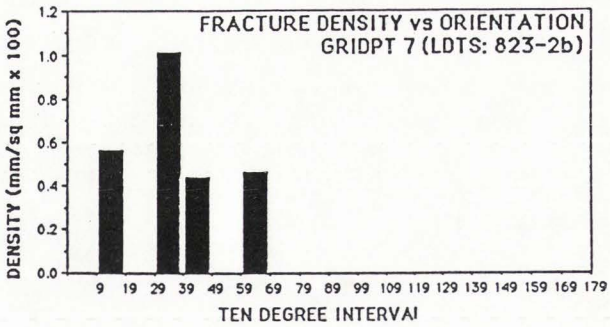

GRIDPT 7
(all TS quartz fractures)
N=30:40-50,50-60=16%
(40-60=32%);80-90=13%

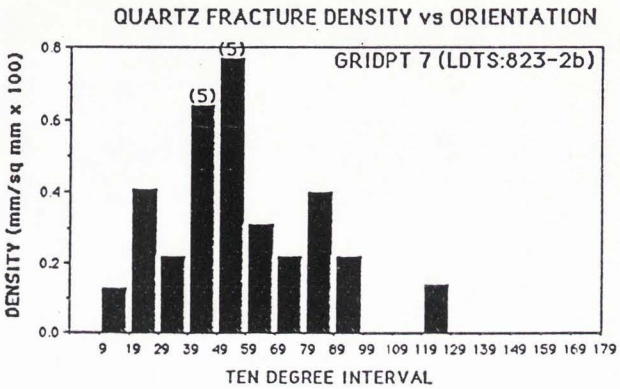

GRIDPT 7
(Outcrop Fractures)
N=29:90-100-61%

AREA 7
(Airphoto Lineaments)
N=22:40-50=28%

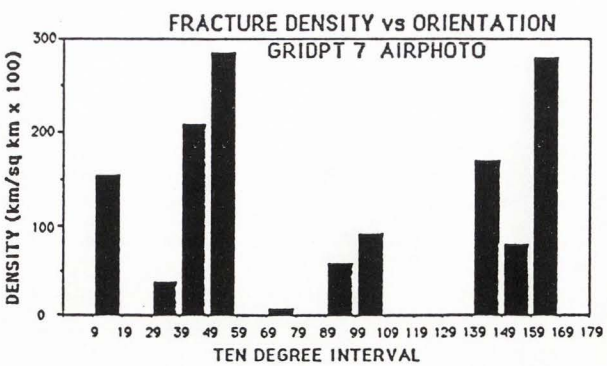

GRIDPT 8 (TS:823-1)
(Lo-defm,open fractures)
N=7: 70-80,80-90,90-100,
110-120,120-130,160-170,
170-180=14%

GRIDPT 8 (TS:823-1)
(Lo-defm,open+closed fractures)
N=14: 80-90,110-120,
120-130=14%

GRIDPT 8 (TS:823-1)
(Lo-defm,closed fractures)
N=7: 20-30,60-70,80-90,
100-110,110-120,120-130
140-150=14%

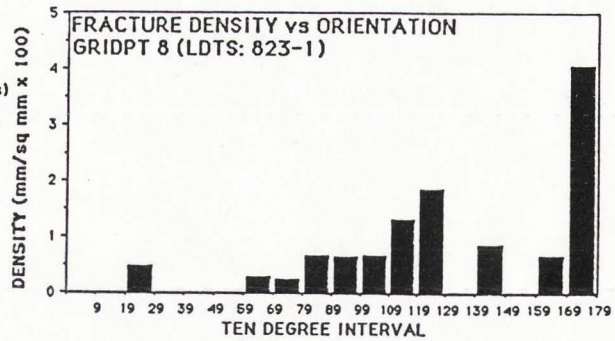

GRIDPT 8
(TS quartz fractures,Lo-defm)
N=63: 110-120=20%

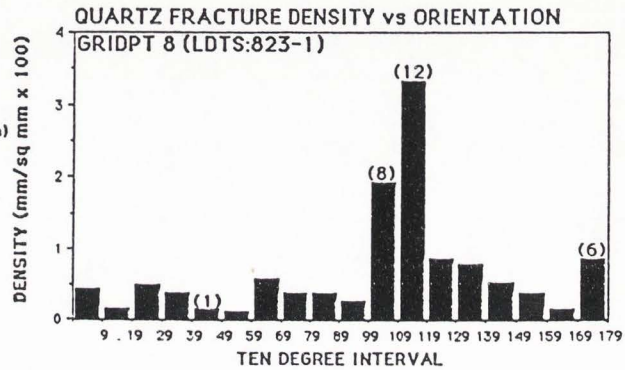

GRIDPT 8
(Outcrop Fractures)
N=25:30-40-56%

AREA 8
(Airphoto lineaments)
N=11:30-40-28%

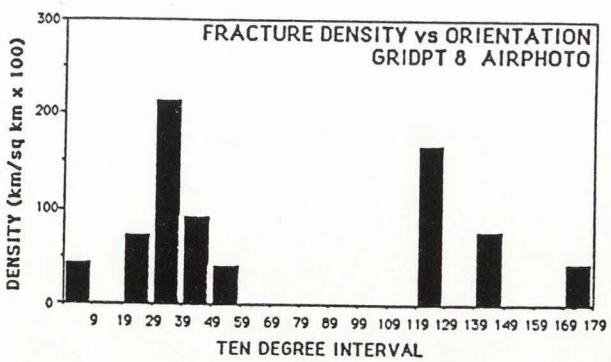

GRIDPT 11 (TS:725-2)
(Lo-defm,open fractures)
N=23: 50-60,60-70,70-80=18%

GRIDPT 11 (TS:725-2)
(Lo-defm,open+closed fractures)
N=35:50-60=18%,
110-120=15%

GRIDPT 11(TS:725-2)
(Lo-defm,closed fractures)
N=12: 50-60,110-120,
140-150=16%

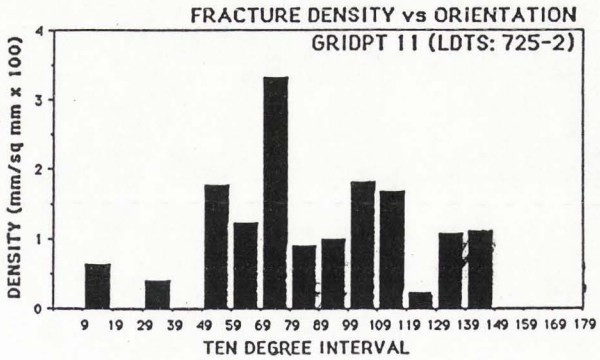

GRIDPT 11
(Outcrop Fractures)
N=87:110-120=40%

GRIDPT 12(TS:721-4c)
(Lo-defm?,closed fractures)
N=11: 0-10,10-20-28%

GRIDPT 12 (TS:721-4c)
(Lo-defm?,open+closed fractures)
N=12: 0-10,10-20-25%

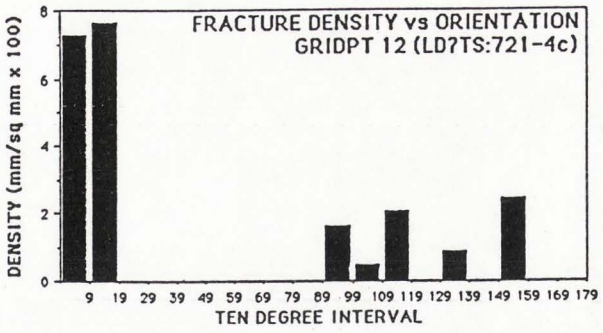

GRIDPT 12 (TS:725-1d)
(HI-defm?, open fractures)
N=6: 120-130,130-140-33%

GRIDPT 12 (TS:725-1d)
(HI-defm?,open+closed fractures)
N=13: 120-130,150-160-24%

GRIDPT 12 (TS:725-1d)
(HI-defm?, closed fractures)
N=7: 100-110,150-160-28%

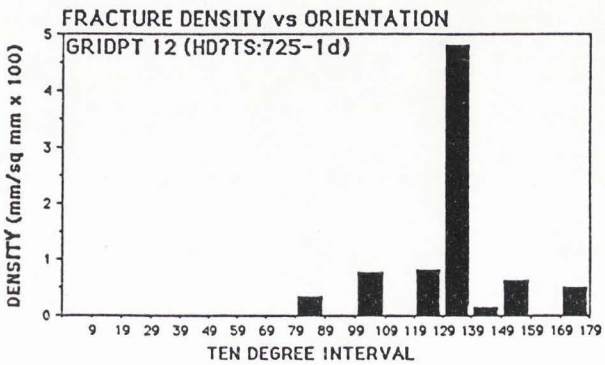

GRIDPT 12
Thinsection
(all fracture data)
N=25:150-160-16%

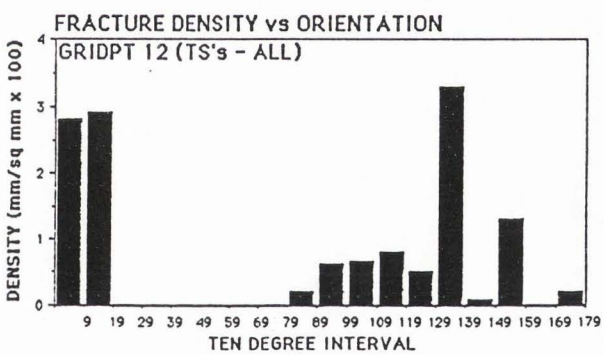

GRIDPT 12
(Outcrop Fractures)
N=54:30-40-100%

GRIDPT 14 (TS:82-2c)
(Lo-defm?,open fractures)
N=15: 150-160,160-170-20%

GRIDPT 14 (TS:82-2c)
(Lo-defm?,open+closed fractures)
N=77: 10-20-12%

GRIDPT 14 (TS:82-2c)
(Lo-defm?,closed fractures)
N=62: 10-20-14%

GRIDPT 14 (TS:82-2b)
(Hi-defm?, open fractures)
N=5: 0-10,10-20,20-30,
60-70,170-180-20%

GRIDPT 14 (TS:82-2b)
(Hi-defm?,open+closed fractures)
N=16: 60-70-26%

GRIDPT 14 (TS:82-2b)
(Hi-defm?, closed fractures)
N=11: 50-60-28%

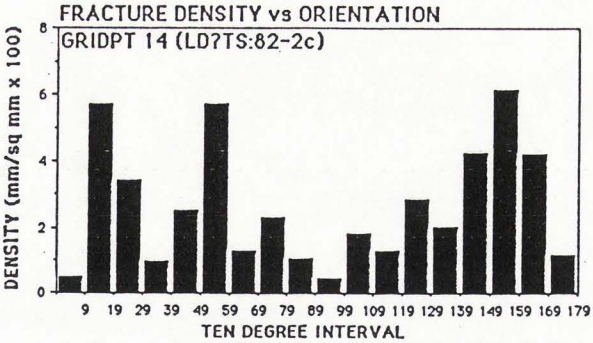

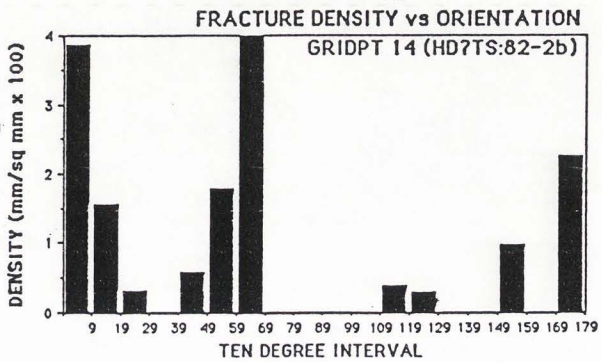

GRIDPT 14
Thinsection
(all fracture data)
N=93:10-20-10%;
50-60,150-160 " 9%

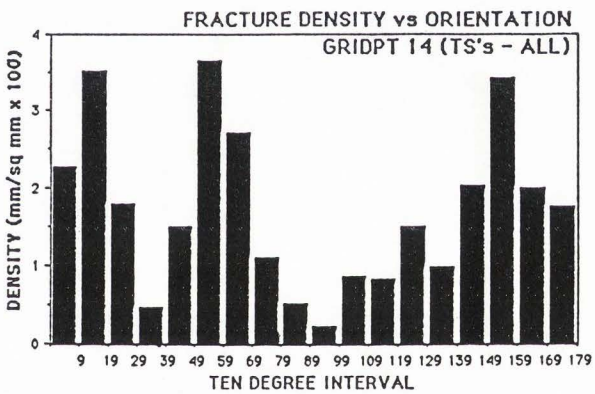

GRIDPT 14
(Outcrop Fractures)
N=127:90-100-34%,
20-30-25%

AREA 14
(Airphoto lineaments)
N=9:90-100-44%,
40-50 22%

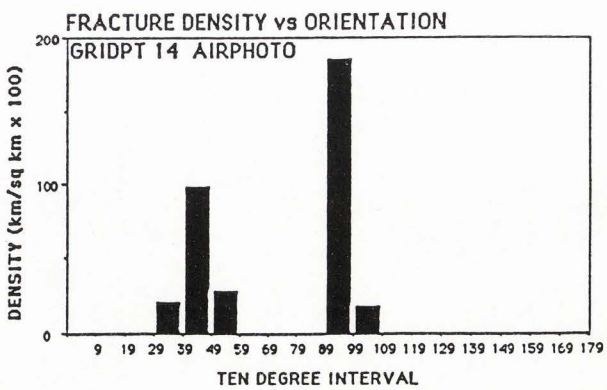

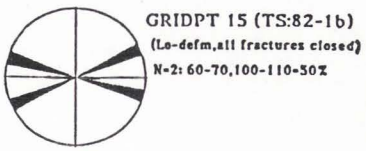

GRIDPT 15 (TS:82-1b)
(Lo-defm,all fractures closed)
N=2: 60-70,100-110=50%

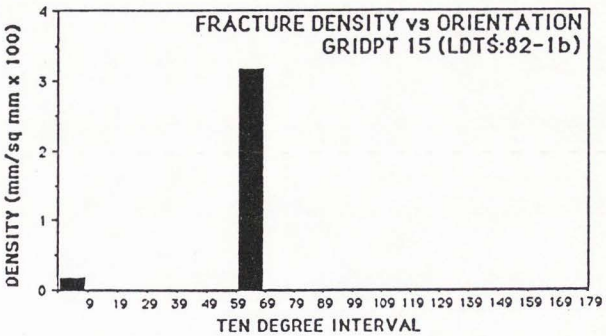

GRIDPT 15
(Outcrop Fractures)
N=48:70-80=30%,
140-150=21%,
80-90=19%,
120-130=17%

GRIDPT 16 (TS:81-3b)
(Lo-defm,open fractures)
N=5: 50-60=40%

GRIDPT 16 (TS:81-3b)
(Lo-defm,open+closed fractures)
N=11: 50-60,130-140=18%

GRIDPT 16 (TS:81-3b)
(Lo-defm,closed fractures)
N=6: 130-140=33%

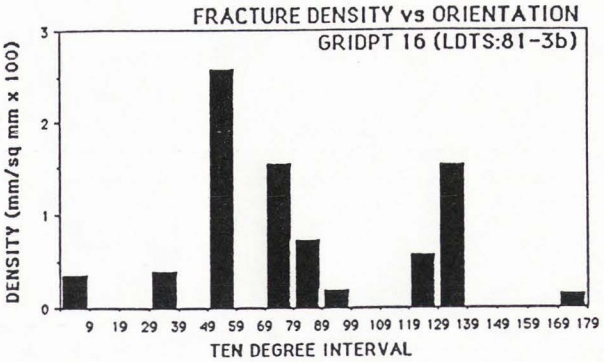

GRIDPT 16 (TS:81-3a)
(HI-defm, closed fractures)
N=13: 110-120,160-170=24%

GRIDPT 16 (TS:81-3a)
(HI-defm,open+closed fractures)
N=15: 110-120,160-170=20%

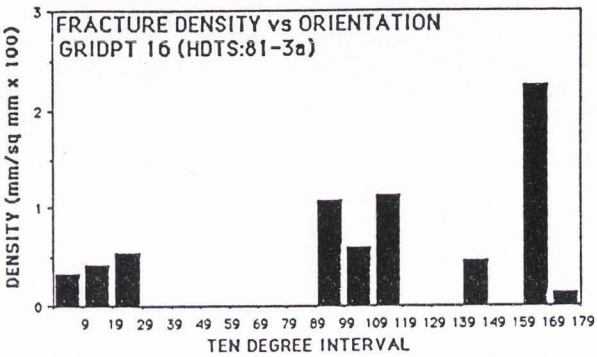

GRIDPT 16
(TS quartz fractures,Lo-defm)
N=27: 0-10,120-130=14%

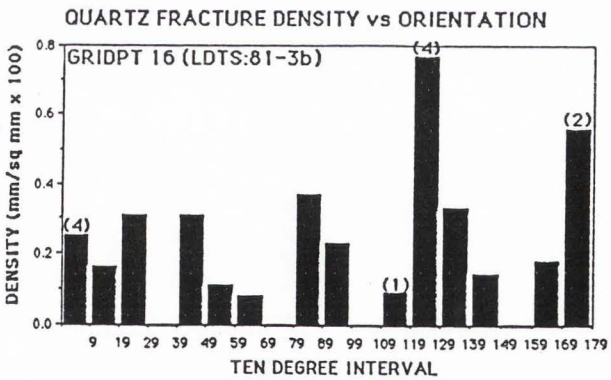

GRIDPT 16
(TS quartz fractures,Hi-defm)
N=38: 150-160=14%

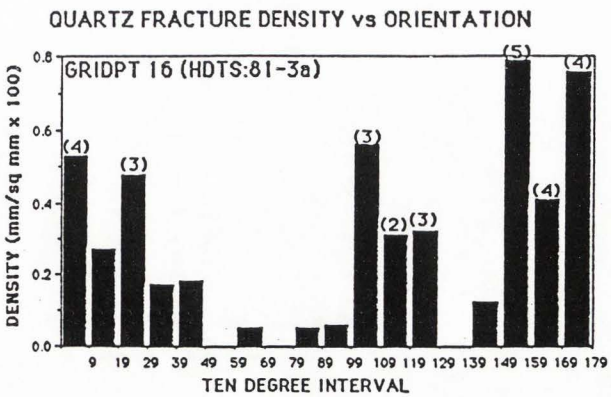

GRIDPT 16
Thinsection
(all fracture data)
N=26:90-100-12%

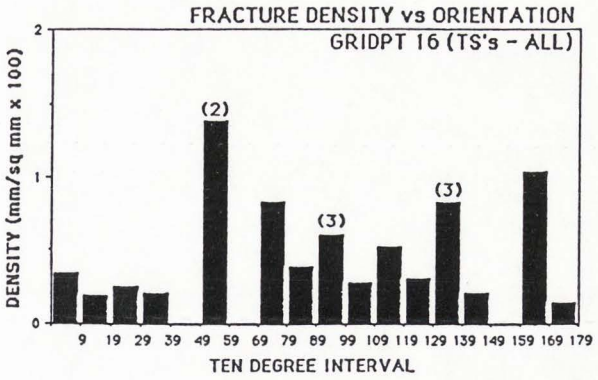

GRIDPT 16
(TS quartz fractures,
HI- + Lo-defm)
N=65: 0-10-12%

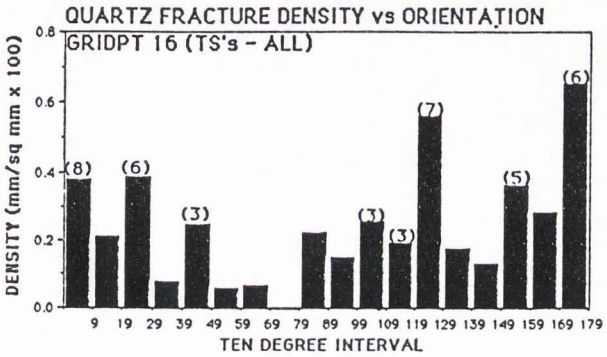

GRIDPT 16
(Outcrop Fractures)
N=62:30-40-10%,
140-150-33%

GRIDPT 17 (TS:727-2a)
(Lo-defm,open fractures)
N=5: 50-60,70-80=40%

GRIDPT 17 (TS:727-2a)
(Lo-defm,open+closed fractures)
N=8: 50-60,70-80,160-170=25%

GRIDPT 17 (TS:727-2a)
(Lo-defm,closed fractures)
N=3: 160-170=67%

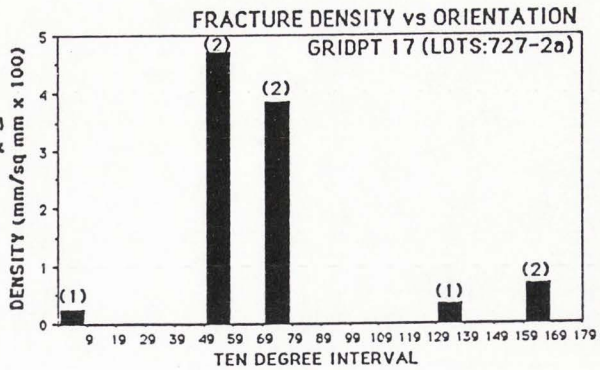

GRIDPT 17
(TS quartz fractures)
N=35: 70-80,150-160=12%

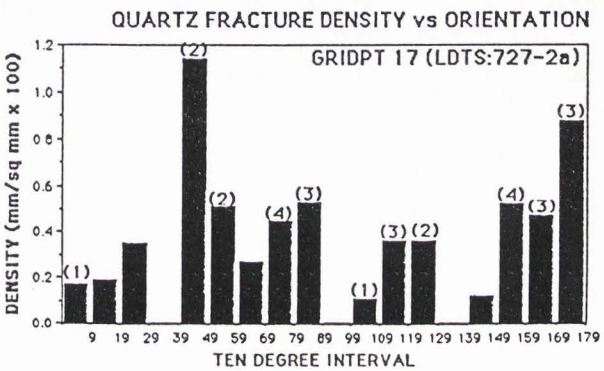

GRIDPT 17
(Outcrop Fractures)
N=22:40-50=55%

GRIDPT 18 (TS:727-1c)
(Lo-defm,open fractures)
N=4: 0-10,140-150,160-170,
170-180=25%

GRIDPT 18 (TS:727-1c)
(Lo-defm,open+closed fractures)
N=24: 140-150=16%

GRIDPT 18 (TS:727-1c)
(Lo-defm,closed fractures)
N=20: 10-20,60-70,130-140,
140-150=15%

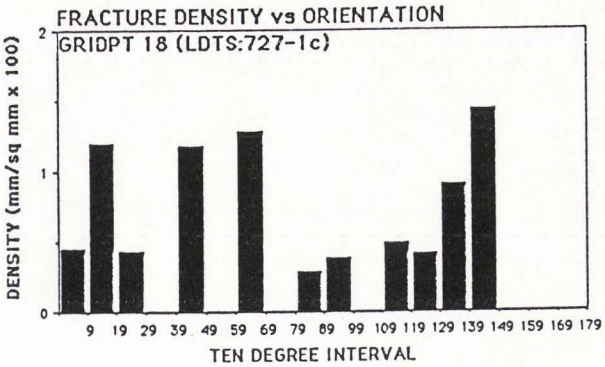

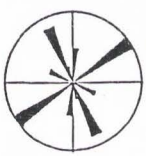

GRIDPT 18
(Outcrop Fractures)
N=24:50-60=34%,
150-160=29%

AREA 18
(Airphoto lineaments)
N=4:40-50=50%

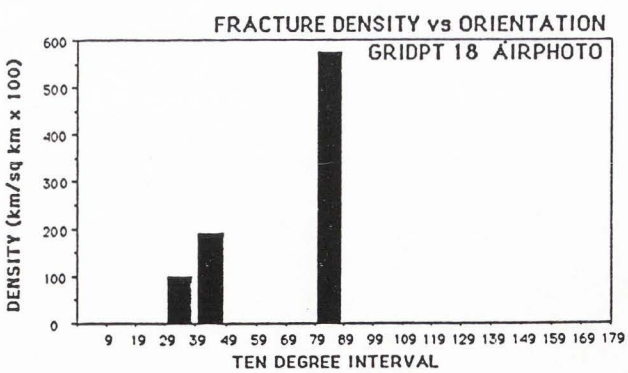

GRIDPT 19 (TS:726-3b)
(Lo-defm,closed fractures)
N=21: 20-30,160-170-20%

GRIDPT 19 (TS:726-3b)
(Lo-defm,open+closed fractures)
N=23: 160-170-22%

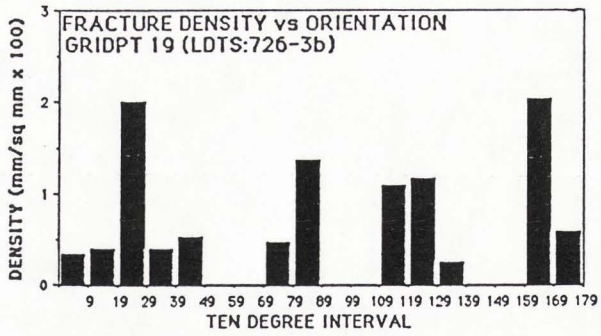

GRIDPT 19 (TS:726-3c)
(Hi-defm?,closed fractures)
N=13: 20-30,130-140-24%

GRIDPT 19 (TS:726-3c)
(Hi-defm?,open+closed fractures)
N=14: 20-30,130-140-22%

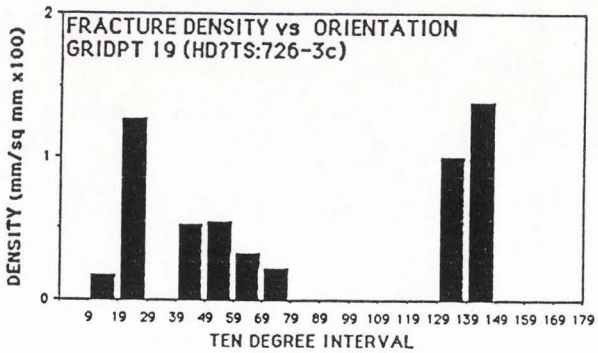

GRIDPT 19 (TS:726-3a)
(Hi-defm?,closed fractures)
N=9: 50-60-56%

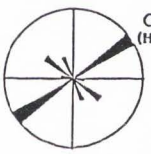

GRIDPT 19 (TS:726-3a)
(Hi-defm?,open+closed fractures)
N=12: 50-60-50%

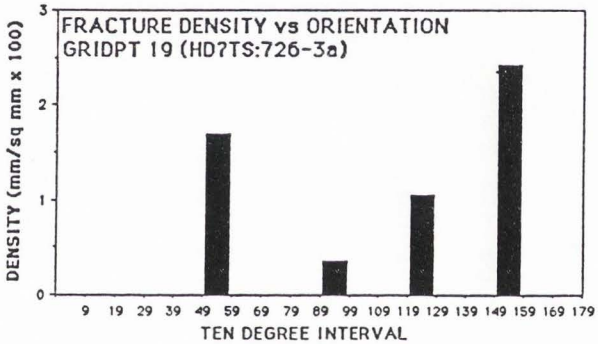

GRIDPT 19
Thinsection
(all fracture data)
N=49:50-60-16%,
20-30-14%,120-130-12%

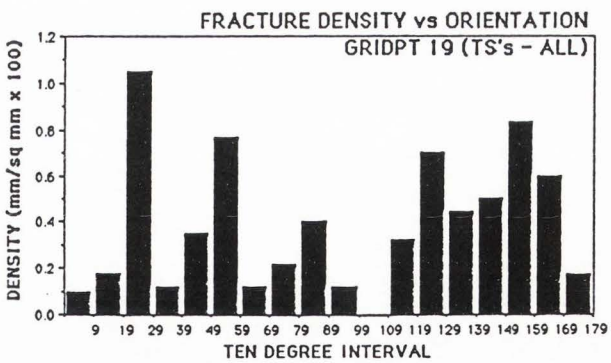

GRIDPT 19
(Outcrop Fractures)
N=34:0-10-44%,
130-140-41%

GRIDPT 20 (TS:726-1a)
(Lo-defm,closed fractures)
N=9: 60-70-44%

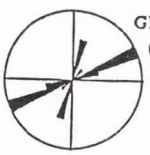

GRIDPT 20 (TS:726-1a)
(Lo-defm,open+closed fractures)
N=12:60-70-42%,
10-20-25%

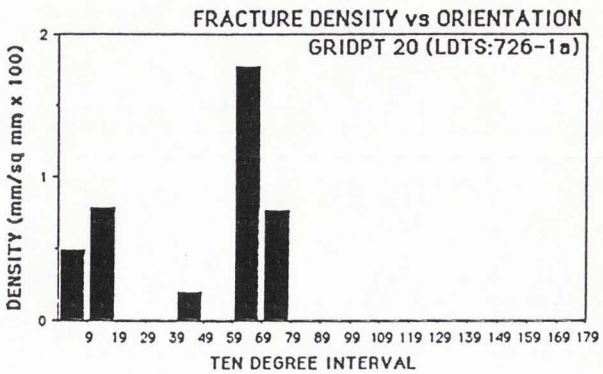

GRIDPT 20
(Outcrop Fractures)
N=43:150-160-72%

GRIDPTS 16,17
(all open fractures)

N=12:
50-60=34%

GRIDPTS 16,17

Thinsection
(all fracture data)

N=34:160-170=14%,
50-60 = 11%

GRIDPTS 16,17
(all closed fractures)

N=22:
160-170=22%

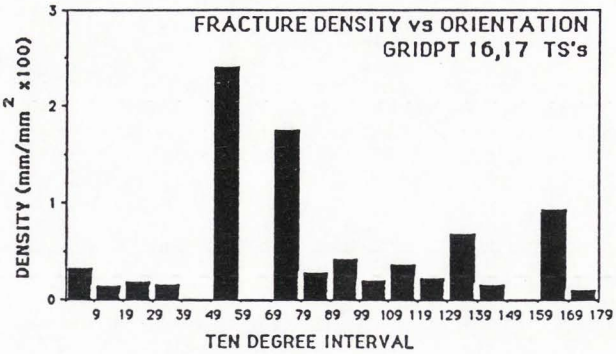

GRIDPTS 16,17
(TS quartz fracture data)

N=100: 0-10,120-130,150-160,
160-170,170-180=10%

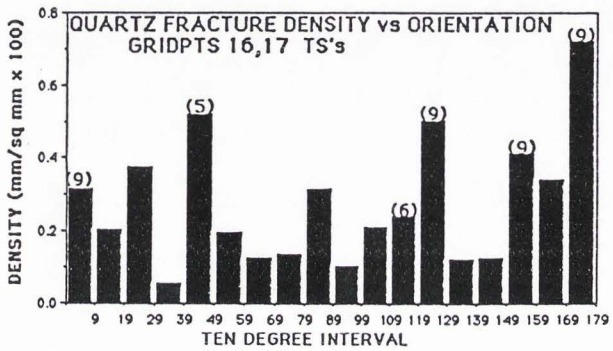

GRIDPTS 16,17
(Outcrop Fractures)

N=84:30-40=30%,
140-150=25%

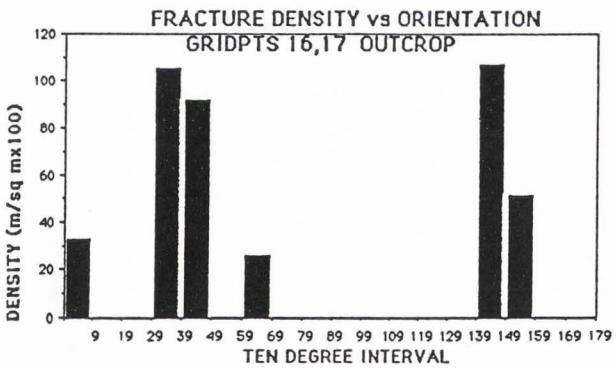

AREA 16,17
(Airphoto lineaments)

N=32:10-20=32%,
20-30=22%

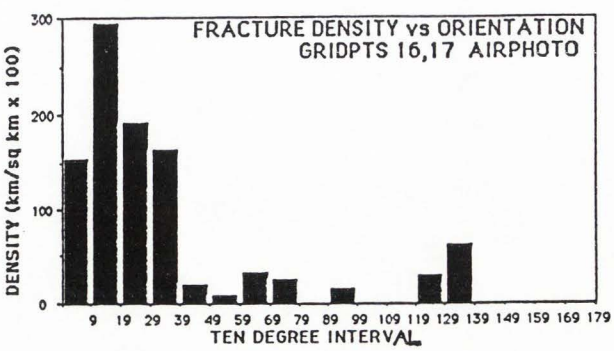

GRIDPTS 19,20
(all open fractures)
N=9: 150-160-22%

GRIDPTS 19,20
Thinsection
(all fracture data)
N=61:50-60-14%,
20-30-12%,120-130-11%

GRIDPTS 19,20
(all closed fractures)
N=52: 20-30,50-60-14%

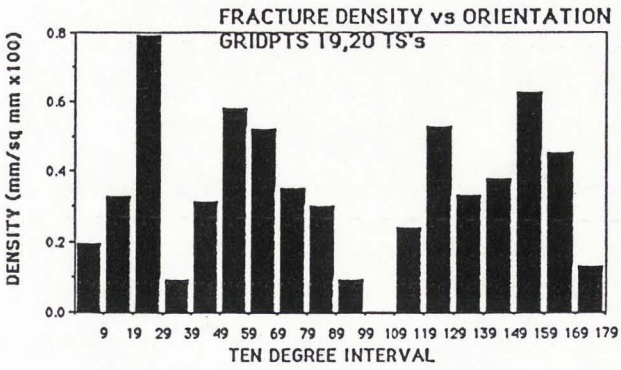

GRIDPTS 19,20
(Outcrop Fractures)
N=77:150-160-40%

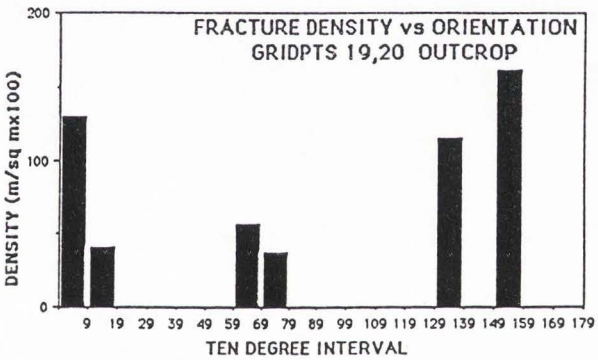

AREA 19,20
(Airphoto lineaments)
N=11:70-80-36%,
60-70-27%

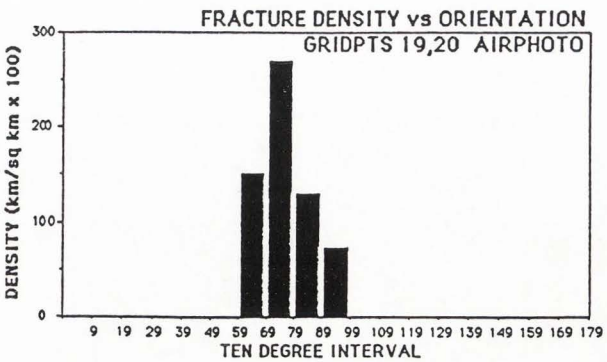

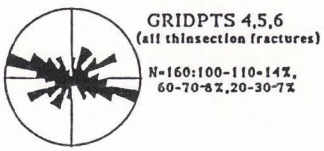

GRIDPTS 4,5,6
(all thinsection fractures)
N=160:100-110-14%,
60-70-8%,20-30-7%

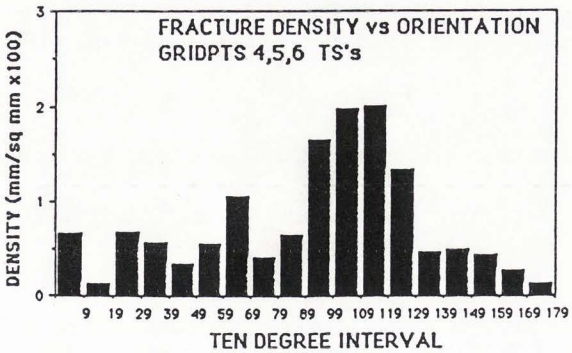

GRIDPTS 4,5,6
(Outcrop Fractures)
N=263:80-90-27%,
100-110-22%,
20-30-17%

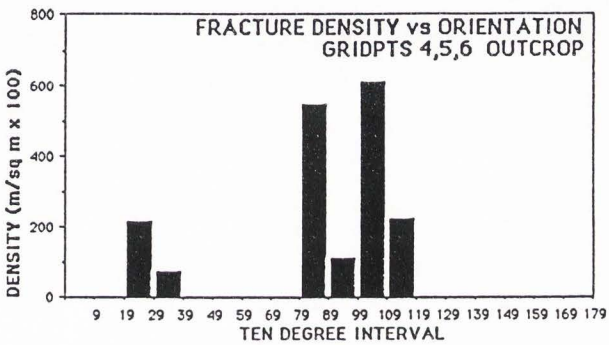

AREA 4,5,6
(Airphoto lineaments)
N=13:90-100-38%,
80-90-31%

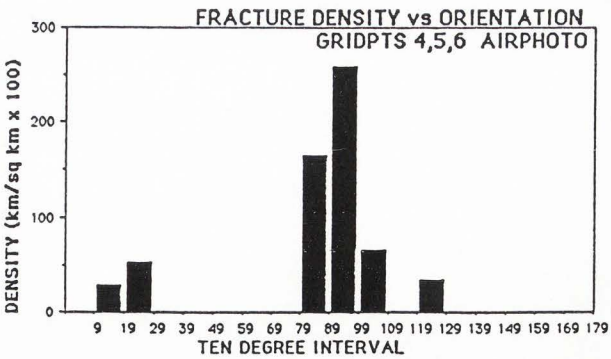

GRIDPTS 7,8,16,17
(all thinsection fractures)
N=53:160-170=12%,
110-120=10%

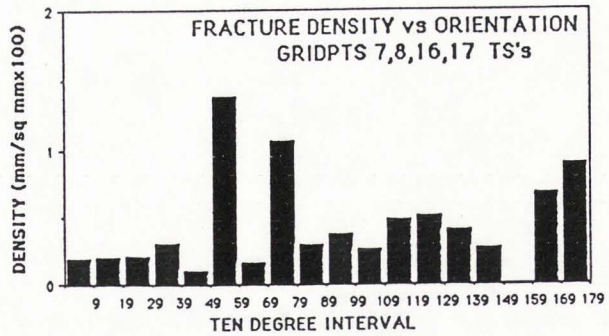

GRIDPTS 7,8,16,17
(all TS quartz fractures)
N=193:110-120=10%;
20-30,170-180=8%;
80-90=6%

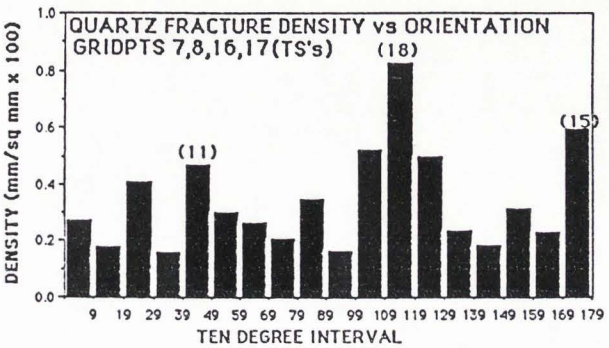

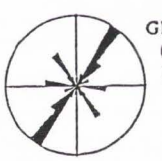

GRIDPTS 7,8,16,17
(Outcrop Fractures)
N=138:30-40=28%,
140-150=15%,
90-100=12%

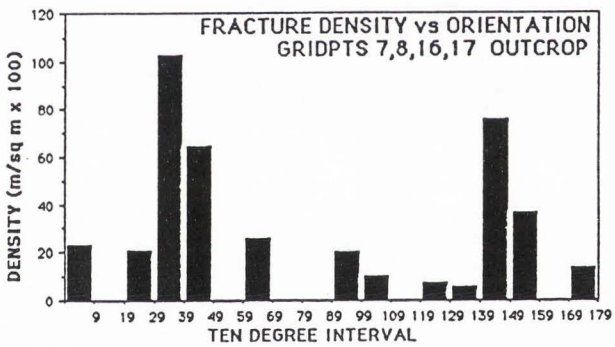

AREA 7,8,16,17
(Airphoto lineaments)
N=65:10-20=18%,
40-50=14%,
(10-50=55%)

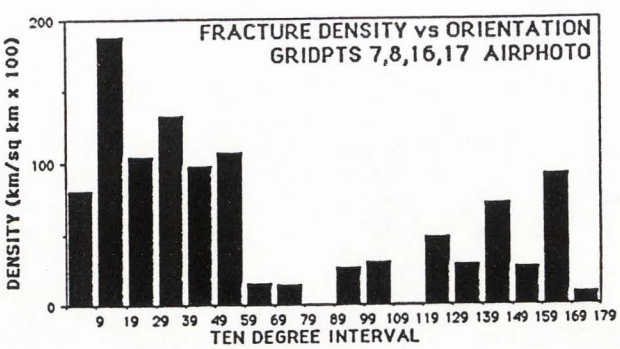

GRIDPTS 1,2,3,15
Thinsection
(all fracture data)
N=92:150-160-10%

GRIDPTS 1,2,3,15
(Outcrop Fractures)
N=309:120-130-32%,
90-100-28%

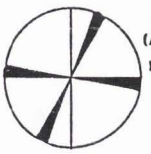

AREA 1,2,3,15
(Airphoto lineaments)
N=2:20-30,90-100-50%

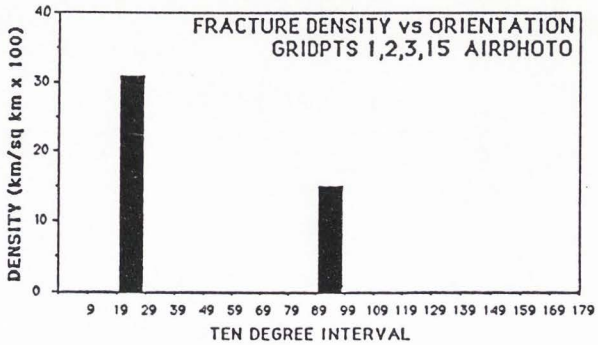

ALL GRIDPTS
Thinsection
(all closed fractures)
N=389:60-70-8%

ALL GRIDPTS
Thinsection
(all open fractures)
N=168:100-110-10%

ALL GRIDPTS
(all thinsection fractures)
N=557: 60-70,100-110-8%

N=1079: 90-100-14%,
30-40-12%,
120-130-10%,
110-120-9%,
20-30-8%

ALL GRIDPT FRACTURE DATA
(OUTCROP)

AIRPHOTO
(All Lineaments)
N=104:90-100-14%;
10-20,40-50-13%

APPENDIX H. TRAVERSE AREA: THIN SECTION PHOTONEGATIVES AND FRACTURE TRACINGS

Appendix H presents copies of thin section photonegatives prepared for (horizontal) thin section fracture and quartz fracture analysis. Fracture tracings from acetate overlays are included below the photonegatives. Generally, in terms of photonegative 'darkness', quartz > open space > microcline > plagioclase (generally altered) > opaques, chlorite. In those thin sections analyzed for quartz fractures, the identifying numbers for the quartz fractures are circled to distinguish them from those for intergranular fractures. These were done for all Traverse thin sections (Points E-I). For some thin sections, dashed lines were used to designate healed or partially healed fractures. Lower case letters were sometimes used to designate fracture 'segments' and the data were treated as if from separate fractures. The mineralogy was mapped in some Traverse thin sections (F:720-1a; G:721-1b; H:822-1; I:721-3a) to investigate possible relations between fractures and mineralogy. For these diagrams, abbreviations for mapped minerals are as follows: Q=quartz, M=microcline, A=plagioclase (usually with albite twinning), C=chlorite, O=opaque, and U or ? = uncertain identity (many of these grains appear to be altered plagioclase). No definite or consistent relations between fractures and mineralogy were discovered. All Traverse thin sections were photographed with 'down' being into the picture. In a few cases, (a few) prominent fractures not appearing in the photonegatives, but visible in thin section, were used in data analyses.

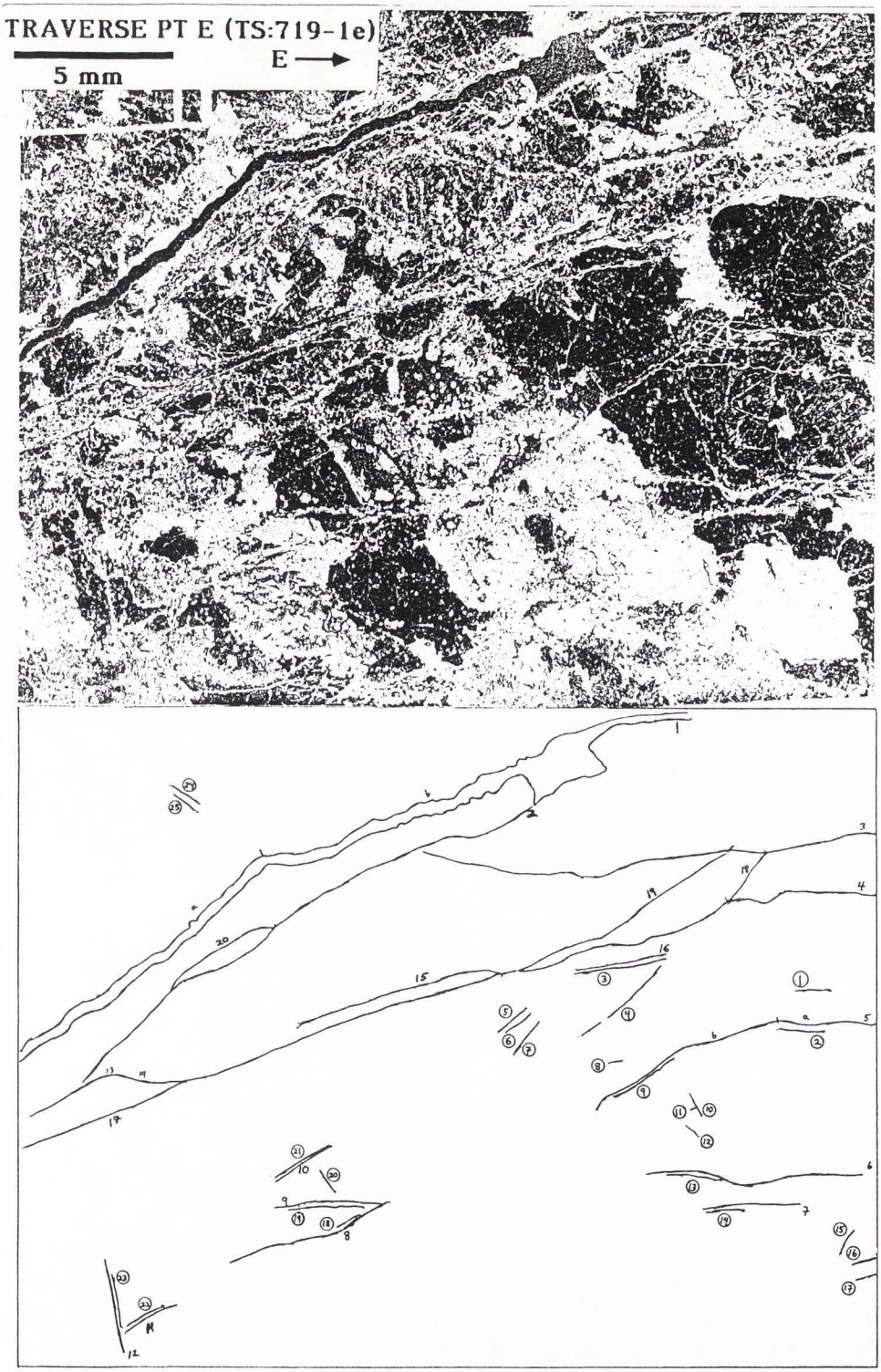
TRAVERSE PT E (TS:719-1e)
5 mm
E

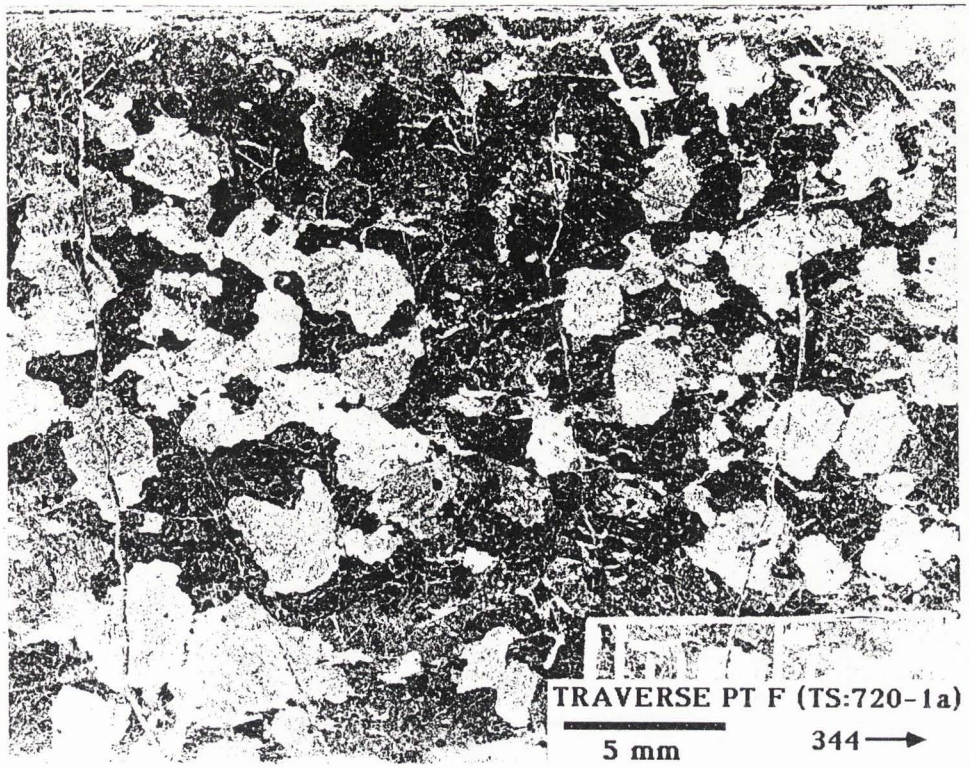
TRAVERSE PT F (TS:720-1a)
5 mm
344

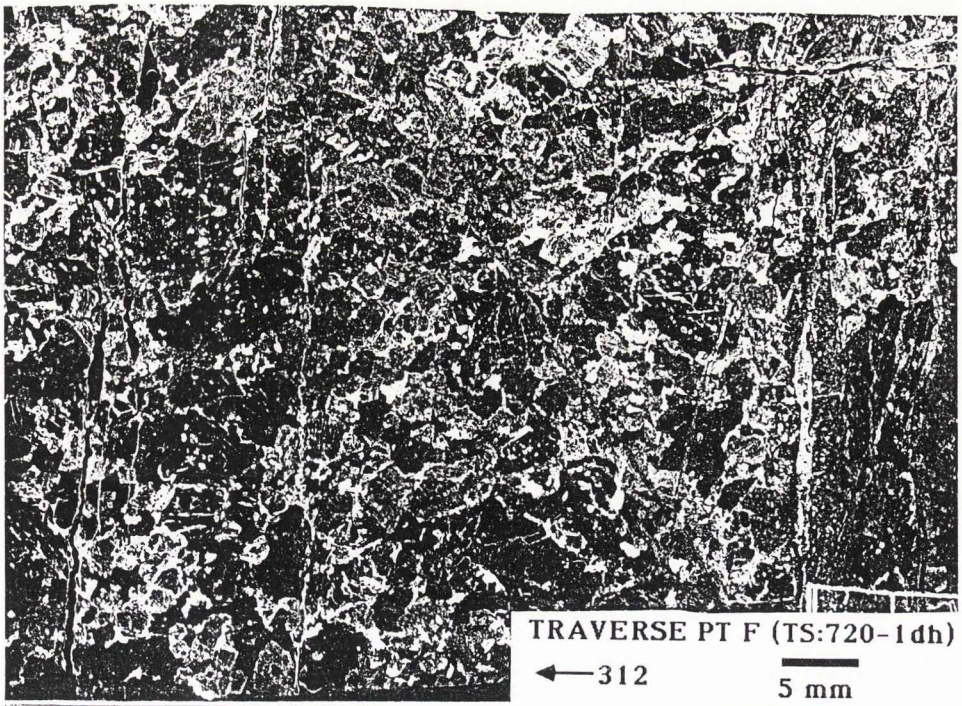
TRAVERSE PT F (TS:720-1dh)
←312
5 mm

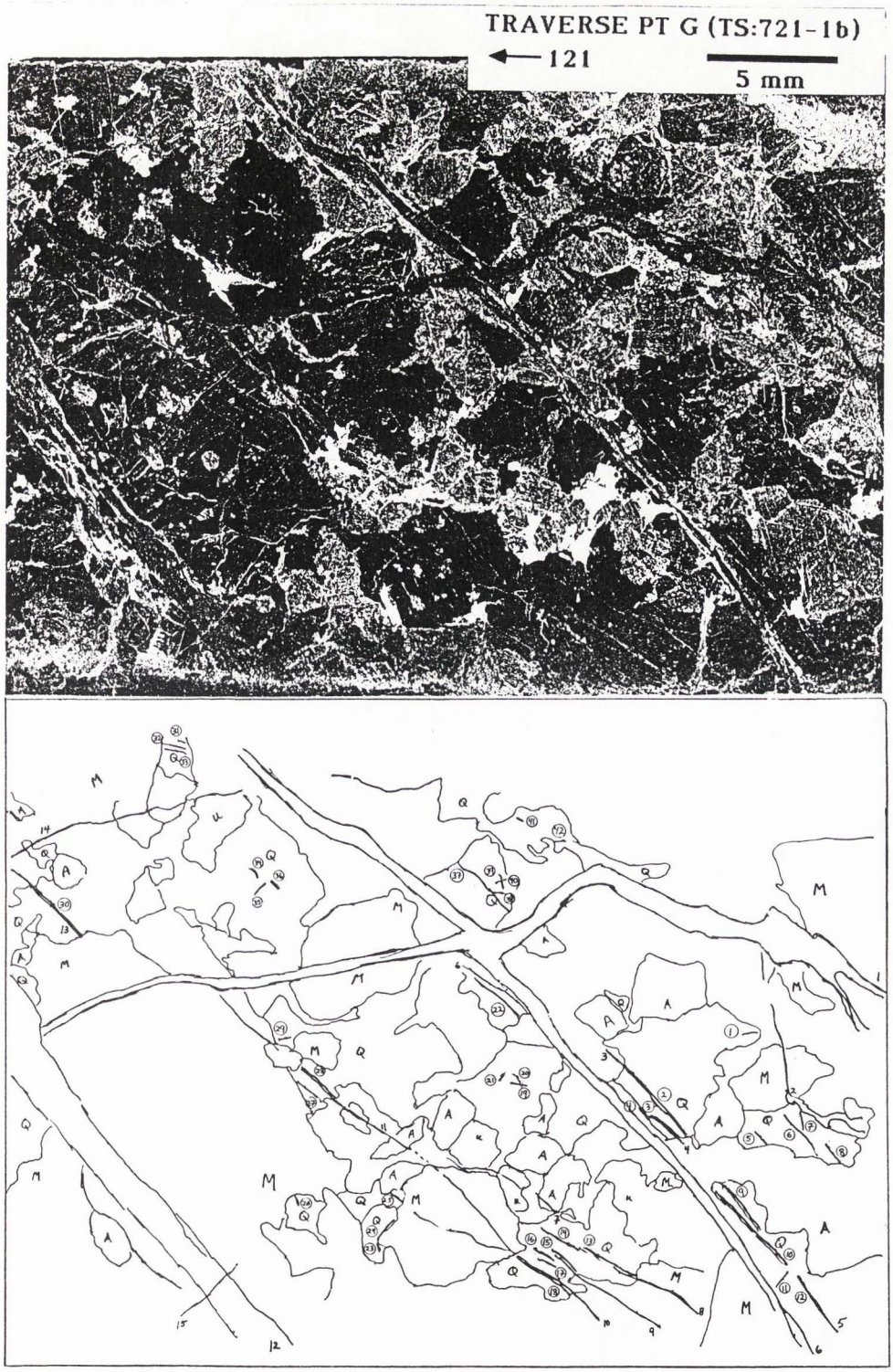
TRAVERSE PT G (TS:721-1b)
121
5 mm

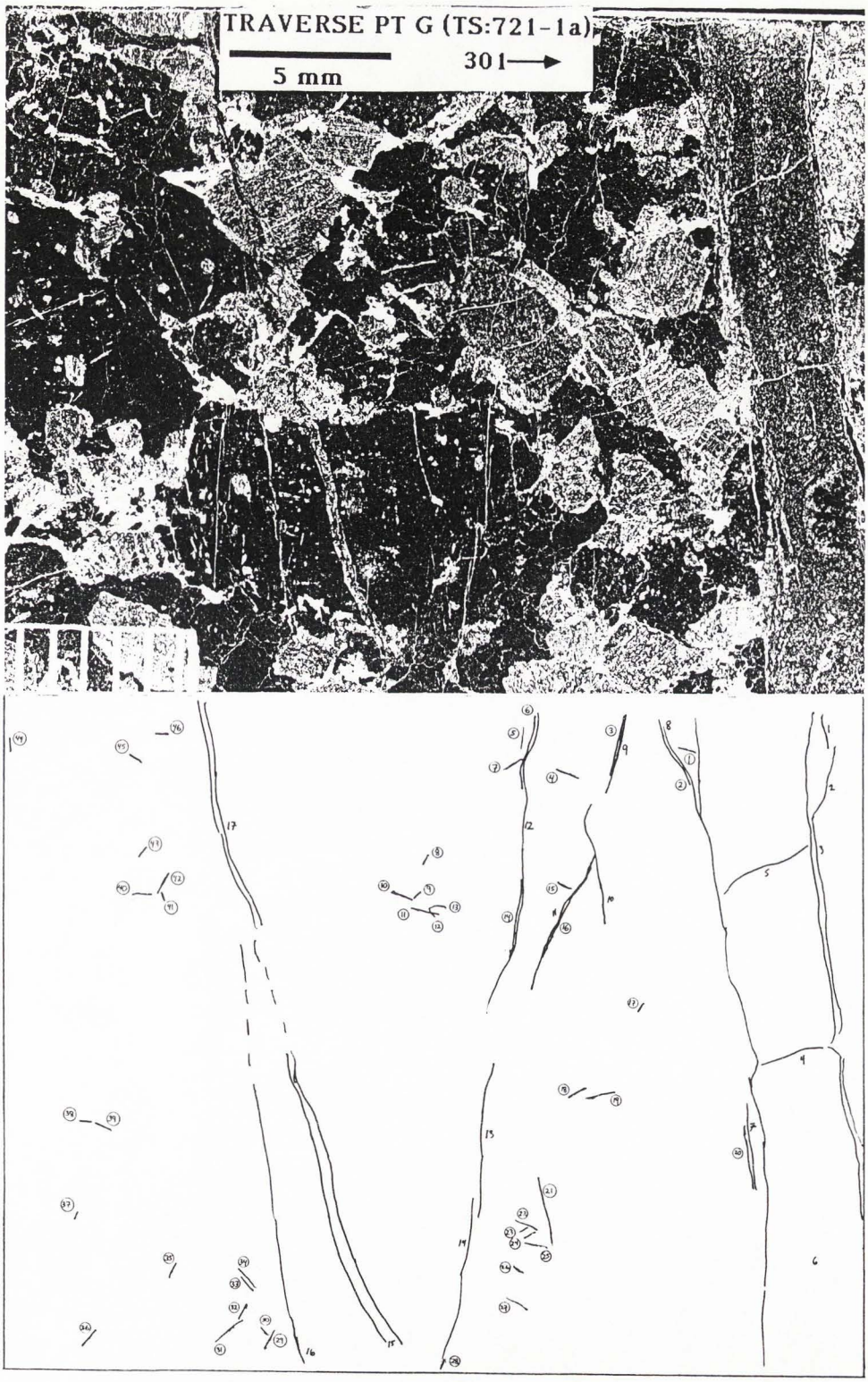
TRAVERSE PT G (TS:721-1a)
5 mm
301

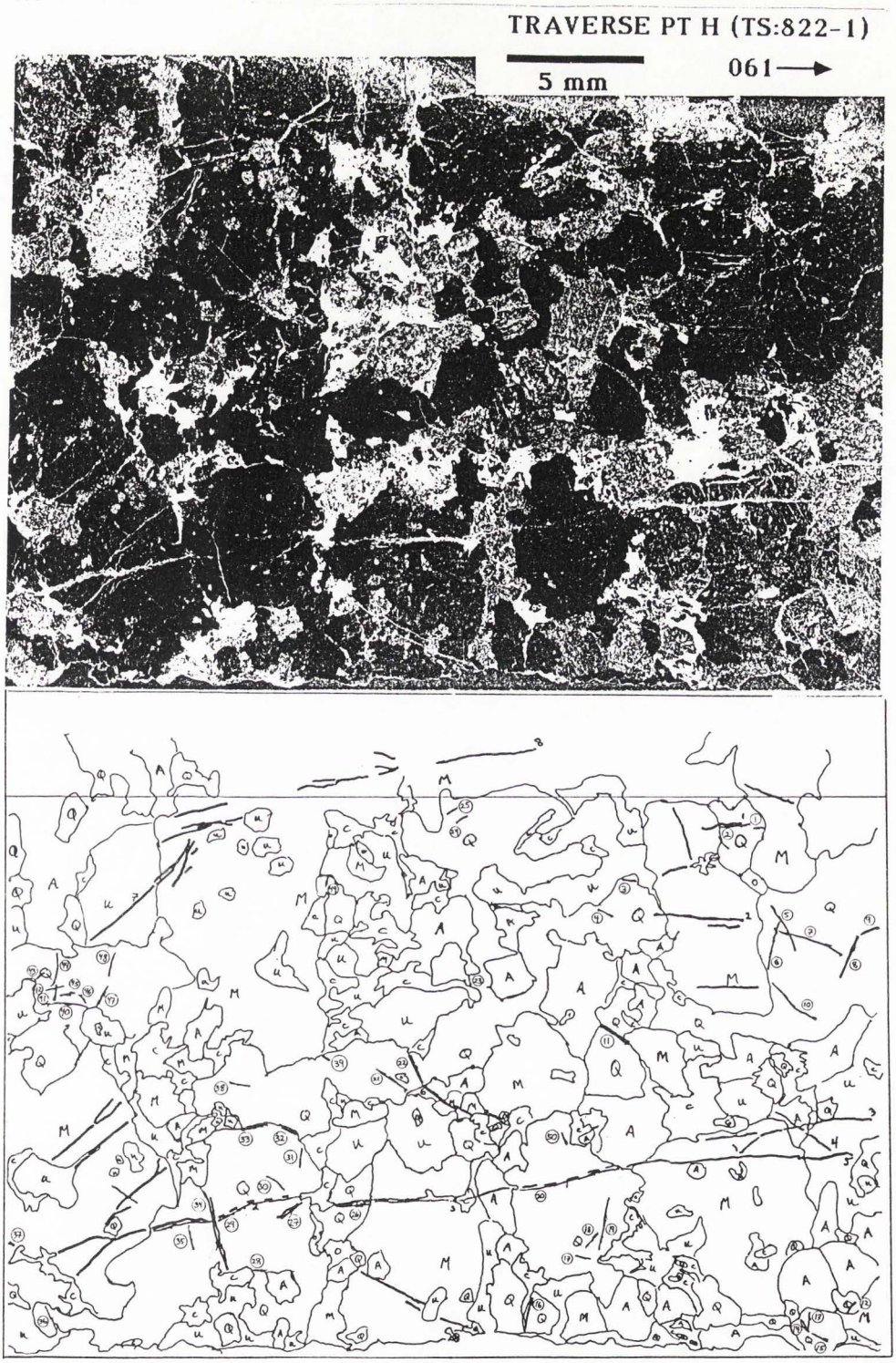
TRAVERSE PT H (TS:822-1)
5 mm
061

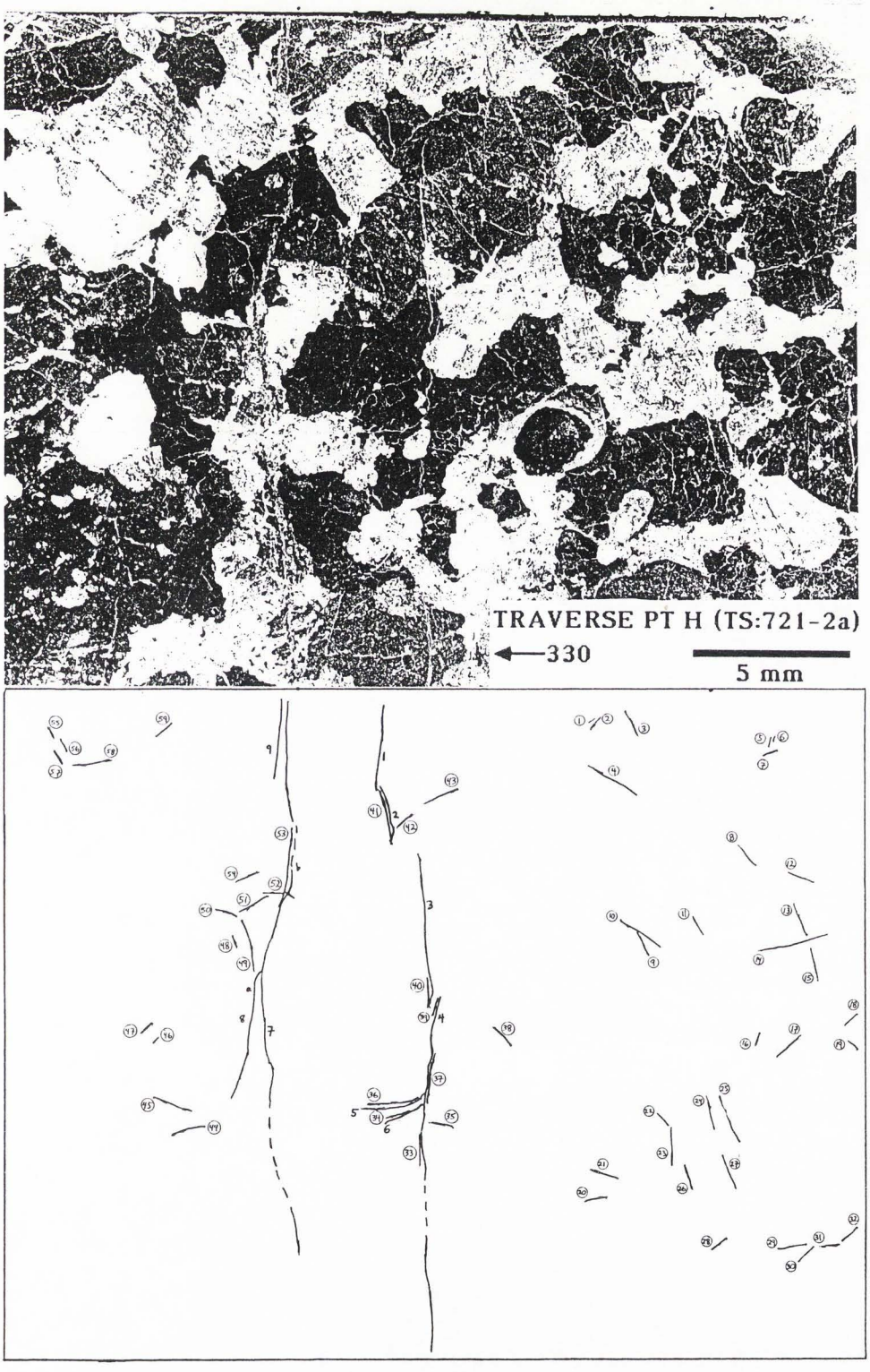
TRAVERSE PT H (TS:721-2a)
330
5 mm

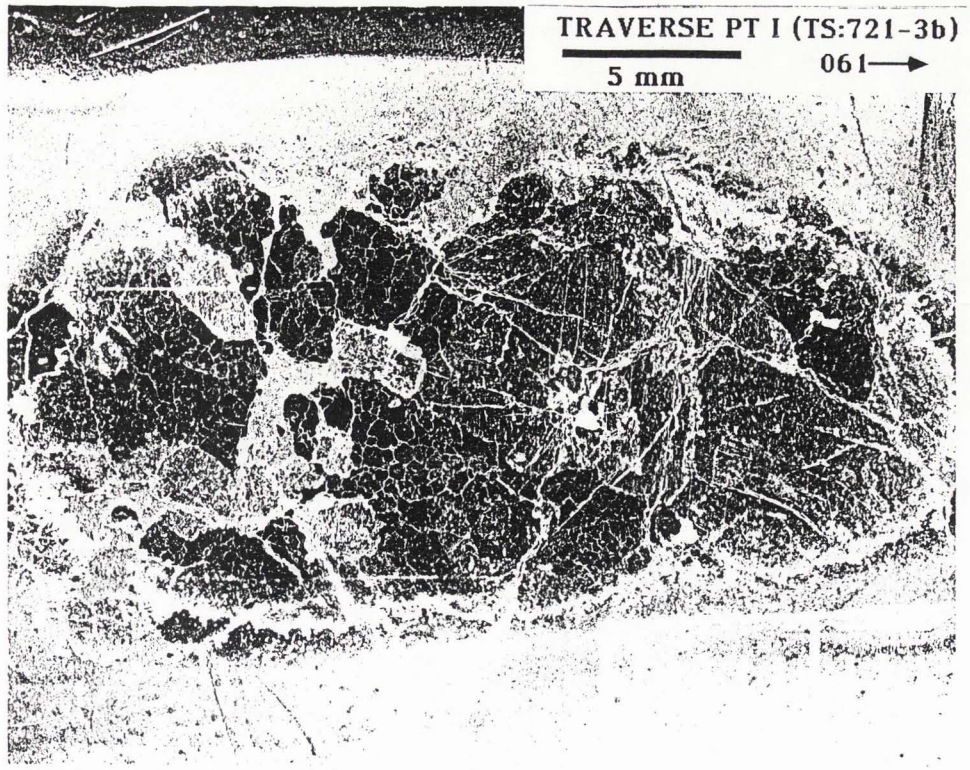
TRAVERSE PT I (TS:721-3b)
5 mm
061

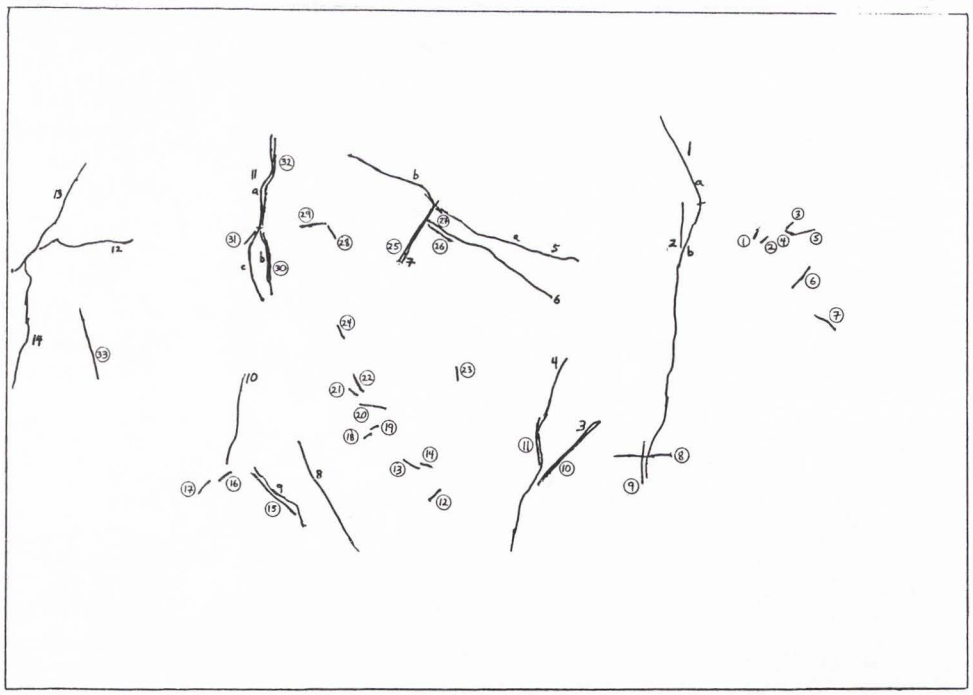

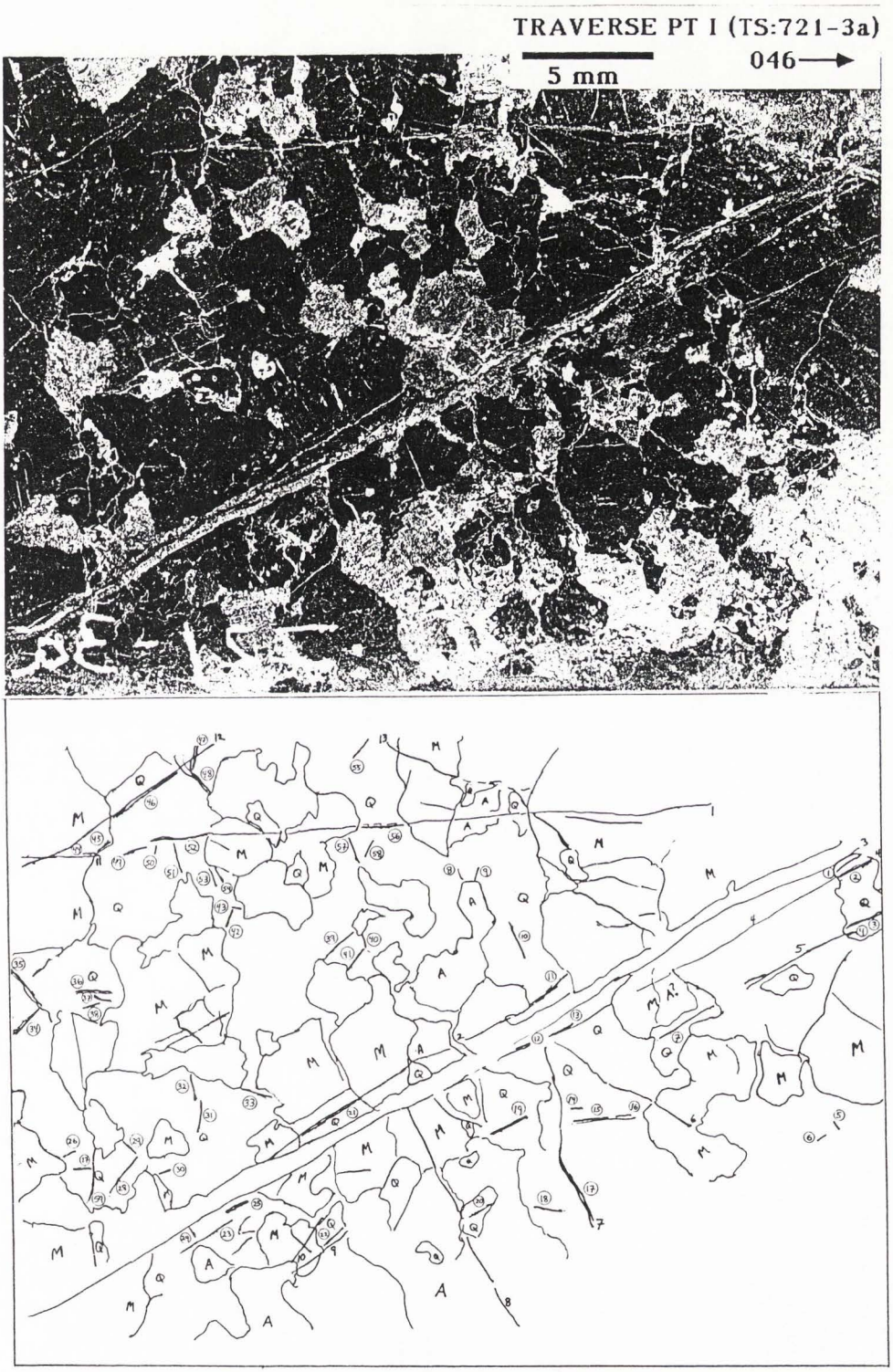
TRAVERSE PT I (TS:721-3a)
5 mm
046

APPENDIX I. GRID AREA: THIN SECTION
PHOTONEGATIVES AND FRACTURE TRACINGS

Appendix I presents copies of thin section photonegatives prepared for (horizontal) thin section fracture and quartz fracture analysis. Fracture tracings from acetate overlays are included below the photonegatives. Generally, in terms of photonegative 'darkness', quartz > open space > microcline > plagioclase (generally altered) > opaques, chlorite. In those thin sections analyzed for quartz fractures, the identifying numbers for the quartz fractures are circled to distinguish them from those for intergranular fractures. These were done for Gridpoints 7,8,16,17. For some thin sections, dashed lines were used to designate healed or partially healed fractures. Lower case letters were sometimes used to designate fracture 'segments' and the data were treated as if from separate fractures. In a few cases, (a few) prominent fractures not appearing in the photonegatives, but visible in thin section, were used in data analyses.

For the following photonegatives (Gridpoint, sample number), 'down' is out of the picture and reported fracture orientations reflect 'true' measurements: 5,727-3dh; 6,824-1b; 7,823-2b; 14,82-2b; 17,727-2a; 19,726-3b; 19,726-3c.

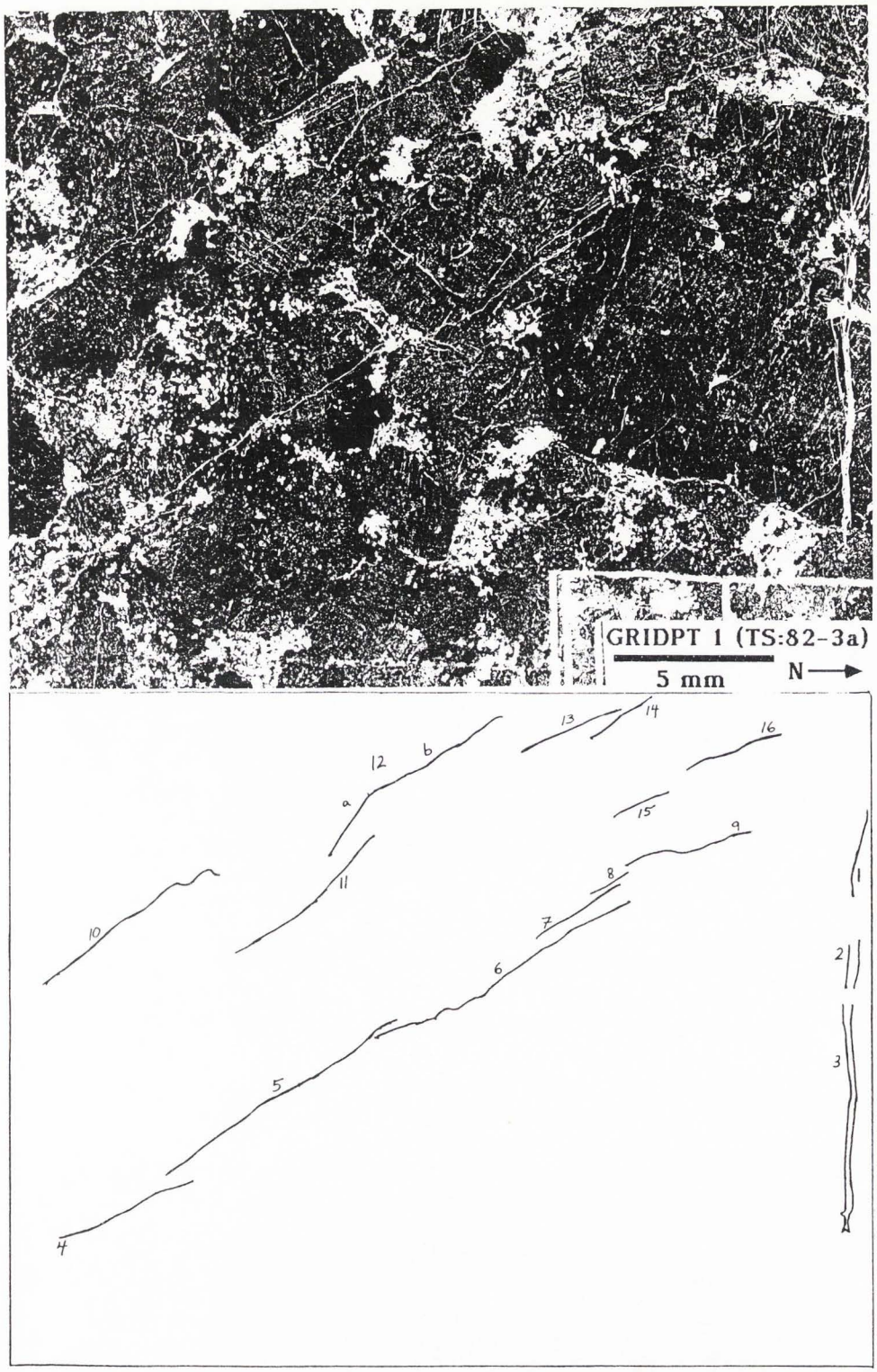
GRIDPT 1 (TS:82-3a)
5 mm
N
1
2
3
4
5
6
7
8
9
10
11
12
a
b
13
14
15
16

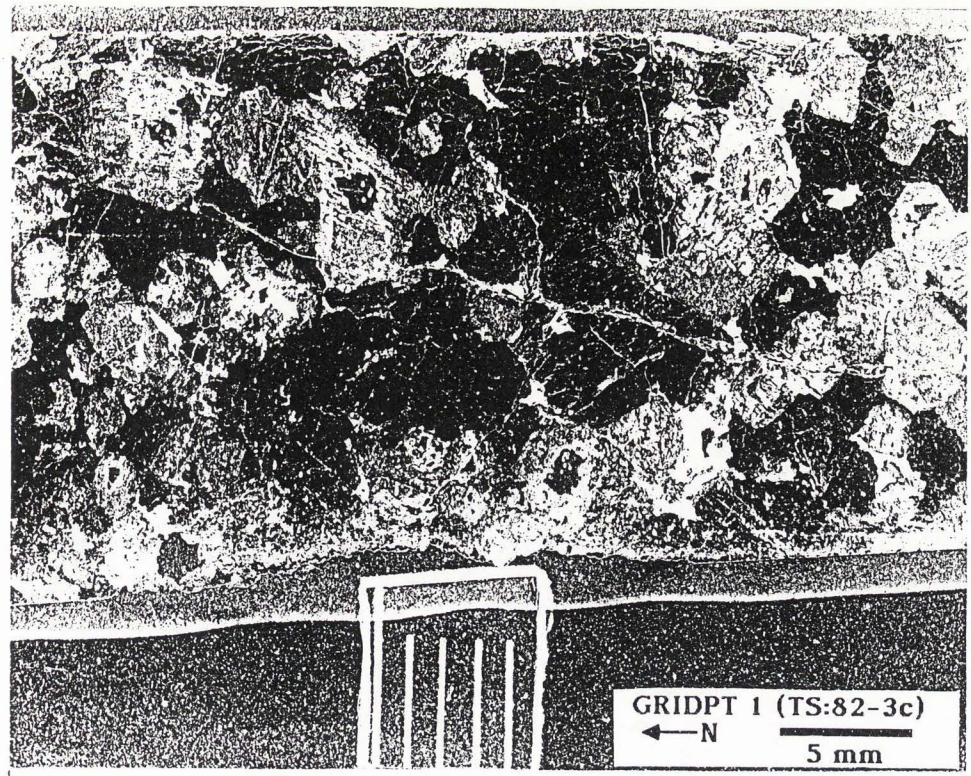
GRIDPT 1 (TS:82-3c)
N
5 mm

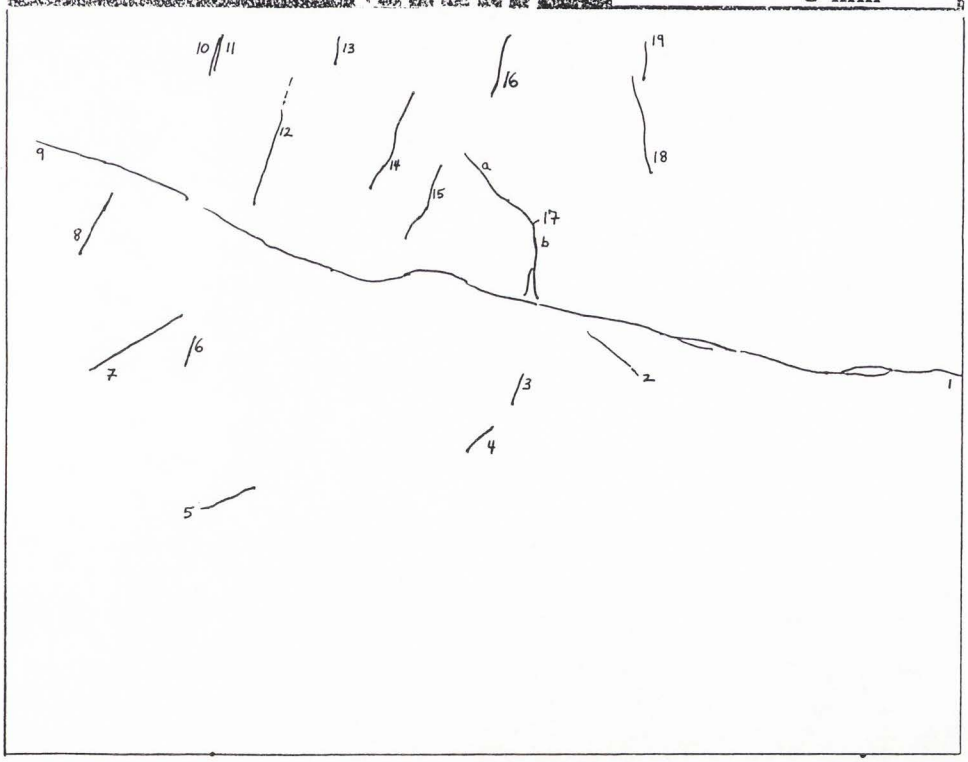
10
11
13
16
19
12
18
9
14
a
15
17
8
b
7
6
3
2
1
4
5

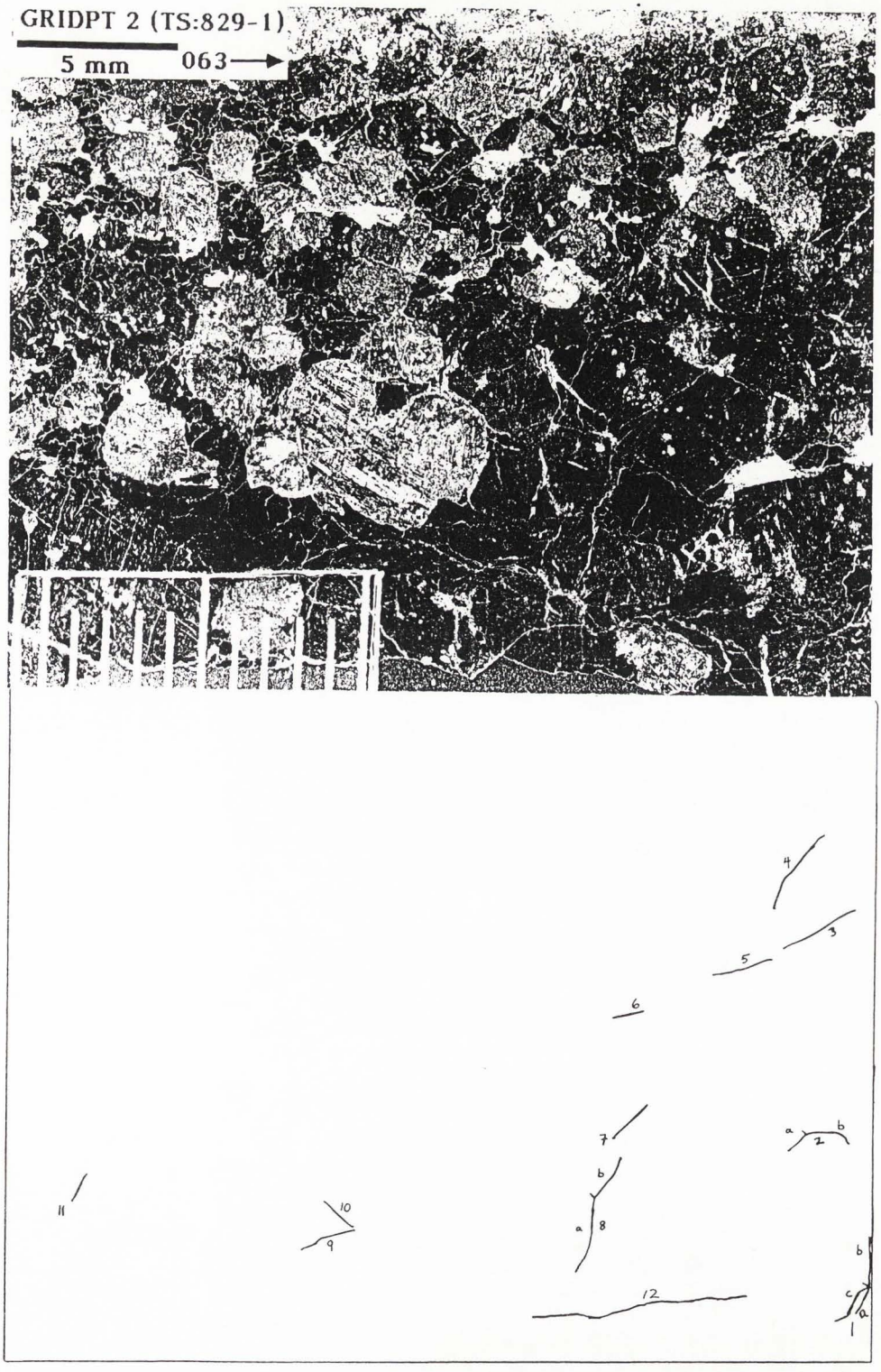
GRIDPT 2 (TS:829-1)
5 mm
063
4
3
5
6
7
b
a
8
2
a
b
11
10
9
12
b
c
a
1

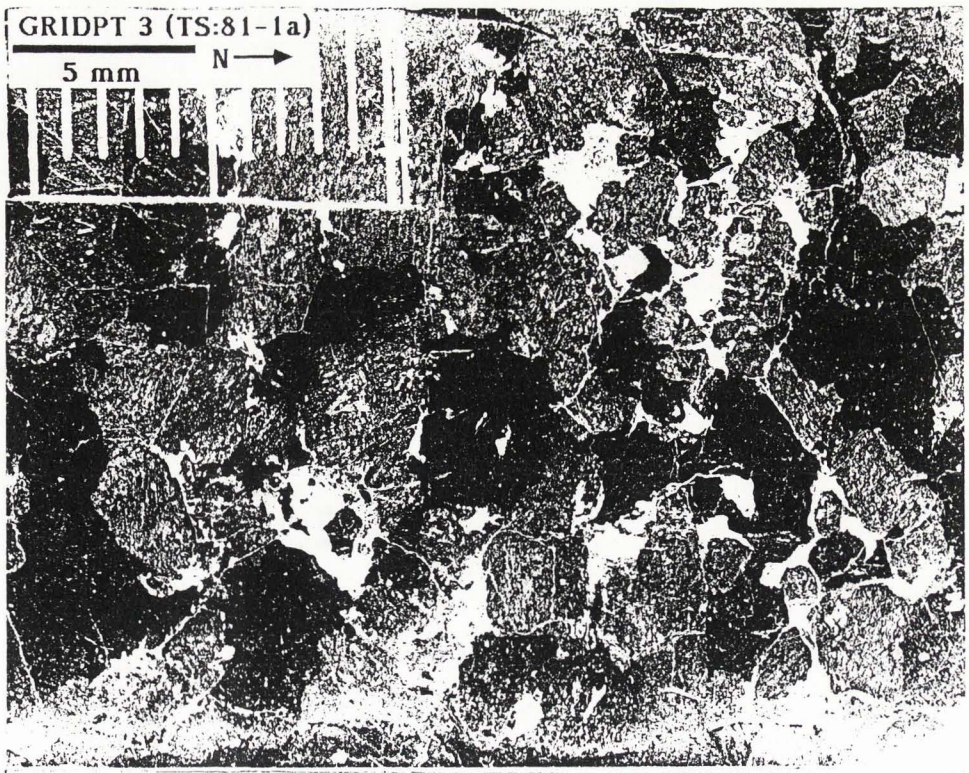
GRIDPT 3 (TS:81-1a)
5 mm
N

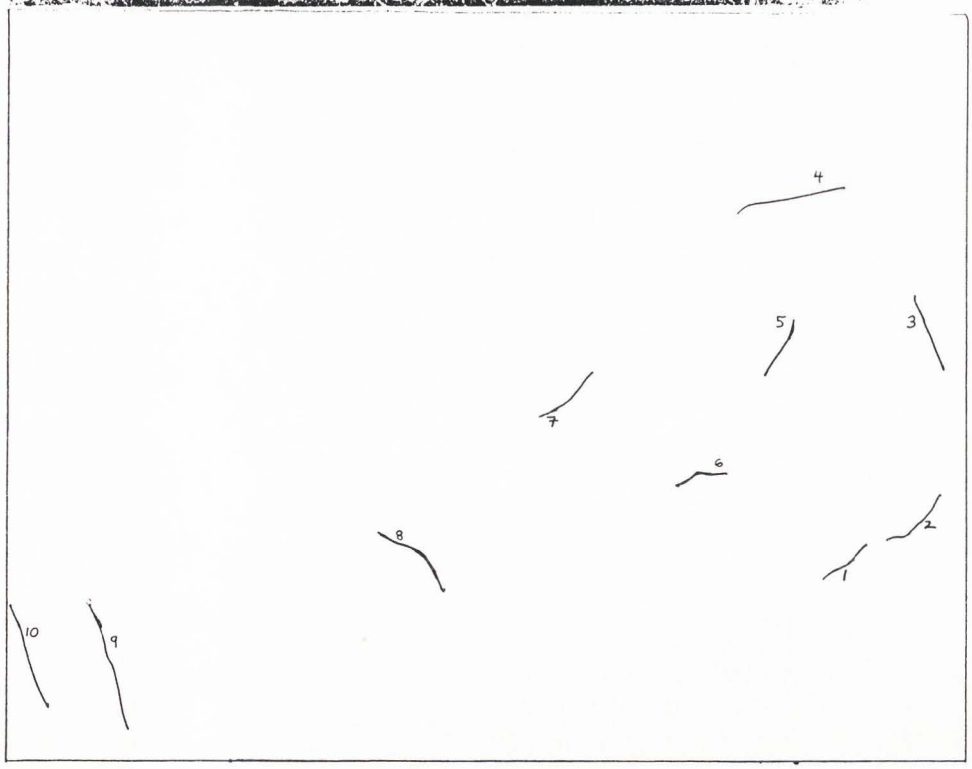
4
5
3
7
6
8
2
1
10
9

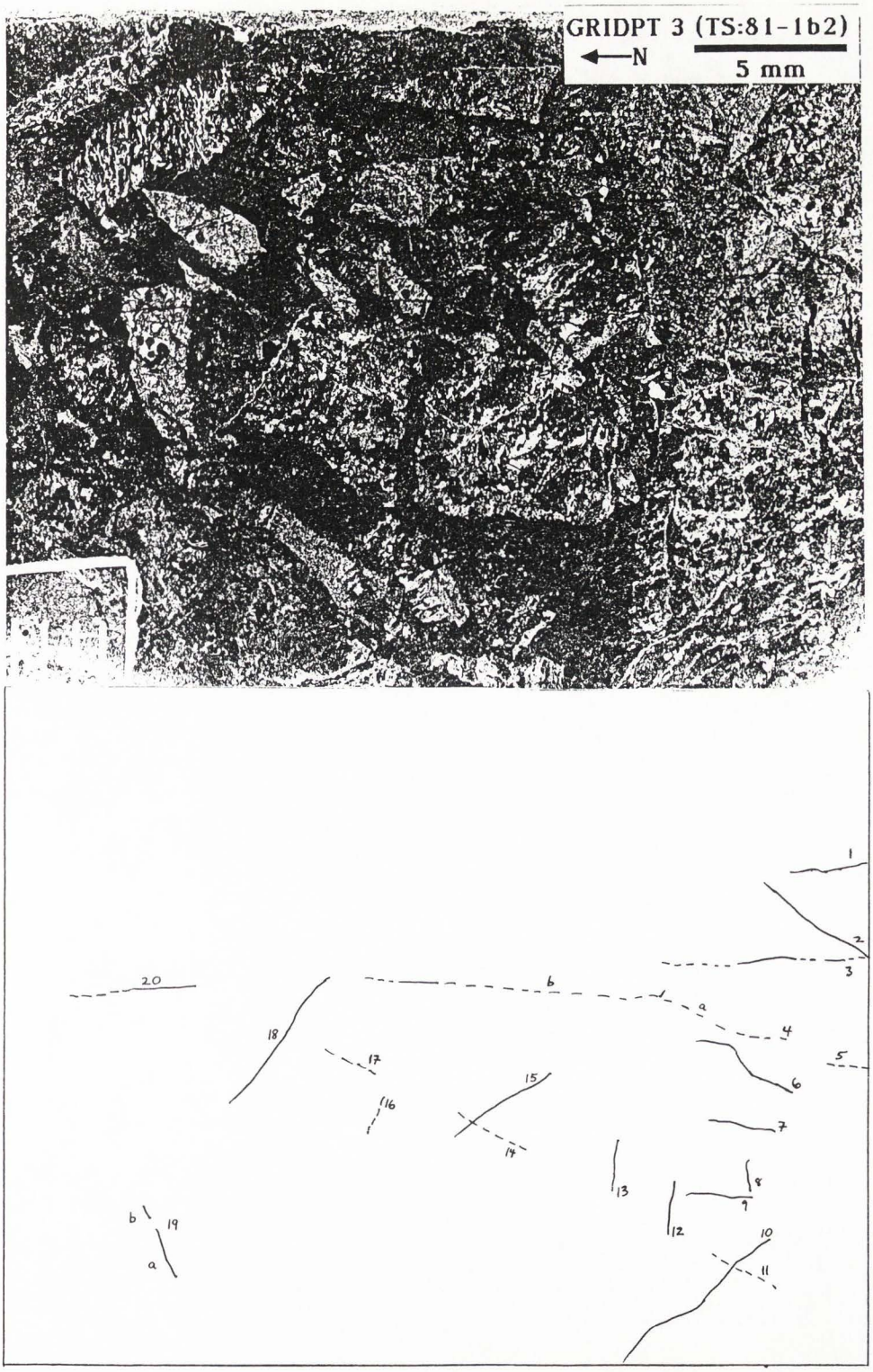
GRIDPT 3 (TS:81-1b2)
N
5 mm
1
2
3
4
5
6
7
8
9
10
11
12
13
14
15
16
17
18
19
20
a
b

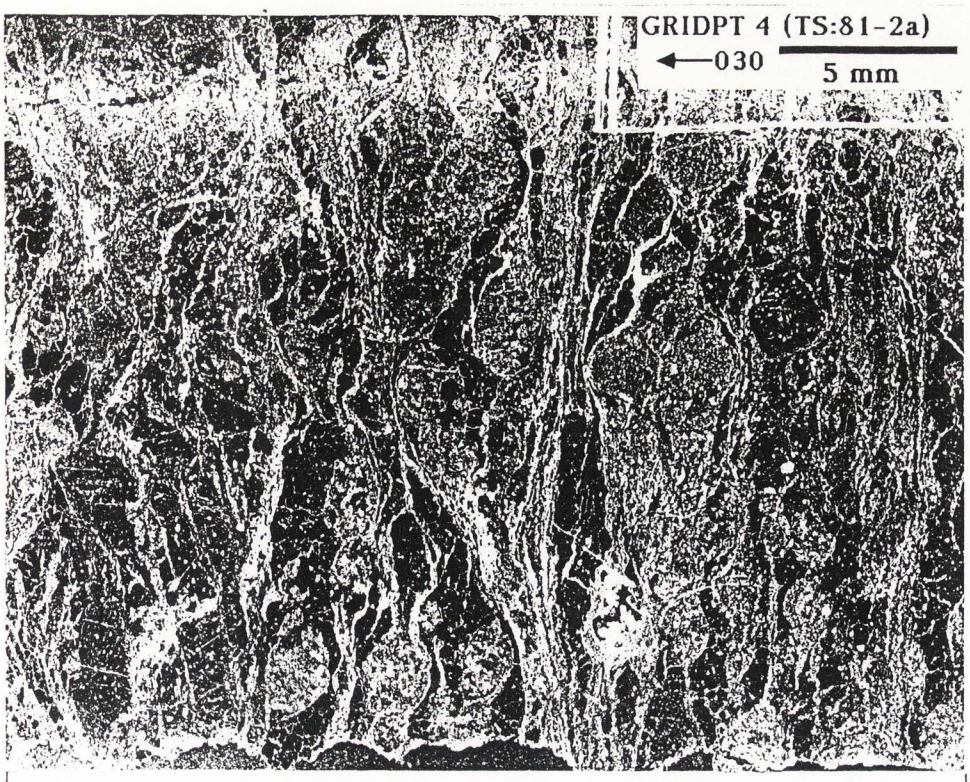
GRIDPT 4 (TS:81-2a)
030
5 mm

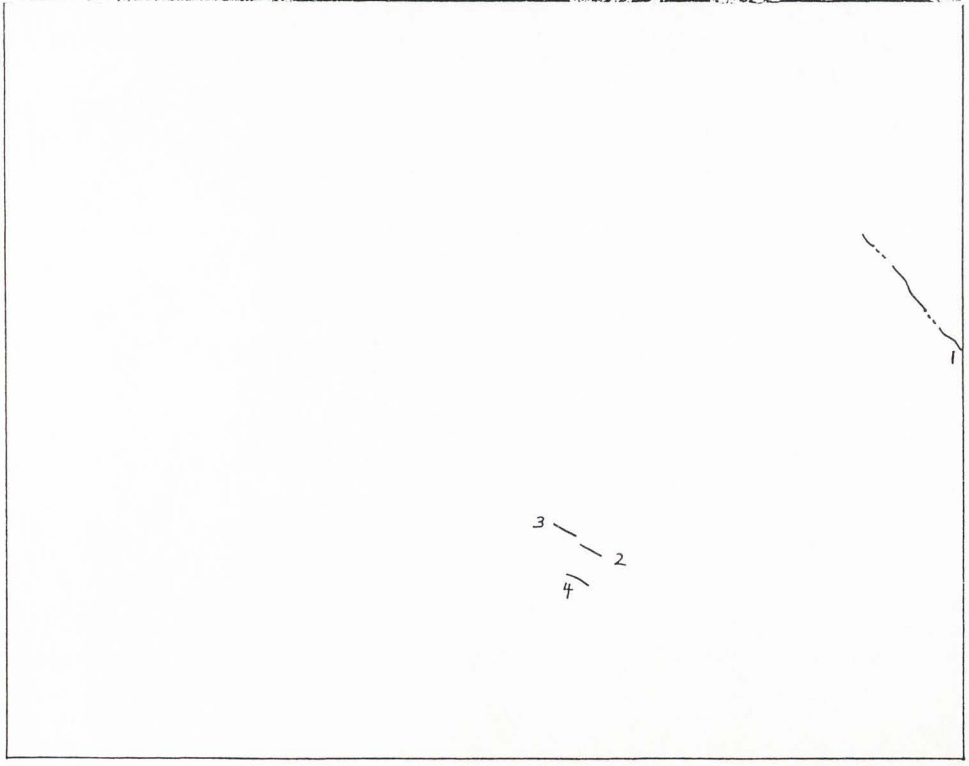
1
2
3
4

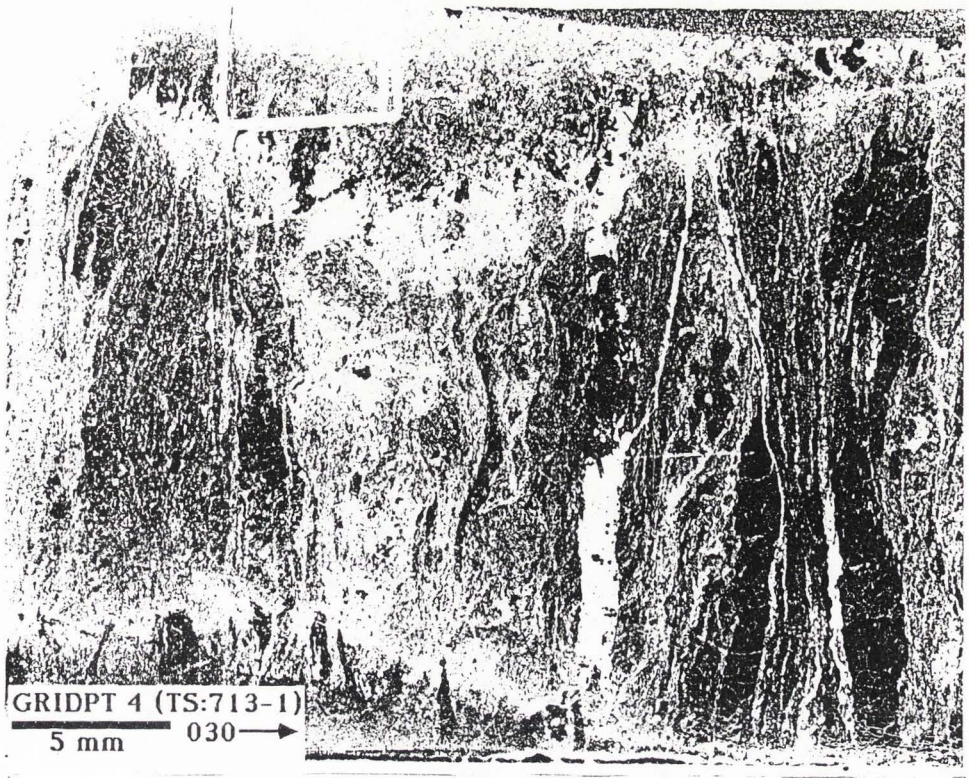
GRIDPT 4 (TS:713-1)
5 mm
030

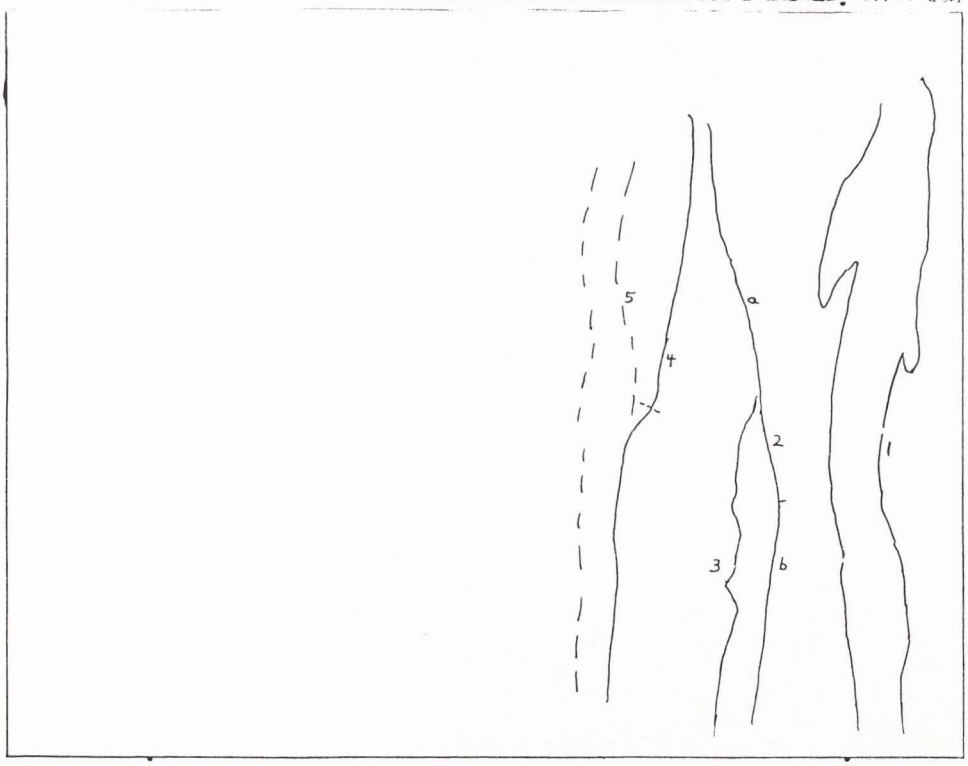
5
a
4
2
1
3
b

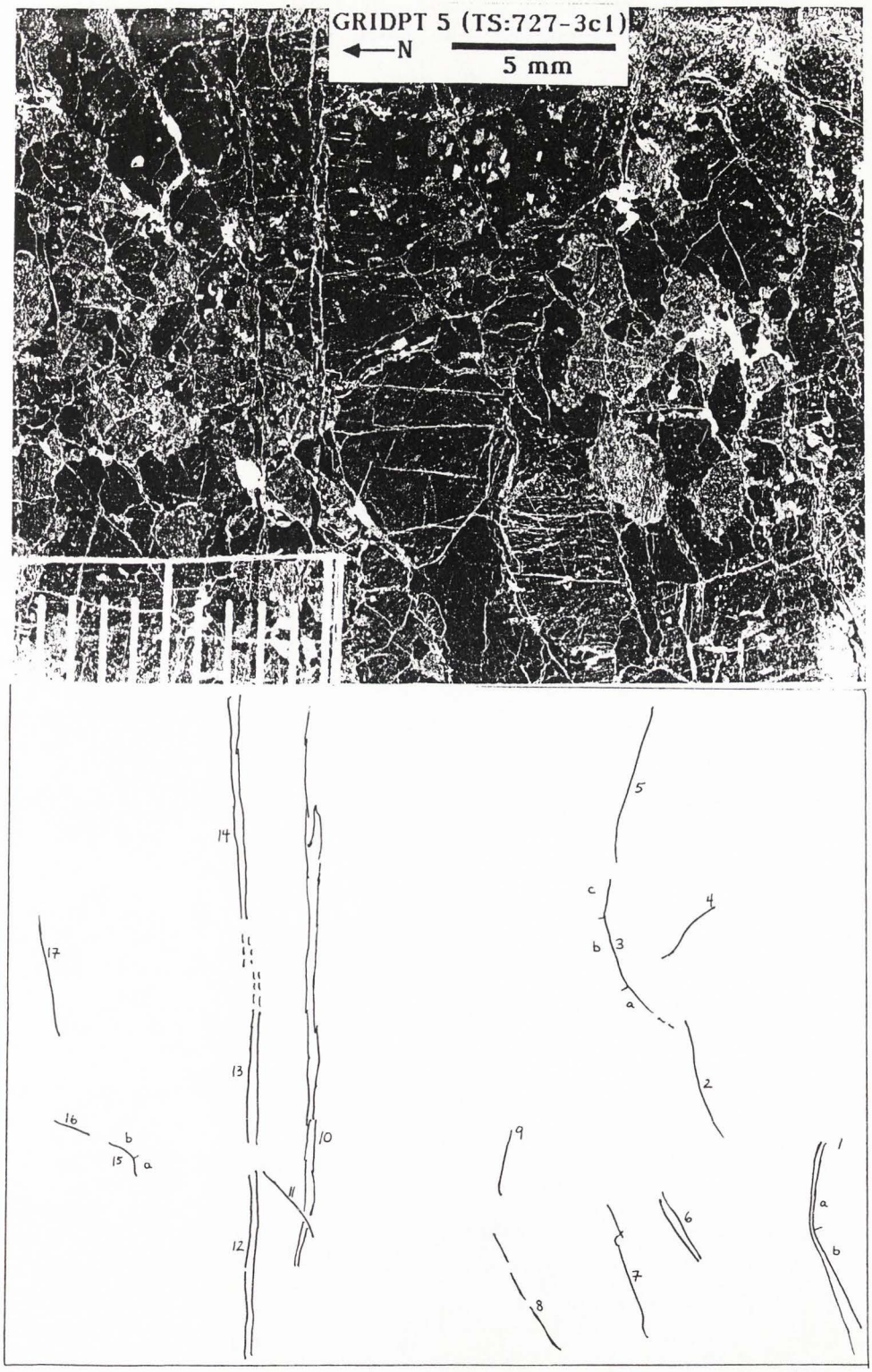
GRIDPT 5 (TS:727-3c1)
N
5 mm
1
a
b
2
3
a
b
c
4
5
6
7
8
9
10
11
12
13
14
15
a
b
16
17

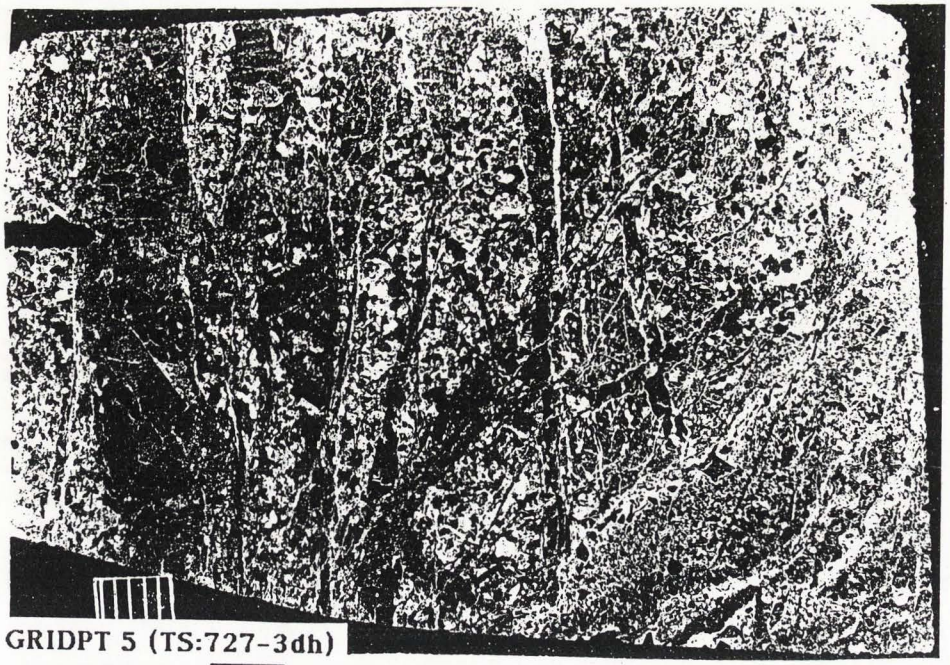
GRIDPT 5 (TS:727-3dh)
010
5 mm

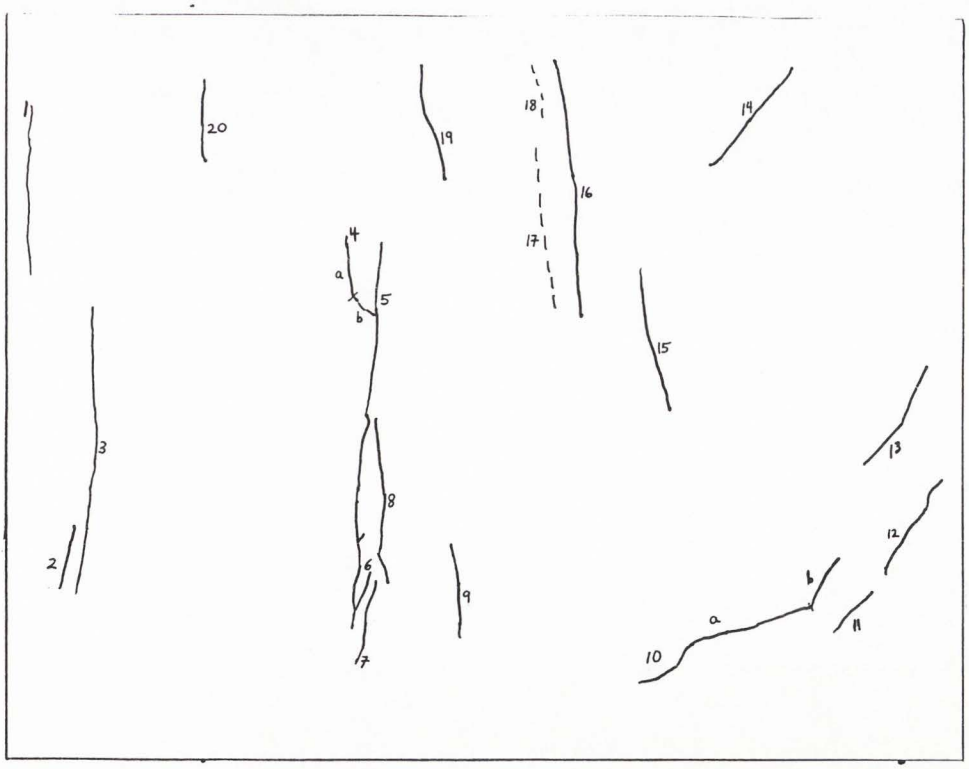
1
20
19
18
14
16
17
4
a
5
b
15
3
13
8
12
2
6
b
9
a
11
10
7

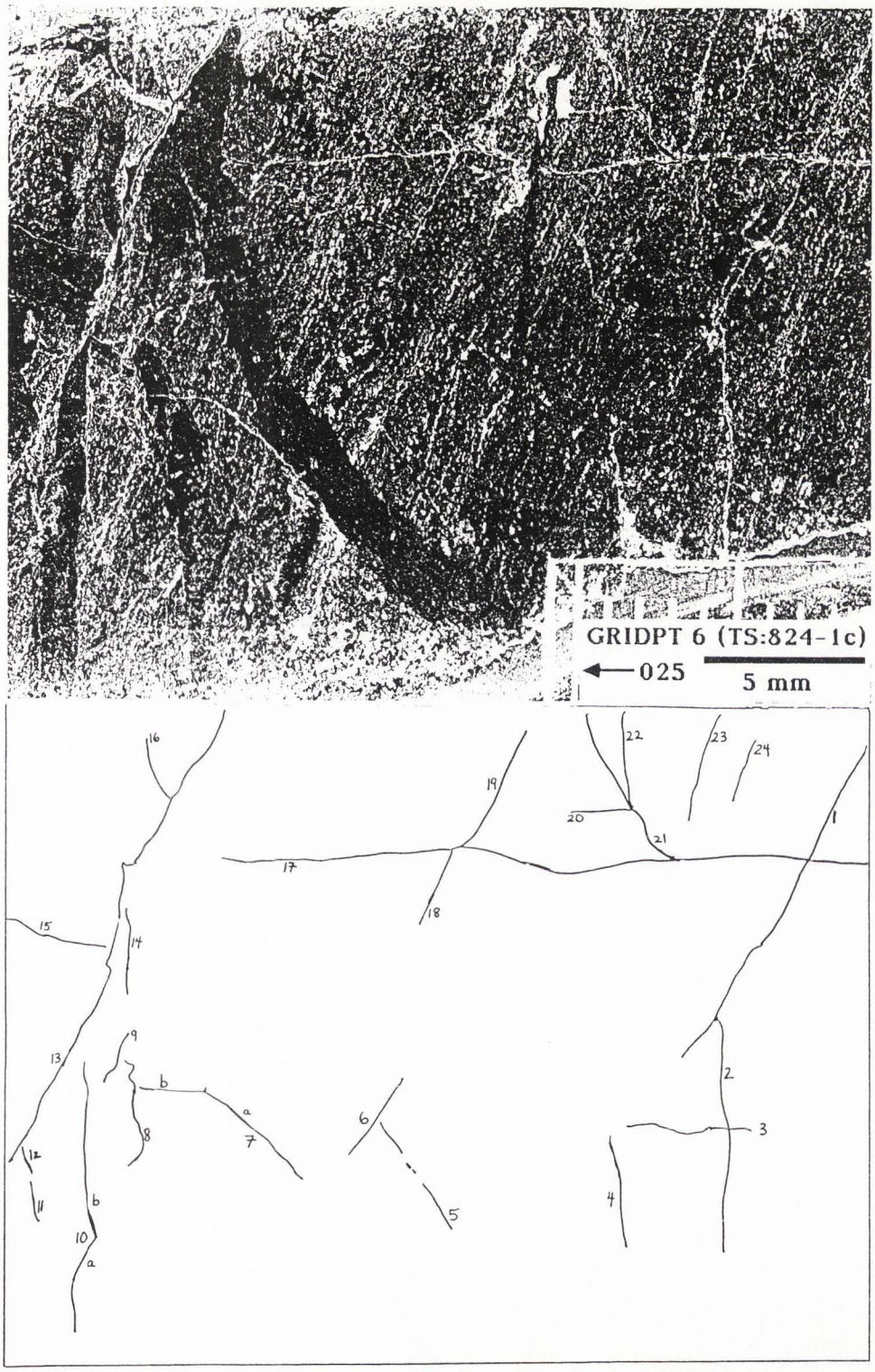
GRIDPT 6 (TS:824-1c)
025
5 mm
1
2
3
4
5
6
7
8
9
10
11
12
13
14
15
16
17
18
19
20
21
22
23
24
a
b

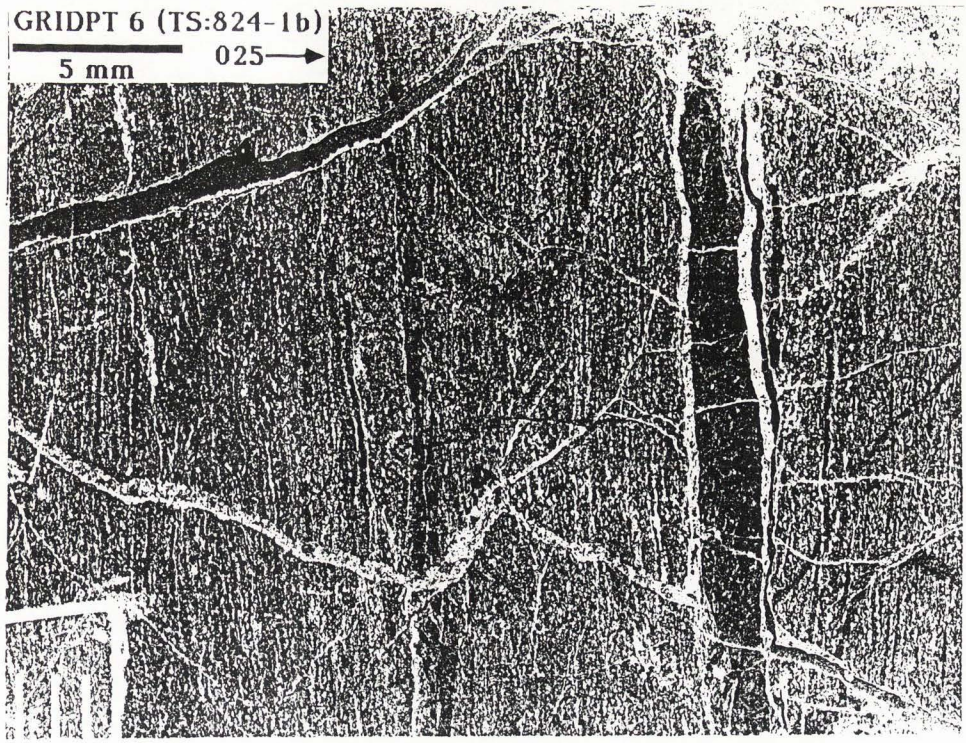
GRIDPT 6 (TS:824-1b)
5 mm
025

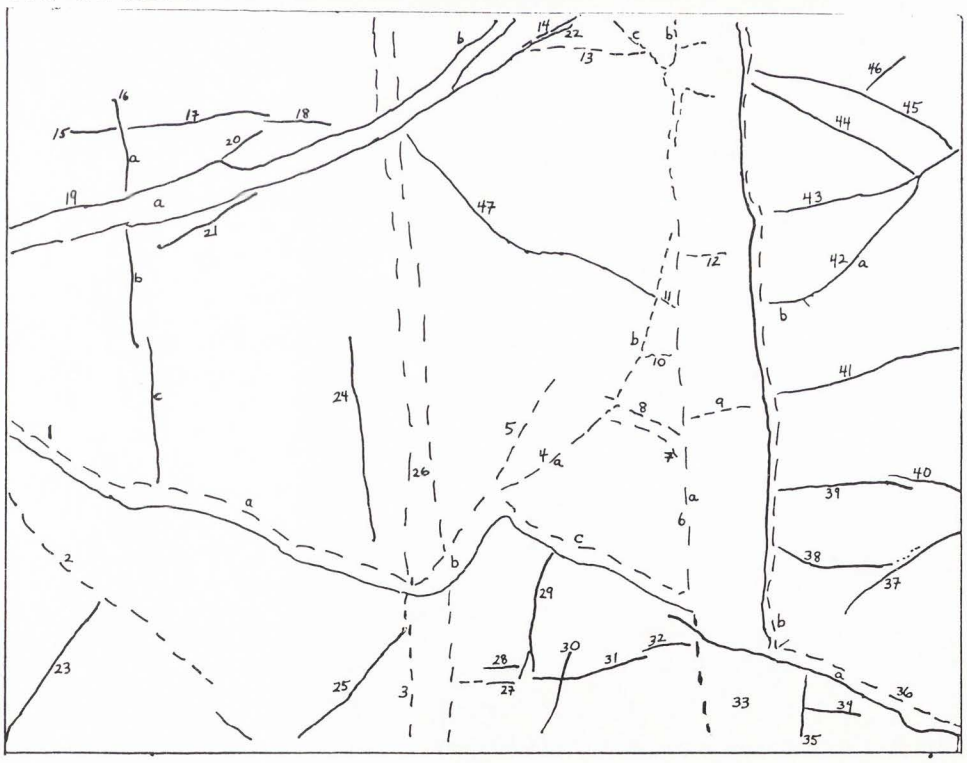
1
2
3
4
5
6
7
8
9
10
11
12
13
14
15
16
17
18
19
20
21
22
23
24
25
26
27
28
29
30
31
32
33
34
35
36
37
38
39
40
41
42
43
44
45
46
47

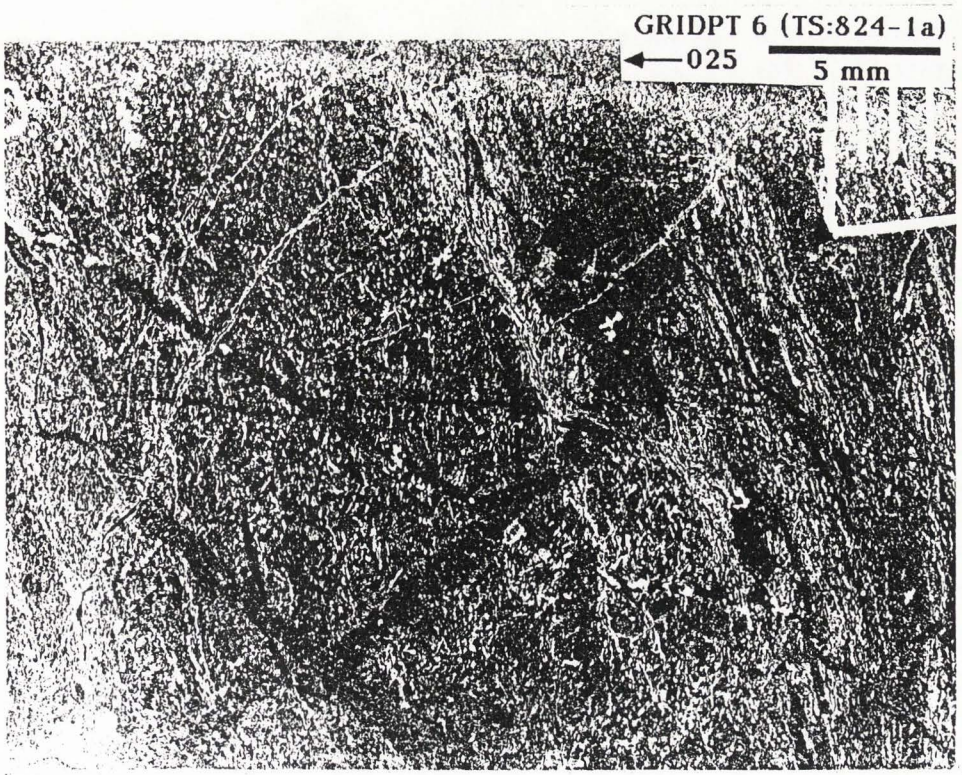
GRIDPT 6 (TS:824-1a)
025
5 mm

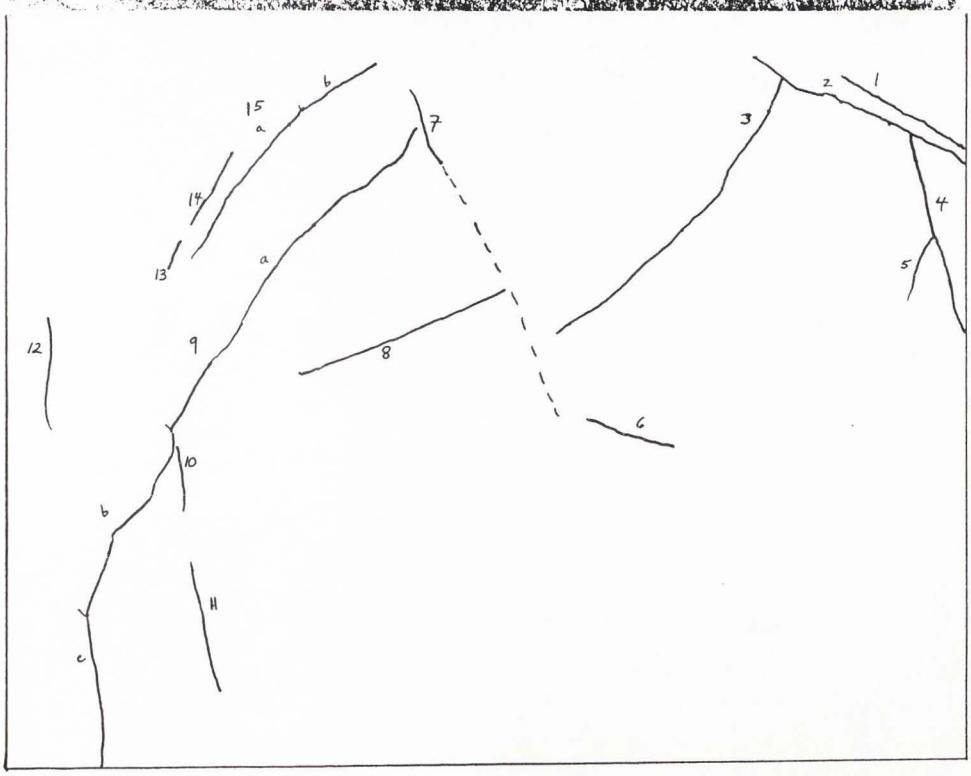
15
a
b
14
13
7
a
12
9
8
10
b
11
c
6
3
2
1
4
5

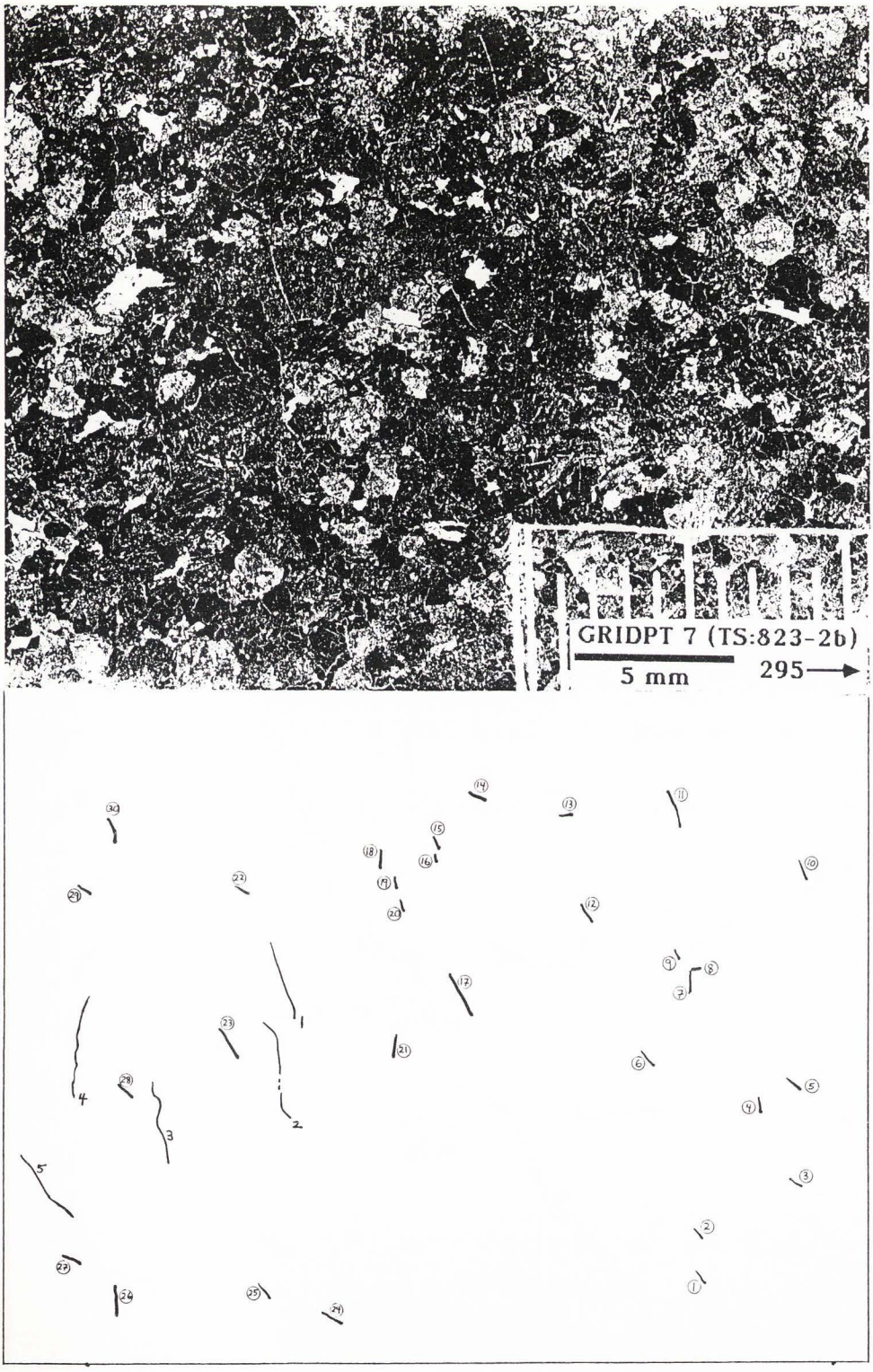
GRIDPT 7 (TS:823-2b)
5 mm
295

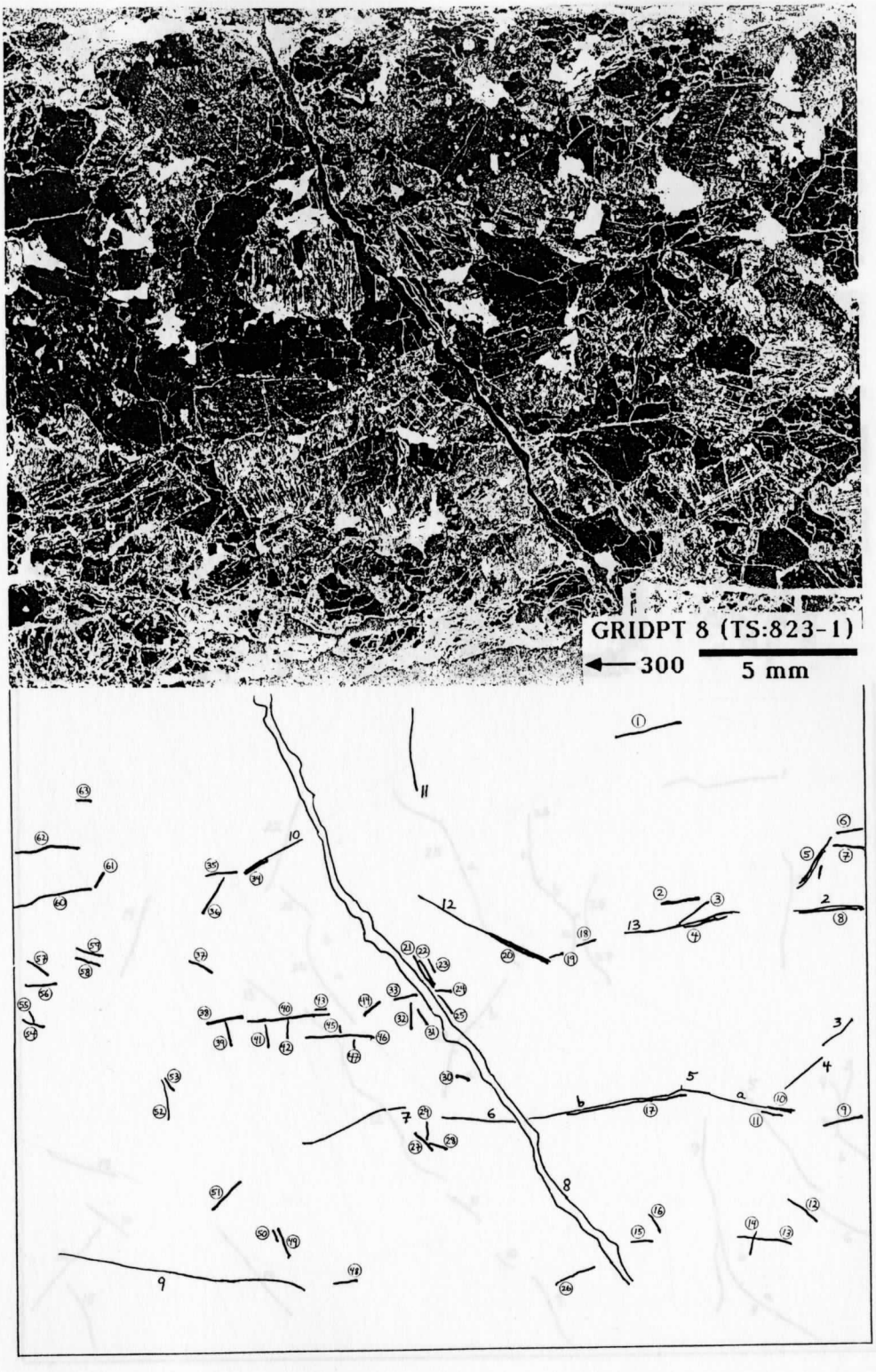
GRIDPT 8 (TS:823-1)
300
5 mm

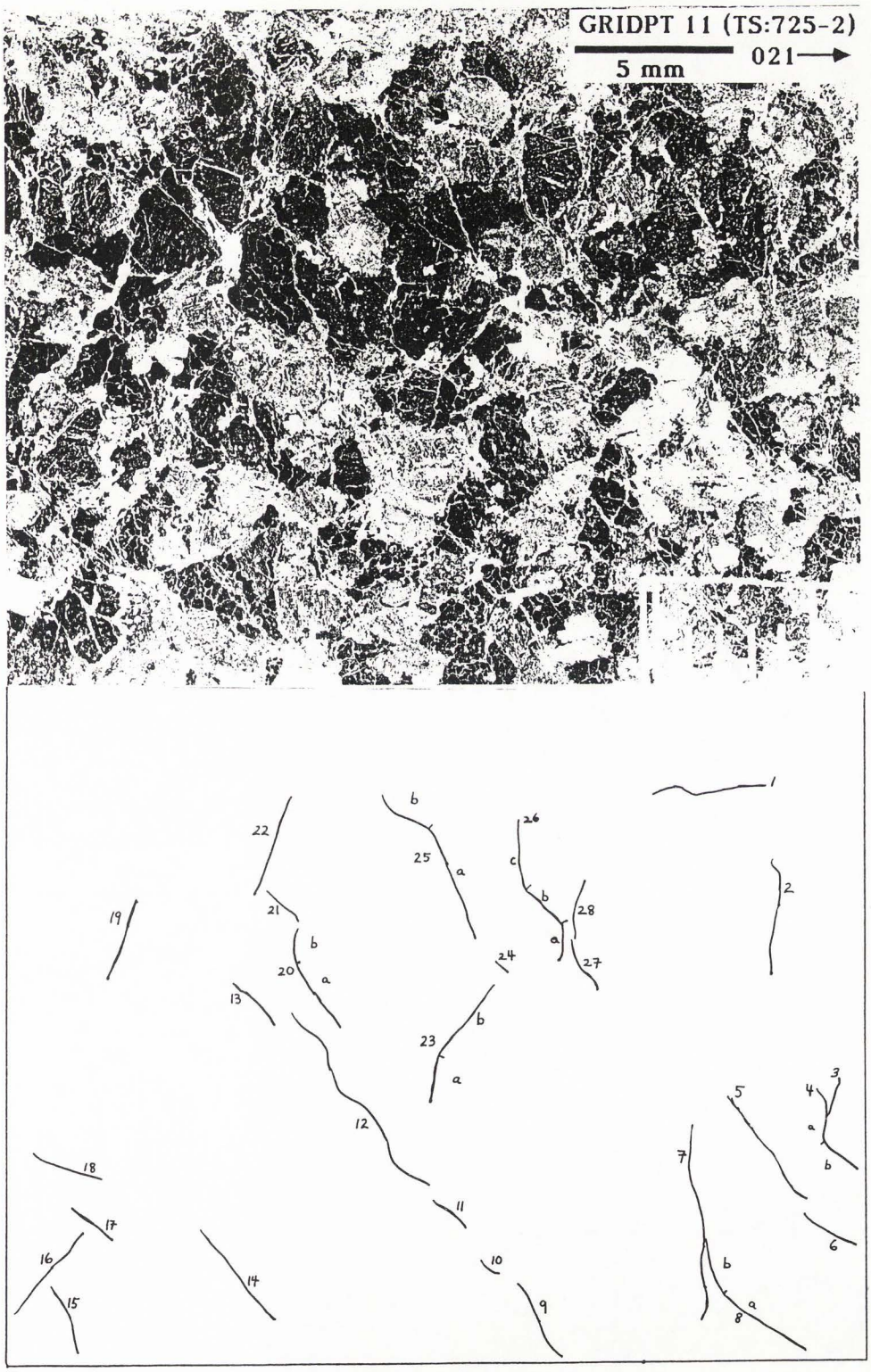
GRIDPT 11 (TS:725-2)
5 mm
021
1
2
3
4
a
b
5
6
7
b
8
a
9
10
11
12
13
14
15
16
17
18
19
20
b
a
21
22
23
b
a
24
25
b
a
26
c
b
a
27
28

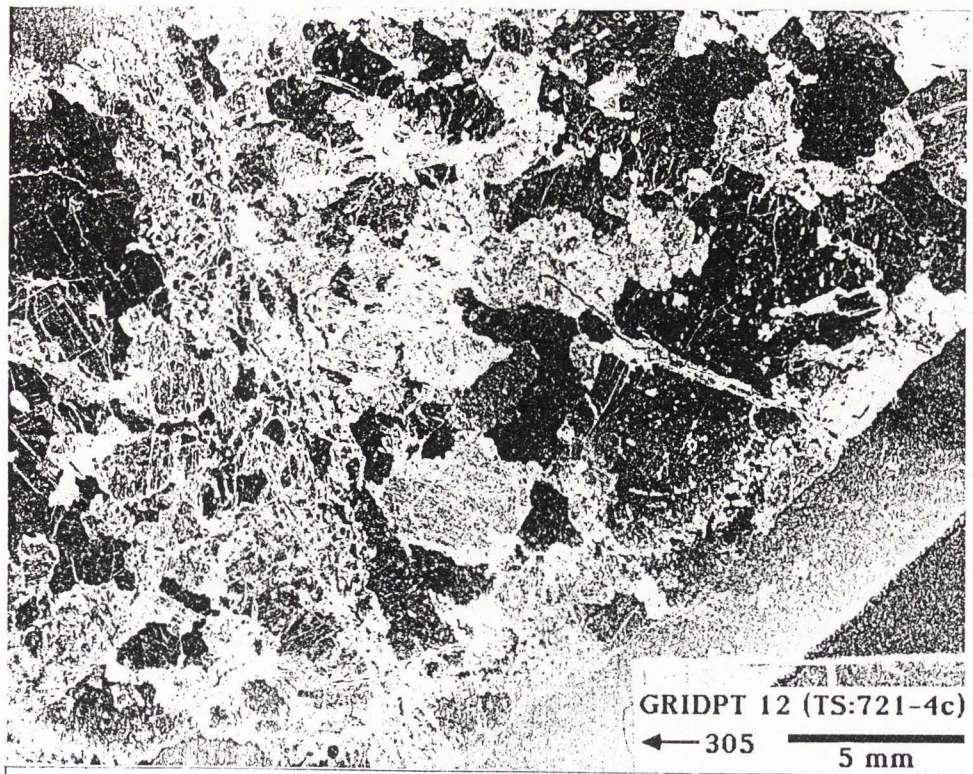
GRIDPT 12 (TS:721-4c)
305
5 mm

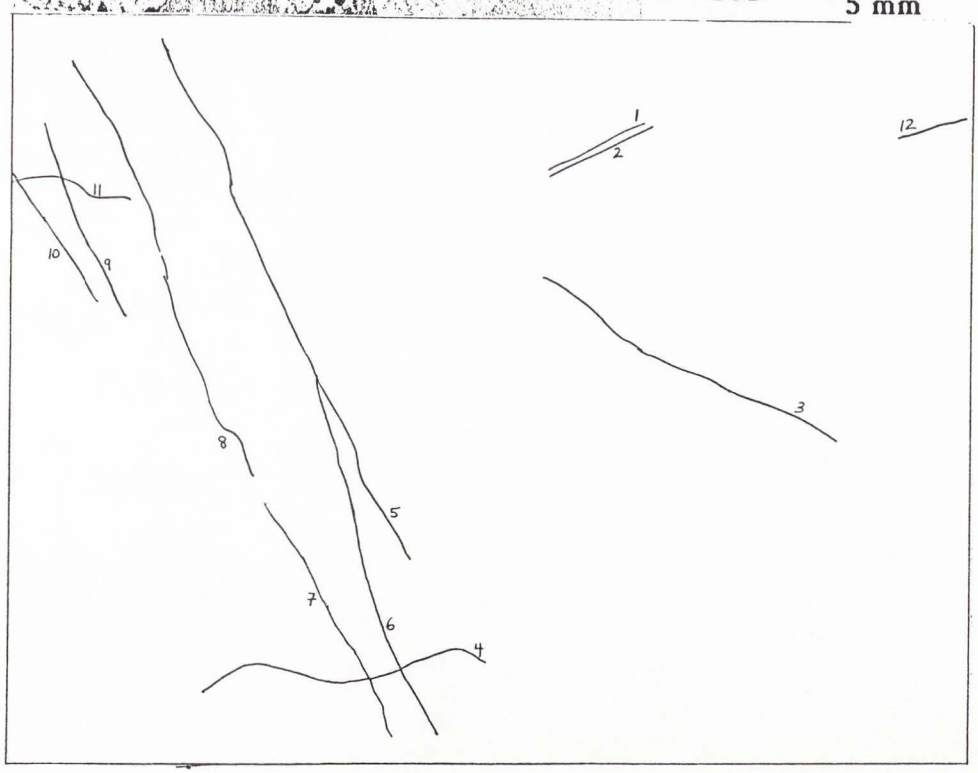
1
2
12
11
10
9
8
3
5
7
6
4

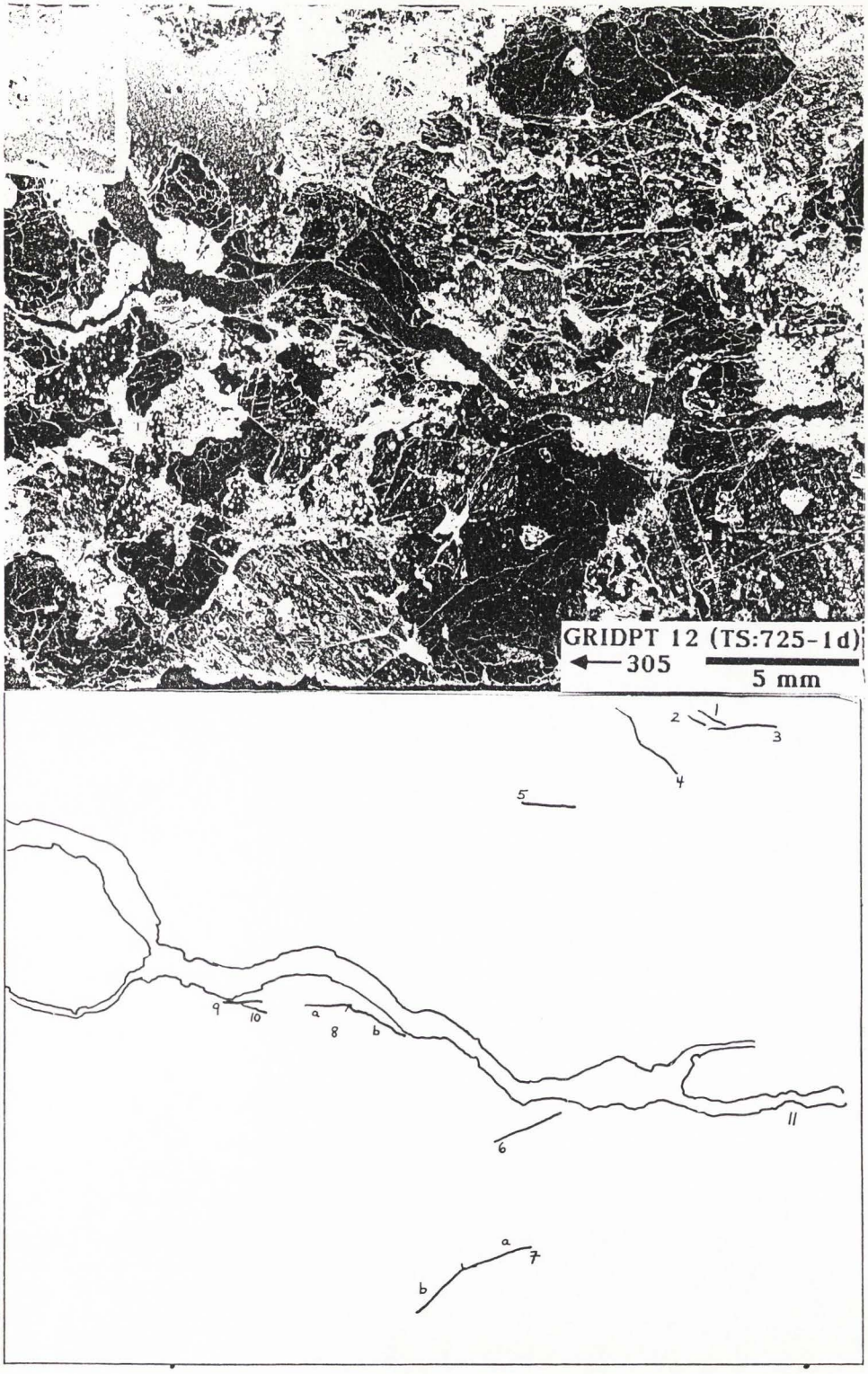
GRIDPT 12 (TS:725-1d)
305
5 mm
1
2
3
4
5
6
7
8
9
10
11
a
b
a
b

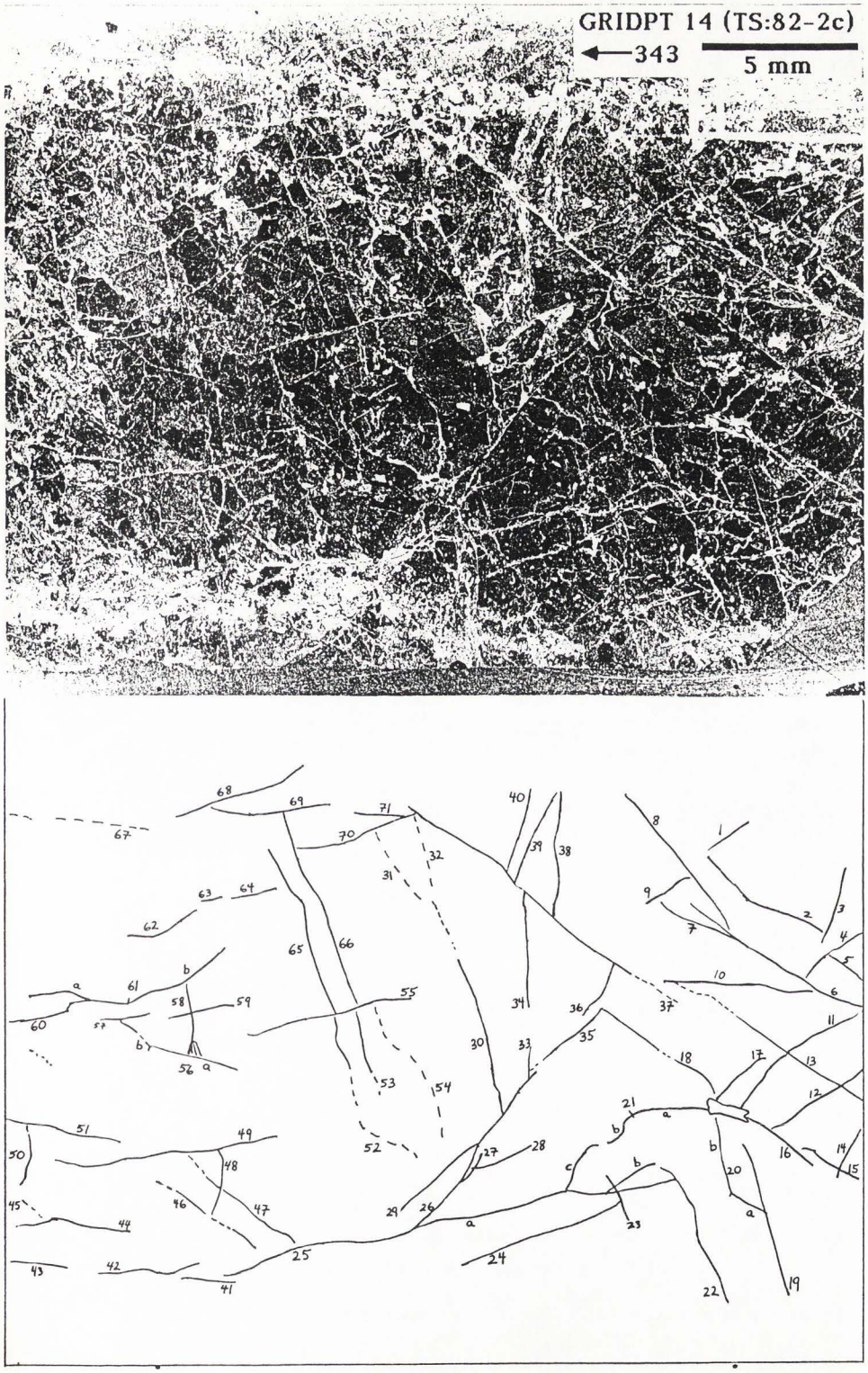
GRIDPT 14 (TS:82-2c)
←343
5 mm

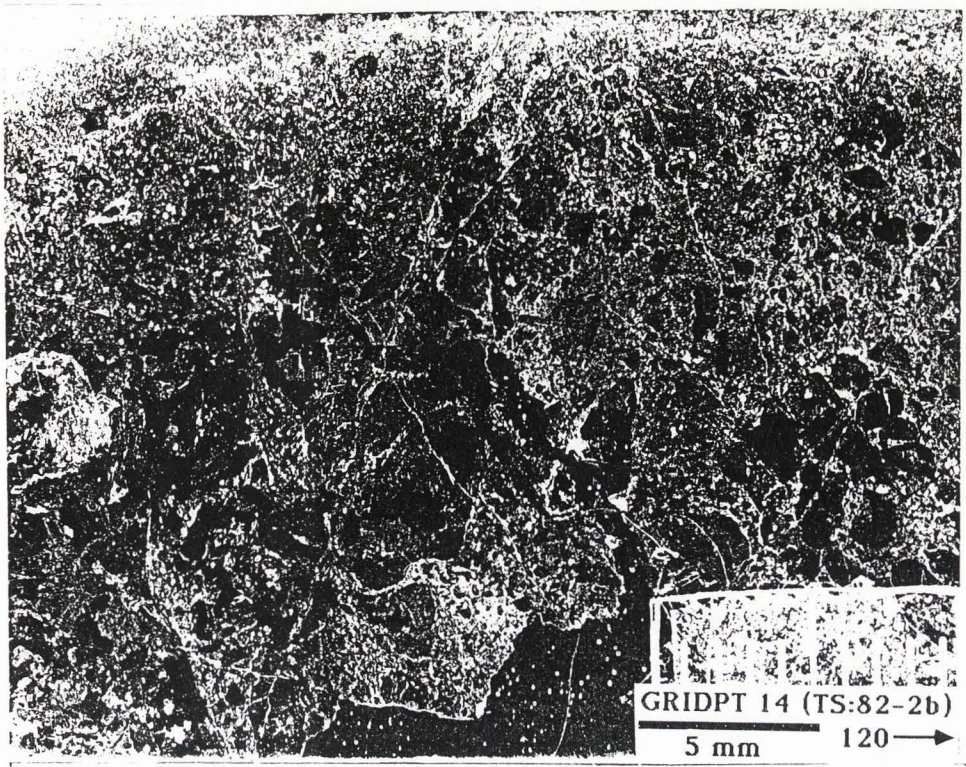
GRIDPT 14 (TS:82-2b)
5 mm
120

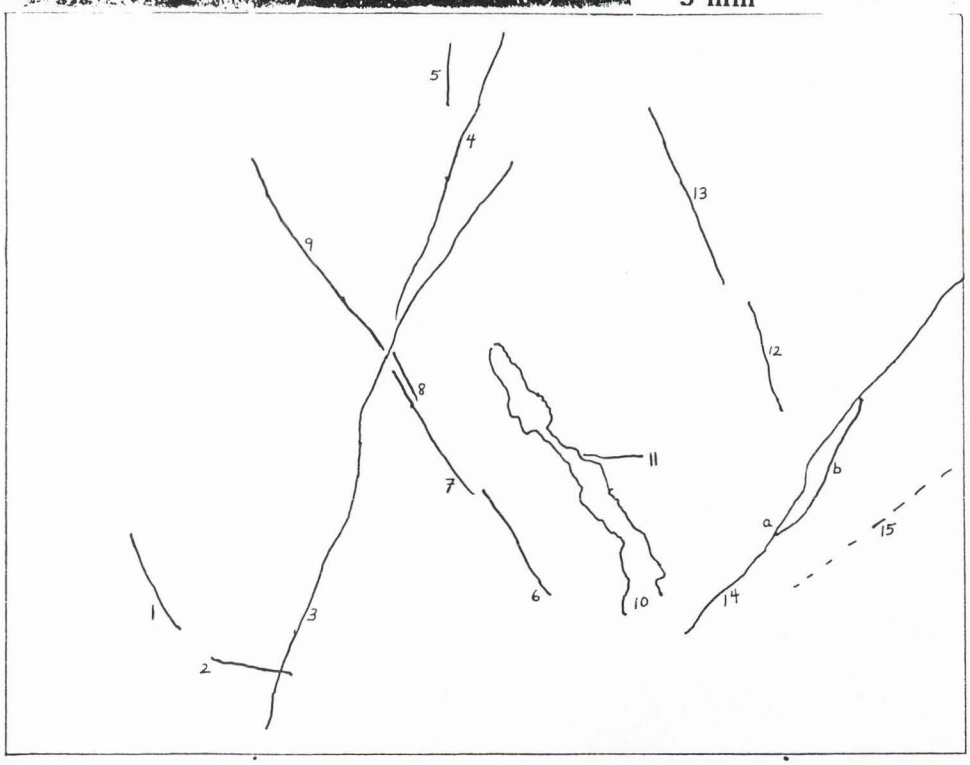
1
2
3
4
5
6
7
8
9
10
11
12
13
14
15
a
b

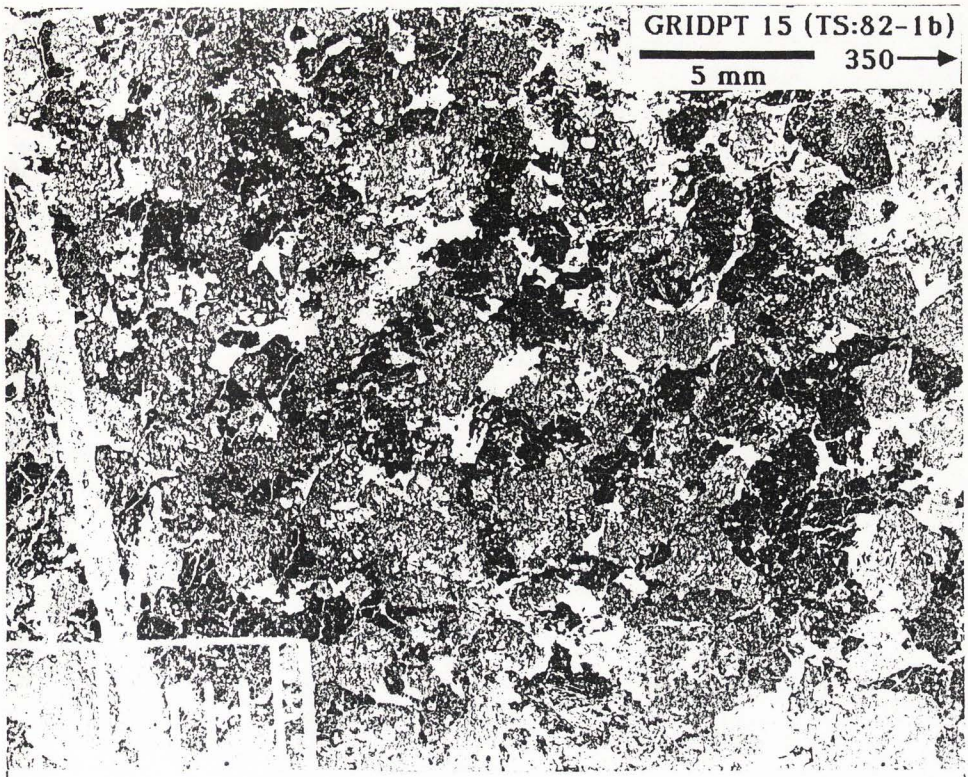
GRIDPT 15 (TS:82-1b)
5 mm
350

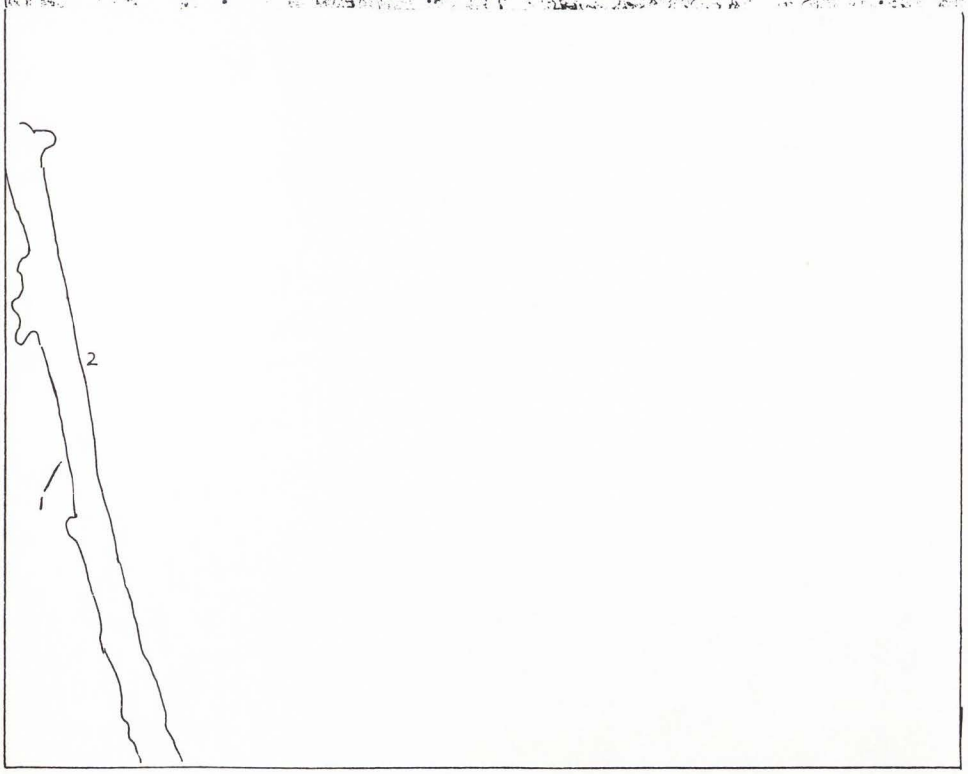
2
1

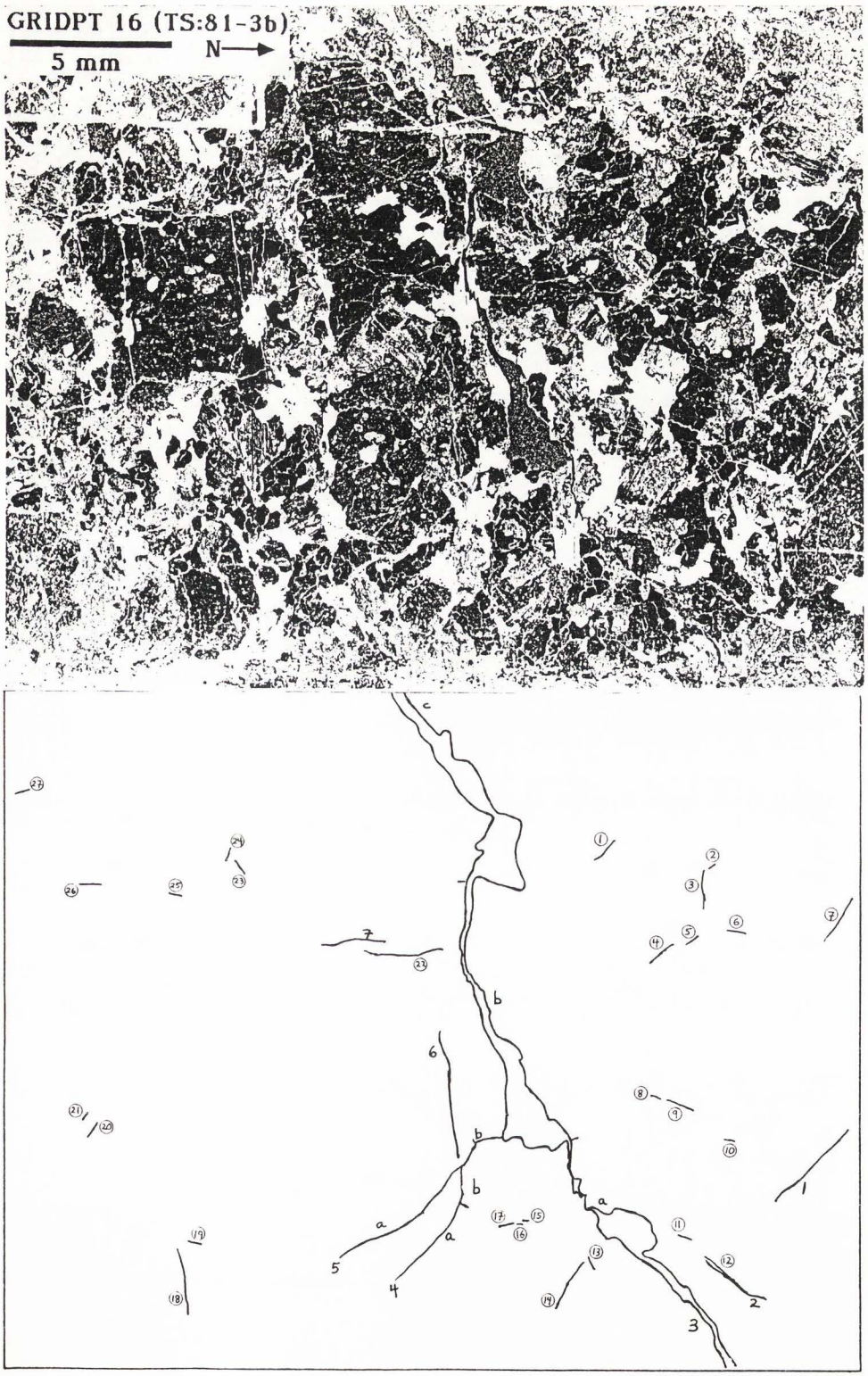
GRIDPT 16 (TS:81-3b)
5 mm
N
c
b
a
1
2
3
4
5
6
7

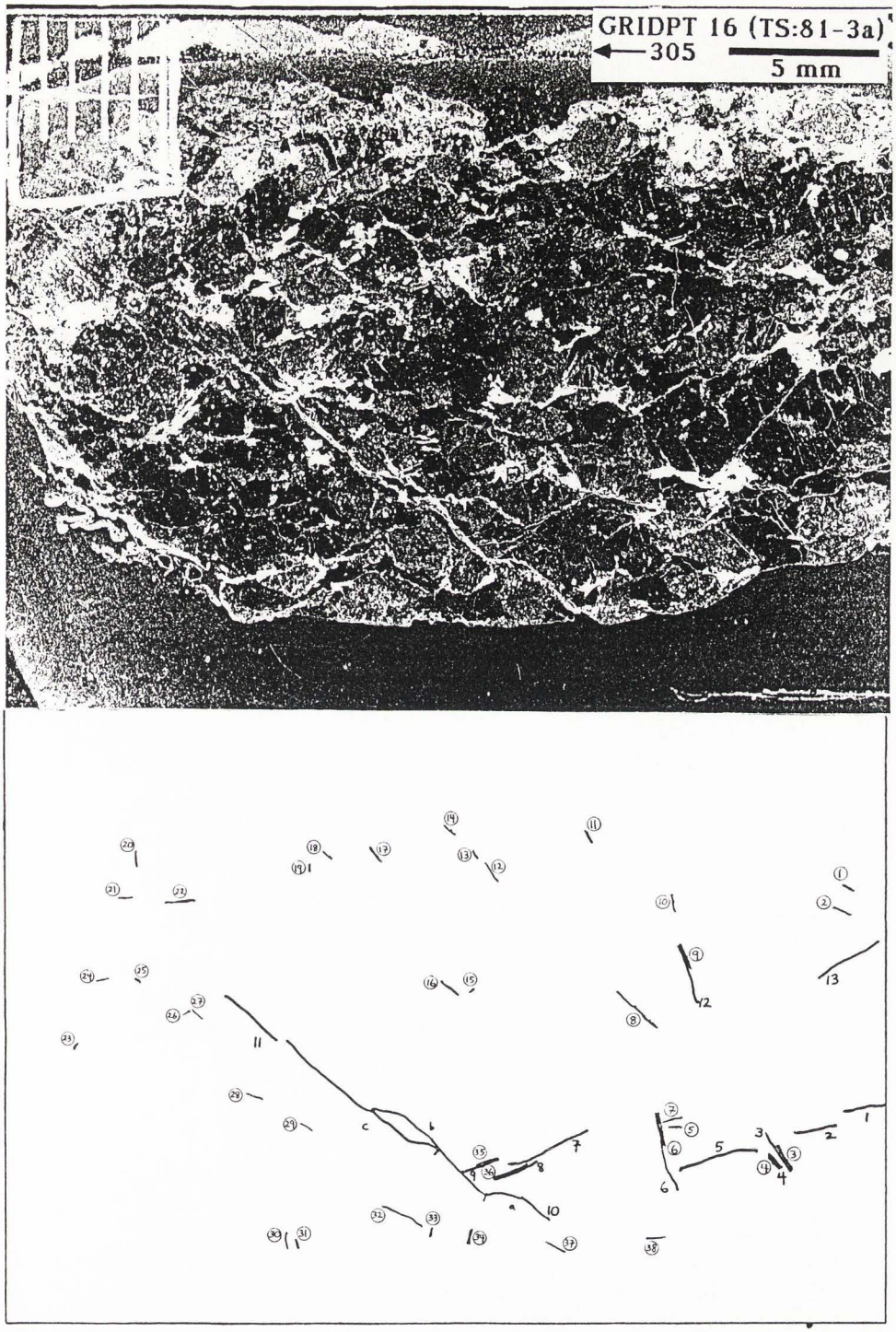
GRIDPT 16 (TS:81-3a)
305
5 mm

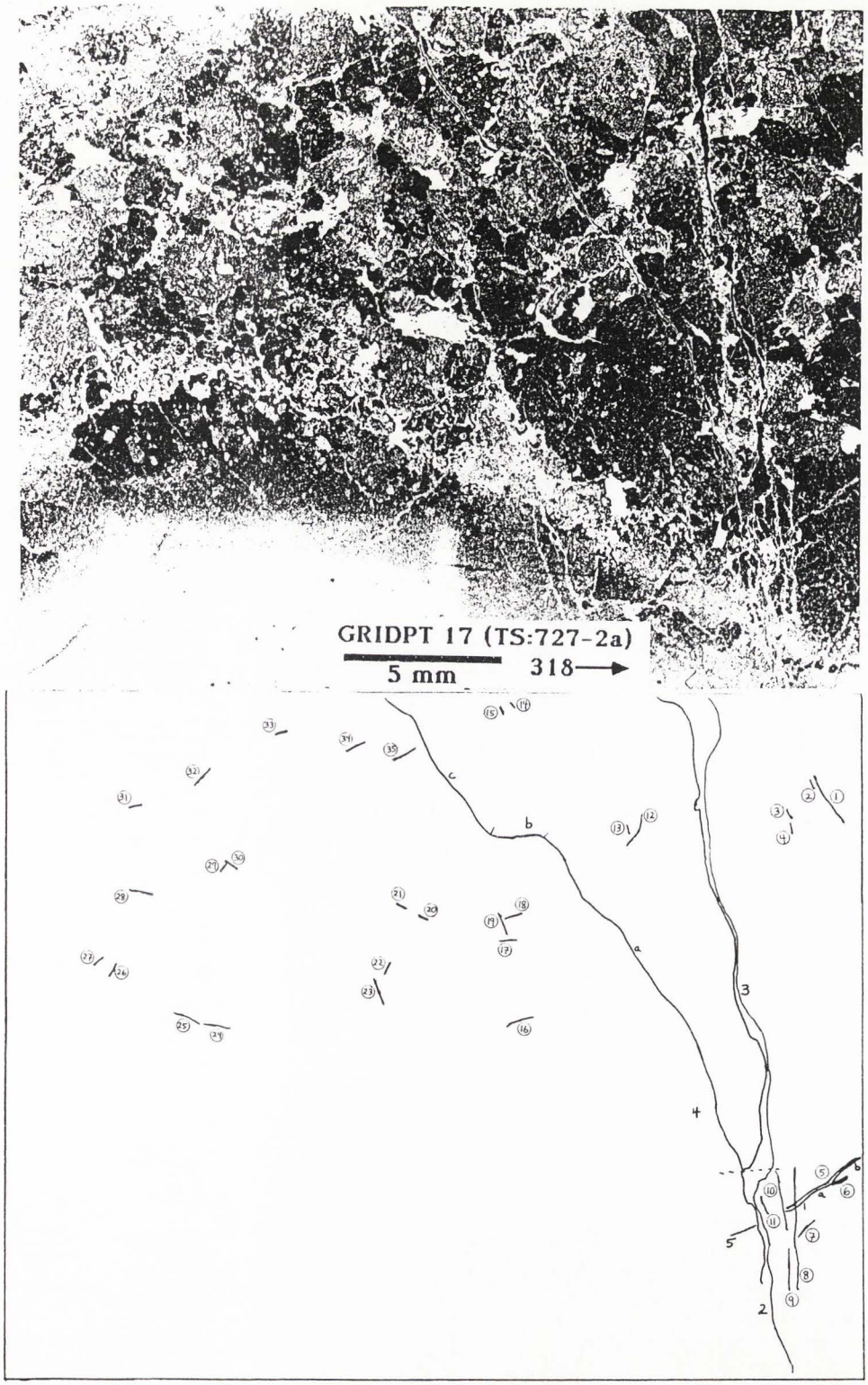
GRIDPT 17 (TS:727-2a)
5 mm
318
a
b
c
1
2
3
4
5

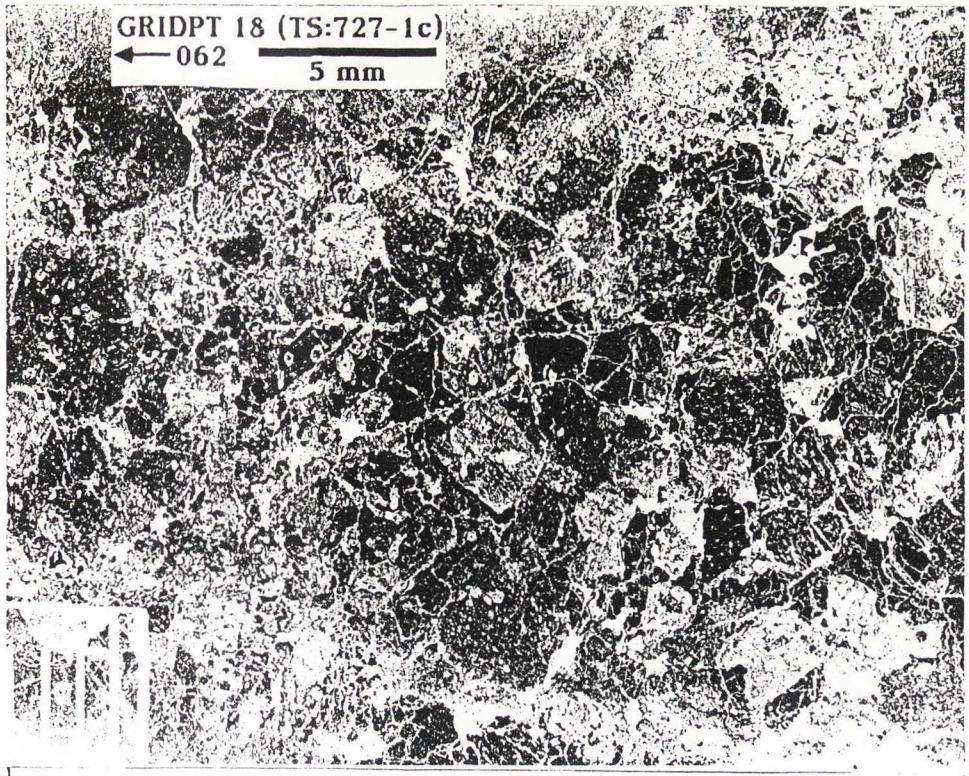
GRIDPT 18 (TS:727-1c)
062
5 mm

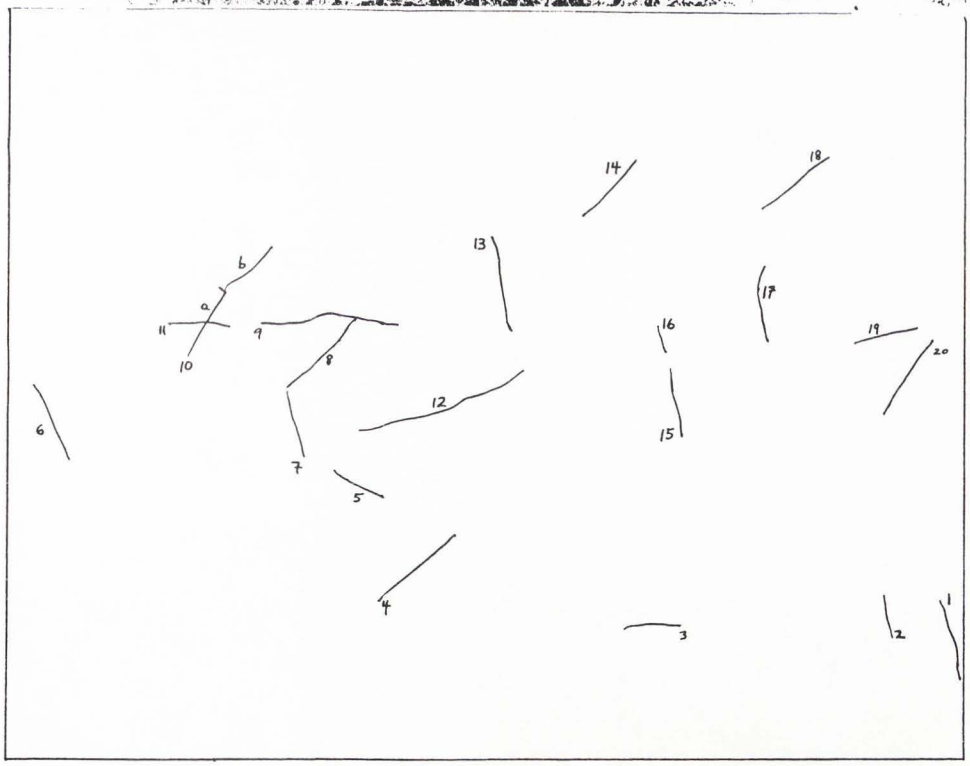
1
2
3
4
5
6
7
8
9
10
11
12
13
14
15
16
17
18
19
20
a
b

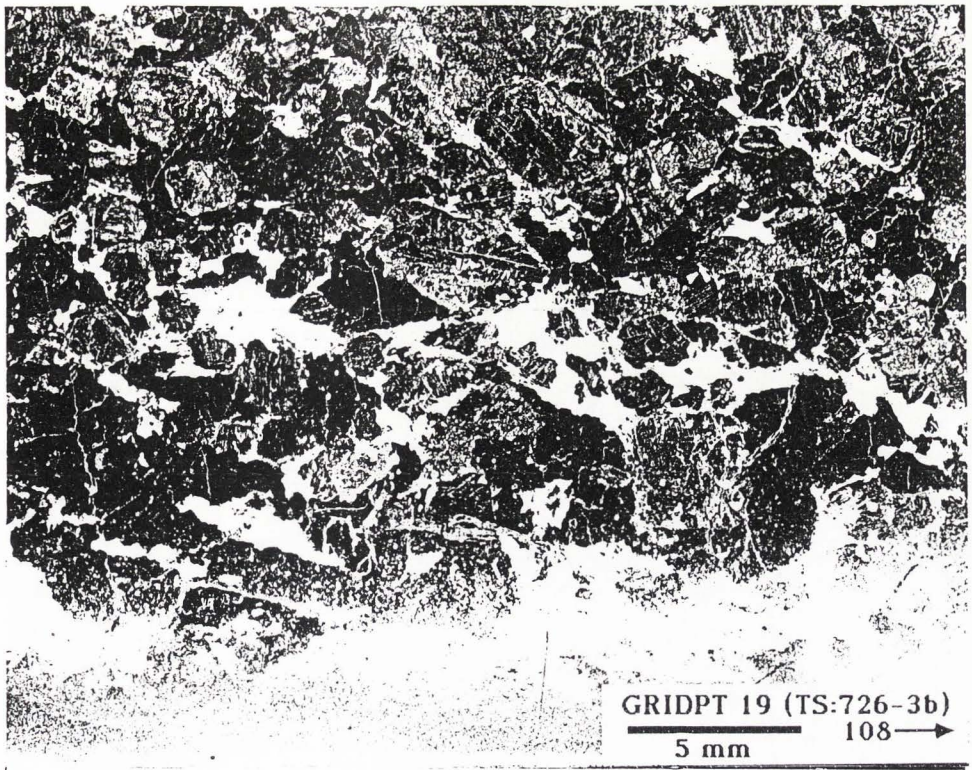
GRIDPT 19 (TS:726-3b)
5 mm
108

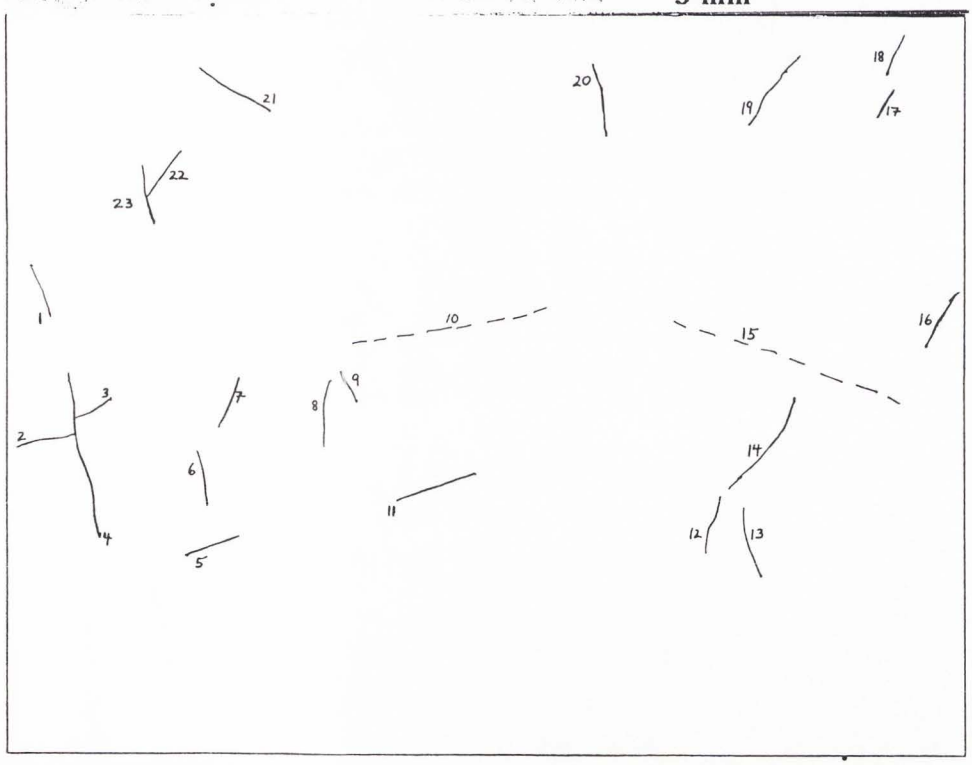
1
2
3
4
5
6
7
8
9
10
11
12
13
14
15
16
17
18
19
20
21
22
23

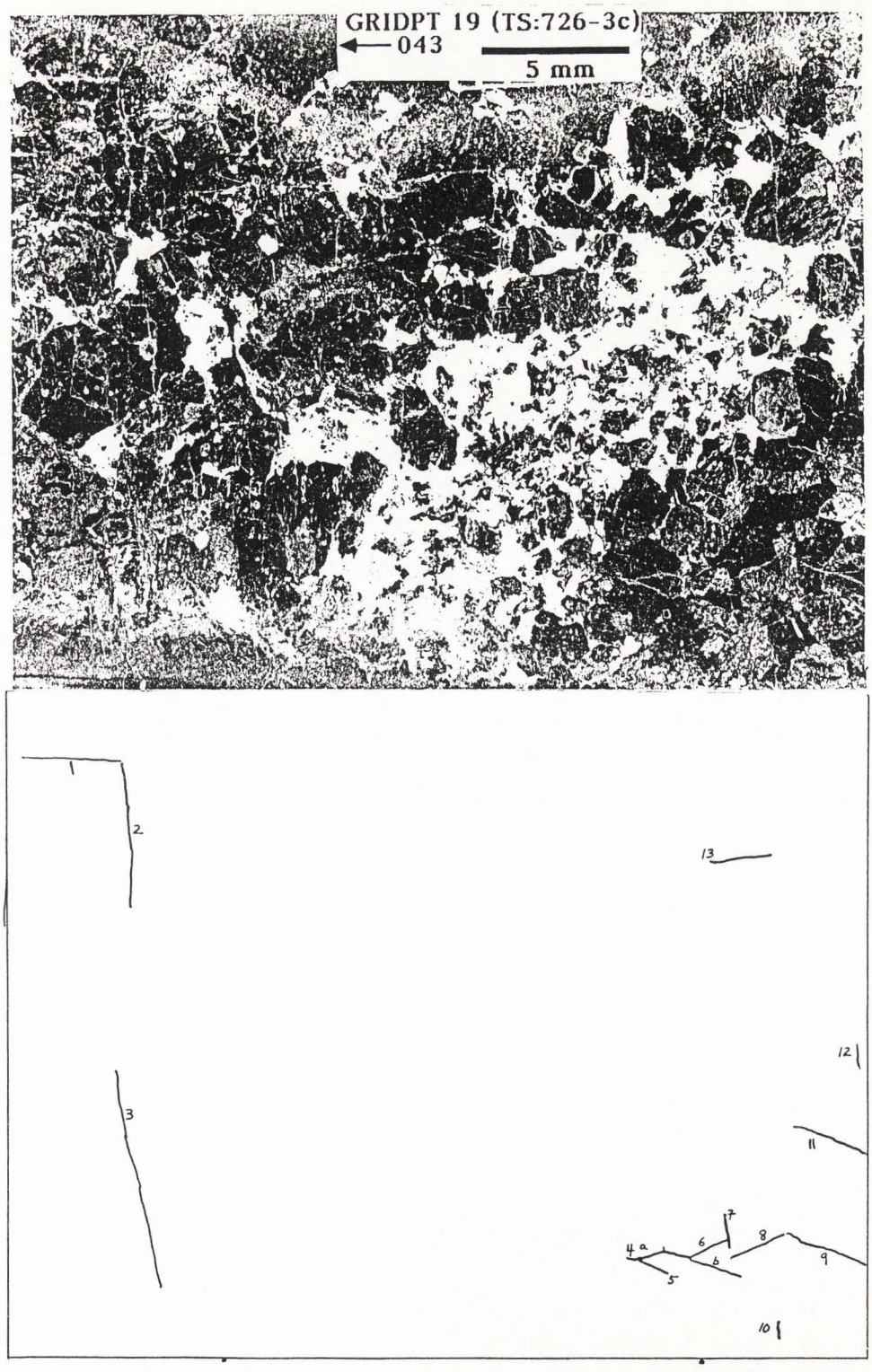
GRIDPT 19 (TS:726-3c)
043
5 mm
1
2
13
12
3
11
7
6
8
4a
b
9
5
10

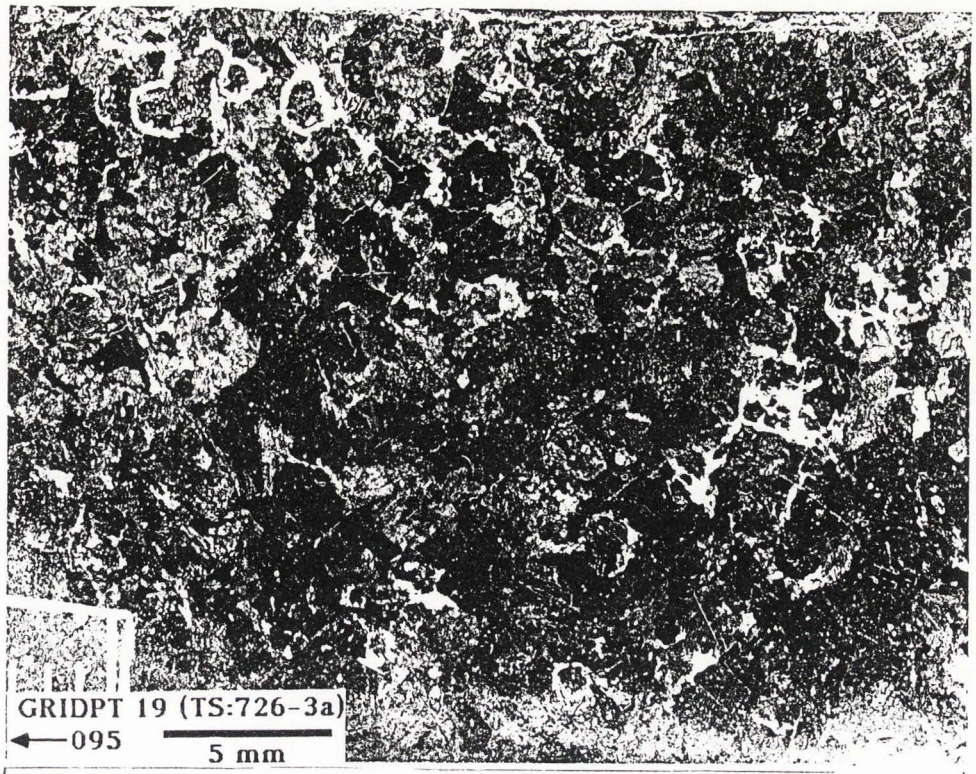
GRIDPT 19 (TS:726-3a)
←095
5 mm

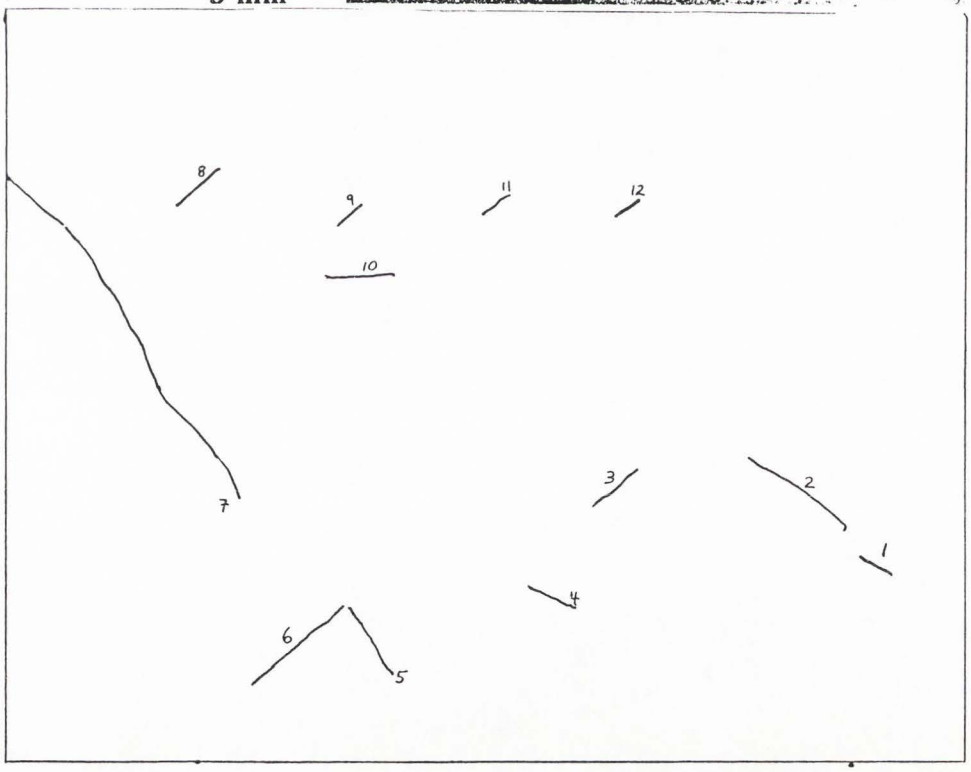
8
9
11
12
10
7
3
2
1
4
6
5

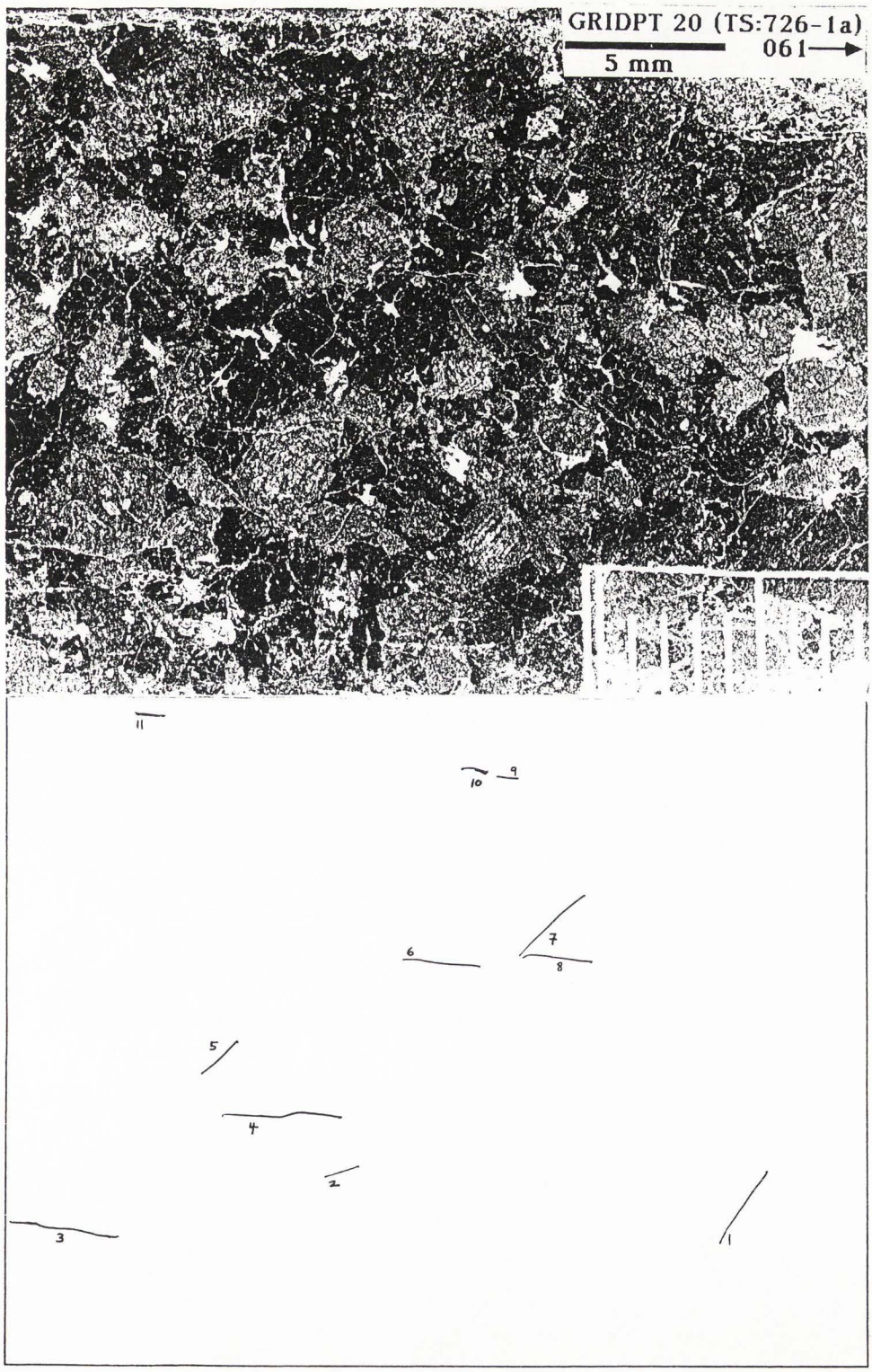
GRIDPT 20 (TS:726-1a)
5 mm
061
11
10
9
6
7
8
5
4
2
3
1